Design of Coated Magnetic Iron-Oxide Nanogels for Drug Delivery Systems

by

Sara Rahmani

A thesis
presented to the University of Waterloo
in fulfillment of the
thesis requirement for the degree of
Master of Applied Science
in
Chemical Engineering

Waterloo, Ontario, Canada, 2011

Author's Declaration

I hereby declare that I am the sole author of this thesis. This is a true copy of the thesis, including any required final revisions, as accepted by my examiners. I understand that my thesis may be made electronically available to the public.

Abstract

Intelligent and more advanced therapeutic agents, capable of sensing and responding to their environment, are required to treat more complicated and complex diseases. Among all recently developed therapeutic agents, hydrogels are not only intelligent to sense and respond to external stimulus, but also they can be synthesized and designed in the cellular and sub-cellular size scale, which enhance their therapeutic ability. Most body physiological processes are regulated as a consequence of pH gradient in different compartments of the body; besides, changes in pH are also associated with disease or damaged sites within the body. A unique feature of hydrogels is that they can provide a network for loading and release of drugs. Therefore, the drug loaded within pH-responsive nanogels are able to locally release onto the target sites because of their small size, and capability to sense and respond to environmental changes.

The goal of this research is to design and implement novel pH-responsive magnetic nanogels for drug delivery that respond to changes in pH. Semi-continuous emulsion polymerization was conducted to synthesize polyampholyte nanogels comprising of methacrylic acid (MAA) and 2-(diethylamino) ethyl methacrylate (DEAEMA) in the presence and absence of steric stabilizer poly (ethylene glycol) methacrylate (PEGMA). The synthesized nanogels demonstrated swelling behavior at both acidic and basic pHs. Herein, procaine hydro chloride (PrHy) was utilized as cationic drug to investigate the release behavior from synthesized nanogels under different conditions. PrHy was loaded within

nanogels through hydrophobic interaction and hydrogen bonding, as confirmed by isothermal titration calorimetry. The release study of PrHy molecules from nanogels was conducted by applying the versatile and easy technique of drug selective electrode, in which the concentration of released drug was measured as a function of time.

In order to facilitate the purification and enhance the detection of nanogels, iron oxide particles (Fe_3O_4) were co-precipitated within nanogels to form magnetic nanogels. Subsequently, layer-by-layer coating of polyelectrolytes were performed to control and eliminate the initial burst release of PrHy from nanogel by increasing the diffusion barrier and manipulating the permeability of nanogels. For the purpose of this research low molecular weight chitosan (CS) was used as polycation and poly (sodium 4-styrenesulfonate) (PSS) was acted as polyanion to coat magnetic nanogels. The more layers was applied, the more reduction in burst release was observed, which was revealed by using drug selective electrode to measure the concentration of the released drug from coated nanogels. Besides, layer-by-layer coating prolonged the time require to reach the steady state drug release. Therefore, this synthesized polyampholyte coated iron-oxide nanogels demonstrate great potential for use in controlled drug delivery systems.

Acknowledgements

First and foremost, I would like to acknowledge my supervisor, Professor K. C. Tam, for being an outstanding advisor and mentor for his constant assistance and encouragements to my master research and throughout difficult times I encountered during my graduate studies. For that I will always be grateful. I would like to acknowledge Professor Alexander Penlidis and Dr. Neil McManus for granting me access to the zeta-potential analyzer facility. I also like to extend my sincere thanks to Dr. Eric Croiset and Dr. Boxin Zhao for their valuable advices and comments on this thesis.

I would like to express my gratitude towards University of Waterloo department of Chemical Engineering for providing me the significant opportunity to conduct my master research. I also would like to thank my fellow lab mates for all their assistances and supports. Special thanks need to be given to Payam Ghafari and Andrea Patterson for their kind help to review and edit portions of this thesis. I would like to thank all my dear friends and loved ones who kept me centered and held me up during the difficult times.

Last but not least, this research along with my other achievements in life could not have been accomplished without priceless and continuous love and encouragements I receive throughout my life from my mother and father, Hengameh and Farshid, thanks for being always there for me and making me who I am today. I am also grateful to Pooria Habibbeigi for his supports and encouragements.

Dedication

This thesis is dedicated to

my wonderful parents

Hengameh and Farshid

Table of Contents

List of Figures

List of Tables

Chapter 1

Introduction

1.1 Background

Hydrogels are known as chemically or physically cross-linked organic or inorganic polymers that are able to absorb and retain large amount of water in response to external stimuli without losing their integrity upon dissolution in aqueous phase. Physical cross-linking agents are introduced via non-covalently connections between polymeric chains, due to the reversible sol-gel transition such as physical entanglement, hydrogen bonding, hydrophobic interactions, coordination bonds, and electrostatic interactions. Whereas chemical cross-linking agents are those that covalently connect at least three polymeric chains by cross-linker or chain transfer (Peppas et al., 2000). The development of stimuli-responsive polymer hydrogels, offer the pH-, thermo-, magnetic-, glucose- responsivity to polymeric hydrogels, which sometimes is called ‘’intelligence’’. The chemical structure of the polymeric network, particularly the functional groups on the side chains, characterizes the response mechanisms. Consequently, stimuli-responsive hydrogels have broad-spectrum applications in tissue engineering, diagnosis, drug delivery and biomaterials (Hendrickson et al., 2010b; Kopeček, 2007).

When hydrogels are confined into a spherical space with a diameter ranging from 10 to below 1000 nm are called nanogels. Nanogels are defined as a cross-linked polymeric network capable of swelling in a good solvent (Sasaki and Akiyoshi, 2010). In contrast to the behavior or hard

spheres, nanogels act like soft spheres because of both electrostatic repulsion of charges, which could induce compression as a result of imposing high concentration of nanogels (osmotic deswelling) or higher ionic strength (compression of electric double layers) and steric repulsion of dangling chains tethered on their rough surface (Sasaki and Akiyoshi, 2010). Because of the dominance of polymer-solvent interaction over polymer-polymer interactions, polymeric chains in nanogels without cross-linking agents would dissolve in solvent. Therefore, nanogels depend on the cross-linking in order to maintain their structure stability and integrity (Sasaki and Akiyoshi, 2010). Nanogels demonstrate great potential in smart, controlled, and regulated applications due to their environmentally responsive character. Specifically, they increasingly became recognized as the carrier for therapeutic drugs and diagnostic agents. The porous polymer network structure of synthetic nanogels offers an ideal reservoir for loading drugs, protecting them from environmental degradation and hazards, and also providing a template for post-synthetic modification of the drug carrier (Rhee and Mansour, 2011;Wu and Mansour, 2011).

A responsive drug delivery system is one of the most known technologies for intelligent drug release. In effective drug delivery systems, the drug release must be regulated in response to external biological, physical, or chemical stimuli. Targeting character may be obtained by functionalizing nanogels with receptor-specific ligands. Main requirements for an effective drug delivery systems include small size, extended circulation time, colloidal stability, biocompatibility, biodegradability, and reduced interaction with serum proteins to prevent renal clearance (Rhee and Mansour, 2011;Wu and Mansour, 2011).

Magnetic nanoparticles (MNP) are known as core metallic particles, in which each nanoparticles exhibit inherent magnetic properties. A stable colloidal suspension of single domain magnetic nanoparticles, typically ferrites in aqueous or organic carrier liquids, is defined as a ferrofluid. The general chemical formula for ferrites in MFe_2O_4, in which M represents a divalent ion such iron (Fe^{+2}), nickel (Ni^{+2}), or cobalt (Co^{+2}) (Li et al., 2002).

In this research iron oxide incorporated within nanogels, to form magnetic nanogels, for the enhanced delivery of the encapsulated drug molecules was investigated. In order to control the drug release and also to reduce the burst release of the drug molecules from the magnetic nanogels the layer-by-layer coating technique was applied. Kinetic profile of the drug release was obtained in the lab through manufactured drug-selective membrane electrodes.

1.2 Research Objectives

The goal of this research is to design and apply coated magnetic iron-oxide nanogels for drug delivery applications. The particular goals to be addressed include:

- Synthesis and characterization of polyampholyte nanogels,
- Incorporation of iron oxide within nanogels to forms magnetic nanogels,
- Construction of drug-selective membrane electrode in order to study the kinetic of drug release,
- Studying the drug release from magnetic nanogels under different environmental conditions,

- Coating the magnetic nanogels by layer-by-layer process in order to decrease the burst release of the incorporated drug and also to provide semi-permeable polyelectrolyte around the matrix.

Different characterization techniques were used to characterize the nanogels and to assure the polyampholyte properties of the nanogels. To determine neutralization and microstructure character of nanogels the laser light scattering (LLS) was performed to determine the hydrodynamic radius (R_h), the zeta-potential measurement was conducted to elucidate the overall surface charge of nanogels and coated nanogels to study the binding behavior, and the isothermal titrating calorimeter (ITC) was utilized to determine the binding behavior of drug-nanogels systems.

In order to provide insight into the drug release kinetic profile, the drug selective electrode method was used as an alternative approach to conventional dialysis membrane and centrifugal machine was applied, under different conditions such as varying pH, salt concentration, and concentration gradient. Moreover, in this research the multiple purification steps during layer-by-layer coating process have been eliminated as a result of synthesizing magnetic nanogels.

1.3 Thesis Overview

The work presented herein illustrates the synthesis and characterization of pH-responsive magnetic nanogels along with drug release behavior from the interior of the bare and coated magnetic nanogels. Chapter 2 provides an introduction to polymer nanogels, magnetic nanoparticles, layer-by-layer coating, and their current applications. This chapter offers insight on how unique stimuli-responsive properties of polymer nanogels can be regulated to meet the specific responsive and sensory applications. Chapter 3 discusses the different characterization

techniques utilized throughout the course of the experiments. In chapter, 4, the insight on the drug-selective membrane electrode is provided along with its characterization method. Chapter 5 describes the materials and methods used to synthesize different nanogel systems. In chapter 6, a detailed study on swelling and environmentally responsive behavior of polyampholyte nanogels, containing weak acidic and basic groups, is presented. Chapter 7 elucidates the kinetic profile of drug release from the polyampholyte nanogels. The results of these studies evaluate the influence of hydrophobic interactions on the successful physical incorporation of the drug molecules in the nanogels. Chapter 8 builds upon the synthesis of magnetic nanogels and the coating process of the magnetic nanogels. The layer-by-layer approach was conducted through alternate deposition of positively and negatively charged polyelectrolyte layers onto the magnetic nanogels. The results reveal the elimination of the burst release of the drug molecules from the nanogels as a result of coating layers. Besides, by manipulating the number of polyelectrolyte layers the release of the drug from the nanogels can be controlled and regulated. Finally, chapter 9 summarizes all the research done and the future outlook of this research.

Chapter 2

Literature and Background Review

2.1 Introduction to Hydrogels

Accurately identifying a gel is difficult. This state of material can act both as a solid and liquid, possessing the cohesive properties of a solid and the diffusive transport properties of a liquid. Polymer gels may be defined in the following ways (Hoare and Kohane, 2008):

1. Chemical gels: covalently-linked polymer chains together within the gel's polymeric network.
2. Physical gels: externally-induced topological change in polymer chain conformation by means of a system that reverses gelation.

Hydrogels are known as a cross-linked hydrophilic polymer network, which are able to provide distinct advantages over other biomedical polymers. Some of these advantages can be outlined as (Hamidi et al., 2008; Hoare and Kohane, 2008):

1. Covalent bonds held the polymer network together and offer control and integrity
2. Soft, and the hydrated nature of hydrogel makes them very similar to tissue, cell and other biological matters
3. Vastly controllable material properties
4. Synthesizable over a wide range of sizes

In this study the smart polymeric system refers to both nanogels and microgels interchangeably, even though in nanotechnology, the term ‘nano’ describes technologies that possess size range of 1-100 nm (Whitesides, 2005).

2.1.1 Structural Characteristics of Hydrogels

Hydrogels are described as a physically restricted hydrophilic polymer that can absorb and retain a large amount of water or biological fluids. There is no minimum amount of water a material has to absorb to be called a hydrogel (Kopeček, 2007). The presence of hydrophilic groups such as -*OH*, -*$CONH_2$*-, -*CONH*-, and -*SO_3H* in the polymeric units determines the water absorbance characteristic (Hamidi et al., 2008). The restriction within the hydrogels network is the result of covalent crosslinks between polymeric chains. These covalent bonds provide additional integrity, control, and maintain the robust structure of the gel while swelling or deswelling in aqueous medium, and also offer an environment to encapsulate guest molecules (Matyjaszewski et al., 2007). The characteristic polymeric structure is responsible for a hydrogel’s unique ability to undergo abrupt phase transition from a swollen liquid-like hydrated state to a solid-like collapse state in response to changes in the external stimuli, such as pH, temperature, ionic strength, glucose concentration, and external electromagnetic field. However, the main focus of this research is on the synthesis and characterization of pH- and magnetic responsive nanogels. The changes in the equilibrium volume in a different solvent can vary from monomer to monomer, and depends on the interaction energy of side groups of the monomer with other monomers or solvent. Figure 2.1 illustrates the cross-linked structure of a hydrogel. This demonstration combines the Flory representation of an ideal network with that of an ideal ionic hydrogel. In the former, a crosslink is depicted as a point that has no volume with respect to the rest of the chain.

A crosslink can be imagined as a chain of atoms capable of joining at least two different polymer chains together. Hydrogels can be classified as neutral, cationic (Hu et al., 2007; Marek et al., 2010) , anionic (Brugger et al., 2010; Hoare and Pelton, 2004), and amphiphilic or zwitterionic (Deng et al., 2009; Tan et al., 2006) depending on the origin of the incorporated functional groups. Hydrogels can also be classified based on their size. Macrogels are bulk gels and have a size range of one millimeter to a few centimeter; Microgels are colloidally stable hydrogels that range from 100 nm to several hundred microns. Microgels find great interest in intelligent, controlled and regulated application, due to their environmentally responsive behavior. It should be indicated that the terms nanogels and microgels are usually used interchangeably in the literatures, and through this thesis the term nanogels was used to describe the colloids that been synthesized in this research and the term microgels was utilized in the literature review section according to the referred papers.

Microgels are composed of a porous, covalently-crosslinked, spherical network of randomly oriented polymeric chains that are swollen in a suitable solvent. The microgels possess a cross-linked linear polymeric chain structure with a narrow range of particle size without a discrete core, which makes them appear visually as flawlessly spherical sponges (Kopeček, 2007). Figure 2.1 shows microgels particles collapsed (a) and swollen in a good solvent (b).

(a)

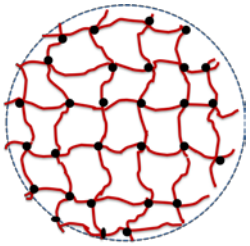

(b)

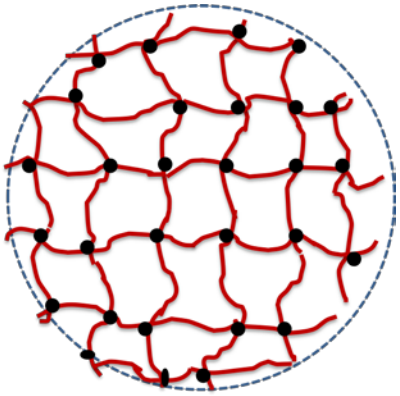

Figure 2.1 Schematic of (a) collapsed and (b) swollen microgels.

2.1.2 Nanogels Classifications

Nanogels are more commonly classified in three ways. The first classification is based on the type of functional groups incorporated into their network. The second classification is based on their responsive behavior, which can be either stimuli-responsive or non-responsive. In the case of non-responsive microgels, they simply swell as a result of absorbing water, while stimuli-responsive microgels swell or deswell upon exposure to environmental changes such as temperature, pH, magnetic field, and ionic strength. Multi-responsive microgels are responsive to more than one environmental stimulus. In the last classification of microgels, they are sorted by the nature of the crosslinks within their network, in which micorgels can be either physically or chemically crosslinked. As mentioned before, crosslinks play an important role to prevent dissolution of the polymer chain and also to keep the network structure of the hydrogels under different environmental conditions (Gupta et al., 2002; Sasaki and Akiyoshi, 2010).

2.1.3 .1 Chemically Cross-linked Nanogels

The chemically crosslinked nanogels formed by covalent interactions are stable and capable of maintaining their robust structure under all environmental condition unless a labile functional

group has been attached to the network. The method commonly used to synthesize chemically crosslinked microgels is copolymerizing monomers with multifunctional crosslinker. Radical polymerization or condensation polymerization is typically used to synthesize chemically crosslinked microgels with size ranging from 100 to 1000 nm (Gupta et al., 2002). A variety of physical properties such as the swelling capacity and viscosity of microgels are dependent on and controlled by the amounts of cross-linked agent used in the microgel synthesis.

Tan et al. (Tan et al., 2005b) synthesized pH-responsive microgels by semi-continuous emulsion polymerization consisting of methacrylic acid-ethyl acrylate (MAA-EA) cross-linked by di-allyl phthalate (DAP). They observed that in order to synthesize stable and compact microgels with 20 mol% MAA, the optimum cross-linking agent density of 1 wt.% was required, so that sufficient cross-linked junctions were formed to maintain a permanent structure in the microgels; otherwise insufficient cross-linked junctions were formed, which produced unstable microgels. Figure 2.2 illustrates that by increasing the cross-linking density, the microgel size decreased and the swelling was inhibited, resulting in a drop in the relative viscosity. In addition, the M_w of the microgels decreased below the 1 wt% crosslink density as a result of the expulsion of polymer chains from the microgel and due to the insufficient crosslinked junction, unstable microgels were formed (Tan et al., 2005b).

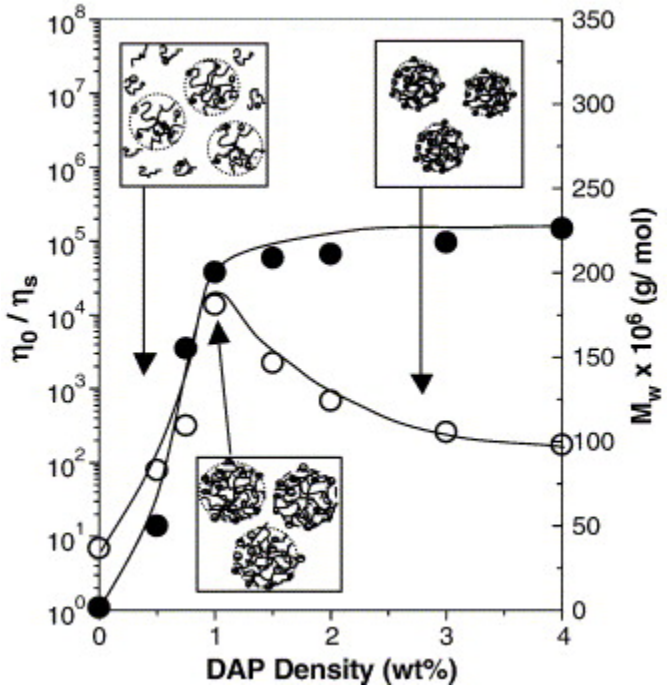

Figure 2.2 The conformation evolution of (MAA-EA) microgels with 20 mol% MAA versus the crosslinking agent density (wt. % DAP). The filled circle shows M_w and the white circle shows the low shear relative viscosity (Tan et al., 2005a).

2.1.4 .1 Physically Cross-linked Nanogels

The formation of physically crosslinked microgels is due to the non-covalent interaction such as hydrophobic interaction, ionic interaction, and hydrogen bonding. This system is vastly applied in the encapsulation of drugs and proteins within the structural network of microgels, because the microgels can release incorporated agents from the interior network by the dissolution of their structure. Therefore, physically cross-linked microgels are of great interest in the field of biodegradable systems that are able to go from the solution state to stable gel state, and vice versa (Morimoto et al., 2005; Sasaki and Akiyoshi, 2010).

The main disadvantage of this system is that they can lose their stability and disintegrate upon exposure to many factors, such as temperature, ionic strength, and polymer composition as a result of weak non-covalent interactions. Therefore, physically cross-linked microgels are less stable compared to their chemically cross-linked counterparts (Hoare and Kohane, 2008).

2.1.5 Nanogels Applications

Latex copolymers have a wide range of applications, including paints, adhesives, synthetic rubber, paper coating, and carpet backing, and toughened plastics (Sudol et al., 1992). Other applications, such as waste water treatment and enhanced oil recovery involving microgel particles. In addition, microgels that have a stable, well-defined morphology (monodisperse) can be applied as opacifying agents, model colloids, calibration standards, and pharmaceutical applications (Sudol et al., 1992). Due to their high water content, which makes them very similar to natural tissue; microgels also have a variety of applications in biomedical field. They usually exhibit very good biocompatibility, and such characteristic makes microgels a very good candidate for biomedical application, e.g. in drug delivery systems, biosensors, contact lenses, catheters, and wound dressing. Moreover, because of their high water content they can also be used as membranes. The diffusion of solute through the microgel networks is facilitated by the water within the gel, and the crosslinks, which are characterized by the pore size of the hydrogels network. Together these determine whether a solute of a specific size is able to pass through the space between the polymer chains (Peppas et al., 2000).

2.1.6 Nanogels Stabilization

Colloidally stable nanogels that are stable against aggregation are crucial factors in designing nanogels. The stability of nanogels results from the equilibrium between attractive and repulsive forces. Interparticle potential in the system is usually attributed to the van der Waals forces, which induce strong short-range isotropic attractions, and electrostatic repulsive forces. These two forces are theoretically explained by the Derjaguin-Landau-Verwey-Overbeek (DLVO) theory. Another force that should be considered especially for coated nanoparticles is steric repulsion (Laurent et al., 2008).

Charged stabilized nanogels maintain a charge balance on the micorgel surface with small ions of opposite sign in the solution phase (counter-ion). Consequently, electrical double-layer forms, in which the nanogel's surface has an electric potential depending on the surface group's charge as shown in Figure 2.3a. When the charges no longer provide practical approach for stabilization, 'hairy particles' can be employed. A common example of 'hairy particles' is the use of poly (ethylene glycol) chains as the stabilizer agent, which (Ottewill, 1982) leads to non-charged 'hairs' extending into the solvent, providing a sterically stabilized system 2.3b.

Nanogels synthesized via emulsion polymerization are not likely to be electrostatically stable, especially around their isoelectric point (IEP). Isoelectric point is the pH in which there are equal numbers of positive and negative charges present. As a result, one should view nanogels as a combination of charged group and 'nano-hair'. From this description, the nanogel's stabilization can occur through the following factors (Ottewill, 1982):

1. Electrostatic effects: caused by the repulsive interactions between similar charges,

2. Steric effects: associated with the unfavourable entropy of mixing of chains from the surfaces of more than one particle,
3. Solvating effects: arising from the association of solvent molecules near an interface or between polymer chains,
4. Attractive effects: arising from the Van der Waals interaction between opposite charges.

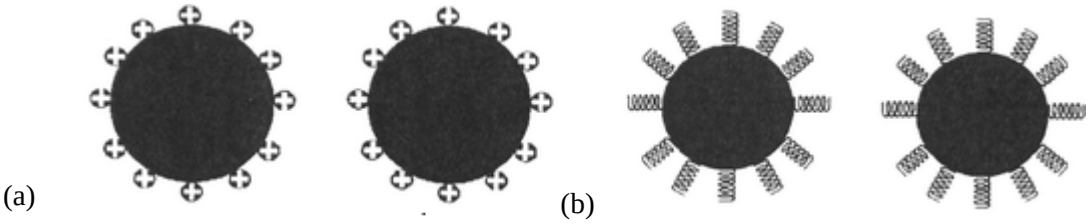

Figure 2.3 Nanogel stability (a) electrostatic stabilization (b) steric stabilization (Laurent et al., 2008).

Electrical double-layer is distributed when electrostatic-stabilized nanogels are in dispersion of high electrolyte concentrations due to shielding of surface groups. The distance D between nanogel particles is decreased when the electrostatic repulsions are shielded. Concurrently, increasing the electrolyte concentration in the medium causes an osmotic effect, resulting in the reduction of solvent in the counter ion cloud. Polymer chains contract due to a loss of water and as a result the distance D between nanogel particles is increased. The deswelling of microgel particles in salt solution leads to van der Waals attractions resulting in flocculation and eventually coagulation.

2.2 Polyampholytes

Polymeric nanogels are functionalized with ionic groups and are known as polyelectrolyte microgels. When both positively and negatively charged functional groups exist and are randomly distributed along a polymer chain, the microgels are referred to as polyampholyte

microgels. Therefore, the properties of polyampholyte microgels are very different from those of polyelectrolyte, due to the presence of the oppositely charged group in the microgel network (Das and Kumacheva, 2006). The conformation of a polyampholyte chain with a net charge is the result of competition between the following two antagonistic effects (Tan et al., 2006):

1. The polyampholyte effect: associated with the attraction between groups of opposite sign, which leads to chain compression,
2. The polyelectrolyte effect: associated with the repulsion between like charges, which tends to expand the polymer chains

Polyampholytes are capable of undergoing volume transition at both low and high pH conditions. Changing pH leads to ionization of acidic or basic groups within the microgel network, causing electrostatic repulsion between like charges, and subsequent swelling of the microgels, this then results in larger microgel size. In other words, the degree of swelling is increased by the repulsion between protonated cationic functional groups at low pH, and deprotonated anionic functional groups at high pH. The intermediate pH, in which there are equal numbers of both cationic and anionic functional groups that are present in their charged state, is known as the isoelectric point (IEP). Isoelectric point leads to microgel deswelling, and also reduces the net surface charge to zero. At the IEP, ion pairing between charged cationic and anionic functional groups is dominant over repulsion between unpaired, like charges.

2.2.1 Block Polyampholytes

There are significant studies on the synthesis and characterization of both linear polyampholyte copolymers and diblock polyampholytes. Polyampholytes with diblock copolymer structure, unlike conventional free radical copolymerization, can be synthesized under living

polymerization conditions (anionic, cationic, or group transfer polymerization), which requires sequential addition of protected monomers (Tan et al., 2006). Dai et al. (Dai et al., 2003) reported on the synthesis and solution behavior of diblock copolymer of poly [2-(diethylamino) ethyl methacrylate-*block*-methacrylate acid] [P (DEAEMA-*b*-MAA)] that was synthesized through the atom transfer radical polymerization (ATRP) technique. They observed that at low pH, the DEAEMA block became hydrophilic due to the protonation of amines; while, at high pH value the MAA block became soluble due to ionization. Therefore, the hydrophile-lipophilic balance (HLB) of the block copolymer was varied at high and low pH values. In other words, micelles with a hydrophobic MAA core and protonated DEAEMA corona shell were formed at low pH condition. On the other hand, at high pH condition hydrophobic DEAEMA core deprotonated and hydrophilic MAA corona shell ionized, as seen in Figure 2.4 (Dai et al., 2003). As illustrated in Figure 2.4 the laser light scattering measurement was performed by this research group to study the micellization behavior of the block copolymer at different pHs. They obtained two hydrodynamic radii of about 2.7 and 70 nm at pH of 3, corresponding to the unimers and micelles, respectively. This happened because of the very low pK_a ~ 5.4 of MAA in contrast to HLB. At intermediate pH, large aggregates formed due to phase separations. By increasing the pH to above 9, only one hydrodynamic radius was detected due to the high pK_a ~ 7.3 value of DEAEMA (Dai et al., 2003). The same pH reversible micellization properties were also observed by other research groups as a result of synthesizing polyampholyte diblock copolymer.

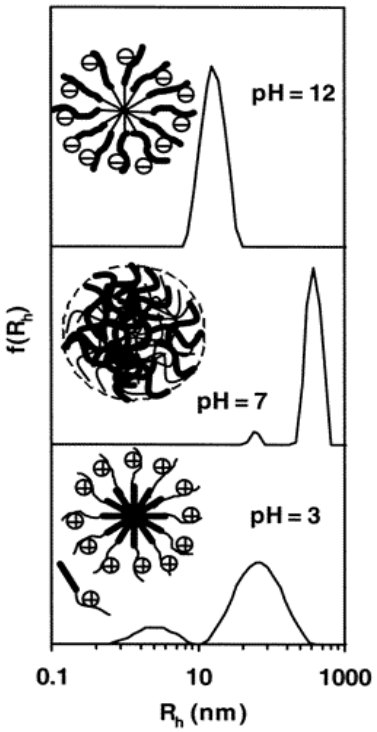

Figure 2.4 The hydrodynamic radius distribution and possible structure of P (MAA-b-DEAEMA) at different pH values (Dai et al., 2003).

2.2.2 Polyampholyte Nanogels

In comparison to linear and block polyampholyte, there are very few investigation on the synthesis and characterization of polyampholyte microgels. In a very recent study, Christodoulakis et al. (Christodoulakis and Vamvakaki, 2010) synthesized a series of pH-responsive polyampholyte core-shell microgels comprising 2-(diethylamino)ethyl methacrylate (DEAEMA) as the ionizable cationic monomer, *tert*-butyl methacrylate (*t*-BuMA) as the hydrophobic monomer, and ethylene glycol dimethacrylate as the cross-linking agent through emulsion copolymerization and following acid hydrolysis to obtain methacrylic acid (MAA) from *tert*-butyl methacrylate (t-BMA). The core of the final microgels consisted of a cross-linked

poly (2-diethylamino) ethyl methacrylate (PDEAEMA) or poly methacrylic acid (PMAA) which was surrounded by a cross-linked PMAA or PDEAEMA shell, respectively. The synthesized sore-shell microgels have been illustrated in Figure 2.5 (Christodoulakis and Vamvakaki, 2010).

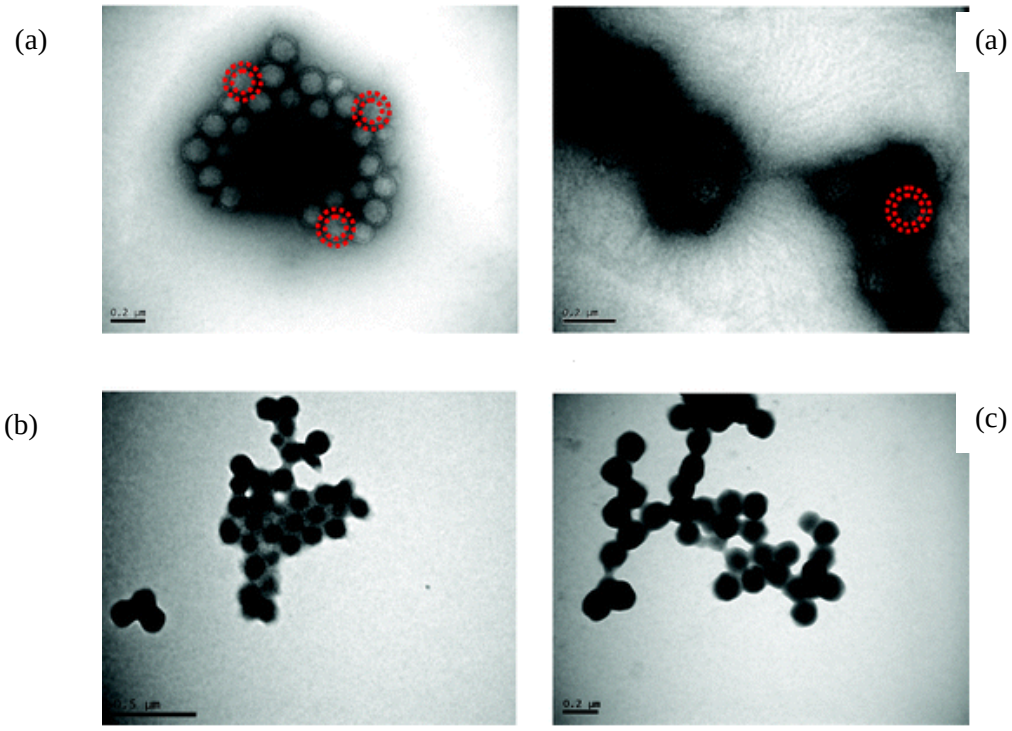

Figure 2.5 TEM images of the (a) P (t-BuMA)-PDEAEMA shell microgels stained with potassium hexachloroplatinate, (b) PMAA core-PDEAEMA shell microgels stained with cadmium nitrate, and (c) PMAA core-PDEAEMA shell microgels stained with potassium hexachlo hexachloroplatinate (Christodoulakis and Vamvakaki, 2010).

From potentiometric titration curves shown in Figure 2.6, it is revealed that acidic and basic ionizable groups of the core and the shell of the core-shell microgels were spatially separated and independently ionized because of the presence of two plateau regions in the titration curve. However, the simultaneous protonation and deprotonation of the basic and acidic segments was observed in the random copolymer microgels due to the presence of single plateau region in the

titration curve. In other words, upon ionization of the DEAEMA segments at low pH value or the MAA segments at high pH condition the core and the shell of the microgels were swollen. Besides, when both the core and the shell of the microgels were neutral at intermediate pH, the microgels collapsed (Christodoulakis and Vamvakaki, 2010).

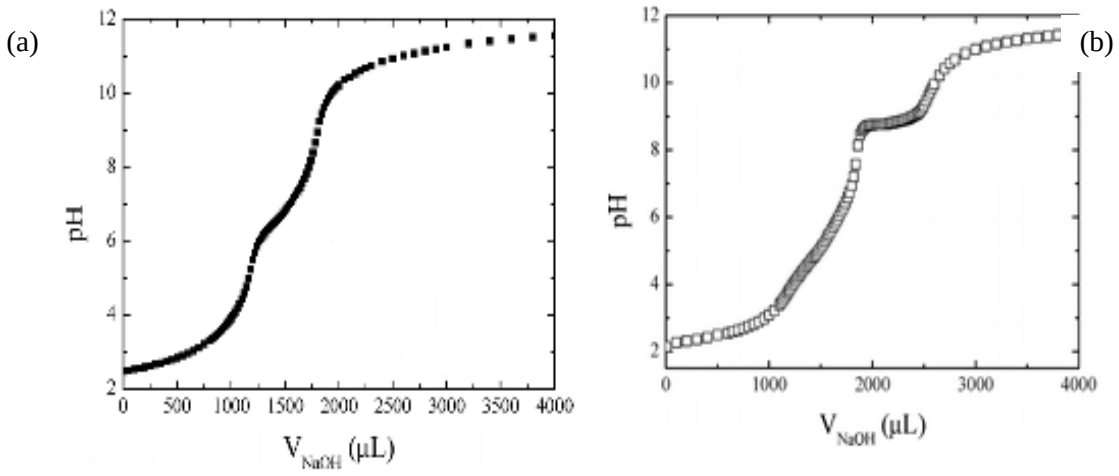

Figure 2.6 Potentiometric titration curves for a 0.2 wt% solution of the (a) PDEAEMA- PMAA random copolymer microgels showing single plateau region, and (b) PDEAEMA core- PMAA shell microgels illustrating two plateau regions (Christodoulakis and Vamvakaki, 2010).

In another study Deng et al. (Deng et al., 2009) performed distillation dispersion copolymerization in acetonitrile (AN) to synthesize polyampholyte nanogels consisting of poly (ethylene glycol) methyl ether methacrylate (PEGMA) as macromonomer, *N*,*N*-(dimethylamino) ethyl methacrylate (DMAEMA) as monomer, and methacrylic acid (MAA) as comonomer. These nanogels demonstrated great swelling ability and also core-shell structure away from isoelectric point (IEP). In addition, the size of the swelled nanogels did not change over time and it reached equilibrium after swelling for 24 hour, as shown in Figure 2.7. Moreover, the swollen

nanogels composed of hollow core and cross-linked network shell, which was formed due to osmotic swelling (Deng et al., 2009).

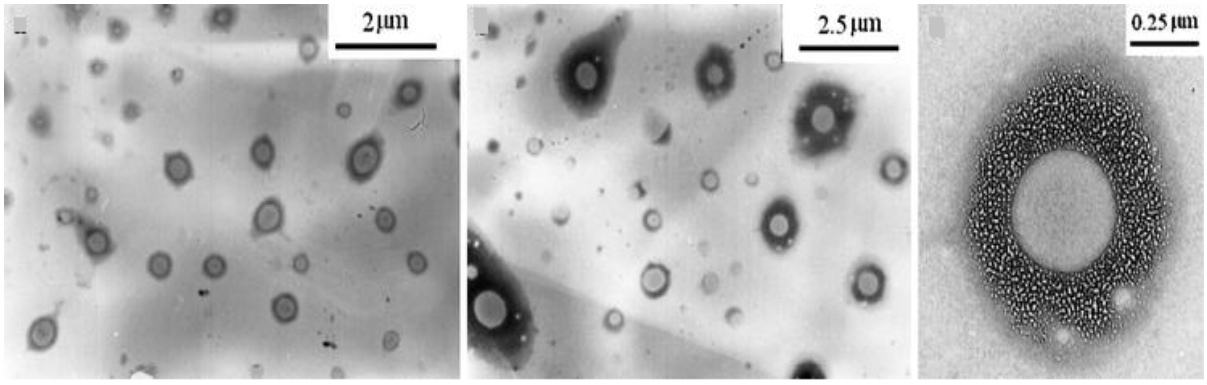

(a) (b) (c)

Figure 2.7 TEM images of P ((MAA-co-DMAEMA)-g-PEGMA) after swelling in pH=1.89 of PBS (a) after 24 h, (b) after 48 h, and (c) hollow core structure of nanogels in (b) (Deng et al., 2009).

2.3 Nanogels Synthesis

As previously discussed, microgels offer very unique characteristics, including tunable chemical structure, high surface area, porous network, good mechanical properties, high water content, and biocompatibility, all of which make them an interesting topic to study and explore (Oh et al., 2008b). There are various synthetic techniques for the production of microgels. Some of these methods are summarized below. Since the microgels associated with this research were synthesized by both emulsion and inverse emulsion polymerization, more focus is given to these methods compared to the other synthesizing techniques.

2.3.1 Emulsion Polymerization

Emulsion polymerization was first introduced on an industrial scale in mid 1930s. Nowadays, it has developed into a very versatile approach that is widely used for the synthesis of stimuli-responsive microgels from hydrophobic monomers (Lovell and El-Aasser, 1997). Figure 2.8 depicts the three steps in the emulsion polymerization. By adding a large amount of surfactant above its critical micelle concentration (CMC) in the continuous phase, usually water, micelles are formed and nucleation occurs. Micelles emulsify the hydrophobic monomers and act as micro-continuous reactors that contain all essential ingredients for the emulsion polymerization reaction. At this stage, both the large monomer droplets stabilized by surfactant and monomer-swollen surfactant micelles exist in the continuous phase. The first step (Figure 2.8a) starts when the water-soluble initiator produces oligoradicals from slightly hydrophobic monomers. Subsequently, these oligoradicals enter the micelles and form particles. In the second step (Figure 2.8b), monomer droplets gradually diffuse through the water phase to the micelle during the course of polymerization to maintain a continuous growth of polymer particles. The last step (Figure 2.8c) corresponds to consumption of monomer droplet and polymerization of any residual monomers in the particle and aqueous phase (Landfester, 2001; Odian, 2004).

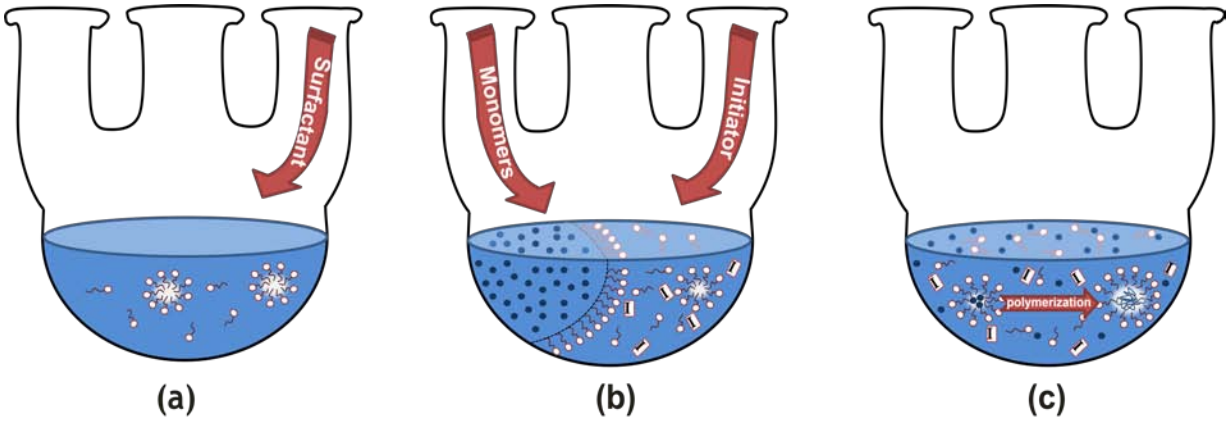

Figure 2.8 Schematic diagram of the three steps involved in the emulsion polymerization. (a) the first step of emulsion polymerization, (b) the second step of emulsion polymerization, and (c) the last step of emulsion polymerization.

Depending on the monomer droplet size, the emulsion polymerization can be classified into macroemulsion and microemulsion. The former refers to emulsion polymerization in which monomer droplets are large (hundreds of micron), and the latter describes emulsion polymerization with small size monomer droplets (nanometer). Hydrophobic microgels are commonly synthesized by microemulsion polymerization. Microemulsions are thermodynamically stable dispersion due to a very low interfacial tension, which can balance the very high dispersion entropy mostly caused by small droplets size (Chern, 2008). Van der Waals interaction between hydrophobic microgels is the dominant driving force for irreversible aggregation of these microgels, due to the high refractive index difference between the hydrophobic microgels and aqueous medium. Therefore, the colloidal stability enhancement obtained using surfactant (which possesses both hydrophobic and hydrophilic domains) to provide electrostatic or steric stabilization to the hydrophobic nanogels.

2.3.2 Inverse Emulsion Polymerization

Inverse emulsion polymerization was first introduced in 1987. Similar to emulsion polymerization, this method involves the addition of large amounts of surfactant above its CMC into the system, which leads to thermodynamically stable water-in-oil (W/O) emulsions. Inverse emulsion polymerization is mostly suitable for polymerization of high molecular weight hydrophilic polymers that are capable of polymerizing in hydrophobic organic solvents. Polymerization occurs inside the water droplets, which act as nanoreactors that can encapsulate a high concentration of hydrophilic monomers that can produce microgels in the presence of hydrophilic crosslinking agents. Unlike emulsion polymerization, this technique does not include the step of monomer diffusion through the continuous medium. Preventing water droplets from aggregation through steric stabilization is another function of nonionic surfactants in the inverse emulsion polymerization (Capek, 2010).

Figure 2.9 shows the schematic diagram of inverse emulsion polymerization; it can be observed that monomer droplets are not present in this system. Moreover, nonionic surfactants possess a unique value known as hydrophile-lipophile balance (HLB), which determines the ratio of hydrophilic to liphophilic portion on the surfactant. The desired HLB value can be obtained by mixing two different nonionic surfactants with different HLB values. Nonionic hydrophobic surfactants are generally used in the inverse emulsion polymerization to convert oil-in-water (O/W) emulsions at room temperature into water-in-oil (W/O) emulsions at higher temperature. The temperature at which this phase inversion occurs is referred to as the phase inversion temperature (PIT) (Odian, 2004).

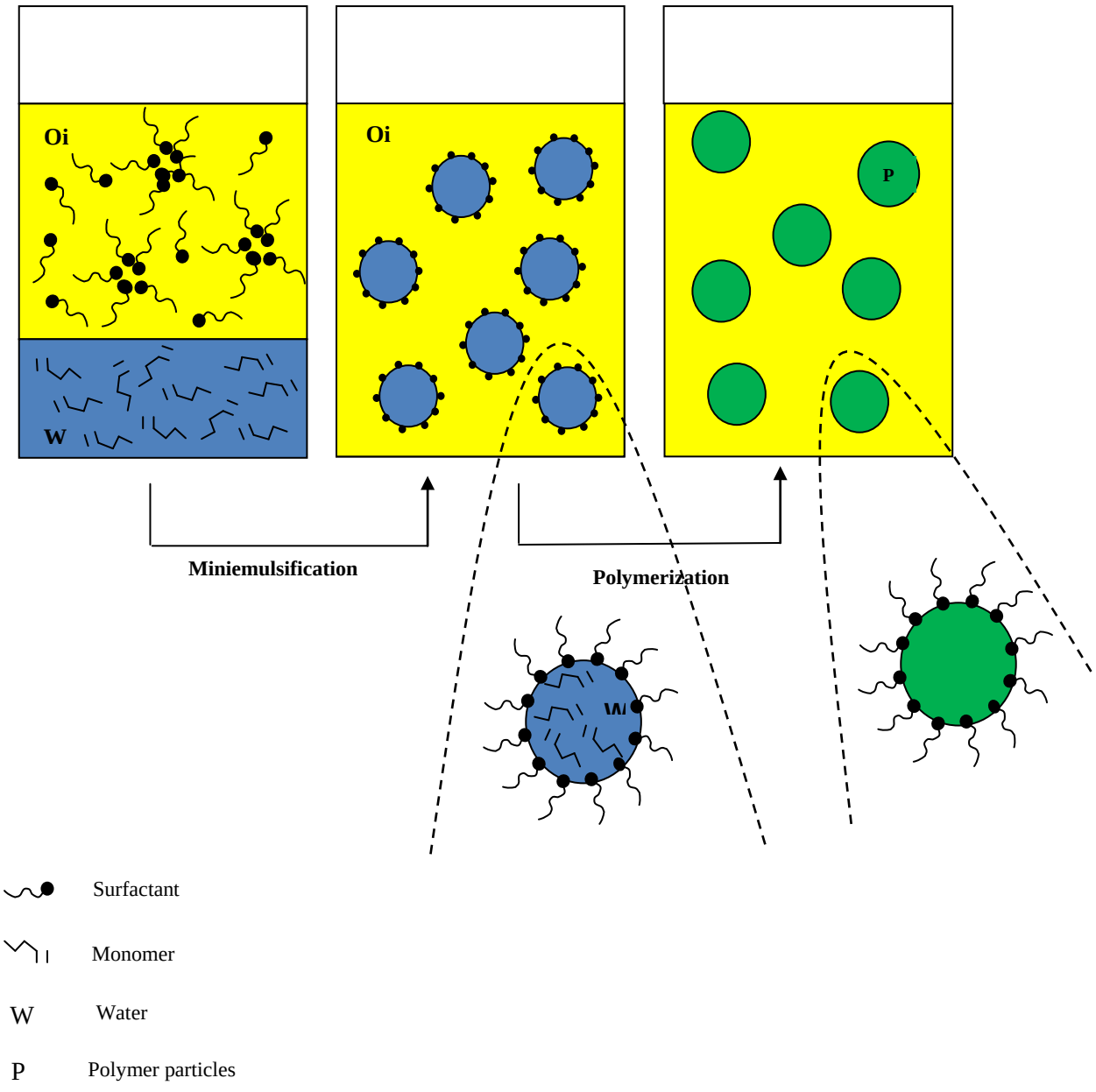

Figure 2.9 Schematic diagram of inverse emulsion polymerization.

2.3.3 Precipitation/Dispersion Polymerization

During the course of precipitation polymerization, the reaction proceeds from a homogeneous mixture of monomer, initiator and solvent to the heterogeneous solution, where produced polymers precipitate out of the solution and form microgels. Dispersion polymerization is a subdivision of precipitation polymerization, and where the growing hydrophobic polymer chains are sterically stabilized, and dispersed in a colloidal solution. In this method, the use of a cross-linking agent is essential for the isolation of the formed microgels, because the synthesized microgels are not swellable but soluble in the medium (Odian, 2004). Peppas et al. synthesized narrow size distribution poly (methacrylic acid-*g*-ethylene glycol) (P (MAA-*g*-EG)) nanospheres through precipitation polymerization for the oral delivery of proteins. They obtained better control over particle size and particle size distribution by controlling monomer concentration in water. They also revealed that increasing the cross-linker concentration during polymerization decreased the equilibrium swelling of the nanospheres (Robinson and Peppas, 2002; Thomas et al., 2006).

2.3.4 Photolithography

Photolithography basically addresses a high throughput nano-molding process with high control over size, shape and composition of formed particle. As shown in Figure 2.10, photolithography consists of five steps. In the first step, the UV cross-linkable polymer, which possesses low surface energy, as a substrate is released on the pre-baked photo resist-coated water. The next step involves molding the polymer into patterns on the silicon wafer by pressing the quartz template onto the polymer and exposed it to the intense UV light. In the third step, the particles

with a thin residual interconnecting film layer are uncovered by removing the quartz template. Subsequently, this residual thin layer is removed by a plasma containing oxygen that oxidizes it. In the last step, the fabricated particles are directly collected by dissolution of the substrate in water of buffer (Glangchai et al., 2008; Sasaki and Akiyoshi, 2010).

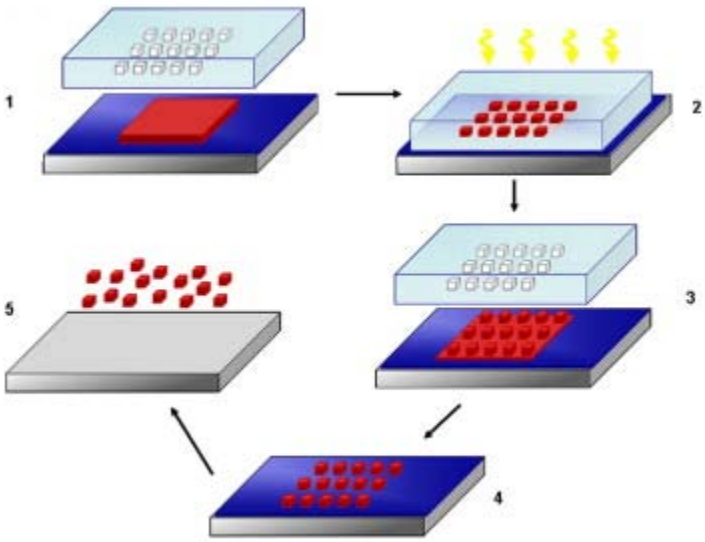

Figure 2.10 Schematic diagram of five steps involved in photolithography (Glangchai et al., 2008).

Photolithography can be classified into Particle Replication in Non-wetting Templates, known as a PRINT process, and Traditional Imprint Lithography based on the non-wetting substrate and wetting substrate, respectively. The former process leads to the fabrication of isolated particles in which the formation of the residual interconnecting film is eliminated, while the latter produces an embossed film that, as explained above, needs to be removed (Petros and DeSimone, 2010;Rolland et al., 2005). Glangchai et al. (Glangchai et al., 2008) successfully synthesized cross-linked hydrogels of poly (ethylene glycol diacrylate) (PEGDA) and GFLGK-DA via the traditional imprinting technique. The imprinted particles were obtained in very small particle size about 50 nm. Moreover, these particles represent a very high efficiency to encapsulate agents,

such as plasmid DNA, antibodies, and model drugs, and release the incorporated agents in response to various external stimuli (Glangchai et al., 2008).

2.3.5 Membrane Emulsification

In the membrane emulsification technique, the to-be-dispersed phase is passed through the membrane (glass or ceramic), which possesses uniform pore size. Under certain conditions the emulsion droplets or microgels with specific morphology are formed on the surface of the membrane and afterwards, with a continuous phase that is flowing across the membrane, these fabricated emulsion droplets or microgels are recovered (Nakashima et al., 2000). These fabricated emulsion droplets can be in different emulsion formation such as water-in-oil (W/O), oil-in-water (O/W), oil-in-water-in-oil (O/W/O), and water-in-oil-in-water (W/O/W) (Oh et al., 2008b). The size of the formed droplet is controlled by the membrane pore size, velocity of the continuous phase, and pressure of the trans-membrane. Figure 2.11 represents the diagram using this synthesizing technique.

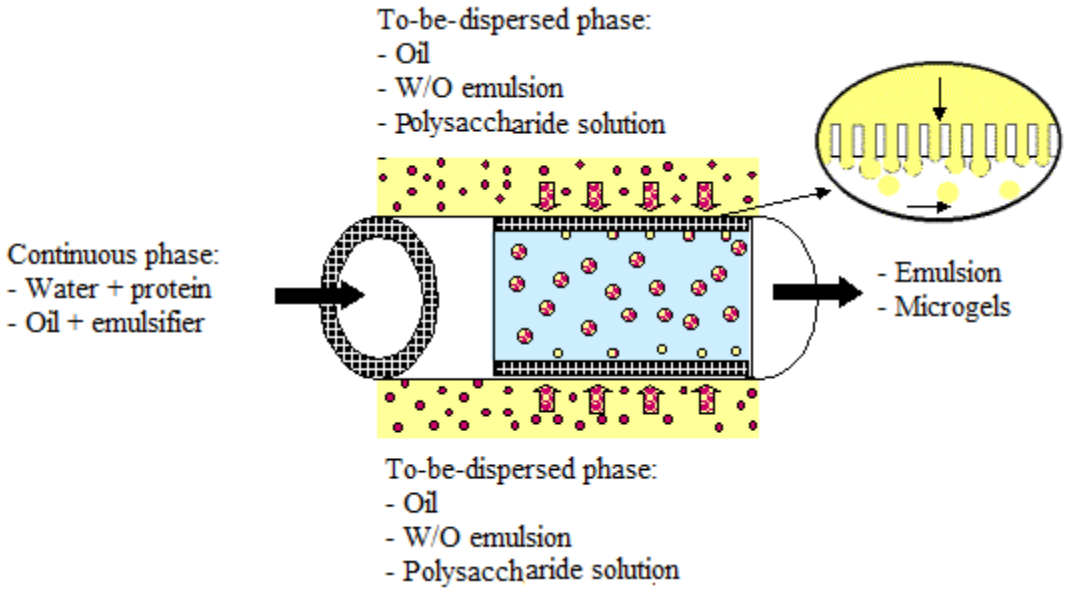

Figure 2.11 Schematic diagram of the membrane emulsification technique (http://www.muschiolik.de/membrane_emulsification_process-desription.htm).

2.4 Nanogels in Nanomedicine

Smart therapeutic system is achieved when the sensing and treatment of a disease or health condition can be performed by the patient himself, without requiring human intervention. The classes of smart therapeutic agents are polymers, which play an active role in nanomedicine. The term nanomedicine was first used to describe technologies under category of nanotechnology with therapeutic applications in human health by the United States National Institutes of Health (Medina et al., 2007). The distinct difference between nanotechnology and nanomedicine lies in the fact that nanotechnology is the development and application of technology with novel properties on nanoscale, while nanomedicines are generally very small devices or systems that utilize the natural, nanoscale properties of the human body. Figure 2.12 summarizes the most common types of polymeric systems used in nanomedicine and their fundamental properties and

characteristics including size, targeting ligand surface chemistry, composition, and physical properties that need to be consider while designing nanoparticles for biomedicine applications.

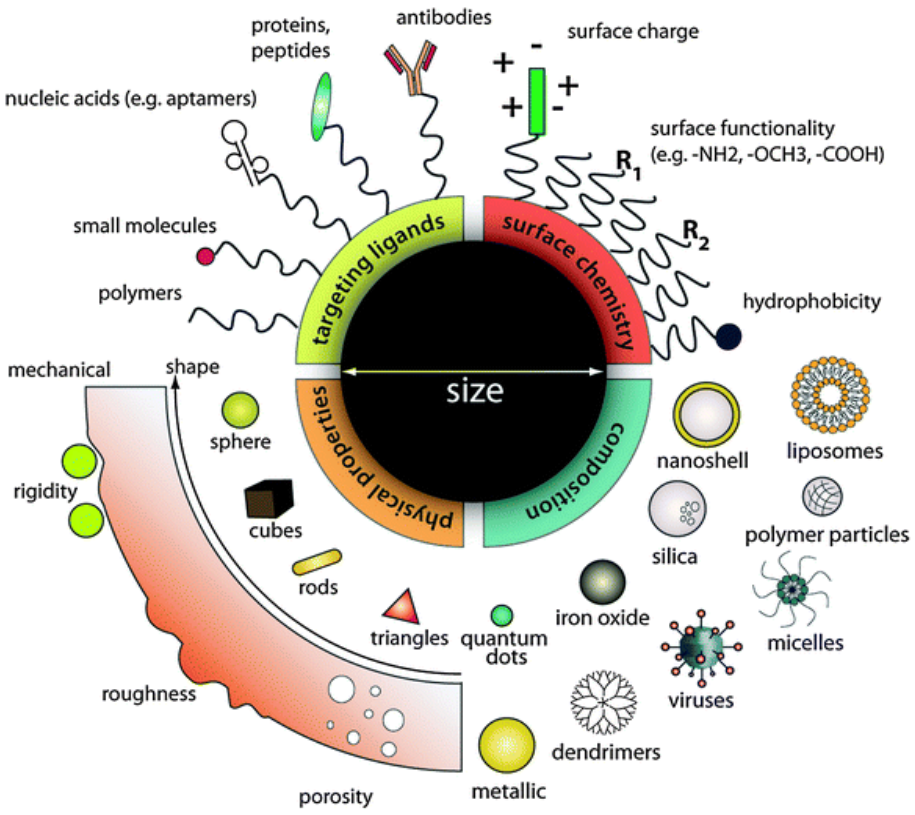

Figure 2.12 Schematic of how properties and characters of nanoparticles can be manipulated while designing nanoparticles for biomedicine applications (Chou et al., 2011).

Responsive hydrogels that respond to changes in their surrounding environment can be exploited in ways that fulfill biomedical purposes. As described earlier, these external changes can be temperature, pH, light, ionic strength and, more specific to the biomedical field, changes in blood glucose level. pH can be named as one of the most important property of the body because it can be manipulated by the body to control nutrient transport and more importantly, because it changes during disease (Peppas et al., 2000). Temperature is another factor in the controlled and smart drug delivery, which is also slightly varied in different body compartments as well as in

diseased tissues. In this study the synthesized pH-responsive magnetite nanogels are developed and characterized to broaden the application of smart polymeric system in the promising area of nanomedicine and, ultimately leads to better healthcare for patients (Peppas et al., 2000).

Since the use of plastics first became widespread in the middle of 20th century, polymers have become an emerging tool in biomedical science. Over 50 years ago the ability to synthesize polymers at small scales was developed and the early polymers synthesized in nanoscales were referred to as lattices or colloids (Peppas et al., 2000). Because of their very small size, existence as multi-components in nature, and the exclusive drug-polymer interaction, polymeric drug carriers have generated increasing interests in the field of medicine (Nahar et al., 2006).To better understand the advantages of responsive hydrogel systems over other synthetic polymer carriers, an overview of other systems is given below (Singh and Lillard, 2009).

2.4.1 Dendrimers

Dendrimers are an extreme state of branched polymers, which are also known as arborols or cascade molecules. Depending on whether synthesis starts at the core, or from the exterior, dendrimers are formed either by divergent (Liu et al., 2007a) or convergent synthesis (Lee et al., 2006). Dendrimers are synthesized with well-defined chemical composition, and possess a 3D spherical morphology and tailored surface multi-valency. The number of branch generations determines the size, valence, and other properties of the dendrimers. Molecular weight for dendrimers can vary from 500 Da to 500 kDa (Duncan and Izzo, 2005). The multivalency property of dendrimers provides a conjugational site for functional groups, drugs, and ligands (Samad et al., 2009).

Although a wide selection of dendrimers and dendrimers-based compounds have been studied, such as dendritic hybrids, dendronized polymers, core-shell morphologies, dendrigrafts, cascade-release dendrimers, cyclodextrin-dendrimer conjugates, and self-assembling dendrisomes, only approximately 25% of all the research has been devoted to biological applications (Duncan and Izzo, 2005). Most of the studies work on new synthetic chemistry of dendrimers. Currently, dendrimers are studied for a variety of biomedical applications, including cancer targeting, gene delivery, radiotherapy, transdermal and ocular drug delivery and imaging contrast agents (Samad et al., 2009).

2.4.2 Self –Assembled Systems

Self-assembled systems can be classified into liposome, micelles and polymersomes, which consist of amphiphilic block copolymers. Supramolecular forces cause the free energy of mixing between water and an amphiphilic polymer chain to decrease; as a result, the self-assembled systems are formed (Rhee and Mansour, 2011).

Liposomes consist of synthetic or natural amphipathic compounds that are self-assembled into synthetic lipid bilayer vesicles. They are known as the most clinically successful approaches to drug delivery. They mostly consist of phospholipids or glycolipids, which are both double chain amphiphiles; therefore, due to the biomimetic resemblance to natural lipid bilayer of cell membrane, they are able to penetrate and enter the cytoplasm, releasing the drug, and ultimately targeting the tumor or cancerous cell. Like cell membrane, liposomes are also stabilized with high amounts of cholesterol (Silverthorn, 2010). Liposomes can carry both hydrophobic and hydrophilic drugs. The former are either encapsulated within the aqueous region of the core or between the lipid layers, the latter is dissolved directly into the lipid bilayer. The most successful

liposome is a drug formulation known as Doxil®, which is currently approved for clinical use in AIDS-related Kaposi's sarcoma. It is a doxorubicin encapsulated in PEGylated liposomes (Gabizon, 2001). Although lisosomes are most stable in an aqueous environment, they are also fairly stable in suspension. Thus, freeze drying and freeze/thaw cycles can cause cell lysis and drug loss (Rhee and Mansour, 2011). In addition, changing the pH and temperature has a significant effect on their property (Sułkowski et al., 2006).

Aqueous micelles are composed of a large amount of surfactant, which makes them a two-phase system, where the surfactant hydrophobic tail organized inward and the hydrophilic head ordered outward. Micelles are known for their ability to transport hydrophobic drugs that are encapsulated within their hydrophobic core (Torchilin, 2007). Critical micellar concentration (CMC) is defined as value in where the surfactants spontaneously forming micelles in water above this value. The risk involved using micelles as a drug carrier is the dilution of micelles to below their CMC during administration. This risk factor has recently been solved by synthesizing a highly stable surfactant with CMC below 10^{-6} M (Kabanov et al., 2002). Although the surfactant in the micelle structure increases their stability, it can further be enhanced by cross-linking the core. Miyata et al. (Miyata, Kanjiro 2005) cross-linked the core of PEGylated polyplex micelles with a disulfide bond to increase their stability during freeze drying. The majority of micelles are spherical in shape, but the shape and size of micelles can change according to the sizes of hydrophobic and hydrophilic blocks. Shapes such as rods, lamellae or others can be synthesized by increasing the hydrophobic blocks. The conventional spherical micelles can have diameter from 10-80 nm. Discher et al. (Torchilin, 2007) synthesized filomicelles characterized as highly stable and cylindrically shaped diblock amphipathic micelle. The anticancer drug known as paclitaxel was encapsulated within the hydrophobic core of these

micelles and transported to the tumors site. They concluded that by manipulating the length and the shape of these PEGylated filomicelles, the circulation time in the blood was increased by up to one week.

Polymersomes, also identified as mesoscopic synthetic polymer vesicles, self-assembled into the core-shell structure, in which the core is aqueous and the shell is diblock amphiphilic copolymers that formed bilayer structure. Although they are very similar to liposomes, they possess a 'hyperthick' hydrophobic block, because of the much larger hydrophobic polymer chains in their structure than their liposomes counterparts. This 'hyperthick' membrane makes polymersomes less permeable and also gives them extra thickness compare to the natural lipid bilayers. Polymersomes have shown great potential as targeting agent in vivo (Discher et al., 2007; Pang et al., 2008). Since they are only quasi-stable, (similar to other self-assembled systems), Discher et al. (Discher, B. M. 2002) synthesized polymersomes into polymer nanoshells by free radical polymerization in order to introduce stability to the system.

2.4.3 Nanoparticles

Synthetic nanoparticles are normally glassy, hydrophobic and amorphous in nature, or they could be highly crosslinked, stiff structured with integrity that cannot be obtained from dendrimers or self-assembled systems. Amorphous polymer nanoparticles acquire a broader size range compared to (1) dendrimers that can only form vessels when they approach the de Gennes dense packing point (Svenson and Tomalia, 2005), or (2) self-assembled systems that are size restricted due to the stability and conformation of the lipid bilayer. Nanoparticles can be synthesized with controllable morphology, from 1 nm to hundred of micron in diameter through emulsion or micro-fabrication process. With these techniques, different morphologies can be fabricated, such

as polygonal structure (Glangchai et al., 2008), cones, bars and arrows (Euliss et al., 2006). Because for biodegradable nanoparticles, the control over degradation kinetics is more convenient, this system has been more developed for drug delivery applications. By reducing the particle size and increasing the hydrophobicity, the uptake of nanoparticles via the M-cells and payer's patches will be raised significantly (Sahoo et al., 1998).

2.4.4 Metallic Nanoparticles

Metallic nanoparticles such as gold, silver, iron, cobalt, nickel, platinum, and other metal composite nanoparticles are among the most investigated materials in the field of biomedicine. Significant development in this area is attributed to iron oxide, gold and composite metal nanoparticles (Chiappini et al., 2010). Because of the accelerated detection (e.g. via electron microscopy, and Localized Surface Plasmon Resonance (LSPR)), availability, and also photothermal properties, gold and silver nanoparticles have been widely investigated (Chiappini et al., 2010). On the other hand, iron oxide nanoparticles' unique magnetic property allows for easy detection by magnetic resonance contrast, and cell separation. Iron oxide nanoparticles offer more attractive property than other metallic nanoparticles. Many research groups have studied magnetic nanoparticles for application in gene and drug delivery, *in vivo* MRI enhancement, and cell labeling and detection (Chou et al., 2011; Lee et al., 2010).

Furthermore, metallic nanoparticles are usually more stable in comparison to other polymeric and biological nanoparticles; metallic nanoparticles can be exploited for different applications due to the diversity and unique properties of metals. However, the toxicity of many metallic nanoparticles raises some concerns regarding their degradation and long term fate *in vivo* (Chou et al., 2011; Lee et al., 2010).

2.4.5 Nanogels

As previously mentioned, hydrogels are a hydrophilic, cross-linked polymer network that can absorb large amounts of water, and based on their size they can be classified as microgels or nanogels. They were one the earliest synthetic polymers that were used in the field of biomaterial. The hydrogel structure, mechanical properties and hydration imitate the human tissue. Because of their biocompatibility, flexibility, high water content, hydrophilicity, versatility, and controllable character. They are among the most successful polymeric systems in biomedicine (Kabanov and Vinogradov, 2009; Kopeček, 2007; Oh et al., 2009; Petros and DeSimone, 2010; Sasaki and Akiyoshi, 2010).

Table 2.1 Summary of some of the nanogels advantages for drug delivery systems.

Nanogels Properties	Advantages
Small size	Increase drug up take
Large surface area	Maximize drug loading
Stimuli responsive	Improve drug release
Cross-linked structure	Enhance internal network
Porous structure	Facilitate drug loading and release
Polymeric network	Protect loaded drug
High water content and hydrophilicity	Facilitate delivery within the body

Table 2.1 summarized some of the advantages of using nanogels for drug delivery systems. Nanogels not only can increase the circulation time of the drug in the blood stream, but also they are capable of actively or passively deliver the drug to the specific tumor sites in the body (Hamidi et al., 2008). Nano size hydrogels have recently found great popularity in the field of biomedicine as they are composed of internally cross-linked, hydrophilic polymer chains with

large free volume, which provide a suitable matrix for drug encapsulation. Crosslinking not only contributes to stability of the hydrogels, compared to other nanostructure systems, but it also gives them a highly porous structure that allows drugs to load into the hydrogel matrix and then successively released from the matrix (Hoare and Kohane, 2008). Although hydrogels are analogous to dendrimers, the difference is that hydrogels can be produced over a wider range of sizes. Functional groups are able to incorporate into the hydrogel polymeric backbone, crosslinks, pendant group, or on the surface. In addition, controlled and targeted drug delivery is improved in hydrogels because therapeutic agents can be entrapped in or conjugated to the polymer network. There are several of methods for synthesizing hydrogels with controllable size and morphology, such as emulsion polymerization, dispersion/precipitation polymerization, and micro/nano fabrication (Oh et al., 2008a). Using hydrophilic monomer for hydrogel synthesis prevents phase separation during the reaction and also using organic solvents, it offers a more compatible environment for biological macromolecules. Cross-link junctions can be obtained either during the course of polymerization, or after the polymerization finished by means of chemical and physical techniques (Hoare and Kohane, 2008;Peppas et al., 2000).

Moreover, hydrogels are able to act as drug conjugates with size manipulation, which make them capable of prolonged circulation of drugs. Because of the high free volume of cross-linked hydrogels, they can encapsulate more drugs in their interior matrix compared to uncross-linked chains. By binding ligand molecules onto the three dimensional surface of hydrogels during polymerization, their surface is decorated with high affinity receptors that resemble the surface receptors of antibodies and cell (Bergmann and Peppas, 2008; Ye et al., 2001).

Using amphiphilic macromolecules in the formation of hydrogels leads to formation of hydrophobicity domains, which have application in the delivery of small hydrophobic drugs. For instance, Missirlis et al. (Missirlis et al., 2005) through inverse-emulsion photo-polymerization synthesized amphiphilic Pluronic nanoparticles, which can be used in the delivery of hydrophobic drugs.

2.4.6 pH-Responsive Nanogels

As mentioned earlier, responsive hydrogels are capable of undergoing considerable changes in shape and volume in response to environmental stimuli, such as pH, temperature, light, ionic strength, or glucose concentrations (Hendrickson et al., 2010b; Oishi and Nagasaki, 2010). pH-responsive hydrogels have attracted specific attention over other polymeric drugs carrier because of the pH variation in different part of the body.

Addition of ionizable functional groups onto the hydrogels network can contribute to the responsive behavior of intelligent hydrogels. The shift from collapse to swollen state occurs when the functional groups are ionized. Buffering capacity of functional groups determines the pH at which the transition occurs. pH-responsive hydrogels can be synthesized from various types of functional groups which can be either acidic or basic. By adding acidic functional group such as carboxylate groups, the hydrogels will swell above the pKa of the acidic moiety; in addition, by incorporating basic functional groups such as a primary, secondary or tertiary amine groups the swelling of hydrogel occurs below their pK_a values. For example, in the hydrogel network of MAA-DEA in which the methacrylic acid functional group works as an acidic moiety and 2-(diethylamino) ethyl methacrylate functional group acts as a basic functionality, causes the hydrogels to swell at both high and low pH environment. As a result, when this hydrogel travels

through the body compartments with pH above 6 and 7, such as small intestine, the acidic functional groups become ionized and subsequently the hydrogel swells and release the incorporated molecules. On the other hand, when this hydrogel passes through the low pH environment, such as stomach with pH ranges between 2 and 4, the hydrogel will also swell because its amine groups become protonated.

2.4.7 Temperature-Responsive Nanogels

Temperature-responsive nanogels in comparison to other responsive system have been extensively investigated. Hydrophilic nanogels are capable of absorbing large amounts of water without changing their structure. However, thermo-responsive nanogels possess some hydrophobic functional groups such as methyl, ethyl or propyl in their structure, which induce a transition temperature at which a discontinuous volume changes occur; in other words, by increasing the temperature the volume of nanogels increase or decrease (Lapointe and Martel, 2009a).

The most common and popular temperature-responsive microgels are those composed of N-isopropylacrylamide (NIPAM), and many research groups have examined the synthesis, characterization, and applications of PNIPAM systems (Brugger et al., 2010; Hendrickson et al., 2010a; Regmi et al., 2010). In 1968 Heskins and Guillet (Heskins and Guillet, 1968) were the first group to determine the lower critical solution temperature (LCST) of PNIPAM in aqueous solution. The linear PNIPAM reversibly changes its conformation from soluble, hydrophilic random coil to an insoluble, hydrophobic globule by increasing the temperature above 32^{o}C. This phase transition is due to the adjustable hydrophilic-hydrophobic balance within the NIPAM monomer unit. Below the LCST, the isopropyl groups disrupt the water structure, and

water cages are formed around these mildly hydrophobic moieties. By increasing the temperature above the LCST, the water cages are disrupted exposing the isopropyl groups that associate due to hydrophobic interactions (entropic part of Gibbs free energy) (Hendrickson et al., 2010a). When cross-linked microgels are synthesized using NIPAM, as a result of thermo-sensitivity of the monomer units, the microgels undergo a volume phase transition temperature (VPTT) near the LCST of PNIPAM. Analogous to LCST, by increasing the temperature above VPTT, the microgels shift from hydrophilic and swollen state to relatively hydrophobic and deswollen state (Hoare and Pelton, 2008).

Poly (2-dimethylamino) ethyl methacrylate (PDMAEMA) exhibits excellent pH-responsive character, however, it is also known for its temperature responsive behaviour. Depending on pH, molecular weight and salt concentration, it possesses a LCST ranging from 32 to 53 ^{o}C (Zhou et al., 2008). Zhou et al. (Zhou et al., 2008) synthesized organic-inorganic hybrid nanoparticle SiO_2-g-PDMAEMA via atom transfer radical polymerization (ATRP). They observed that by increasing the temperature from 20 to 50 ^{o}C the hydrodynamic radius increased from 150 to 1000 nm at pH= 0 and from 500 to 1600 nm at pH= 11; which proves the presence of the temperature-responsive behaviour.

2.4.8 Biomolecule-Responsive Nanogels

Nanogels are presently under intensive studies as a matrix for the controlled release of the encapsulated bioactive molecule, in particular pharmaceutical proteins (Tirelli, 2006). Biomolecule-responsive microgels such as glucose-responsive microgels and protein-responsive microgels that undergo swelling changes in response to specific biomolecules have become

significantly important because of their potential applications in the development of biomaterials and drug delivery systems (Hoare and Pelton, 2008; Lapeyre et al., 2008; Tirelli, 2006).

2.5 Drug Delivery Specifications

The first and vital consideration in developing a new biomaterial system is that the proposed system should not be harmful to the human body either locally or systematically (Farokhzad and Langer, 2006). In other word, the system should be biocompatible; it possesses quality of not having toxic or injurious effect on biological systems. Most of the design and development of drug delivery systems depend upon human biology. The most common and critical characteristics of drug delivery systems are: (Farokhzad and Langer, 2006):

- Targeting
- Stimuli responsiveness
- Size
- Prolong circulation
- Biodegradation
- Reporting and imaging

All these characters are reviewed below.

2.5.1 Targeting

Most of the therapeutic agents used for the treatment of serious diseases especially cancer possess very severe side effects such as hair loss, congestive heart failure, sore mouth and throat, bladder or kidney tract infection, changes in taste or smell, etc. Most of the current therapeutic drugs not only kill the tumor cells but also damage normal cells. An ultimate goal of smart drug

delivery is selectivity and specificity, and targeting can be achieved by functionalizing microgels with receptor-specific ligands (Das et al., 2006). The basic principle of this process is that these biofunctionalized microgels target diseased tissues outside the blood vessels, and while passing through the blood vessels they are taken up by intracellular compartment of targeted cells.

2.5.2 Stimuli-Responsive Behavior

Stimuli-responsive therapeutic agents are those that dynamically respond to environmental changes such as temperature, pH, ionic strength, photons, magnetic field or other phenomena. Diseases interfere with the biological and physicochemical equilibrium of human body, which eventually leads to environmental changes.

2.5.3 Size

The recent growth of nanomedicine is due to the fact that it is on the same length scale as many cellular processes. The size of the drug carrier not only determines the path of drug uptake to the targeted tissues but also specifies the course of delivery. In most cases, nanogels are subjected to intravenous administration. Upon this process the body tends to naturally eliminate administrated nanogels from circulation via different approaches, depending on the hydrodynamic sizes of the nanogels (Deka et al., 2010). For example, particles larger than 4μm will be captured in the lungs, since the smallest capillaries in body are 4μm. Mononuclear phagocytes system (MPS) usually eliminates particles smaller than 4μm. Through histological investigation, particles with a size of 100 nm were able to diffuse through the submucosal layers; whereas, particles with size ranging from 500 nm to 10 μm were concentrated within the epithelial tissue lining (Arifin et al., 2006).

Size is a crucial parameter that needs to be taken into account while designing the nanogels. Nanogels developed for *in vivo* drug delivery should possess size smaller than 200 nm because nanogels larger than 200 nm will be sequestered by reticulo-endothelial system right after intravenous injection. Nanogels smaller than 200 nm remain colloidally stable upon injection and will be in circulation for a sufficient amount of time until they approach the tumor sites (Deka et al., 2010).

2.5.4 Extended Circulating Time

For sustained drug release or constant targeting of a specific tissue, prolong circulation of the therapeutic agent is required. A number of researches have illustrated that hydrophilic, uncharged surface; with hydrogen bond donor groups without any ligand is the most effective synthetic surface to increase the circulation (Chonn et al., 1991). Poly (ethylene glycol) (PEG) chains are one of the most common surface grafting agents that can augment the circulation when attached to the surface of the particles. (Bradley et al., 1998)

2.5.5 Biodegradation

Biodegradation is a crucial character in developing smart drug delivery system that leads to the degradation of the drug carrier after the administration of the drug. By ensuring that the drug carriers do not remain in the body for an extended period, potential side effects of the drugs can be minimized. Balogh et al. (Balogh et al., 2007) illustrated that the elimination of drug carrier can be achieved by controlling the size and charge of the drug carrier. They observed that over 4 days about 50% of positively charged, 5 nm Au-dendrimers nanocomposites were excreted form mice after intravenous injection. For the negatively charged or neutral particles of similar size or

larger, this value was larger. Polymeric systems are very promising candidate in the area of nanomedicine due to their degradation ability.

2.5.6 Imaging

In the field of biomedical engineering, imaging is an important tool for determining the targeting, degradation and biodistribution of the drug carrier. To achieve this goal, the drug carrier should be designed with functional groups or moieties that can easily be traced by conventional medical imaging devices. These instruments include magnetic resonance imaging (MRI), computed tomography (CT), positron emission tomography (PET) and ultra sound imaging. For example, supermagnetic iron nanogels to be developed in this thesis research can be targeted by MRI. Fluorophores and quantum dots are other techniques that can be used as targeted agents (Liu et al., 2007b).

2.6 Magnetic Nanoparticles

Core metallic particles that possess magnetic properties and have a size ranging from 1 to 100 nm are known as magnetic nanoparticles (MNP). They are commonly classified into core materials and coatings (Sun et al., 2008). The most widely used magnetic nanoparticles are iron-based core materials; the core can comprise of magnetite (Fe_3O_4) and/or maghemite (γFe_2O_3). The general formula for magnetite is AB_2O_4, where A stands for *Fe (II)* and B stands for *Fe (III)* (Thorek et al., 2006). The ferromagnetic cubic shape of *Fe (III)* oxide is defined as maghemite. The difference between magnetite and maghemite originates from differences in vacancies on the cation sub-lattice. In particular, in magnetite, half of Fe^{3+} takes up the interstitial tetrahedral (Td) sites, while the other half comprises of the octahedral (Oh) sites along with Fe^{2+}. However, in

maghemite, half of Fe^{3+} occupies the octahedral sites along with cationic vacancies instead of Fe^{2+}. The structure of both magnetite and maghemite is illustrated below; (Laurent et al., 2008).

$$Fe_3O_4: [Fe^{3+}]_{Td}\,[Fe^{3+}Fe^{+2}]_{Oh}\,O_4$$

$$\gamma Fe_2O_3: 0.75\,[Fe^{3+}]_{Td}\,[Fe^{+3}{}_{5/3}V_{1/3}]_{Oh}\,O_4$$

Magnetite will be slowly oxidized to maghemite in an ambient environment; however, in biomedical applications these two materials do not differentiate, and are generally defined as iron oxide (Laurent et al., 2008). Other types of metal ferrites, such as $MnFe_2O_4$, $CoFe_2O_4$, and $NiFe_2O_4$, can be produced by replacing Fe^{2+} with the equivalent metal cations. Magnetic nanoparticles are formed either via synthetic approaches or through commercial production (Sun et al., 2008).

Moreover, reactive functional groups such as amino or carboxyl groups must be present on the surface of nanoparticles to graft molecules onto the nanoparticles and form coatings around the nanoparticles. These chemical groups act as attachments between the core of the nanoparticle and coating like peptide or antibody. Not only do these coatings improve water solubility of the iron oxide nanoparticles, but they also impart stability to the iron oxide nanoparticles. Coatings can form multilayered nanoparticles in which each layer possesses its functional groups; therefore, coatings play an important role in intracellular targeting and internalization of nanoparticles (Sun et al., 2008; Zou et al., 2010).

Super-paramagnetic is the magnetic property in which nanoparticles are only magnetized in the presence of an applied magnetic field; in the other words, by removing the magnetic field the super-paramagnetic particles such as Fe_2O_3 and Fe_3O_4 do not retain its magnetism (Park et al., 2007). In addition, the iron oxide core of the super-paramagnetic nanoparticles is less than 30 nm

in diameter. Moreover, super-paramagnetism reduces aggregation and physical interactions of nanoparticles, and also increases the relaxation rates and magnetic resonance contrast of the nanoparticles (Liu et al., 2010; Sun et al., 2008). Thus, super-paramagnetic particles have a promising application in biomedicine; because, in the dispersion they are not only subject to strong magnetic interaction but are also readily stabilized in the physiological condition (Xu and Sun, 2007). Furthermore, conversion of Fe_3O_4 to γFe_2O_3 occurs by oxidation of super-paramagnetic iron oxide through oxidizing agents or oxygen exposure. During this process, as Fe^{2+} in the magnetite lattice oxidizes the color of the solution switches from black-brown to red-brown (Thorek et al., 2006).

Iron oxide magnetic nanoparticles have demonstrated great biocompatibility and a minimum toxicity compared to other metallic nanoparticles. There are three different processes involved in the cellular targeting of the magnetic nanoparticles (Sun et al., 2008; Thorek et al., 2006):

- Passive targeting: the cellular uptake of nanoparticles occuring through a natural mechanism, such as endocytosis,
- Physical targeting: the physical manipulation of magnetic nanoparticles by means of magnetic field, which facilitate the localization of the magnetic nanoparticles within desired area,
- Bimolecular targeting: the biomolecules, such as antibody and peptide are conjugated within the magnetic nanoparticles, in order to facilitate their binding to the specific receptor on the cell or tissue.

Detection of the magnetic nanoparticle is a significant challenge. Due to the very small size of the individual particles and non-fluorescent properties of the magnetic nanoparticles, they cannot

be detected by standard analysis methods, such as light microscopy. Indeed, ultra sensitive microscopy approaches and elemental analysis techniques such as electron microscopy and magnetic resonance imaging (MRI) are used to study magnetic nanoparticles (Sun et al., 2008).

In summary, as schematically illustrated in Figure 2.13 magnetic nanoparticles demonstrate notable properties including, super-paramagnetism, biocompatibility, feasible synthesize, post-synthesize coating and modification, and also a high ratio of surface area to volume, which make them an attractive system in the field of biomedicine (Dias et al., 2011).

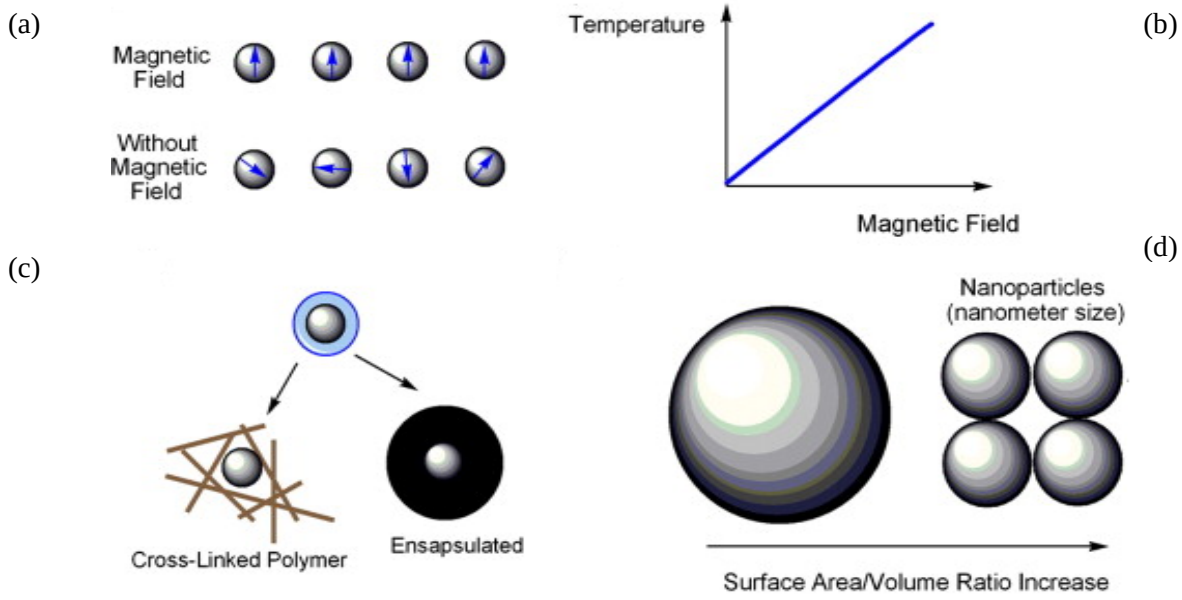

Figure 2.13 Schematic of the significant properties of iron oxide magnetic nanoparticles for biomedical applications (a) super-paramagnetism, (b) heat effects as an influence of external magnetic field, (c) versatility in the synthesis and coating process, and (d) nano-size particle possesses high surface to volume ratio (Dias et al., 2011).

2.6.1 Synthesis of Magnetic Nanoparticles

Control of the nanoparticles size and homogenous dispersion of magnetic nanoparticles are two main challenges regarding the synthesizing magnetic nanoparticles. Various approaches have been investigated to synthesize magnetic nanoparticles, such as co-precipitation, reverse micelles, and thermal decomposition. Subsequently, after the magnetic nanoparticles are formed, three purification techniques can be employed in order to remove excess and unreacted materials: centrifugation, gel-exclusion chromatography (GEC), and magnetic sorting (Laurent et al., 2008) . Herein lie some of the techniques to synthesize magnetic nanoparticles.

The co-precipitation of ferrous or ferric salts with strong bases like ammonium hydroxide (NH_4OH) or sodium hydroxide ($NaOH$) in aqueous medium is the most common and efficient approach to synthesize magnetic nanoparticles, due to the fact that magnetic nanoparticles are easily and economically synthesized in large scale by this process (Gupta and Gupta, 2005). Through this process different types of polymers like poly(ethylene glycol), dextran, and dendrimer can be coated onto the nanoparticles surface to prevent aggregation and provide steric repulsion that creates a balance between attraction and repulsive forces between the nanoparticles (Veiseh et al., 2010). The advantages of the co-precipitation technique is that it is easy and can be readily produced in large quantities; despite the fact that the control over nanoparticle shape, size, crystallinity, and magnetization is restricted to the kinetic control of the growth of the nanoparticles (Hyeon, 2003;Thorek et al., 2006). The following is the general chemical reaction for co-precipitation of the magnetic nanoparticles (Laurent et al., 2008):

$$2\,Fe^{+3} + M^{+2} + 8\,OH^{-} \rightleftharpoons MFe_2O_4 + 4\,H_2O$$

In this reaction M can be a divalent ion such as iron (Fe^{+2}), nickel (Ni^{+2}), or cobalt (Co^{+2}). Because of thermodynamic consideration, complete precipitation of this reaction is occurring in oxygen free environment between pH=8 and pH=14, and the stoichiometric ratio $Fe^{+3:}\ Fe^{+2}$ is 2:1 (Laurent et al., 2008). Stabilization then occurs by introducing strong bases, either nitric acid (HNO_3) which gives a positive charge on the surface of the particle due to adsorption of H_3O^+ ions or tetramethylammonium hydroxide ($(CH_3)_4NH_4OH$), which provides a negative charge to the nanoparticles as a result of OH^- ions adsorption (Laurent et al., 2008). This method produces polydisperse size distribution magnetic nanoparticles and also causes cluster-like aggregations (Thorek et al., 2006). Figure 2.14 demonstrates the general form of this method. Commonly, this process consists of the following two steps (Laurent et al., 2008):

1. Once the concentration of the species has reached the critical super-saturation stage, a short burst nucleation happened,
2. By diffusing the solutes to the surface of the nanoparticles, nuclei encounter a slow growth.

Moreover, in order to form monodisperse magnetic nanoparticles, nucleation should be prevented during the growth process; in other words, these two steps should be separated from each other (Laurent et al., 2008).

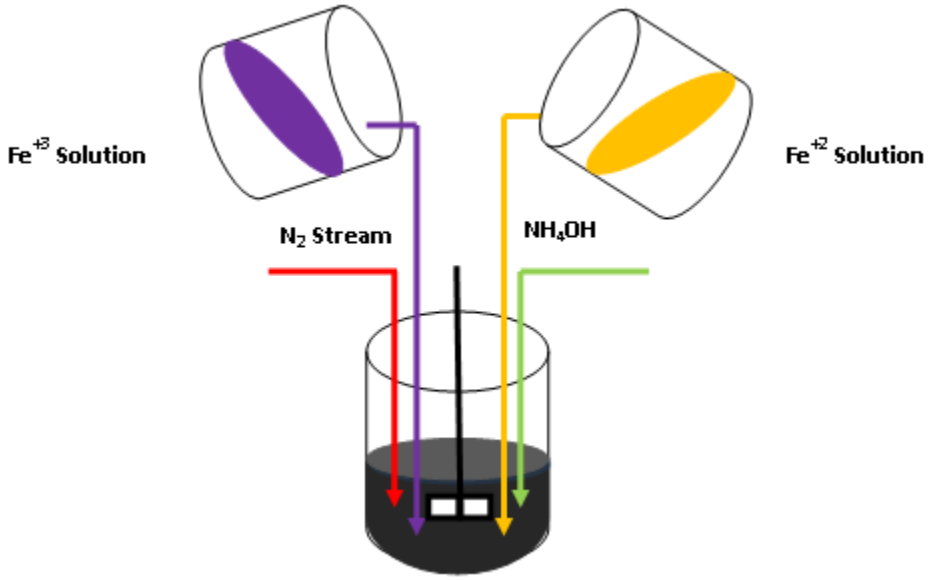

Figure 2.14 Schematic of co-precipitation approach for synthesizing magnetic nanoparticles.

Another method to synthesize magnetic nanoparticles involves reverse micelles, which provide templates to control the nanoparticle size and dispersity. This system involves the dispersion of surfactant molecules in a continuous hydrocarbon phase along with the formation of well-defined nanodroplets in the aqueous phase (Laurent et al., 2008). Calero et al. (Calero-DdelC and Rinaldi, 2007) synthesized cobalt ferrite nanoparticles with size range of 3-10 nm via reverse micelles. In order to form reverse micelles they used sodium bis (2-ethylhexyl) sulfosuccinate (AOT) as a surfactant, which separated bulk organic medium from the aqueous phase. They mixed a solution of reverse micelles consisting the aqueous ammonium hydroxide (NH_4OH) as the precipitating agent with another solution of reverse micelles consisting of a mixture of metal salts (Fe^{+3}:$2Co^{+2}$) at room temperature. Even though the particle has a narrow size distribution due to the grafting of AOT surfactant onto the surface of the nanoparticles, they were highly hydrophobic.

Another technique to synthesize magnetic nanoparticles is known as thermo decomposition. Park et al. (Park et al., 2004) were able to successfully synthesize monodisperse magnetic nanoparticles in large-scale via thermo-decomposition of a metal-oleate precursor, which formed from the reaction between sodium-oleate and metal chloride, in high boiling point 1-octadecene as a solvent. The general overview of this process is represented in Figure 2.15. In this process by controlling the temperature of the solvent, the nucleation and growth phases were separated. They observed at nucleation phase that one oleate ligand was dissociated from the metal-precursor at temperature from 200 to 240 ^{o}C, and the remaining two oleate ligands were dissociated at 300 ^{o}C, where the main magnetic nanoparticles growth occurred. Then, the magnetic nanoparticles were allowed to grow further at the boiling point of the solvent (1-octadecene), which was 320 ^{o}C, for 30 minutes. Subsequently, the formed magnetic nanoparticles were washed with ethanol and precipitated by centrifugation at room temperature. Although the reaction stoichiometry represents only about 2 grams corresponding to magnetite, they were able to synthesize 40 g of monodisperse magnetic nanoparticles through this process (Park et al., 2004). Figure 2.16 shows the TEM images of synthesized MNP via thermal-decomposition.

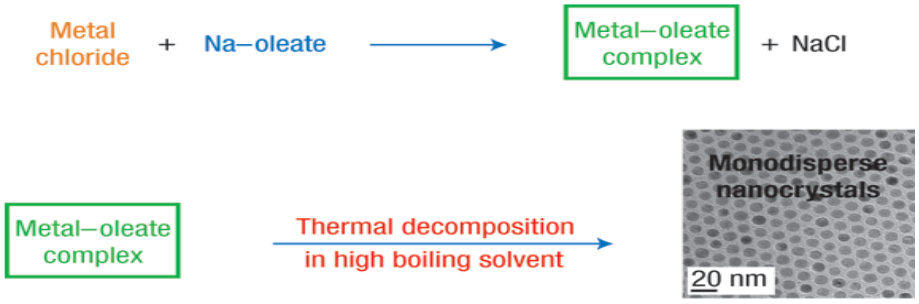

Figure 2.15 Schematic of thermal-decomposition method to synthesize magnetic nanoparticles from metal-oleate complex in a high boiling solvent (Park et al., 2004).

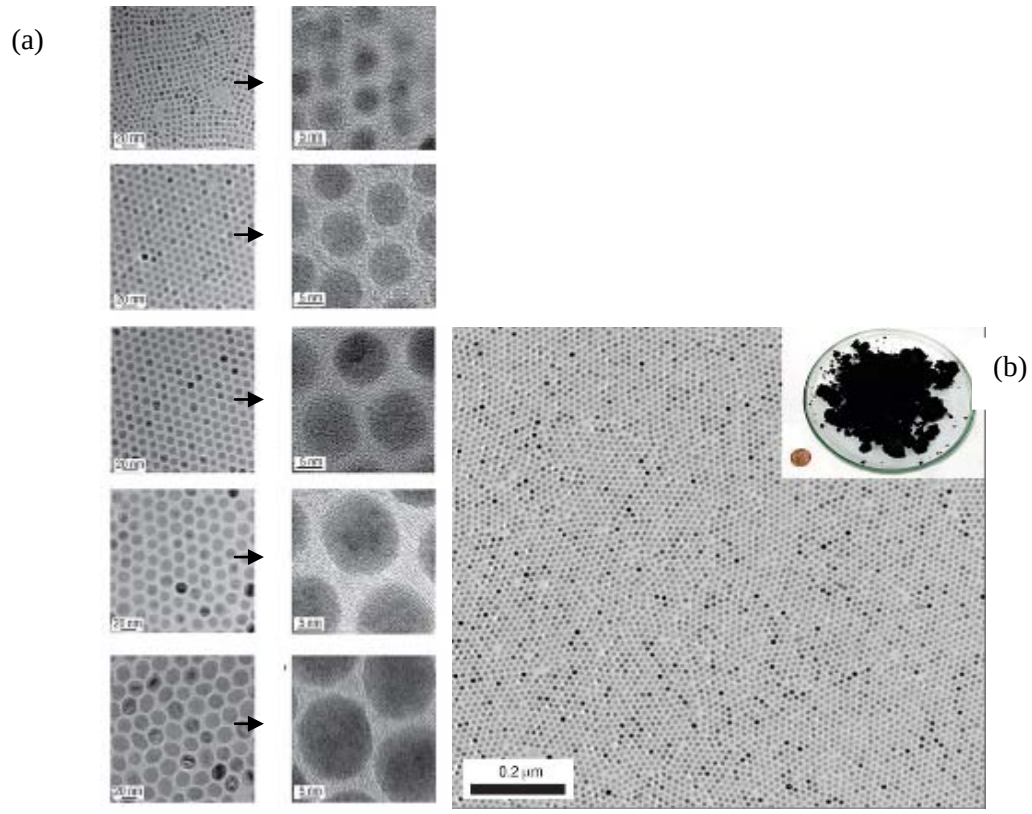

Figure 2.16 TEM images of synthesized MNP via thermal-decomposition where (a) highly monodisperse synthesized MNP (b) 40 g (high-scale) formed monodisperse MNP in comparison to 1 cent (Park et al., 2004).

2.6.2 Surface Modification of Magnetic Nanoparticles

Magnetic nanoparticles possess high surface-to-volume ratio, which promote their aggregation due to the high surface energy, strong magnetic dipole-dipole interactions, and hydrophobic surface. Therefore, their stabilization through coating with specific molecules and polymers is crucial in order to form colloidally stable magnetic nanoparticles; otherwise, for *in vivo* applications, aggregation of magnetic nanoparticles can lead to rapid recognition by macrophage cells and undesired elimination from circulation through RES, and ultimately cause unexpected responses (Dias et al., 2011; Laurent et al., 2008). Similar to microgels, stabilization of magnetic

nanoparticles can also be achieved through electrostatic and/or steric repulsion. The former can be predicted by understanding the diffusion potential through the Debye-Huckel length and the zeta potential (ζ) which both depend on the pH and ionic strength; however, the latter is quite difficult to follow and quantify particularly for magnetic nanoparticles, but it is well-explained for polymers (Dias et al., 2011; Laurent et al., 2008).

In iron oxide magnetic nanoparticles, the surface iron atoms act as Lewis acids and coordinate with molecules that donate one-pair electrons (Dias et al., 2011). In aqueous solutions, the iron atoms coordinate with water, which impart hydroxyl groups on the iron oxide surface. These hydroxyl groups are amphoteric and are able to react with both acids and bases (Gamarra et al., 2010). The surface of the magnetite can be either positive or negative, based on the pH of the solution. Around the isoelectric point (IEP) of magnetic nanoparticles, which is observed at pH 6.8, the surface charge density$\Sigma()$ is too small and the particles are not stable in water and simultaneously form aggregation. Therefore, in order to obtain stable magnetic nanoparticles both electrostatic and steric stabilization should be introduced (Gamarra et al., 2010). In particular, because of coordination and dissociation with water, the surface of iron oxide nanoparticles is dominated by hydroxyl groups in aqueous medium, which leads to protonation and formation of positive surface charges (Fe^{+3}-OH^{+}_{2}) below the isoelectric point and deprotonation and the formation of negative surface charges (Fe^{+3}-O^{-}) above the isoelectric point (Dias et al., 2011).

Coating of the magnetic nanoparticles not only forms a steric barrier to prevent nanoparticles agglomeration, but also provides a platform for surface modification and biocompatibility of the magnetic nanoparticles. Therefore, stabilization leads to the more stable nanoparticles in water

and biological medium preventing adsorption of plasma protein, which may induce the formation of larger nanoparticles and faster recognition by macrophage cells, and subsequent clearance of the nanoparitcles by immune system (RES) (Laurent et al., 2008). As shown in Figure 2.17, a variety of monomers, polymers, and inorganic materials can be applied for this purpose.

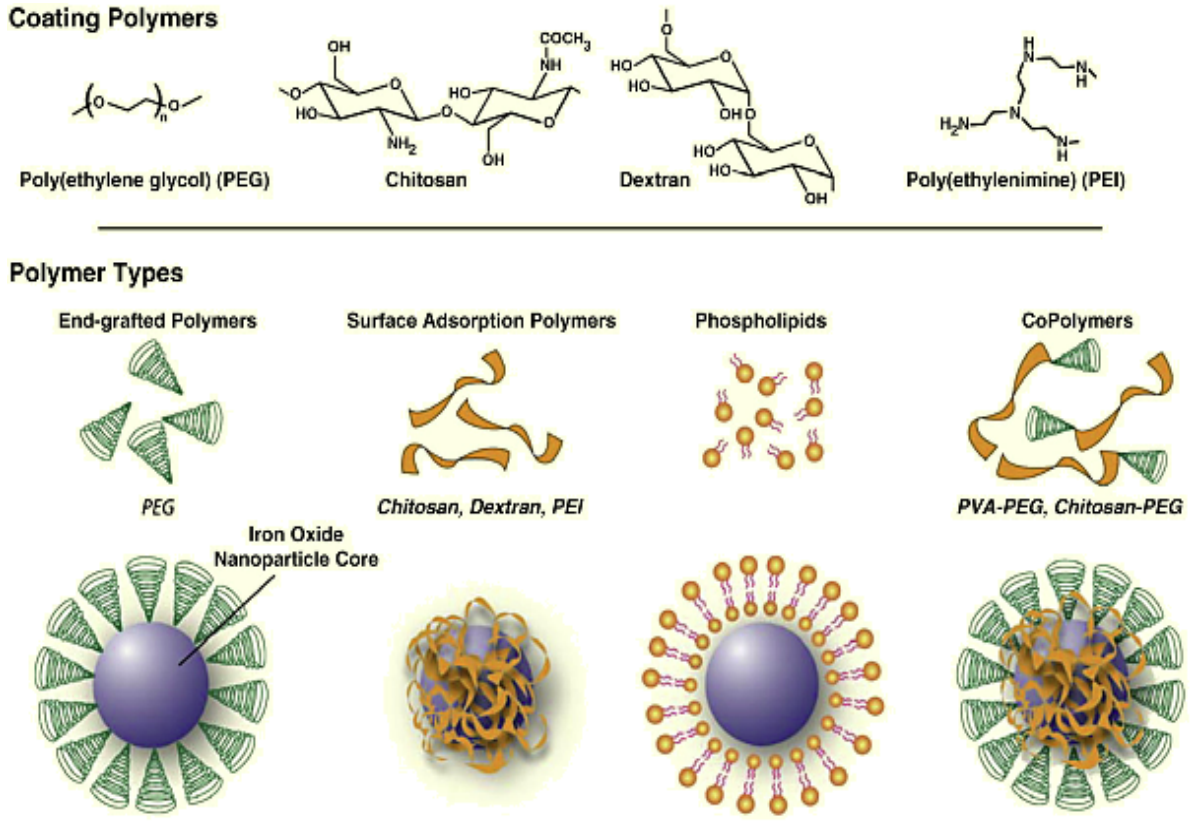

Figure 2.17 Schematic of different kind of polymers exploited as a coating onto the MNP (Veiseh et al., 2010).

The coating of magnetic nanoparticles can be obtained either as a one-step synthesis or as a post-synthetic process, or it can be done by in-situ or encapsulation (Dias et al., 2011). In other words, the result of coating through encapsulation, end-grafting, hydrophobic interaction, or hyper-branching produces more homogeneous hydrophilic nanoparticles. In addition, properties of the coating, along with the size of nanoparticles, determine the body site, which would take up the

nanoparticles. For example, the hydrophilic surface could extend the circulation of the magnetic nanoparticles in blood and enhance the diffusion into marrow and lymph. Conversely, the hydrophobic surface could increase the chance of magnetic nanoparticles being trapped in the liver or spleen (Hong et al., 2008).

Poly (ethylene-glycol) methacryalte (PEGMA) and poly (elthylene-glycol) (PEG), which contain one hydroxyl functional group on every monomer unit, are among the most common materials used for surface modification, especially for biomedical applications due to their biocompatibility, water solubility, and hydrophilicity (Laurent et al., 2008). Grafting on the surface of magnetic nanoparticles is efficient in decreasing non-specific adsorption (such as protein plasma), increasing the stability of magnetic nanoparticles in plasma, and enhancing the circulation time (Xie et al., 2007) .

One of the efforts in this area was conducted by Xie et al. (Xie et al., 2007) through PEGylating of iron oxide nanoparticles with a homemade ligand dopamine-PEG-*COOH*. They were able to synthesize monodisperse 9 nm Fe_3O_4 magnetic nanoparticles in organic medium, and then grafted with dopamine (DPA), which is known for its high affinity to Fe_3O_4 surface linked to one of the carboxylic groups in the PEG by EDC/NHS reaction. As a result of this linkage, the dopamine-PEG-*COOH* ligand was covalently grafted onto the magnetic nanoparticles to replace the original organic coating, oleate and oleyamine, of the magnetic nanoparticles, and rendered the hydrophobic magnetic nanoparticles water-soluble. Figure 2.18 illustrates schematically the synthesize process.

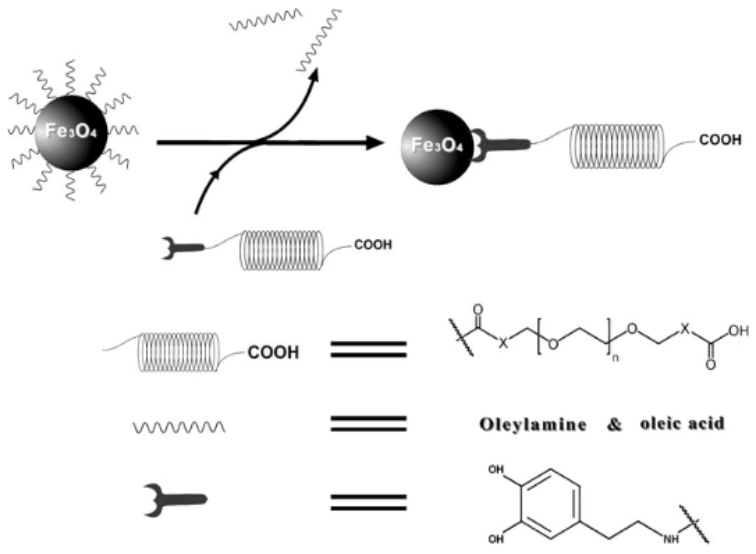

Figure 2.18 Schematic of surface modification of Fe_3O_4 magnetic nanoparticles by DPA-PEG-*COOH* (Xie et al., 2007).

The stability of the formed coated magnetic nanoparticles was investigated in phosphate buffered saline (PBA) plus 10% (FBS). As shown in Figure 2.19 only about a ~10-20 nm increment in size was observed in comparison to nanoparticles in water. This could be due to the interaction with the FBS in the incubation environment. This small change in size was also improved by introducing higher molecular weight PEG, which caused the formation of the dense coating and subsequent reduction of these interactions; thus all four types of PEG demonstrated great stability without significant size enhancement (Xie et al., 2007). They observed through DLS that by changing the length or molecular weight of the PEG, the overall size of the magnetic nanoparticles could be manipulated, while the core size remained the same. For instance, as shown in Figure 2.20, by coating the magnetic nanoparticles with PEG 3000, the overall diameter increased from 9 to 50 nm, whereas by applying PEG 20000, the overall diameter of the magnetic nanoparticles increased to 90 nm in aqueous solution. Along with DLS, the zeta potential measurement also confirmed the formation of PEG coating around the magnetic

nanoparticles, due to the negatively charged surface. Furthermore, this group confirmed that all four types of synthesized PEGylated magnetic nanoparticles, PEG 600, 3000, 6000, and 20000, showed a much lower uptake by macrophages cell in contrast to dextran coated magnetic nanoparticles (Xie et al., 2007).

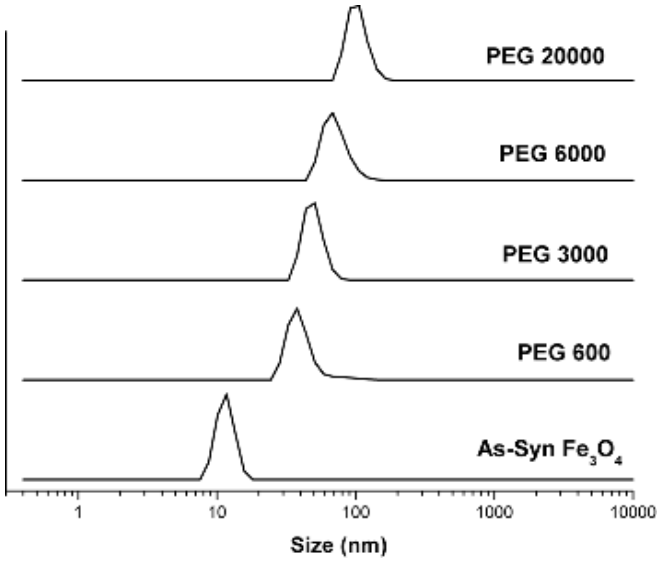

Figure 2.19 DLS curves, showing the hydrodynamic sizes of the different PEG molecular weight utilized to coat the Fe_3O_4 magnetic nanoparticles (Xie et al., 2007).

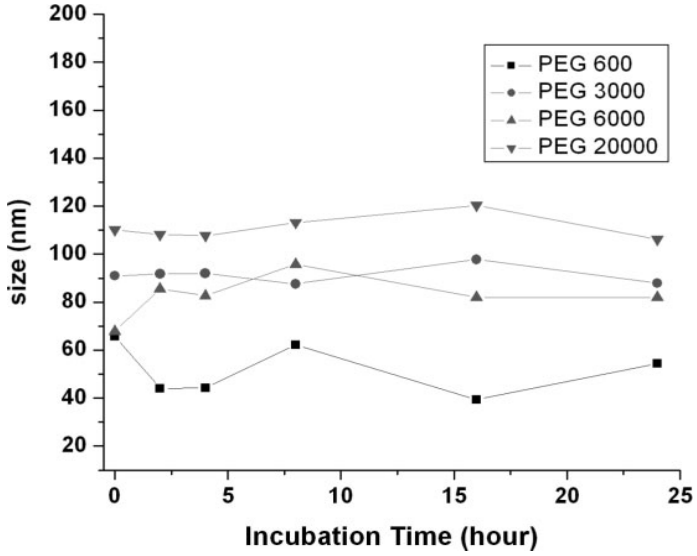

Figure 2.20 Hydrodynamic radius (size) of the Fe_3O_4 magnetic nanoparticles coated with different M_w of PEG and incubated in PBS and 10% FBS for 24 hours at 37 ^oC (Xie et al., 2007).

Barrera et al. (Barrera et al., 2009) synthesized monodisperse colloidally stable magnetic nanoparticles through the thermal decomposition technique, in which an iron precursor decomposed in a high boiling point solvent in the presence of a non-polar surfactant; afterward, the hydrophobic magnetic nanoparticle was covalently coated with PEG-silane. PEG-silane was prepared in a two steps process. In the first step, terminal hydroxyl groups in mPEG were converted to carboxylic acids (mPEG-*COOH*) with the help of strong oxidizing agent; in the next step, through amidation reaction at 180 ^oC under N_2 atmosphere, carboxyl groups (mPEG-*COOH*) reacted with $–NH_2$ in 3-aminopropyl triethoxysilane (APS). The stability of PEG-coated magnetic nanoparticles was confirmed by zeta potential and dynamic light scattering measurements. From the DLS measurement, an increase of 35 nm in size was observed. As shown in Figure 2.21a, the nanoparticles were stable in water for pH of 3-9, except at the isoelectric point around pH=7.5. These charges were correlated to ions absorbed on the PEG-silane layer surrounding the nanoparticles from the solution, because the PEG-silane segments

did not carry any ionizable groups. In addition, the particle stability was further confirmed by varying the ionic strengths, as seen in Figure 2.21c and Figure 2.21d, through varying *NaCl* concentrations from 0.038 M to 0.32 M at pH=7. Although the hydrodynamic radius fluctuated between 35 and 45 nm, no significant aggregation was reported, as revealed by DLS measurements shown in Figure 2.21b (Barrera et al., 2009).

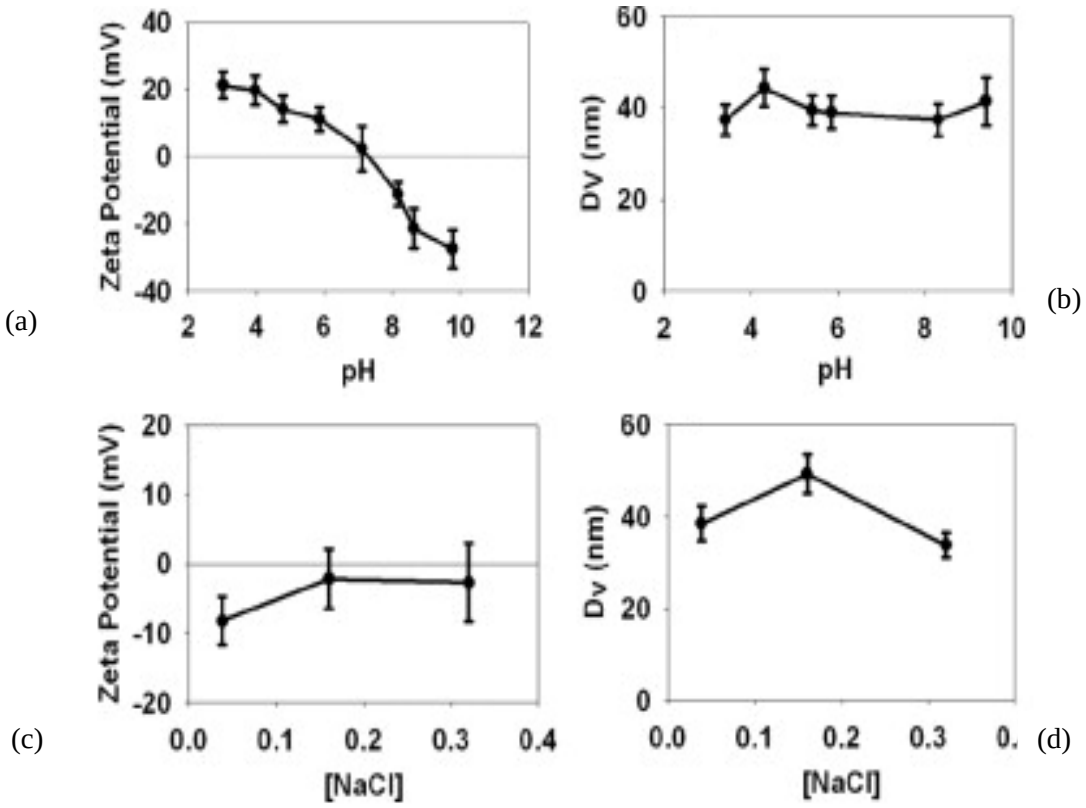

Figure 2.21 (a) zeta potential measurement as a function of pH, (b) hydrodynamic radii as function of pH, (c) zeta potential measurement as a function of *NaCl* concentration, and (d) hydrodynamic radius as a function of *NaCl* concentration (Barrera et al., 2009).

The only drawback regarding coating of magnetic nanoparticles is due to the fact that coatings provide strong thermodynamic stabilization that causes the steric repulsion of magnetic nanoparticles from each other; thus, the particles do not agglomerate and opportunity to capture

them is reduced. An efficient solution is to control the stability of the formed clusters, so that the clusters stay stable to further aggregations, while maintaining their ability to be captured for separation applications (Barrera et al., 2009).

Ditsch et al. (Ditsch et al., 2005) were able to synthesize clusters with controlled size and stability. They investigated the effects of (*I*) varying molecular weight of the coating polymers, and (*II*) addition of the second polymer on the stability and aggregation of magnetic nanoparticles. As shown in Figure 2.22, the magnetic nanoparticles were synthesized by co-precipitation of iron oxide salts in an aqueous solution; afterward, synthesized magnetic nanoparticles were coated in two steps with optimal molecular weight of random copolymer consisting of styrene sulfonic acid, acrylic acid, and vinyl sulfonic acid. In the first step, a limited amount of low molecular weight polymer was added, which caused the formation of clusters due to insufficient coating. In the second step, low molecular weight hydrophilic polymer was added to provide additional coating of the magnetic nanoparticles. In this step, the clusters were completely stabilized over a wide range of ionic strength and pH with no effect on the cluster size (Ditsch et al., 2005).

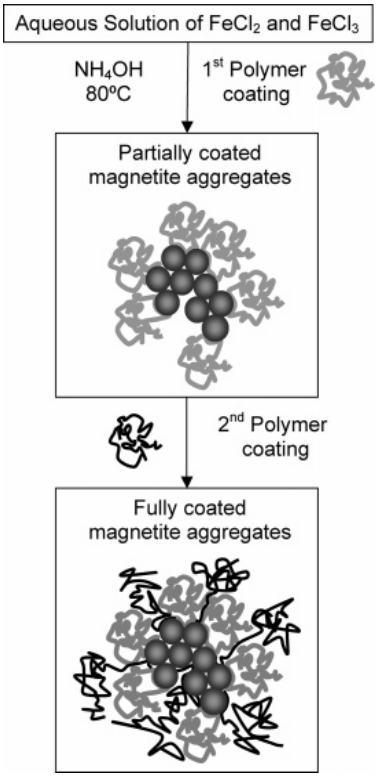

Figure 2.22 Schematic of the coating process of the synthesized magnetic nanoparticles (Ditsch et al., 2005).

They observed that by adding high molecular weight polymer in the first step produced smaller size clusters, due to the formation of thicker coating and steric stabilization. In contrast, by using low molecular weight polymer, larger size clusters formed. However, the largest size cluster produced in this step was not large enough to be captured with a high gradient magnetic separator (Ditsch et al., 2005). Therefore, they concluded that changing the molecular weight of a single coating is insufficient for forming stable clusters. In another set of experiments, they noticed that the instability and subsequent clustering was more susceptible by adding a limited amount of coated polymer or by reducing the density of attachment groups, because of the incomplete coating of the surface of the magnetic nanoparticles. They also realized that the size of the clusters coated with more hydrophobic coatings decreased more slowly as a result of the

added polymer, because of the larger polymer size and greater steric repulsion associated with the hydrophobic groups. Although this system was stable in water due to strong surface charges and interparticle electrostatic repulsion, however with a slight change in the ionic strength, instability occurred (Ditsch et al., 2005). Thus, as a final experiment, they examined the effect of adding a secondary polymer as a coating. The role of the secondary coating was to cover the vacant sites on the surface that were not sufficiently covered by the primary polymer coating.

In addition, by adding a low molecular weight secondary polymer, the cluster size remained constant, while, a higher molecular weight polymer formed a larger size cluster, due to bridging interactions (Ditsch et al., 2005). These effects were illsutrated in Figure 2.23. As illustrated in Figure 2.23a, before the addition of a second polymer, the particle size increased slowly; when the second polymer became larger that the first polymer (around X_w = 85) the particle size increased due to bridging. This also confirmed the incomplete coating. Figure 2.23b indicated that by adding large amounts of the first polymer the cluster size increased, but in lower values in comparison to adding less amount of the first polymer. It also indicates that the bare surface of the magnetic nanoparticles is still present and Figure 2.23c demonstrated the stability of the final particle as a result of adding the second polymer (Ditsch et al., 2005).

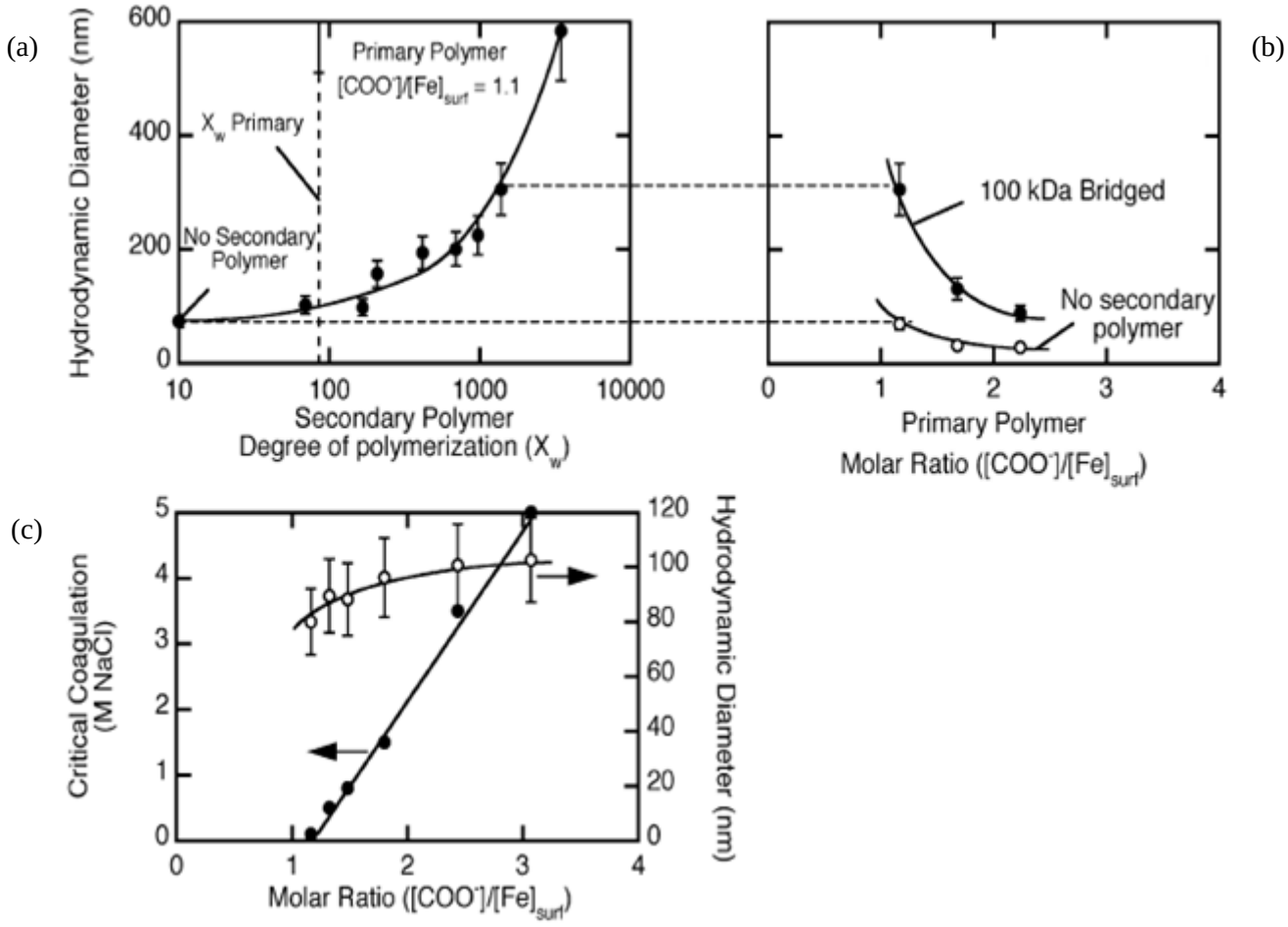

Figure 2.23 (a) the particle size as a function of secondary polymer (acrylic acid) size for clusters starting at 74 nm, (b) cluster size vs. different ratios of second polymer to surface iron, and (c) stability of the final particle as a result of adding the second polymer (Ditsch et al., 2005).

In another study, Sondjaja et al. (Sondjaja et al., 2009) prepared magnetic nanoparticles via co-precipitation technique and grafted the magnetic nanoparticles with double hydrophilic block copolymer (DHBC), poly (ethylene oxide)-block- poly (acrylic acid) (PEO-b-PAA). In this structure, one block enhanced the colloidal stability of nanoparticles, while the other block acted as polyelectrolyte and caused interaction with the precursor. Subsequently, the synthesized nanoparticles were then passed through a high-gradient magnetic separator. The PEO-b-PAA not

only controlled the particle growth, but also acted as stabilizer and clustering agent. They reported that clustering of magnetic nanoparticles, which formed larger aggregates of magnetic nanoparticles more than 100 nm in size, was required in order for magnetic nanoparticles to be permanently and effectively trapped in a magnetic separator; otherwise, the nanoparticles with size less than 50 nm could not be trapped and efficiently separated by the magnetic separator. By altering the iron loading-to-polymer ratio, they observed that inadequate amounts of polymer destabilized the nanoparticles resulting in clusters formation. This phenomenon occurred as a result of the van der Waals attraction between the regions of the nanoparticles that were not sufficiently coated with the polymer; thus, the nanoparticles aggregated at these uncoated regions. Figure 2.24 demonstrates that the cluster yield was inversely proportional to the ratio of grafting group (COO^-) to surface iron atoms ($Fe_{Surface}$). These plots illustrate that when a polymer was in excess ($R > 0.8$) there was less than 10% cluster yield and the magnetic nanoparticles size were around 126 nm. However, by decreasing the polymer amount ($R \leq 0.2$) the magnetic nanoparticles aggregated due to incomplete surface coverage, and yielded more than 87% clusters with a size of about 280 nm. This group was able to successfully obtained homogenous magnetic nanoparticles clusters, which were also colloidally stable for about 48 hours in aqueous solution (Sondjaja et al., 2009).

(a)

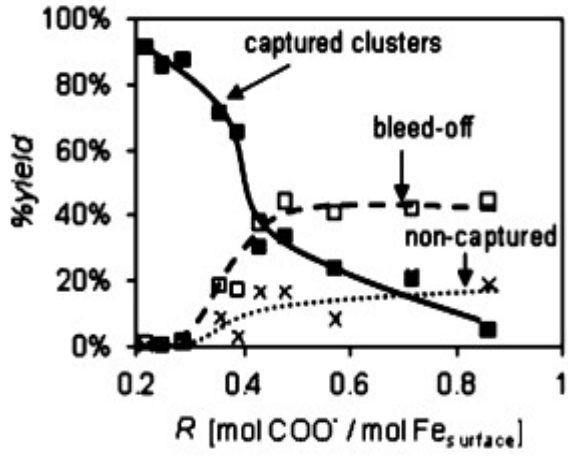

(b)

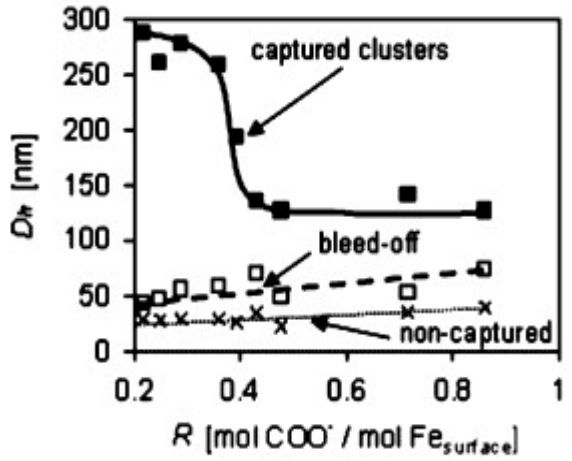

Figure 2.24 Graphs of (a) yield, and (b) hydrodynamic radius versus R for three different solutions: (■) permanently captured clusters solution, (□) bleed off solution, and (×) non-captured particles solution (Sondjaja et al., 2009).

Super-paramagnetic iron oxide nanoparticles coated with hydrophilic polysaccharide known as dextran, which act as contrast agents for MRI, have been approved for the Food and Drug Administration (FDA). Hong et al. (Hong et al., 2008) successfully synthesized dextran-coated Fe_3O_4 via a one-step conventional co-precipitation method with a novel modification using hydrazine hydrate as reducing agent and precipitator. This process is illustrated in Figure 2.25.

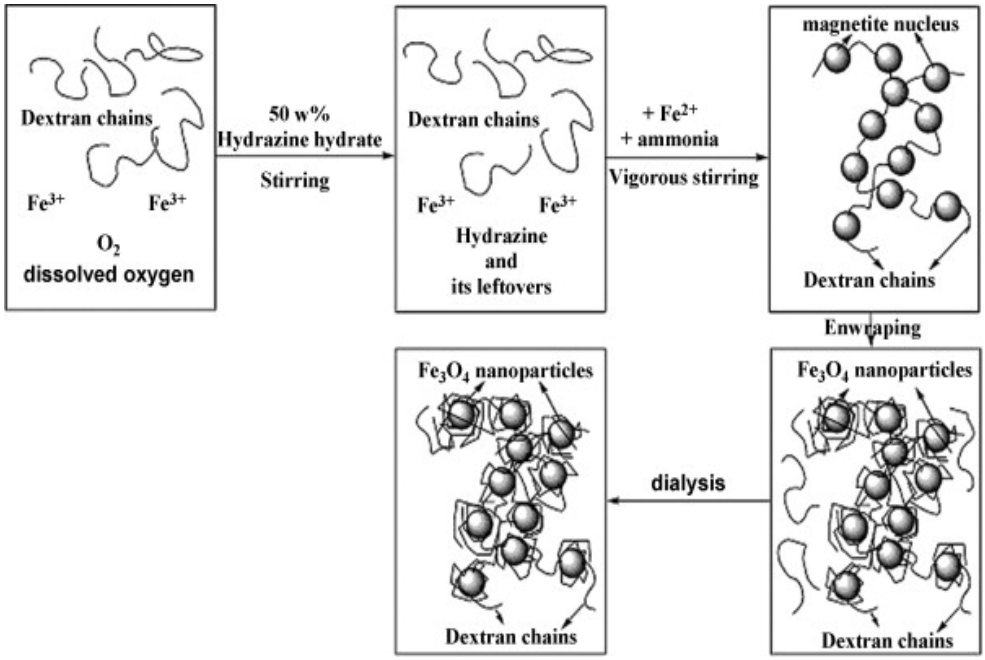

Figure 2.25 Schematic of the coating process of the Fe_3O_4 magnetic nanoparticles with dextran (Hong et al., 2008).

This group (Hong et al., 2008) investigated the particle size and coating efficiency of dextran on the synthesized magnetic nanoparticles. They observed that by increasing the weight ratio of dextran to magnetic nanoparticles to more than 2.5, the size and aggregation of magnetic nanoparticles decreased dramatically and the magnetic nanoparticles dispersion was enhanced due to the steric hindrance provided by dextran. By increasing the ratio to 7.5, as a result of adsorption of magnetic nanoparticles with entanglement of dextran chains aggregation was minimized. Although increasing the molecular weight of the dextran significantly increased the size of the magnetic nanoparticle, resulting in more dextran coming in contact with magnetic nanoparticles, only a minor impact on the coating efficiency was observed. Figure 2.26 shows that by coating the magnetic nanoparticles with dextran, the size was decreased and the colloidal stability was improved (Hong et al., 2008).

(a) 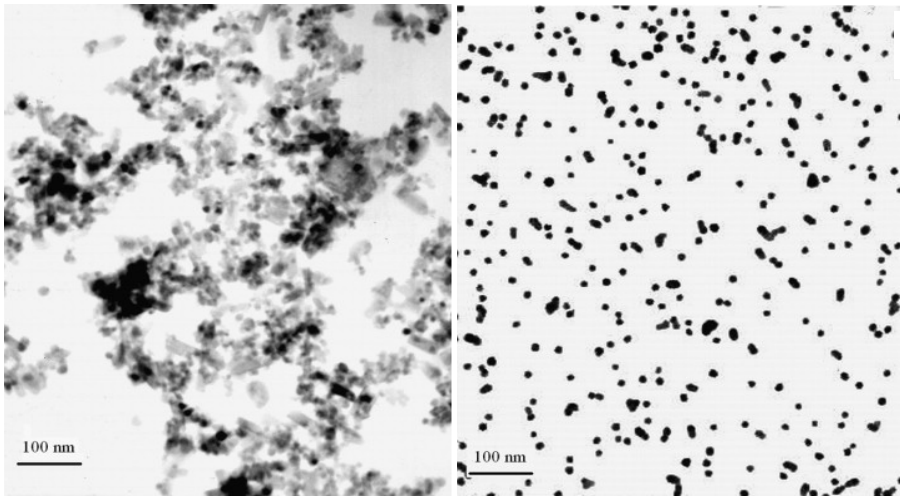

(b)

Figure 2.26 TEM images represent (a) bare magnetic nanoparticles, and (b) dextran-coated magnetic nanoparticles (Hong et al., 2008).

In another study of dextran coated magnetic nanoparticle, Gamarra et al. (Gamarra et al., 2010) observed that the so-called Endorem, which was the colloidal suspension of iron oxide nanoparticles coated with dextran, had a great potential for use as a contrast agent in MRI detection. They observed a transition temperature from Fe_3O_4 to the γFe_2O_4 phase by deferential scanning calorimetry (DSC). As shown in Figure 2.27, the DSC curve consisted of an endothermic and exothermic peak. The former at 166.6^{o}C represented the melting temperature of mannitol ($C_6H_{14}O_6$), which existed to increase the colloidal stability, the latter at 253.1 ^{o}C corresponded to the oxidation of Fe_3O_4 to γFe_2O_3, which was further confirmed by the reduction in O_2 concentration (Gamarra et al., 2010).

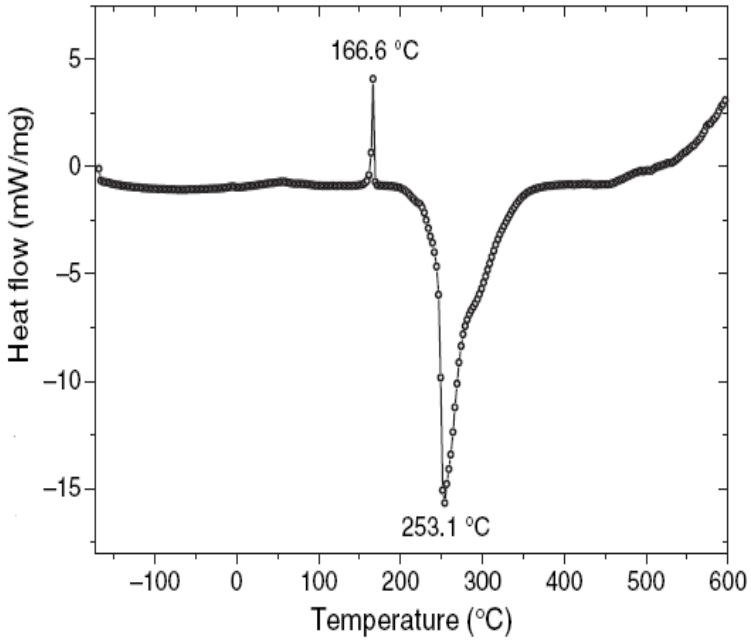

Figure 2.27 DSC graph of dextran-coated Fe_3O_4 magnetic nanoparticles (Gamarra et al., 2010).

Another polysaccharide that has been widely studied as a coating agent is chitosan. Its natural properties, such as biocompatibility, biodegradability along with antibacterial activity, and also its affinity for many biomacromolecules leading to bioadhesion makes this polysaccharide an interesting and promising system for further investigation (Lopez-Cruz et al., 2009). Lopez-Cruz et al. (Lopez-Cruz et al., 2009) successfully prepared Fe_3O_4 magnetic nanoparticles by thermal decomposition and functionalized them with carboxylic group. Later, further functionalization of magnetic nanoparticles occurred by coating them with both chitosan oligosaccharide and low molecular weight chitosan. They studied the effects of chitosan molecular weight on the morphology and colloidal stability of the nanoparticles. The coating process was done through covalent linkage, carbodiimide activation, between amine groups in chitosan and carboxyl groups on the magnetic nanoparticles using EDC and NHS, which is shown in Figure 2.28.

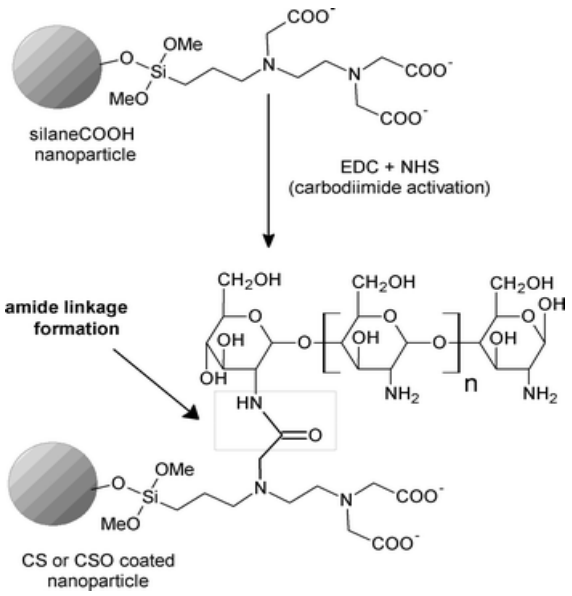

Figure 2.28 Schematic of coating process of the *Fe_3O_4-COOH* magnetic nanoparticles with chitosan oligosaccharide (Lopez-Cruz et al., 2009).

As can be seen in Figure 2.29, this research group (Lopez-Cruz et al., 2009) demonstrated that coating the magnetic nanoparticles with chitosan and chitosan oligosaccharide influenced the morphology of the primary magnetic nanoparticles. In the former, aggregated clusters were observed, while in the latter a single core was produced. They noticed that the size and size distribution of the magnetic nanoparticles did not change and remained at 11 nm in diameter with different coatings. In other words, using chitosan oligosaccharide as a coating resulted in magnetic nanoparticles as distinct entities, while using chitosan as a coating produced magnetic nanoparticles clusters. In this case, particles in each cluster possessed 11 nm mean diameter (Lopez-Cruz et al., 2009).

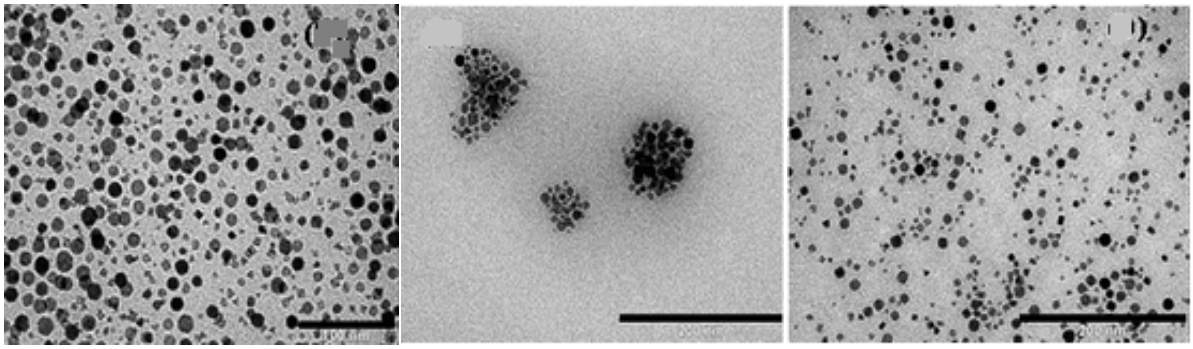

(a) (b) (c)

Figure 2.29 TEM images represent (a) *Fe_3O_4-COOH* magnetic nanoparticles, (b) chitosan-coated *Fe_3O_4* magnetic nanoparticles, and (c) chitosan oligosaccharide-coated *Fe_3O_4* magnetic nanoparticles (Lopez-Cruz et al., 2009).

Moreover, Lopez-Cruz et al. (Lopez-Cruz et al., 2009) observed a wide size distribution of the chitosan coated nanoparticles. A very low stability was observed at pH greater than 6, due to the deprotonation of amino groups of the chitosan segments, which also indicated that the stabilization in this system was facilitated by electrostatic repulsion. However, chitosan oligosaccharide coated nanoparticles had a narrow size distribution and were also colloidally stable at pH=6 or higher, which confirmed that its stability was a result of steric repulsion rather than electrostatic repulsion. In addition, Figure 2.30 illustrates the zeta potential of the three different systems as a function of pH. It showed that at low pH, coated magnetic nanoparticles were positively charged as a result of protonation of the amino groups, which further confirmed the presence of chitosan on the surface of the nanoparticles (Lopez-Cruz et al., 2009).

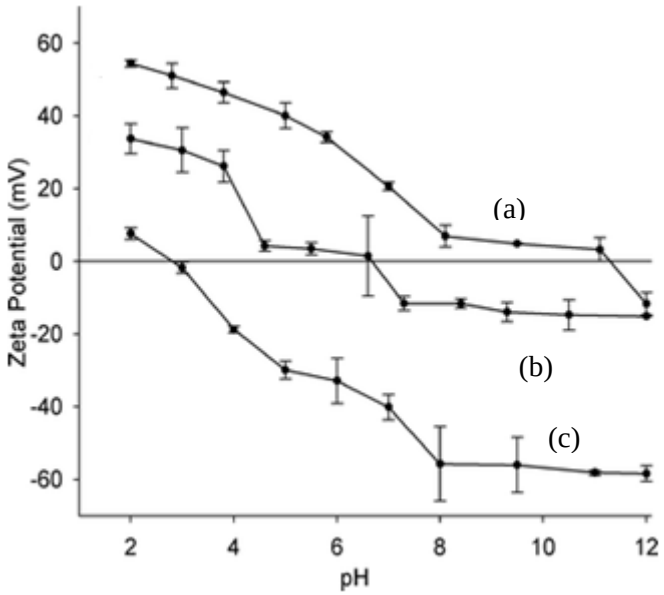

Figure 2.30 Zeta potential graph as a function of pH for (a) chitosan oligosaccharide-coated Fe_3O_4 magnetic nanoparticles, (b) chitosan-coated Fe_3O_4 magnetic nanoparticles, and (c) Fe_3O_4-*COOH* magnetic nanoparticles (Lopez-Cruz et al., 2009).

Another technique for coating magnetic nanoparticle is to use thick and dense inorganic materials such as silica. As a result of their rigid structure, inorganic materials are able to protect magnetic nanoparticles from interacting with each other and also with their environment. Yi et al. (Yi et al., 2006) synthesized iron oxide particles via thermal-decomposition and then used reverse microemulsion to form a silica coating on the nanoparticles. Following dispersion of polyoxyethlylene (5) nonylphenyl, which acted as a surfactant, in cyclohexane by sonication, reverse microemulsion was produced by the addition of iron oxide nanoparticles in cyclohexane and ammonium hydroxide. Afterwards, tetraethyl orthosilicate (TEOS) was added and the solution was agitated overnight. The TEOS was hydrolyzed and condensed during this process and ultimately formed silica coating on the nanoparticles. As can be seen from Figure 2.31, this

research group studied three different structures with different coating thickness, which was derived from this iron oxide coated silica template (Yi et al., 2006).

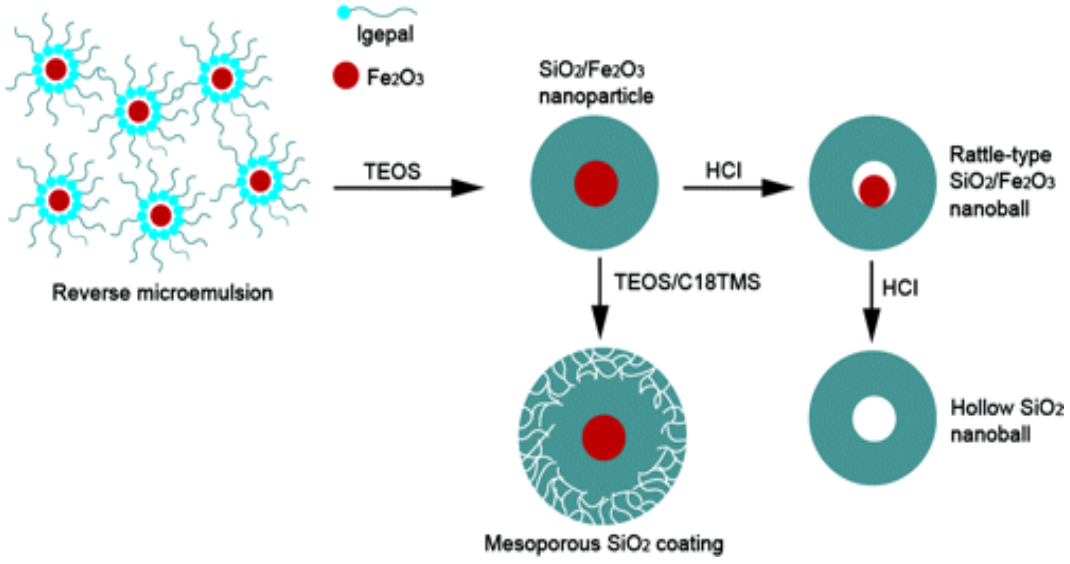

Figure 2.31 Schematic of the reverse microemulsion polymerization of silica coated iron oxide and the three other structures formed from the template (Yi et al., 2006).

In another study, a pH-responsive polymer was applied to coat magnetic nanoparticles. Zhou et al. (Zhou et al., 2009a) utilized the atom transfer radical polymerization (ATRP) technique to graft poly ((2-dimethylamino) ethyl methacrylate) (PDMAEMA) onto the surface of magnetic nanoparticles (*Fe_3O_4-Br*), which were synthesized through the co-precipitation process. The general procedure is shown in Figure 2.32. Due to the biocompatibility, hydrophilicity, and pH sensitivity of PDMAEMA, the reported hybrid nanoparticles with core-shell structure demonstrated great potential to load drugs into the polymer shell. In addition, this system was confirmed to be able to release the drugs in a steady and controllable manner by changing the pH (Zhou et al., 2009a). This research group observed more stable dispersion of magnetic hybrid nanoparticles in comparison to ungrafted magnetic nanoparticles. As illustrated in Figure 2.33, at

low pH value, the amine groups on the PDMAEMA segments were protonated; thus, the hydrodynamic radius was increased by decreasing pH. This phenomenon was attributed to the electrostatic repulsion, strong polymer-solvent interaction, and also geometrical restriction that resulted in polymer chains extension along the radial direction. On the other hand, at high pH value the PDMAEMA segments were deprotonated, the high grafting reduced the available space, and also polymer-polymer interactions were stronger than polymer-solvent interaction; thus polymer chains agglomerated and reduced the hydrodynamic radius (Zhou et al., 2009a; Zhou et al., 2009b).

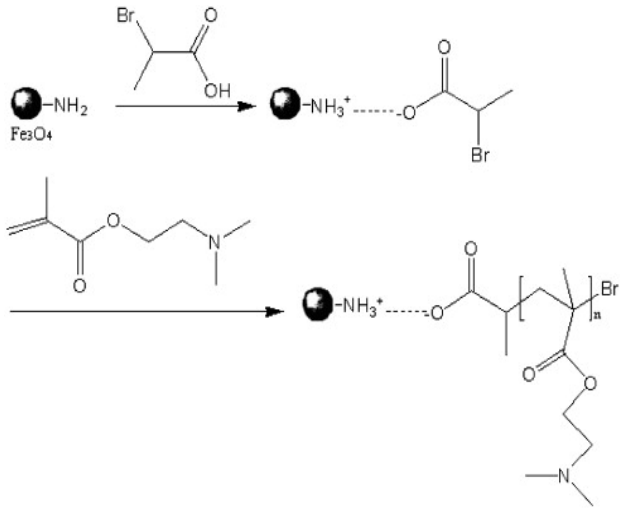

Figure 2.32 Schematic of the synthesizing of the magnetic nanoparticles grafted with PDMAEMA (Zhou et al., 2009a).

This research group incorporated the model drug, phenolphthalein, into the polymer shell, and subsequently studied the release of the drug. As can be seen in Figure 2.34, the release of the drug is significantly faster at pH=3 than pH=7, because of the protonation resulting in the expansion of the hybrid magnetic nanoparticles, where more drug molecules were able to diffuse from the magnetic hybrid nanoparticles (Zhou et al., 2009a; Zhou et al., 2009b).

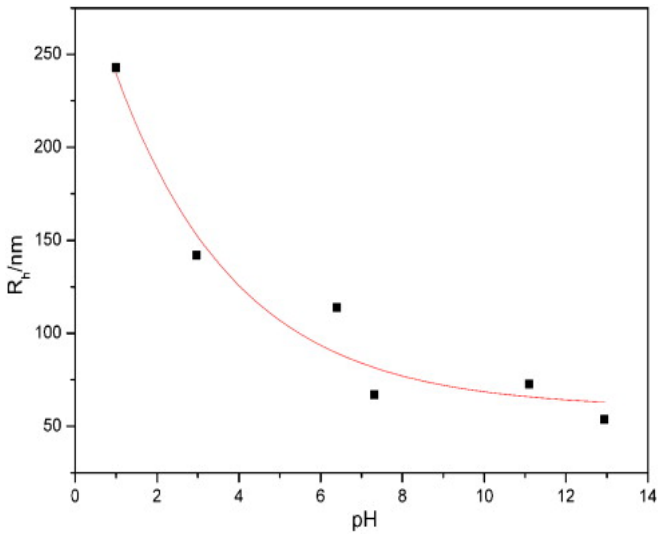

Figure 2.33 Hydrodynamic radius of Fe_3O_4 / PDMAEMA as a function of pH (Zhou et al., 2009a).

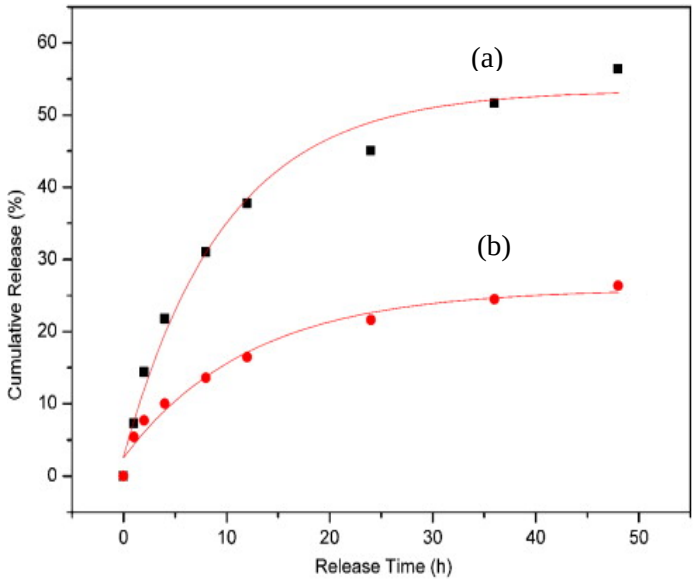

Figure 2.34 Release profile of phenolphthalein from the Fe_3O_4 / PDMAEMA at (a) pH=3, and (b) pH=7 (Zhou et al., 2009a).

2.7 Nanogels and Magnetic Nanoparticles

Because of the specific characteristics and properties of iron oxide magnetic nanoparticles conjugated within nanogels or microgels, and also their promising potential in the field of biomedicine, this system has attracted increasing attention in recent years. In the following section we will briefly describe some of the most recent studies in this field.

Deka et al. (Deka et al., 2010) developed a novel approach to incorporate both magnetic nanoparticles and oligonucleotide through the pH-responsive nanogels. They synthesized nanogels based on a copolymer of divinyl benzene (DVB) and vinyl pyridine (VP) via surfactant free emulsion polymerization. Then, the iron oxide nanoparticles (IONPs) were separately synthesized and wrapped into an amphiphilic polymer shell consisting of poly (maleic anhydride *alt*-1-tetradecene). Subsequently, these iron oxide nanoparticles were coated with diamino-PEG through EDC reaction in order to introduce better stability to the nanoparticles.

Afterward, the PEG-coated iron oxide nanoparticles and oligonucleotide were both simultaneously loaded within the nanogels by mixing a specific concentration of both solutions for 24 hours with nanogels solution at pH=3.5, where the nanogels were swollen. When the pH was increased to pH=7, the nanogels collapsed, and the excess amounts of both iron oxide nanoparticles and oligonucleotide not incorporated within the nanogels were removed by the electro-magnets (Deka et al., 2010). As described in Figure 2.35 they were able to successfully entrap iron oxide and oligonucleotide within the pH-responsive nanogels. In this study, iron oxide nanoparticles were not covalently attached to the nanogels network, and they escaped from the nanogels network once the nanogels swelled due to changes in the pH. As shown in Figure 2.36, both iron oxide nanoparticles and oligonucleotide were released from the nanogels by

switching the pH of the loaded nanogels solution from pH=7 to pH=3.5, where the nanogels were in swollen state (Deka et al., 2010).

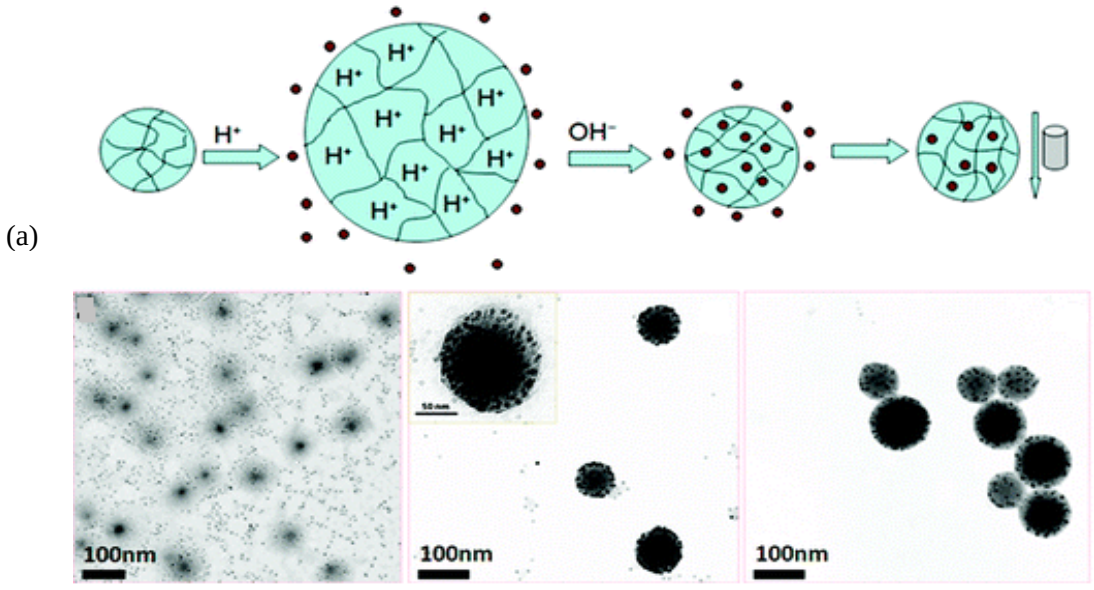

Figure 2.35 Schematic and TEM images of (a) general picture of loading of IONPs and oligonucleotide within nanogels at acidic pH where nanogels swell and then increased the pH so that nanogel deswell (b) IONPs and oligonucleotide in the nanogels solution (c) IONPs and oligonucleotide entrapped within nanogels at swelling state (d) removal of excess IONPs and oligonucleotide from the solution by magnet (Deka et al., 2010).

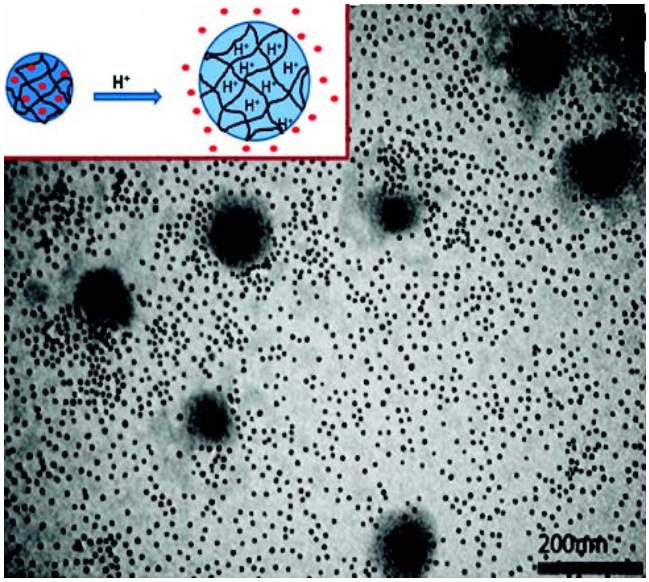

Figure 2.36 TEM image of the IONP and oligonucleotide release from the nanogels at pH=3.5, which induced swelling of the nanogels (Deka et al., 2010).

In another study utilizing microgels as a carrier for drug, Bhattacharya et al. (Bhattacharya et al., 2007) synthesized colloidally stable magnetic hybrid microgels, which are also sensitive to temperature and pH. These core-shell microgels consist of thermo-sensitive N-vinylcaprolactam (VCL)-rich shell, acetoacetoxyethyl methacrylate (AAEM)-rich core, and pH-responsive vinylimidazole (VIm) and were polymerized via batch copolymerization. Afterwards, up to 15 wt% ferric oxide was incorporated into the microgels by co-precipitation of aqueous solution of $FeCl_3$ and $FeCl_2$ with NH_4OH. From dynamic light scattering, they observed the reduction in microgel shell thickness and partial collapse of the microgel network, as a result of magnetic nanoparticles incorporation. Maximum swelling of microgels occured at pH=4, and was correlated to the complete ionization of VIm segments.

In addition, the volume phase transition temperature of microgels was observed at 28 ^{o}C, which was different from the LCST of linear PVCL at 32 ^{o}C, due to the presence of the pH-

responsive VIm segments. In other words, they confirmed that the VPTT can be shifted towards higher temperature by manipulating the amounts of VIm in the microgels or the pH of the system, and this effect is shown in Figure 2-37 (Bhattacharya et al., 2007).

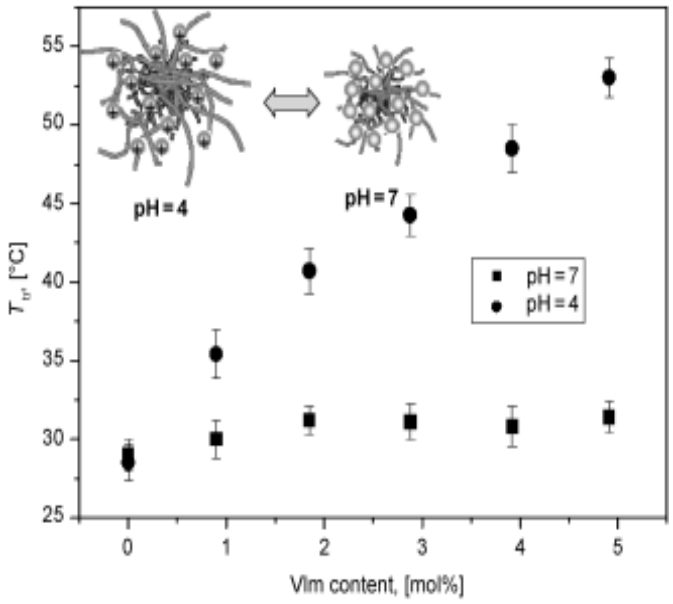

Figure 2.37 The effect of VIm content and pH on the volume phase-transition temperature of VCL-AAEM-Vim microgels (Bhattacharya et al., 2007).

They observed that low magnetic nanoparticles content was clearly noticeable inside the VCL-rich core of the microgels; however, when high magnetite content was used, the microgels partially deformed and aggregation of magnetic nanoparticles occurred at the microgels shell. These microgels remained colloidally stable and are pH-responsive inspite of the incorporation of large amounts of magnetic nanoparticles into them. Nevertheless, the degree of swelling and consequently the hydrodynamic radius shifted to lower values for the magnetic microgels in contrast to bare microgels as shown in Figure 2.38. This phenomenon can be attributed to the effective interaction between the microgels network and magnetic nanoparticles (Bhattacharya et al., 2007).

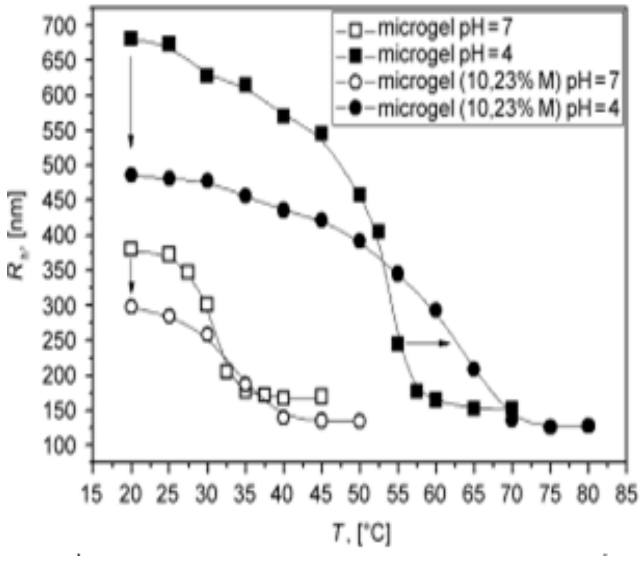

Figure 2.38 Hydrodynamic radius of the hybrid maicrogels, and bare microgels at pH=4 and pH=7 (Bhattacharya et al., 2007).

As a result of the incorporation of iron oxide mostly onto the shell of the microgels, the electorphoretic measurements of hybrid microgels represented in Figure 2.39 signify a strong positive charge at low pH. In addition, due to the presence of magnetic nanoparticles, the electrophoretic mobility was significantly higher in comparison to bare microgels. In a basic environment, the microgels shell partially collapsed due to the deionization of VIm segments, and also the negative charges of the magnetic nanoparticles were effectively shielded by the polymer coating. Therefore, at pH 7-10, hybrid microgels demonstrated the same trend as bare microgels, although they possessed strong negative charges (Bhattacharya et al., 2007).

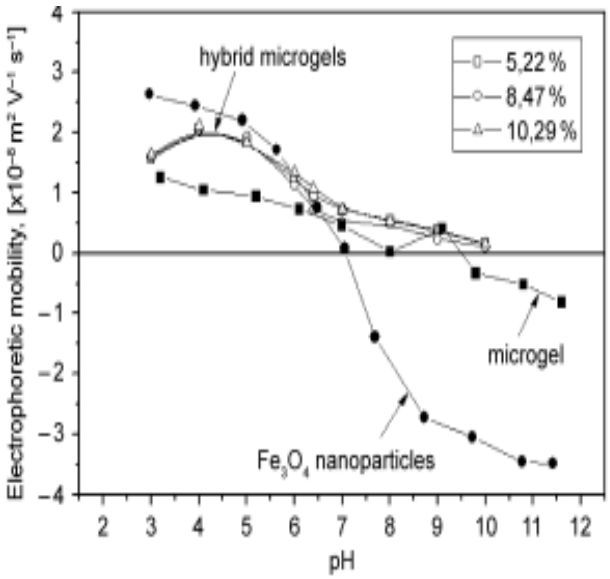

Figure 2.39 Electrophoretic mobility of the hybrid microgels, bare microgels, and magnetic nanoparticles (Bhattacharya et al., 2007).

Jaiswal et al. (Jaiswal et al., 2010) were able to successfully encapsulate iron oxide magnetic nanoparticles, which were synthesized by co-precipiaiton with a size of ~10 nm, into nano-hydrogels matrix, with a size of ~200 nm. Nano-hydrogels consisting of poly (N-isopropylacrylamide) (PNIPAAm)-chitosan were synthesized through free radical polymerization. Figure 2.40 shows the TEM images of the encapsulation of the magnetic iron oxide nanoparticles within the matrix of nano-hydrogels. Chitosan plays an important role in this system; it imparts biodegradability to the system, acts as cross-linking and surface active agents during polymerization. It controls the growth of the nano-hydrogels, and also improves the lower critical solution temperature (LCST) by increasing the weight ratio of chitosan to NIPAAm. Furthermore, they noted that the LCST of PNIPAAm increased from 32 to 42 ^{o}C, which is known as hyperthermia temperature, as a result of the encapsulation of iron oxide nanoparticles into nano-hydrogels. Therefore, this system showed great potential for hyperthermia treatment of

cancer, because the LCST could be shifted either through grafting chitosan or/and by encapsulating the magnetic nanoparticles (Jaiswal et al., 2010). The former was attributed to reduction in the mobility of water molecules as they were trapped in cross-linked nano-hydrogels matrix. On the other hand, the latter was suggested to be responsible for the dipole-dipole interactions, which inhibits the collapsed of the cross-linked polymer segments (Jaiswal et al., 2010). They observed no significant changes in the size of magnetic nano-hydrogels, after the encapsulation of magnetic nanoparticles into nano-hydrogels matrix, in comparison to the nano-hydrogels, before the encapsulation of the magnetic nanoparticles. As seen in Figure 2.41, by increasing the feed ratio of chitosan to PNIPAAm, the nano-hydrogels size decreased due to the adsorption of free positively charged chitosan onto the negatively charged PNIPAAm chain (Jaiswal et al., 2010).

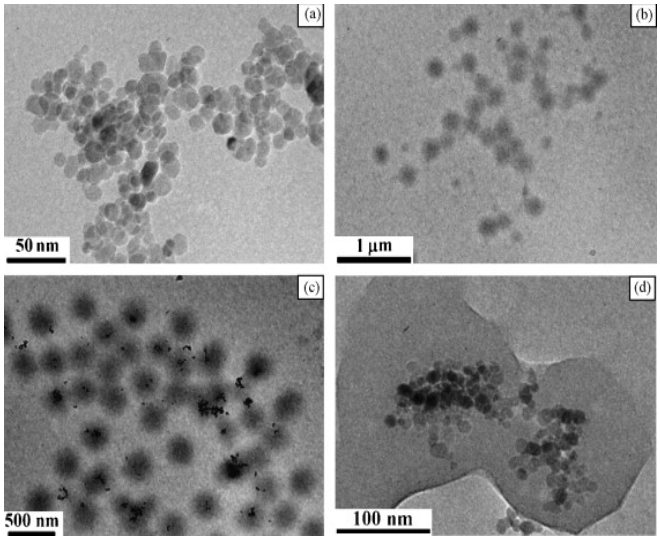

Figure 2.40 TEM Images (a) bare Fe_3O_4 magnetic nanoparticles, (b) nano-hydrogels particles, (c) MNP encapsulated within the nano-hydrogels matrix, and (d) magnified version (Jaiswal et al., 2010).

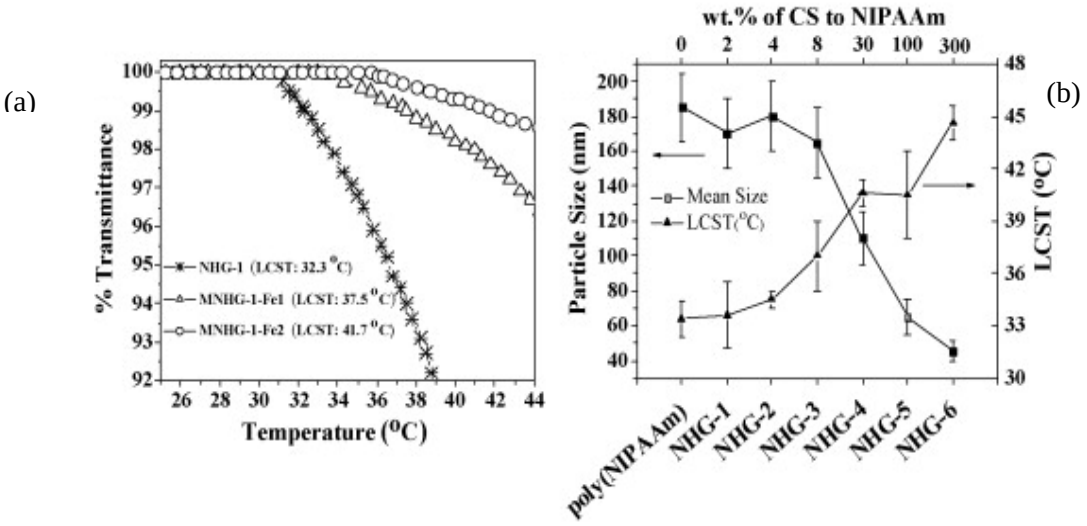

Figure 2.41 Determination of the LCST by transmittance as a function of the temperature at different compositions (a) illustrate shift in LCST as a result of MNP encapsulation, and (b) particle size and LCST of different nano-hydrogels compositions, by increasing the chitosan feed percentage from NHG-1 to NHG-6 (Jaiswal et al., 2010).

Sun et al. (Sun HanWen et al., 2009) synthesized super-paramagnetic Fe_3O_4 nanogels via the co-precipitation approach. As shown in Figure 2.42, the synthesized nanogels were stabilized by coating poly (ethylene glycol) methacrylate (PEGMA) as monomer and N, N'- methylene-bis-(acrylamide) (MBA) as cross-linking agent onto the surface of the nanogels by photochemical polymerization under UV irradiation. In photochemical reaction, magnetic nanogels absorbed a majority of the photons due to a larger cross section area, in comparison to the monomer and the cross-linking agent (Sun HanWen et al., 2009). Therefore, valence band holes and conduction band electrons were formed on the surface of the magnetic nanoparticles. A high tendency of the valence band holes to absorb electron caused the formation of free radical formation in the PEGMA, which induced photochemical polymerization and grafting of PEGMA on the surface of the nanogels (Sun HanWen et al., 2009).

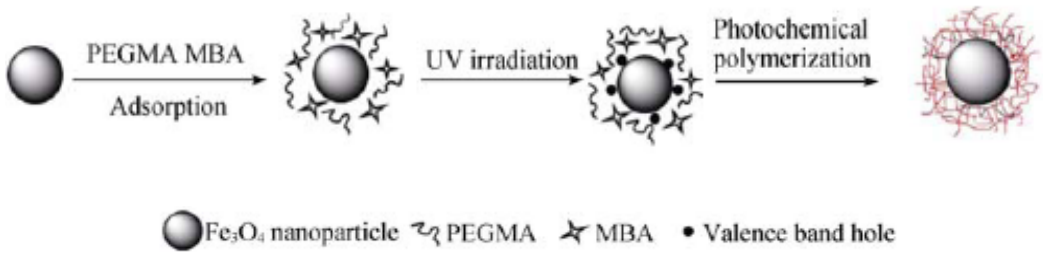

Figure 2.42 Schematic of photochemical polymerization of the magnetic nanoparticles by UV irradiation (Sun HanWen et al., 2009).

Sun et al. (Sun HanWen et al., 2009) investigated the drug delivery application of these stabilized magnetic nanogels using the anti-cancer drug, doxorubicin. As illustrated in Figure 2.43a, by increasing the quantity of doxorubicin into the coated-magnetic nanogels solution to 130 μg, 110 μg was encapsulated by the nanogels. They concluded that the high drug-loading capacity was attributed to the grafted PEGMA chains, which provide looser internal structure for the nanogels. In addition, Figure 2.43b demonstrates the release profile of doxorubicin from the nanogels. Drug release reached a maximum value of 85.4% after 90 hrs through desorption and diffusion of the drug into the medium (Sun HanWen et al., 2009).

(a)

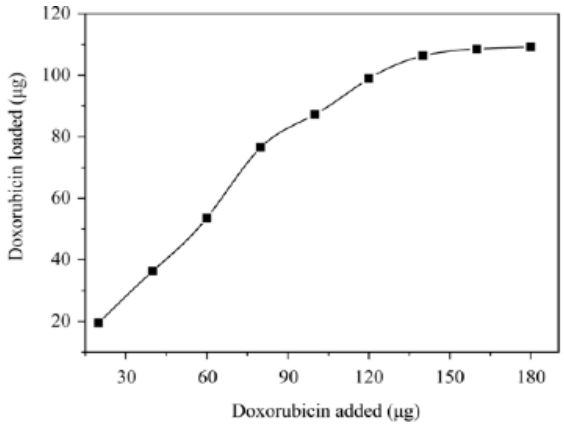

(b)

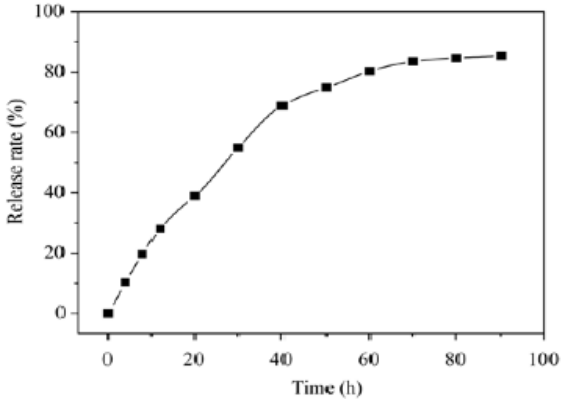

Figure 2.43 (a) Loading profiles of doxorubicin and (b) release profile of doxorubicinprofile from the magnetic nanogels (Sun HanWen et al., 2009).

Lapointe et al. (Lapointe and Martel, 2009a) reported the synthesis of thermo-responsive hydrogels with embedded magnetic nanoparticles. The thermo-responsive hydrogels consist of PNIPAAm synthesized by free radical polymerization, which was then inpregnated by dextran-coated Fe_3O_4 nanoparticles. Magnetic nanoparticles are able to produce heat when placed in an external magnetic field. This feature was applied in this system to provide the required heat for the actuation of the thermo-responsive hydrogels. They took advantage of thermo-responsive behavior of the hydrogels, in which a volume change of the hydrogels was induced when temperature was decreased to below the transition temperature. As shown in Figure 2.44, by

increasing the temperature beyond the LCST, the PNIPAAm hydrogels embedded with magnetic nanoparticles lost more than 90% of their mass over 6 hours. Whereas, when there was no embedded magnetic nanoparticles the volume lost was as high as 88% (Lapointe and Martel, 2009a).

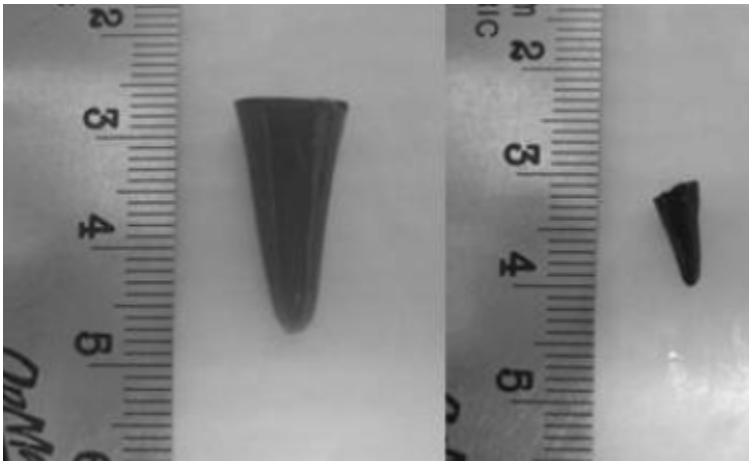

Figure 2.44 The volume reduction of PNIPAAm hydrogels embedded with magnetic nanoparticles (Lapointe and Martel, 2009a).

They (Lapointe and Martel, 2009a) also observed that hydrogels with embedded magnetic nanoparticles possessed a shorter stabilization (response) time of about 30 minutes, while hydrogels without magnetic nanoparticles stabilized in about 24 hours. This phenomenon was related to the fact that the internal structure and the surface characteristics of the hydrogels were altered as a consequence of embedding iron oxide nanoparticle into them, Moreover, as can be seen in Figure 2.45, by embedding magnetic nanoparticles into hydrogels the volume transition occurred at a higher temperature of 34 ^{o}C, compared to bare PNIPAAm hydrogels (Lapointe and Martel, 2009a).

(a)

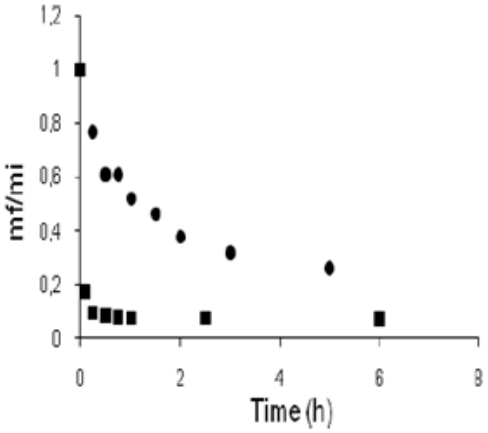

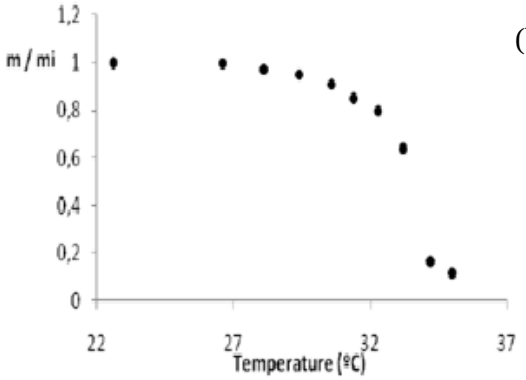

(b)

Figure 2.45 (a) Mass loss rate for samples with and without embedded magnetic nanoparticles, and (b) Volume changes of the hydrogels embedded with magnetic nanoparticles occurred at 34^{o} C (Lapointe and Martel, 2009a).

Menager et al. (Menager et al., 2004) utilized a different approach to encapsulate magnetic nanoparticles in microgels. In this study, stable colloidal dispersion of magnetic particles was prepared by the co-precipitation technique. They used inverse emulsion and miniemulsion polymerization to incorporate iron oxide nanoparticles in the final microgels. In this process, the cross-linking agent and the hydrophilic acrylamide monomer were added to the magnetic fluid, which was colloidally stable, by adjusting the ionic strength and pH. These magnetic microgels were stable in water at pH=7 because of electrostatic repulsion induced by negative charge citrate ligands, which covered the magnetic nanoparticles (Menager et al., 2004).

(a) 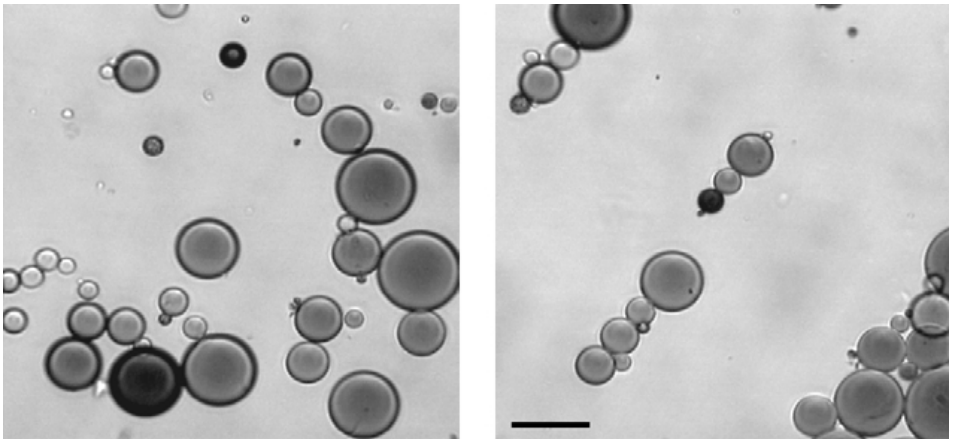 (b)

Figure 2.46 TEM images of magnetic microgels (a) without magnetic field (b) under magnetic field (Menager et al., 2004).

These magnetic microgels exhibited fast and reversible response to a weak magnetic field, as illustrated in Figure 2.46. The synthesized magnetic nanoparticles swelled when placed in the right solvent, which is demonstrated in Figure 2.47. Because this reversible swelling was only induced by the diffusion of water and ions from the solution into the microgels through the porous medium of the microgels, there was no reported release of the magnetic content (Menager et al., 2004).

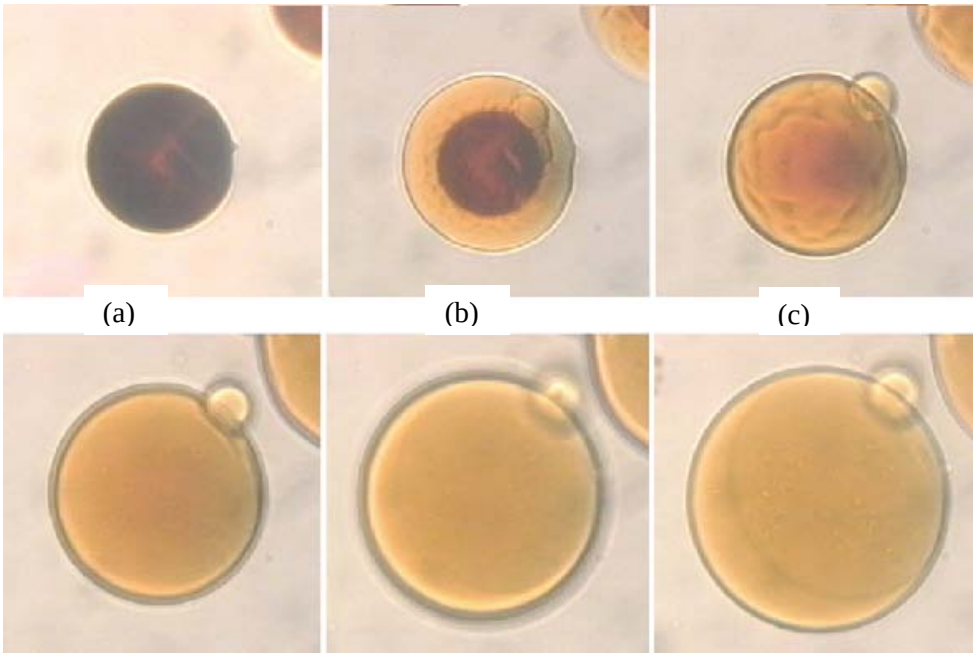

Figure 2.47 Optical micrographs of the swelling degree of magnetic microgels, (a) In dried state, (b) 0.7 s, (c) 1.8 s, (d) 3.9 s, (e) 6.6 s, (f) 16 s after adding water (Menager et al., 2004).

In another study, Lee et al. (Lee et al., 2010) synthesized magnetic nanoparticles via the co-precipitation approach, and then conjugated them within pH-responsive microgels. Microgels were prepared using methacrylic acid (MAA), ethyl acrylate (EA) and di-allyl phthalate (DAP), which is the cross-linking agent. They developed these microgel iron oxide nanoparticles (MGIO) for the cell labeling applications. Due to the high MRI contrast of MGIO nanoparticles, which could be feasibly cellular tracked by MRI, great cellular uptake of these nanoparticles was observed. They confirmed that MGIO nanoparticles were effective for labeling and detecting stem cell and progenitor cells after the transplantation (Lee et al., 2010).

2.8 Magnetic Nanoparticles Applications

Because of the biocompatible and magnetic properties, magnetic nanoparticles have been evaluated as novel cancer therapeutic agents. The heat produced as a consequence of natural magnetic properties can be used to induce the release of a heat-sensitive probe or to destroy cancerous cells. Besides, magnetic nanoparticles have a great potential for use in the therapeutic treatment and can be exploited as magnetic resonance imaging (Berry, 2009; Gupta and Gupta, 2005; Sun et al., 2008). The summary of magnetic nanoparticles applications is illustrated in Figure 2.48.

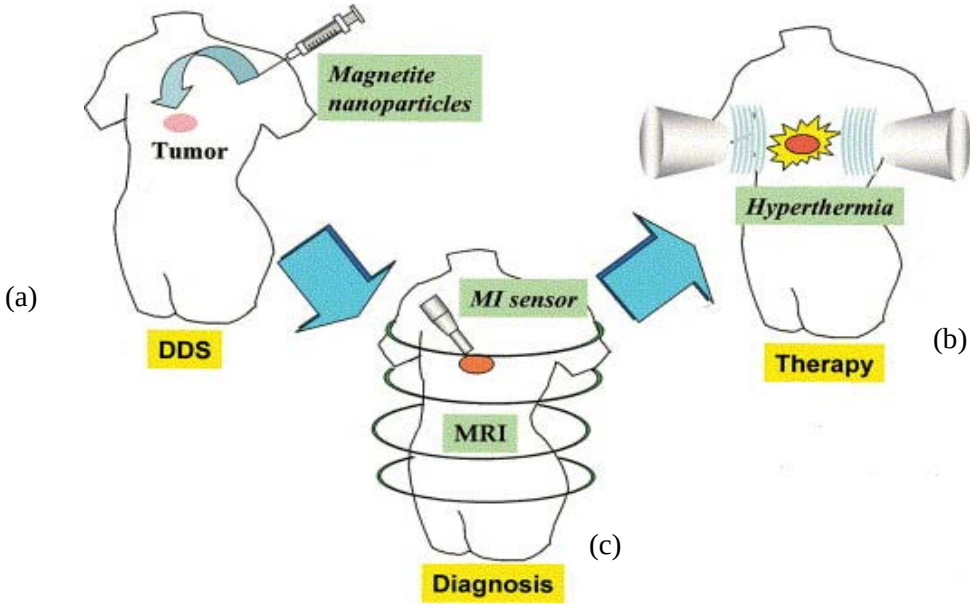

Figure 2.48 Schematic of magnetic nanoparticles (MNP) applications, (a) through the Drug Delivery Systems (DDS) functionalized MNP build up in the tumor tissue, (b) as a diagnosis tool for cancer by magnetic resonance imaging (MRI) or for magnetoimpedance (MI) sensor, (c) as a hyperthermia treatment for cancer (Ito et al., 2005).

2.8.1 Magnetic Resonance Imaging and Cell Labeling

Due to its noninvasive character, and also ease of analysis, magnetic resonance imaging (MRI) is the most common technique for detecting and tracking magnetic nanoparticles. It is also a powerful imaging instrument in clinical medicine that provides high spatial resolution of contrast difference between tissues without ionized radiation (Berry, 2009; Veiseh et al., 2010). MRI is capable of detecting super-paramagnetic nanoparticles because of their magnetic susceptibility, which results in sturdy magnetic field distortions. MRI and other optical imaging devices have made feasible the *in vivo* tracking of magnetic nanoparticles uptake by tumor or cell (Gupta and Gupta, 2005). Furthermore, MRI accelerates the detection and separation of cells labeled with MRI-visible particles, such as iron oxide nanoparticles (Gupta and Gupta, 2005).

Regarding the recent development in stem cell and progenitor cell based therapies; labeling cell and tracking the injected cells by MRI are anticipated to ultimately change the treatment of many fatal diseases (Thorek et al., 2006). The important factor in cell labeling is the loading of sufficient quantity of iron oxide into the cells. This can be achieved via two strategies. In the first method, the internalization efficiency increased by simply using higher concentration, and in the other technique, electrostatic interactions concept were employed by using different form of transfection agents (Thorek et al., 2006). Moreover, large particles can be introduced into the cells to make them detectable, as a substitute of introducing millions of particles into the cells. It was found that MRI could detect micro-sized iron oxide nanoparticles in vitro in agarose sample, in cultured cells and in mouse embryos. This technique provides cells with a capacity to accommodate approximately 100 pg of *Fe* (Chen et al., 2011; Chou et al., 2011). Cell labeling has become a popular technique for sorting and separating specific cells from others. The use of

antigens and receptors is common for separating cancer and stem cells. The cell labeling approach is achieved through coating magnetic nanoparticles with antibodies or peptides, which are capable of binding to a desired surface receptor. Because of the magnetic properties of these nanoparticles, only cells that are labeled with magnetic nanoparticles should respond to an external magnetic field, and only those targeted cells can ultimately be collected for further investigation. For example, Yoon et al. (Yoon et al., 2006) incorporated CD10 antibody into silica-coated $CoFe_2O_4$ magnetic nanoparticles for the purpose of targeting leukemia cells. By means of TEM images and magnetic capture, they confirmed the binding and internalization of magnetic nanoparticles. In order to efficiently separate and distinguish cancer cells and stem cells, which are magnetically labeled, from multicellular fluids such as blood; a powerful quadruple magnetic flow-through device was developed recently (Chou et al., 2011; Lee et al., 2010). Although the presence of magnetic nanoparticles can not be directly proved by magnetic-based cell labeling technique, the qualitative information regarding the efficiency of labeling targeted cells can be provided by this approach. However, this technique can be utilized to separate rare cells in a multicellular environment for further investigation (Dias et al., 2011; Faraji et al., 2010; Laurent et al., 2008; Sun et al., 2008).

The parameters, such as magnetic nanoparticles diameter, targeting molecules size, magnetic nanoparticles distribution, and formulation widely influence the MR signal intensity, and detection of nanoparticles accumulation. As a result, predicting the sufficient amount of local nanoparticles concentration for MRI detection is complex. Considering magnetic nanoparticles for biomedicine applications, MRI is known as an important and powerful *in vivo* imaging technique (Berry, 2009; Gupta and Gupta, 2005).

2.8.2 Drug Delivery systems

The most common application of magnetic nanoparticles is their utilization in the area of site-specific drug delivery application, particularly in cancer treatment where serious side effects are caused by conventional chemotherapy and radiotherapy (Veiseh et al., 2010). Widespread pharmaceutical agents delivered by magnetic nanoparticles are chemotherapy drugs such as doxorubicin, methotrexate, and paclitaxel, which are hydrophobic drugs and due to the electrostatic interaction they can be physically or chemically conjugated with nanoparticles layers. They are concentrated to the area of interest by their modified targeting ability, where the drug will be released in a controlled manner. Consequently, through this technique significant reduction in the dosage of drugs occurs, which ultimately reduces the side effects (Sun et al., 2008; Thorek et al., 2006; Veiseh et al., 2010). Parameters such as the size, charge, surface morphology, and surface chemistry of magnetic nanoparticles have major impact on both the blood circulation time and also bioavailability of the particles within the body (Berry, 2009; Gupta, 2005).

By modifying the surface chemistry of iron oxide nanoparticles with different functional groups, drugs can be incorporated onto the surface of nanoparticles through mild chemistry and/or suitable cross-linking agents. For instance, Veiseh et al. (Veiseh et al., 2005) synthesized iron oxide nanoparticles via co-precipitation and then the surface was covalently coated with an amine terminated PEGylated saline; afterwards, an anticancer drug methotrexate (MTX) via EDC/NHS (*N*-hydroxysuccinimide) mediated coupling was loaded onto the surface synthesized magnetic nanoparticles. This study confirmed that loaded iron oxide nanoparticles with MTX could increase the glioma cell (common and lethal form of primary brain tumor) uptake. This

technique can be extended to other drugs as well, but the major problem is the fact that some chemically active groups for coupling must be present for the conjugation of the drugs (Veiseh et al., 2005).

Conversely, through physical absorption, the drugs can also be loaded into the iron oxide nanoparticles. This technique is more versatile compared to the chemically incorporated method, since many drugs do not have appropriate functional groups for coupling or they may loose their activity after coupling. Silica nanoparticles are favored for drug delivery, due to their porous structure. Piao et al. (Piao et al., 2008) through hydrolysis of $FeCl_3$ in aqueous solution produced spindle-shaped akagenite (β-$FeOOH$) nanoparticles and subsequently performed a three-step process on these β-$FeOOH$ nanoparticles, which was called wrap-bake-peel process. As illustrated in Figure 2.49, this process included the following steps: (1) silica coating, (2) heat treatment, and (3) silica removal by $NaOH$ to achieve hollow iron oxide nanoparticles. As shown in Figure 2.49, depending on the process of silica removal, hematite or magnetite water-dispersible nanoparticles can be obtained. Then the anticancer drug doxorubicin (DOX) was loaded into these hollow nanoparticles (Piao et al., 2008).

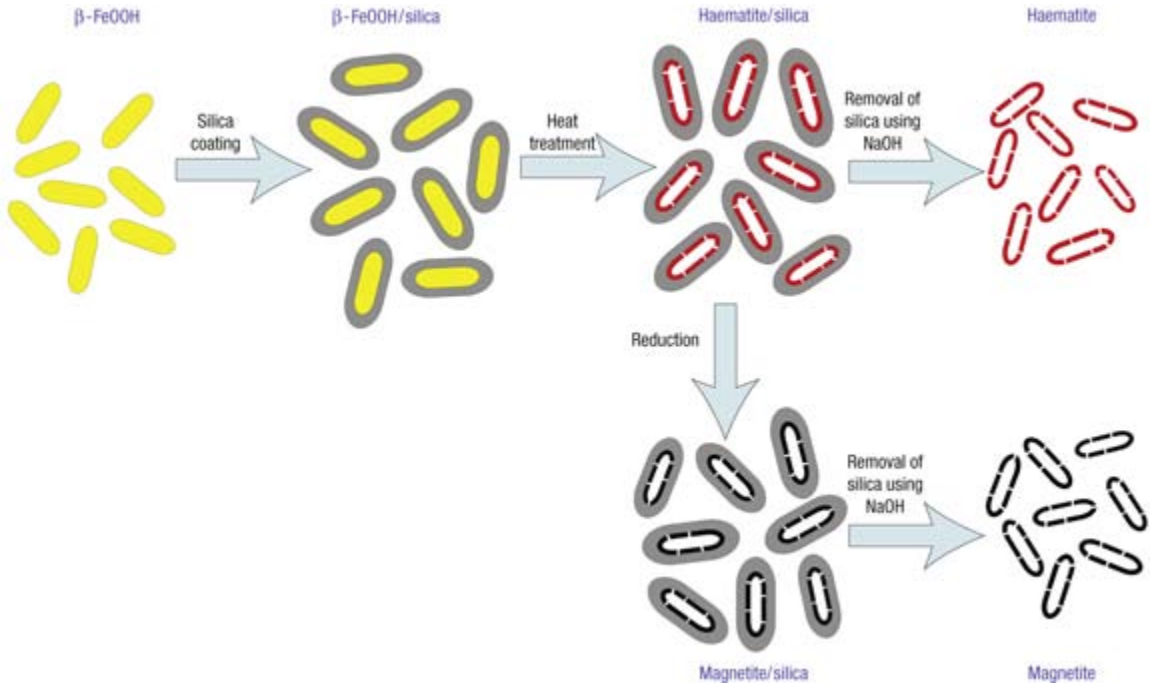

Figure 2.49 Schematic diagram of the formation of hollow iron oxide nanoparticles by wrap-bake-peel process (Piao et al., 2008).

In another study, Park et al. (Park et al., 2007) synthesized iron oxide nanoparticles with PEG and lecithin layers, which were loaded with doxorubicin (DOX). They studied the drug effects on the nanoparticle by investigating loading efficiency and release kinetics of the doxorubicin from the layered coated nanoparticles both *in vitro* and *in vivo*. As shown in Figure 2.50, they observed that over 30 hours, 60% of the loaded doxorubicin was released from the DOX-PEG-MPs or DOX-lecithin-MPs.

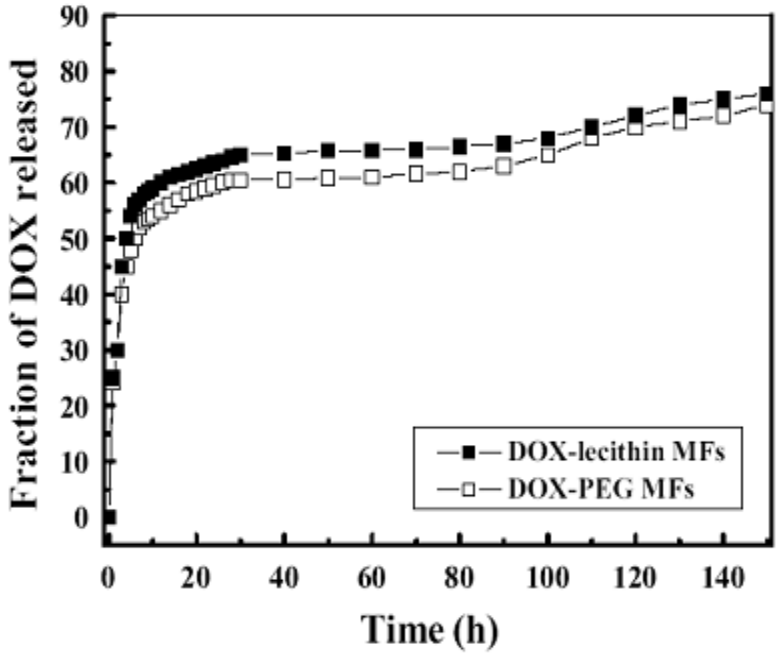

Figure 2.50 DOX released from each of the DOX loaded PEG-magnetic nanoparticles and lecithin magnetic nanoparticles over 150 hour (Park et al., 2007).

Combining cellular targeting and MR contrast with the drug's therapeutic effect is the main objective of using magnetic nanoparticle as drug carrier. The most fundamental drug delivery system is formed by applying these three concepts, and this drug carrier is able to target diseased cells, offer delivery therapy at the cellular level, and provide diagnostic information (Sun et al., 2008).

2.8.3 Gene Therapy

In recent years, gene delivery has been a field of great interest and intense research. Analogous to drug delivery, plasmid DNA and small interfering RNA (siRNA) can be easily conjugated with nanoparticle layers. These incorporations occur generally as a result of electrostatic interaction; however, cross-linking between functional groups on the nanoparticles surface and

linear sequences can also lead to the incorporation of DNA and siRNA into the nanoparticles (Sun et al., 2008; Veiseh et al., 2010). The main obstacles in obtaining an efficient gene delivery system are lack of specificity in targeting, short *in vivo* half-life, and low permeability through cell membrane (Berry, 2009). Because of the fact that nanoparticles have to be delivered to the nucleus for the transfection of the plasmid DNA, the research in this area is also related to cellular and intracellular targeting approaches (Sun et al., 2008).

Berry et al. (Berry, 2008) delivered plasmid DNA and green fluorescent protein (GFP) using the cell penetrating peptide (CPP), HIV virus derived TAT peptide, which transport the DNA into the nucleus. On the other hand, some research groups exploited a magnetofection method, in which magnetic properties of magnetic nanoparticles are used to physically deliver DNA-loaded magnetic nanoparticles into the cells through external magnetic field. In the magnetofection method, the magnetic nanoparticles were coated with the polycation polyethylenimine to make them positively charged in order to conjugate magnetic nanoparticles with negatively charged plasmid DNA (Gupta, 2005). Although each of the two approaches can be used separately to deliver or change genetic information, a combination of both bimolecular and magnetic targeting methods would be the ideal technique to effectively accomplish gene delivery *in vivo*.

Moreover, iron oxide nanoparticles demonstrate great enzyme mimicry. They are able to catalyze reacting peroxidise substrate such as o-phenylenediamine (OPD), di-azo-aminobenzene (DAB), and 3, 3, 5, 5-tetramethylbenziidne (TMB) into their colourful oxidized states, because of the presence of H_2O_2 (Gao et al., 2007). In contrast to peroxides, which denature and lose their activity very rapidly in harsh environment such as high pH and temperature, iron oxide nanoparticles are capable of sustaining a broad pH or high temperature. In fact, the catalytic

activity of iron oxide nanoparticles is 40-fold higher than that of peroxides. In addition, because of the magnetic properties of iron oxides, they can be easily separated and recovered; therefore, permitting recycling and repeated applications (Gao et al., 2007).

2.8.4 Hyperthermia

Local heating of cancer or tumour cells leading to necrosis is known as hyperthermia; in other words, instead of killing the cancerous cell with drugs, the targeted nanoparticles become hot under the magnetic field, and the heat generated would kill the diseased cell (Berry, 2009; Laurent et al., 2008). To reduce the adverse side effects, and the exposure of surrounding healthy cells to the hyperthermia treatment, the treatment should be restricted solely to the targeted cells; which is one of the major challenges with hyperthermia. Exploiting magnetic nanoparticles targeting of cancer cells is a promising approach to enhance localization of this treatment and overcome the challenge; since targeted magnetic nanoparticles are capable of accumulating at the desire site and subsequently be heated by the magnetic field during which the electromagnetic energy is converted to heat and raised the temperature of the targeted site (Berry, 2009; Piao et al., 2008). Because of the susceptibility of tumour cells to high temperature in comparison to normal cells, hyperthermia is capable of specifically delivering magnetic nanoparticles to the tumour cell, and generates heat locally to damage them, without affecting the normal tissues (Dias et al., 2011).

The heat progression rate defined as specific absorption rate (SAR) is an important parameter in hyperthermia. Factors such as size distribution, shape, surface functional groups, frequency, and amplitude of the magnetic field viscosity of the surrounding medium have great influence on

the value of SAR. Due to the high biocompatibility, sufficient SAR value of the iron oxide nanoparticles have been reported (Berry, 2009; Dias et al., 2011; Ito et al., 2005).

Ito et al. (Ito et al., 2004) delivered magnetic nanoparticles-loaded immuneliposome to SkBr-3 breast cancer cells and subsequently heated the cancerous cell up to 45 ^{o}C by high frequency magnetic field. Their investigation revealed a killing efficiency of greater than 90% for the targeted breast cancer cells. Although side effects such as inflammation and immune response *in vivo* are still present as a result of necrotic cellular death, hyperthermia treatment with magnetic nanoparticles demonstrates great influence on targeted cellular therapy for cancer (Ito et al., 2004).

2.9 Layer-by-Layer Coating

The layer-by-layer coating approach involves the sequential adsorption of oppositely charged polyions onto the outer surface of particles that is permeable, stable and compatible, resulting in the reversal of the terminal surface charges after deposition of each layer; thus, allowing the controlled release of the encapsulated materials through these layers. The first report on sequential adsorption of oppositely charged colloids dated back to 1966 by Iler et al. (Antipov and Sukhorukov, 2004). Versatility, simplicity, control over structure, robustness, and low cost are the most significant advantages of layer-by-layer coating approach in preparing multilayered films that contributed to the popularity of this technique over the last two decade (Tang et al., 2006). In other words, the availability of a wide variety of material that can be used as coatings, diversity of precursor and core materials, and versatility of coating techniques increased the biomedical applications of the layer by layer coatings approach (Tang et al., 2006) .

In layer-by-layer coating by means of alternate adsorption of oppositely charged polyions, nanoparticles, and biomolecules, ultrathin layers can be formed. The produced layers acquire tuneable properties to their environment and also possess thickness in the nano- to micro- range (Wong and Richtering, 2008). The fundamental of this technique is the use of electrostatic attractions between oppositely charged polyelectrolytes; as a result, layers with controllable thickness, different compositions, functional groups, and morphologies are produced onto the surface (Burke and Barrett, 2004).

Although electrostatic interaction play an important role in the formation of layer-by-layer coating film, hydrogen bonding, covalent bonding, charge transfer, biological recognition, and hydrophobic interaction could also contribute to the formation of layer-by-layer coatings. Therefore, in physiological conditions, the stability of layers was enhanced as a result of these multiple interactions in layer by layer coatings (Tang et al., 2006; Wong and Richtering, 2008). In this approach not only there is more control over the position and order of multiple layers, but also by altering the number of polyelectrolyte layers, the concentration of incorporated chemicals can be changed. Moreover, the coated layers are able to protect and retain the encapsulated materials from environmental hazards, and by changing the coating layers the solubility of the coated materials in different solvents can be manipulated. Another advantage of this method is the selective permeability for different materials. By manipulating the thickness, porosity, structure, and chemistry of the coating layers, the permeability of the coated component can be tuned (Tang et al., 2006; Wong and Richtering, 2008).

As a result of great success of layer-by-layer coating on planar and rigid substrate, this technique was expanded to three-dimensional hard or soft porous colloidal particles, such as

nano- micro- gels. Consequently, interface characterized porous colloidal particles that are able to incorporate biomacromolecules within their network, due to their high surface-to-volume ratio, gain special attention as a depositing template for layer-by-layer surface engineering in order to achieve sustained and controlled release of the drug (Wong and Richtering, 2008). Application of layer-by-layer procedure in the field of drug delivery offer higher efficiency, lower toxicity, and enhanced patient convenience in comparison to conventional techniques (Tang et al., 2006). Layer-by-layer coating has illustrated wide perspective for encapsulating, and controlling the delivery of drugs. The controlled release of incorporated drug from the layer-by-layer coated material depend on the permeability or breakdown of the multilayer structure, and can further be extended by employing the polyelectrolytes possessing semi permeable properties (Tang et al., 2006). For example, for polyelectrolyte layers formed by electrostatic interaction, pH is a dominant driving force for structural alteration. By placing coated component in a medium with a pH close to the pK_a of one of the polyelectrolytes, the charge density of that polyelectrolyte is decreased. Consequently, the intermolecular binding of the multilayers are loosen due to the repulsive forces between polyelectrolytes of similar charges. These repulsive forces are no longer compensated by the attraction forces of the oppositely charged polyelectrolytes. This phenomenon leads to permeabilization and decomposition of the polyelectrolyte layers and ultimately the release of incorporated components (De Geest et al., 2009).

In order to form functionalized particles, magnetic nanoparticles have potential to utilize the layer by layer approach to accomplish both “localizing” of encapsulated drugs to a desired site followed by “switching” to release the encapsulated materials (Tang et al., 2006). Polyelectrolytes employed in the layer-by-layer coating can be arranged in two groups of natural

or synthetic, which can further be categorized as fully or partially charged, and into strong or weak interactions. In weak polyelectrolytes, the charges are manipulated by pH. Furthermore, natural polyelectrolytes including natural polypeptides or polysaccharides have the advantage of forming diverse configuration due to the folding and unfolding of the chains (Wong and Richtering, 2008). The polyions that predominately employed in the layer-by-layer coating are (Tang et al., 2006; Wong and Richtering, 2008):

- Polyanions: poly (sodium 4-styrenesulfonate) (PSS), poly (acrylic acid) (PAA), poly (vinyl sulfate) (PVS), sodium alginate (SA), sodium carboxylmethyl cellulose (CMC), chondroitin sulfate sodium salt (CS),deoxyribonucleic acid (DNA), dextran sulfate sodium salt (DS), tannic acid (TA), and gelatin B (GB).
- Polycations: chitosan (CH), poly (allylamine hydrochloride) (PAH), poly (dimethyldiallylammonium chloride) (PDDA), poly (ethylenimine) (PEI), gelatin A (GA), poly-L-lysine (PLL), and protamine sulfate C (PS).

The layer-by-layer approach is a very simple and versatile process, a standard approach for coating formation on both a solid planar and nano/micro gels illustrated in Figure 2.51a and describe below (De Geest et al., 2006; Tang et al., 2006):

- Aqueous solution of polyelectrolyte, nanoparticles, or proteins is prepared and the pH is adjusted in such a way that the components are oppositely charges.
- A solution of nanogels or a planar substrate possessing a surface charge for layer-by-layer deposition is prepared.
- Alternately polyelectrolyte solution is added to the nanogel solution or alternately the planar substrate is immersed in the polyelectrolyte solution, inducing the surface charge

reversion. For instance, immersing a negatively charged substrate in a positively charged polyelectrolyte solution leading to net charge reversal to positive due to the adsorption of positively charged polyelectrolyte. Then, by further immersion in a negatively charged polyelectrolyte a charge reversal to overall negative will occur.

- Subsequently after each immersion into polyelectrolyte solution or addition of polyelectrolyte solution, the coated planar substrate is rinsed with distilled de-ionized water or in case of coated nanogels they can either be filtered or centrifuged; in order to remove excess or unbound polyelectrolyte chains. The water should carry a pH that reserved the respective coated components (Antipov and Sukhorukov, 2004).
- Previous steps can be repeated until all the desired layers have been deposited, and multilayered coated substrate or nanogels are obtained with desirable structure and thickness.

The surface charge reversal upon deposition of layers is the only crucial factor that should be taken into account for successful deposition; which can be obtained by proper selection of deposition conditions. Afterwards, by means of electrostatic interactions a variety of polyelectrolyte materials could be adsorbed onto the surface of substrate, forming layered structure with specific properties (Antipov and Sukhorukov, 2004). Moreover, by using different materials such as organic or inorganic nanoparticles, biomolecules, lipids, or viruses in the coating process, various shapes of multilayer coating can be produced. Properties such as mechanical strength, elasticity, electrical characteristics, and other properties make polymers as suitable building blocks for the formation of layer-by-layer coating in contrast to their low-molecular weight analogues (Antipov and Sukhorukov, 2004). In this work, layer-by-layer

technique was used to develop coating onto the magnetic nanogels to better control the burst release of the drug from the nanogels network.

(a)

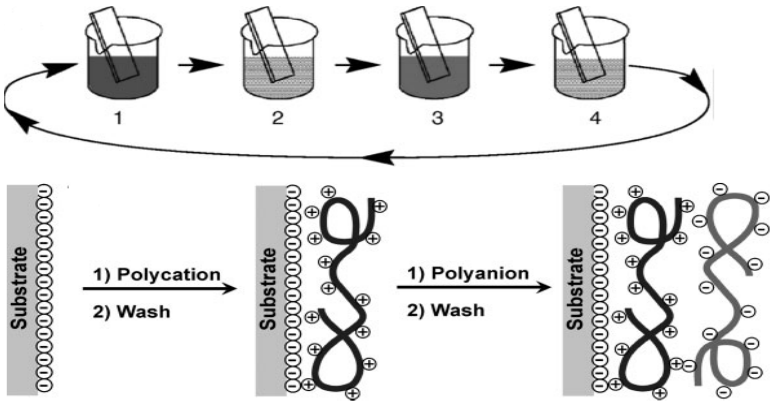

(b)

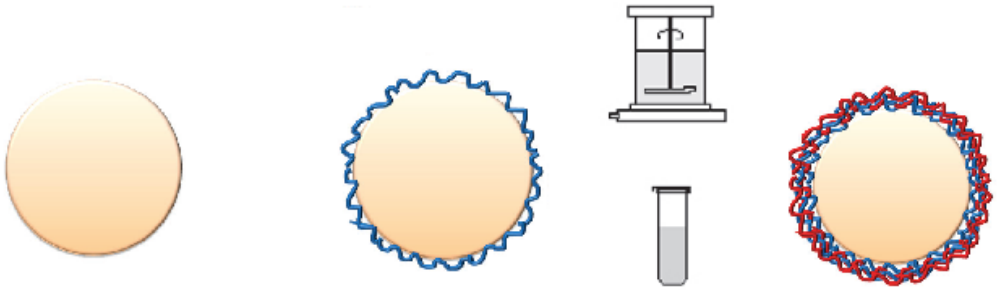

Figure 2.51 Schematic of layer-by-layer coating on (a) planar substrate (b) nanogels. Polyelectrolyte is added into a system adsorb onto the template surface inducing the surface charge reversal. Then, the excess or loosely adsorbed polyelectrolyte is removed by washing of planar substrate or centrifugation or filtration of nanogels; afterwards, oppositely charged polyelectrolyte is added. The desired number of layer is added by repeating this circle (De Geest et al., 2009; Tang et al., 2006).

One of the first studies on the layer-by-layer coating on the colloidal particles was conducted by Sukhorukov et al. in 1998 (Sukhorukov et al., 1998). They investigated this technique on the charged polystyrene latex particles by alternate deposition of PSS/DNA as polyanion and PAH/PDADMAC as polycation and subsequent centrifugation. The formation of the layers was confirmed by zeta-potential measurement. They observed that when the concentration of the next

polyelectrolyte layer was at or above saturation, a reversal of the electrophoretic mobility occurred, which confirmed the deposition of the charged layer. Furthermore, they concluded that centrifugation between each consecutive adsorption was required in order to prevent the aggregation of large numbers of particles, although centrifugation had some disadvantages such as reduction of particle number, which made deposition difficult (Sukhorukov et al., 1998).

In a recent study, Diez-Pascual et al. (Diez-Pascual and Wong, 2010) performed layer-by-layer assembly of polysaccharides and polypeptides onto negatively charged Poly (NIPAM-co-MAA) microgels. Poly (L-lysine) bromide salt (PLL) and chitosan were used as polycation and poly(glutamic acid) sodium salt and dextran sulfate were employed as polyanion in this research followed by three ultracentrifugation cycle after each deposition up to 12 polyelectrolyte layers. They observed, as depicted in Figure 2.52, that microgels retained their thermo-responsive behavior upon coating with different layers of polyelectrolyte. For example, the uncoated microgels possessed a hydrodynamic radius of 330 nm at 20 ^{o}C, and then exhibited the R_h of 180 nm upon heating to around 32-33 ^{o}C. This was due to a volume phase transition of the PNIAPAM chain. During cooling, the microgels returned to their original size (Diez-Pascual and Wong, 2010). On the other hand, the coated microgels demonstrated the same trend upon heating, which indicated the preservation of the thermo-responsive nature of the microgels. Moreover, they noticed that by depositing polycation layer, the R_h decreased remarkably, while by adsorbing polyanion layer the R_h increased again. The former phenomena contributed to the collapse of the microgels as a result of electrostatic attraction between negatively charged microgels and the first positive PLL or chitosan layer. The latter one was related to the fact that by depositing the negative layer, PGA or DEX, the positive charges had to be shared between the

microgels and the new absorbed polyelectrolyte, which further weakened the attraction between the microgels and the polycation and caused the R_h to increase (Diez-Pascual and Wong, 2010).

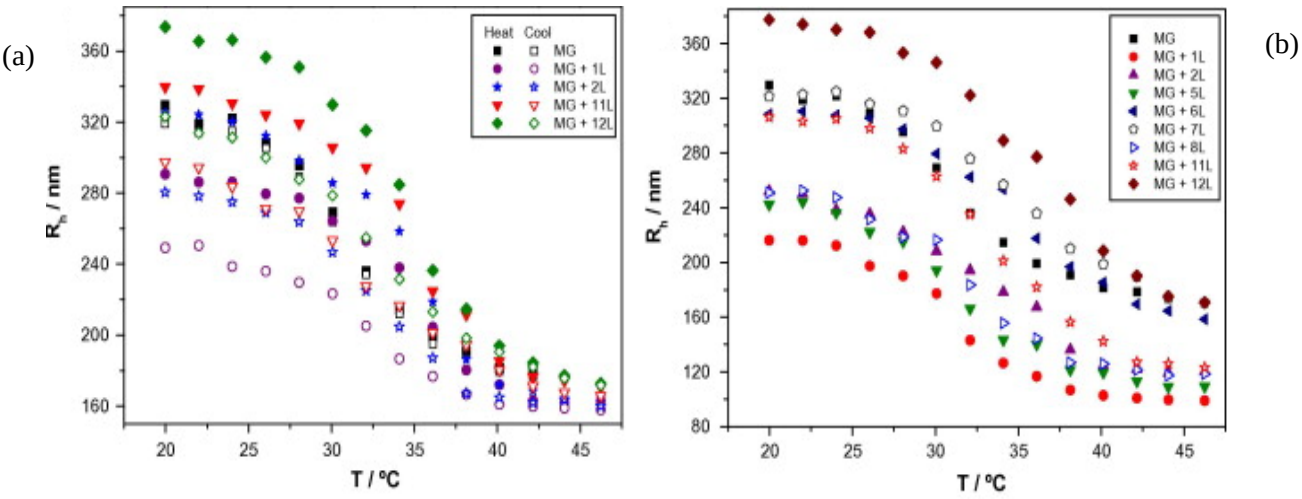

Figure 2.52 Hydrodynamic radius (R_h) vs. temperature for different layers of (a) microgels with PLL/PGA, and (b) microgels with chitosan/dexstran (Diez-Pascual and Wong, 2010).

They (Diez-Pascual and Wong, 2010) observed that in the swollen state, both polysaccharide and polypeptide coating demonstrated the same R_h profile, increment and reduction in R_h as a result of absorbing negatively and positively charged layers, respectively. However, in the collapsed state, this effect was only seen for polysaccharide coating microgels. As can be seen in Figure 2.53, the net surface charge of the microgel became positive and negative upon adsorbing polycation and polyanion, correspondingly (Diez-Pascual and Wong, 2010).

Although chitosan adsorption demonstrated higher charge reversal in comparison to PLL, which was attributed to higher number of functional groups and also charge density when chitosan presented, the overall trend for both polysaccharide and polypeptide was similar. Furthermore, this group confirmed that by increasing the number of layers onto the microgel the mobility was deceased unlike layer-by-layer assembly onto the planar substrate. This was

explained as a result of the soft and porous structures of the microgels, which promote diffusion of the polyelectrolytes into and out of the microgels, causing neutralization of the accessible charges (Diez-Pascual and Wong, 2010).

(a)

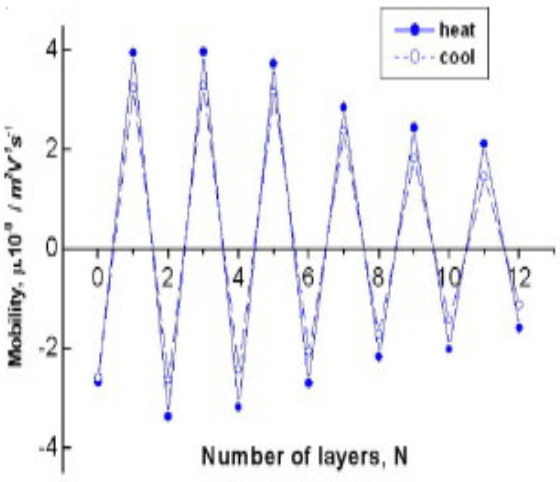

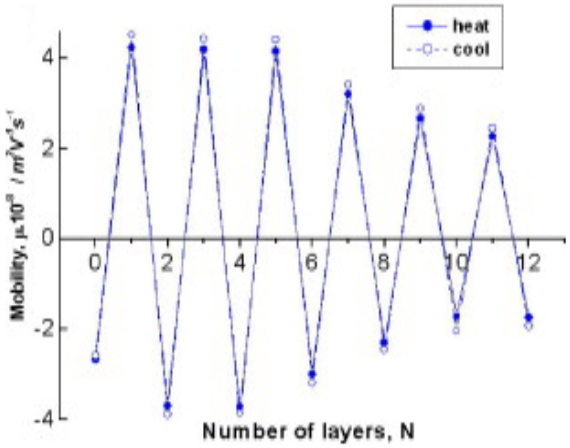

(b)

Figure 2.53 Plots of electrophoretic mobility vs. the number of layers deposited onto the (a) microgels with (PLL/PGA), and (b) microgels with (chitosan/dextran) (Diez-Pascual and Wong, 2010).

Nolan et al. (Nolan et al., 2005a) studied the influence of temperature and film thickness on the controlled pulsatile release of insulin from microgel thin films, consisting of poly (N-isopropylacrylamide-co-acrylic acid), which were constructed by layer-by-layer assembly technique. The presence of NIPAM induced a temperature responsive behavior, whereas acrylic acid caused a pH sensitivity of the system. This group took advantage of the pH sensitivity and swelling of the system at high pH condition to load insulin into the microgels. The layer-by-layer assembly preformed by deposition of PAH as polycation and the insulin incorporated microgels at pH=7.4 was served as negatively charged layer. Figure 2.54 illustrates that they were able to form insulin loaded microgels thin films in a uniform manner up to 30-layer film (Nolan et al., 2005a).

(a)

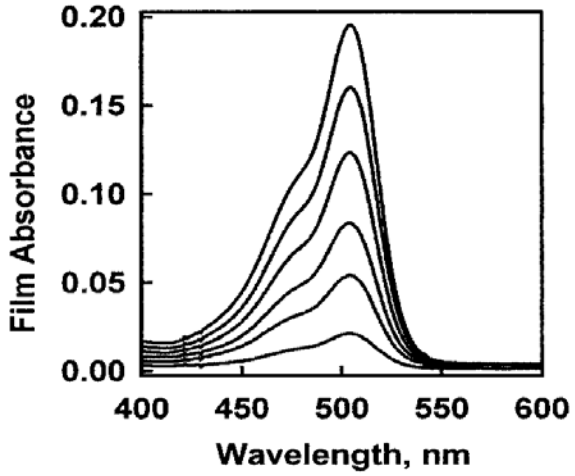

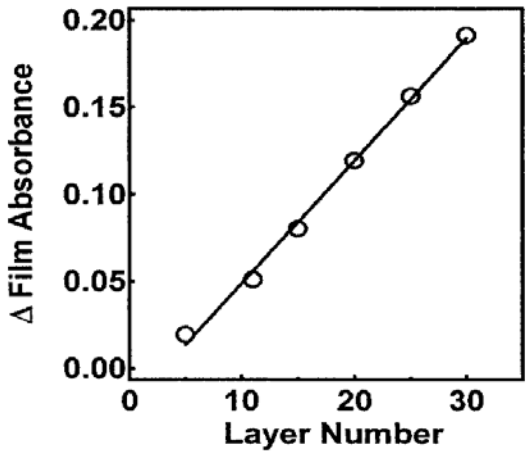

(b)

Figure 2.54 Successful formation of insulin loaded microgel thin film up to 30-layer film. (a) By increasing layer number, film absorbance is increased, and (b) film absorbance vs. layer number (Nolan et al., 2005a).

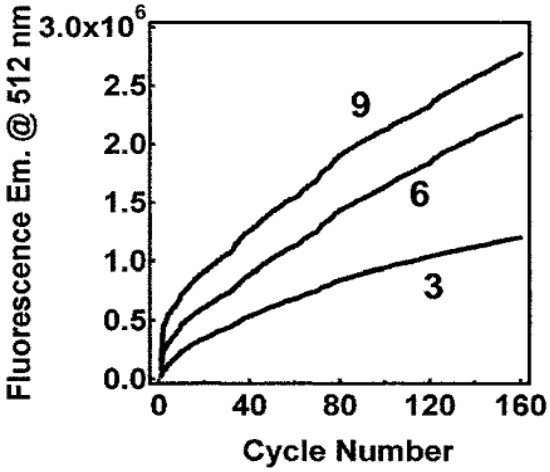

Figure 2.55 The influence of number of layers (3- 6- 9- layers) on the release of the insulin from microgels thin film. The more the layers, the longer time insulin can retain within the microgels (Nolan et al., 2005a).

They (Nolan et al., 2005a) observed that by increasing the number of layer and subsequently enhancing the film thickness, the released of the insulin can be extended to the longer period of time. For instance, as can be seen in Figure 2.55, over a month release of the insulin from the 3-

layer film reached a plateau. Whereas, the 6- and the 9- layer film yet showed an upward slope. Therefore, there was strong connection between the number of film layer, thickness of the film, and insulin release (Nolan et al., 2005a).

Xu et al. (Xu et al., 2010) prepared super-paramagnetic mesoporous silica coated Fe_3O_4 nanoparticles. Afterwards, the synthesized nanoparticles were loaded with chemotherapeutic agent (PM-19) and then alternately coated with total of 10 layers of PAH and PSS, respectively. Once the net surface charge of the magnetic nanoparticles is negative at pH 2-3, which was above its isoelectric point, the PAH was deposited onto the nanoparticles, and subsequently negative PSS was deposited onto the positively charged nanoparticles. This process is schematically demonstrated in Figure 1.56.

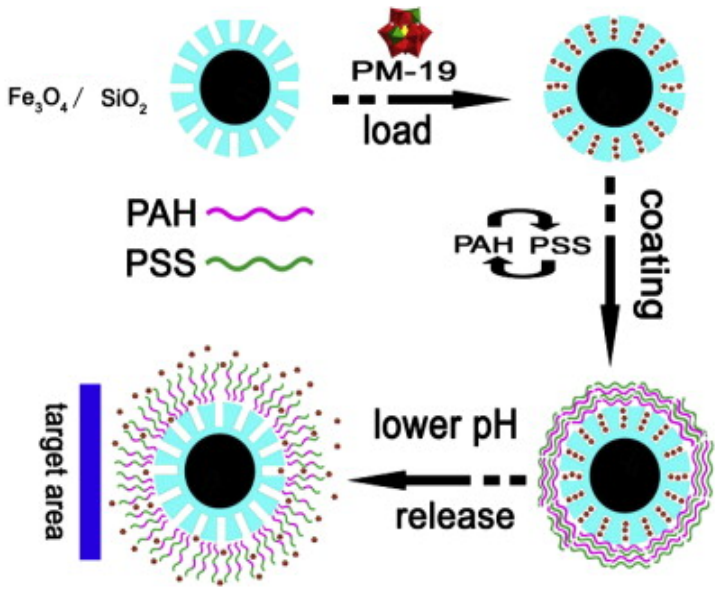

Figure 2.56 Schematic of drug loading, coating, and drug release as a result of decreasing the pH from the silica coated magnetic nanoparticles (Xu et al., 2010).

Xu et al. (Xu et al., 2010) studied the effect of layer-by-layer coating on the release profile of PM-19, as depicted in Figure 2.57. They observed that both the coated and uncoated nanoparticles could release about 70% of the loaded drug at pH=1.4 over 48 hours; whereas, at high pH, such as pH=8, the coated and uncoated nanoparticles demonstrated different patterns, where the release was 23% and 97%, respectively. These results confirmed that the release of drug depended mainly on the polyelectrolyte multilayers (Xu et al., 2010). Because the release of the drug from uncoated magnetic nanoparticles were not affected by pH; whereas, the coated nanoparticles showed pH-control behavior, for example, at pH=1.4 the polyelectrolyte multilayers of the coated nanoparticles swelled, causing more release of the drug and at pH=8 polyelectrolyte multilayers were contracted and restricted the release of the drug (Xu et al., 2010).

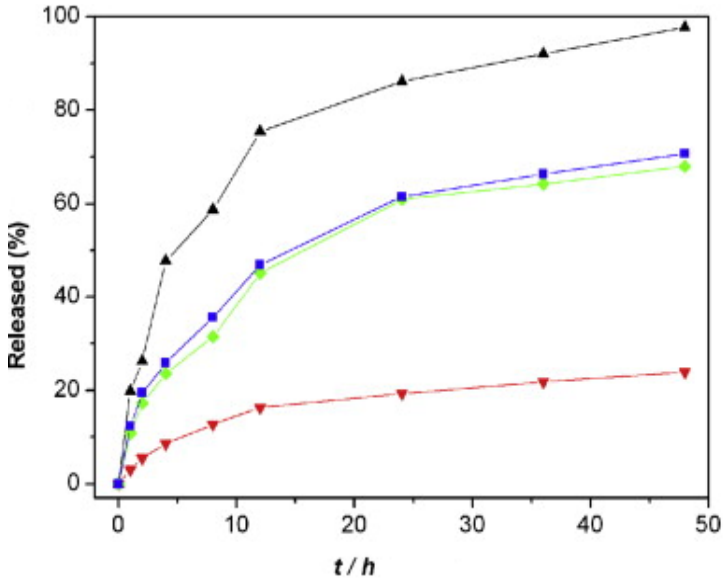

Figure 2.57 Drug release profile in (▲) pH 8, (▀) pH=1.4 from non-coated magnetic nanoparticles, (■) pH=1.4, and (◭) pH=8 from coated magnetic nanoparticles (Xu et al., 2010).

De Geest et al. (De Geest et al., 2006) introduced a novel class of biodegradable microgels surrounded by polyelectrolyte membrane through layer-by-layer technique, and these microgels were capable of releasing the encapsulated drug without applying any external trigger. The rupture of the microgels occurred, when the swelling pressure of the microgels exceed a critical value upon degradation of the microgels; degradation was due to the hydrolysis of the cross-links and the reduction in the cross-link density. They (De Geest et al., 2006) synthesized cross-linked dextran-hydroxyethyl methacrylate microgels, which possessed positive or negative charges through linking MAA or DMAEMA to the dextran backbone, respectively. Afterwards, six layers of PSS as polyanion and PAH as polycation were consecutively deposited, by centrifugation technique onto the synthesized microgels, as depicted in Figure 2.58a. The zeta-potential measurements confirmed the incorporation of both MAA and DMAEMA charged groups, and also the PSS and PAH layers onto the microgels, as can be seen in Figure 2.58b. In the case of MAA and PSS, negative zeta-potential was observed, while in case of DMAEMA and PAH, positive zeta-potential was measured, which were in agreement with the expected values. Besides, it was proven that the coating could also be performed on neutral microgels, and the driving force, which were hydrophobic interactions and physical entanglements, were strong enough to keep the layers in place (De Geest et al., 2006).

(a)

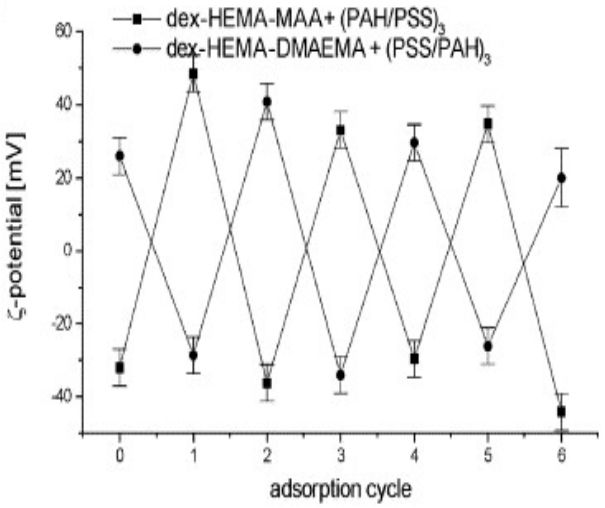

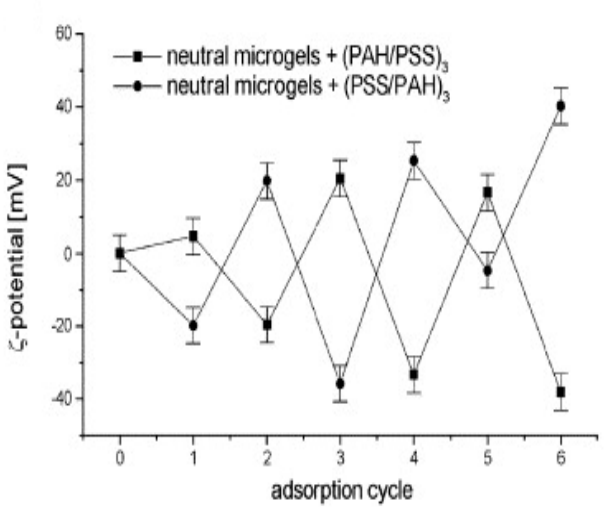

(b)

Figure 2.58 Zeta-potential vs. the layer number, during the layer-by-layer coating of (a) positively and negatively charged microgels, and (b) neutral microgels (n=5) (De Geest et al., 2006).

By means of confocal microscopy, they (De Geest et al., 2006) concluded that only the oppositely charged polyelectrolytes were able to migrate into the microgels during the layer-by-layer coating. They also illustrated that the microgels wall was pH-dependent, and it was more permeable at pH=7 than at pH=9. Moreover, by increasing the number of polyelectrolyte layers the microgels became more impermeable at pH=7, as well as more mechanically stable. As can be seen in Figure 2.59, a burst release of the encapsulated material from uncoated microgels did not occur when microgels were coated; in other words, the coated microgels demonstrated slower release profile in comparison to the uncoated microgels and the majority of the release in the coated microgel occurred in a few hours, which further confirmed the pulsatile release of the encapsulated material in this case (De Geest et al., 2006). Figure 2.60 describes the process of layer-by-layer coating the microgels, and ruptured of the layer aonce the swelling pressure reached the critical value, the point in which cross-linked could no longer hold the microgels together.

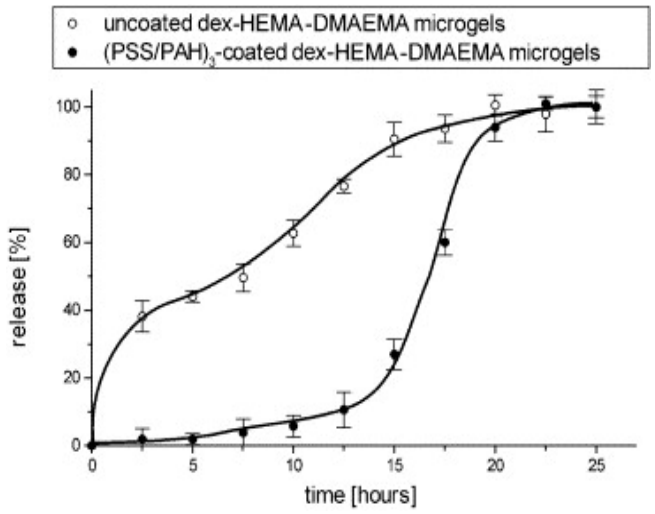

Figure 2.59 Release of the encapsulated material from (open circle) uncoated microgels, (closed circle) coated positively charged microgels (De Geest et al., 2006).

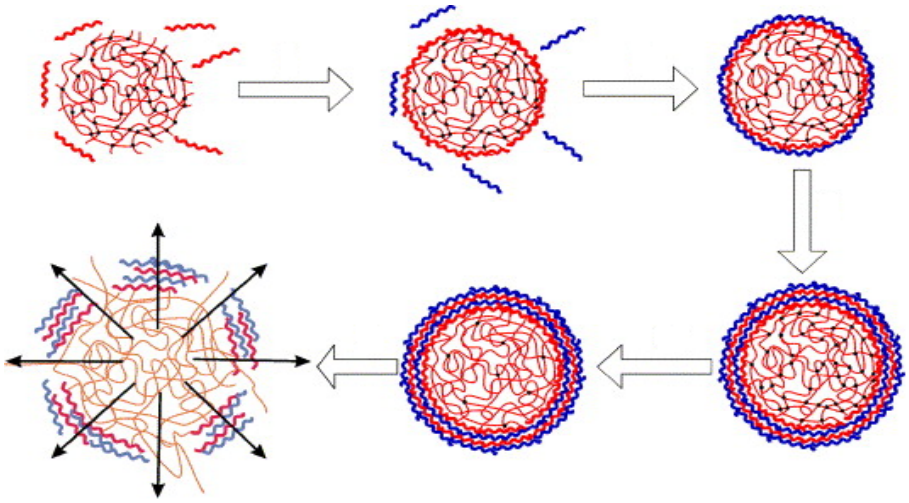

Figure 2.60 Schematic of the sequential adsorption of oppositely charged polyelectrolytes onto the degradable microgels. Degradation occurred by hydrolysis of the cross-links and reduction in cross-links density. Layers ruptured when the swelling pressure of the microgels reached a critical value (De Geest et al., 2006).

Chapter 3

Characterization Techniques

3.1 Laser Light Scattering

The incident light is scattered in all directions by each illuminated particle, when a coherent light is focused on a dilute colloidal solution, where the solvent molecules and colloidal particles have different refractive indices. The scattered lights from different particles are captured in a photomultiplier tube, and generate a net scattering intensity *I(t)* or photon counts *n(t)*. Ideally, under condition that all the particles are stationary, the scattered light intensity in each direction is independent of time and would be constant (Chu, 1970). Conversely, in reality, all the particles are under Brownian motion, which leads to instability of the intensity pattern on the detection plane and if the detection area is sufficiently small it causes fluctuation in *I(t)*. The fluctuation rate depends on different relaxation process, such as translational diffusion, rotational diffusion and internal motion of the particles. The faster the relaxation is, the faster the fluctuation is going to be. In general, laser light scattering (LLS) could be classified as follow (Chu, 1970):

1. Inelastic light scattering: raman, fluorescence and phosphorescence,
2. Elastic light scattering: no absorption.

However, in the field of polymers and colloids, light scattering is usually referred to as static light scattering (elastic) and dynamic (quasi-elastic) light scattering measurements. Static light scattering (SLS) measures the time-average intensity, and this method is a classic and absolute

analytical technique that has been widely applied to characterize both synthetic and natural macromolecules (Chu, 1970). The static light scattering determines the parameters, such as molar mass or weight-average (M_w), second virial coefficient (A_2), z-average radius of gyration or RMS radius (R_g), and particles structure. Dynamic light scattering (DLS) measures the intensity fluctuation over a very short period of time (μs). The reason why dynamic light scattering is also named quasi-elastic is as follows. Because of the Doppler Effect the detected frequency of the incident light that scatters from moving particles will be slightly higher or lower than the detected frequency of the original incident light, depending on whether the particles move towards or away from the detector (HUGLIN, 1977). Therefore, the frequency distribution of the scattered light is slightly broader that the incident light. The frequency augmentation (~ 10^5- 10^7 Hz) is so small in contrast to the incident light frequency (~ 10^{15} Hz) that it is very difficult to detect it in the frequency domain. Accordingly, dynamic light scattering is sometimes referring to as photon correlation spectroscopy (PCS) (HUGLIN, 1977). From dynamic light scattering, parameters such as translation diffusion coefficient (D_T) hydrodynamic radius or stokes radius (R_h), polydispersity, and particles size distribution can be obtained.

In summary, dynamic light scattering collects the fluctuation in the scattered intensity and applied them to determine the autocorrelation function. Then, from the decay of the autocorrelation function the diffusion coefficient is measured. Light scattering measurements were analyzed by the Stokes-Einstein Equation to obtain hydrodynamic radius (R_h):

$$R_h = \frac{k_B\, T}{6\, \pi \eta\, D_T}$$

R_h: Hydrodynamic radius particles.

k_B : Boltzmann's constant,

T: Absolute temperature,

η: Viscosity of the continuous phase,

D_T: Diffusion coefficient for the colloid,

3.2 Isothermal Titration Calorimetry

Isothermal titration calorimetry (ITC) is an appropriate instrument to study the thermodynamic properties of colloidal systems such as: enthalpy (ΔH), entropy (ΔS), heat capacity (C_p), and Gibbs free energy (ΔG). The schematic diagram of ITC is shown in Figure 3.1. ITC consists of 3 major components: sample cell, syringe, and reference cell. The sample cell is filled with the sample solution, while the syringe containing a titrant (ligand) that is injected over a specific time period into the sample cell under continuous stirring (http://www.med.yale.edu/wmkeck/biophysics/VP_ITC_MANUAL_11_20_02a.pdf).

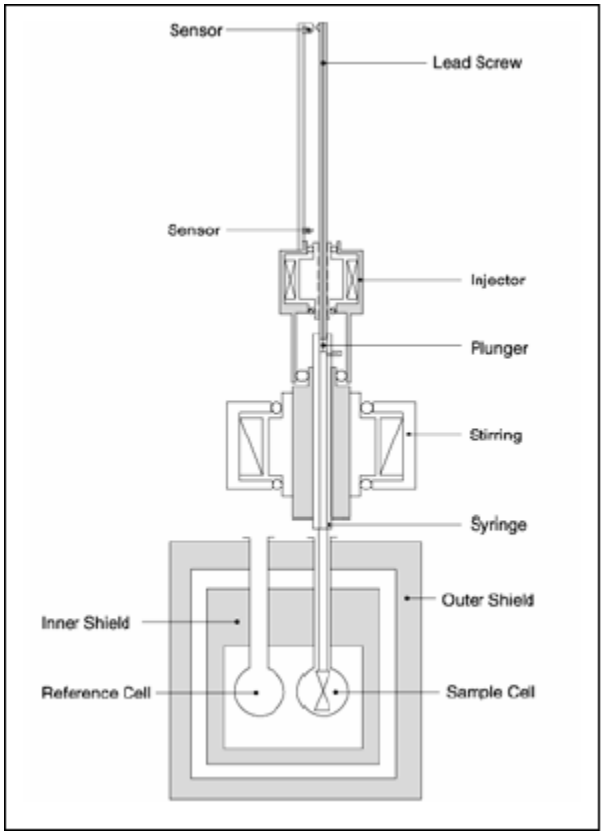

Figure 3.1 Schematic diagram of Isothermal Calorimetry (ITC).

(http://www.med.yale.edu/wmkeck/biophysics/VP_ITC_MANUAL_11_20_02a.pdf)

ITC measures the heat exchange between two systems when specific amount of reactants are added. In other words, ITC measures the temperature difference between the sample and reference cell and converts it into units of power known as the differential power (DP). This power is needed to maintain the reference and sample cell at the same temperature by exchanging the heat between them which is associated to either an exothermic or endothermic process The former one occur when the sample cell is hotter than the reference cell and this causes the DP to deflect in the negative direction, while the latter deflects the DP in the positive direction as a result of hotter reference cell compare to sample cell. The degree of binding and interaction occuring between ligand (in syringe) and colloidal solution (in sample cell) is directly

proportional to the amount of heat that causes the exothermic or endothermic process. The ΔH of interactions can be calculated by integrating the DP peaks with respect to time.

3.3 Differential Scanning Calorimetry

Differential scanning calorimetry (DSC) is a precise instrument to study thermal transition of colloidal systems. Like ITC, DSC consists of a sample and reference cell. The temperature difference between sample and reference cells, during heating or cooling of the sample cell at the constant heating or cooling rate, is measured and correlated into the units of power known as differential power (DP). The exothermic reaction occurs when the sample cell is hotter that the reference cell and this causes the DP to deflect in the negative direction, likewise, the endothermic reaction deflects the DP in the positive direction as a result of hotter reference cell compare to sample cell.

3.4 Zeta-Potential Analyzer

Zeta potential analyzer is an instrument that measures the electrophoretic mobility and zeta potential of the colloidal system to verify colloidal stability and ensure that the ionic functional groups were incorporated into the nanogel during copolymerization. Electrophoresis is defined as the motion of charged colloidal particle towards the oppositely charged electrode when subjected to a uniform electric field. The equation to measure electrophoresis mobility is as follow:

$$\mu_e = \frac{q}{6\pi\eta r}$$

μ_e: Electrophoresis mobility,

q: Charge on the colloidal particle

η: Solution viscosity

r: Particle radius

As illustrated in Figure 3.2, by dispersing colloidal particles into a solution, an electrical double layer formed around the particle between the charged particle and the solution medium, as a result of the presence of counter ions. The inner layer associated to the particle that contains counter ion is known as the Stern layer, while the outer layer contains mobile ions and is known as diffuse layer. The loss of counterions from the diffuse layer induces a charge at the slipping plane. Zeta potential is a potential difference at the slipping plane when a voltage is applied to the colloidal solution. In this experiment a Laser Doppler Eelctrophoresis (LDE) is used to track the movement of charged particles. When light is scattered form a moving particle, its frequency is shifted depending on the velocity and direction of the movement. The velocity at which the charged colloidal particle moves toward the oppositely charged electrode is proportional to the zeta potential.

Since colloidal systems, especially nanogels, have a large ratio of surface area to volume the electrical double layer is more apparent in these systems. The zeta potential value of -30 to 30 mV means that the system is electrically unstable and may lead to aggregation. On the other hand, zeta potential greater than -30, +30 is considered as stable system. The higher the zeta potential, the greater is colloidal stability.

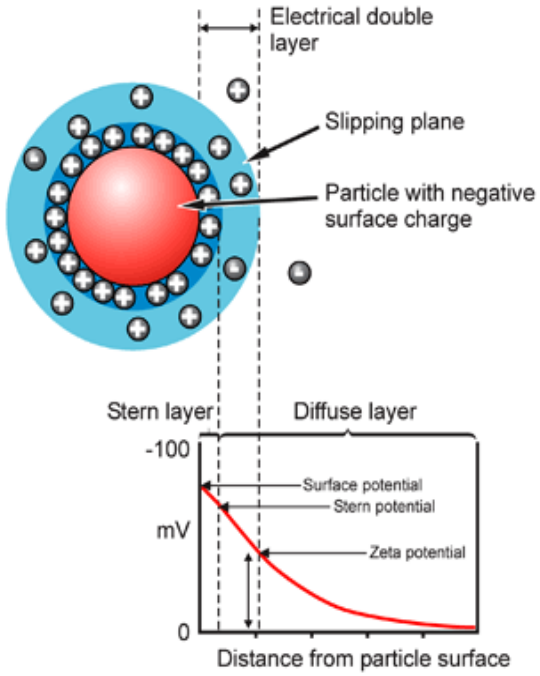

Figure 3.2 Schematic diagram of zeta potential and electrical double layer (http://www.malvern.com/LabEng/technology/zeta_potential/zeta_potential_LDE.htm).

Zeta-potential may be calculated from the following equation using either the Huckel or Smoluchowski approximation of 1 or 1.5 respectively for Henry's Function $f\,(k_a)$:

$$\zeta = \frac{3\eta\mu_e}{2\varepsilon f(k_a)}$$

η: Solution viscosity

μ_e: Electrophoresis mobility

ε: Sample dielectric constant

$f(ka)$: Henrys' function, (k: inverse of Debye length, a: particle radius)

3.5 Potentiometric and Conductometric Titration

Potentiometric and conductometric titrations were performed to provide further insight into the ionization and neutralization degree of nanogels; besides, the exact acid and base composition of nanogels can be determined. Simultaneous measurements of pH and conductivity were performed using a Metrohm 809 Titrando autotitrator. All experiments were conducted in a closed jacked vessel, where the temperature was maintained at 25 ^{o}C under continuous stirring. By gradually titrating acid or base into the system, the pH can shift from a range of 2-11. From the pH and conductivity curves the actual mole percent of monomer segments used during the course of polymerization can be calculated based on the method developed by Homola and James (Homola and James, 1977).

3.6 High-Gradient Magnetic Separation

High-gradient magnetic separator (HGMS) recovers and separates the magnetic nanoparticles as a result of their unique magnetic properties. This instrument possesses a column filled with magnetically prone wires, fine-grade stainless steel wool; and placed between the poles of the electromagnets. During the process, the magnetic field is set at 2 T (Sondjaja et al., 2009). Figure 3.3 illustrates the common technique to use high gradient magnetic separator.

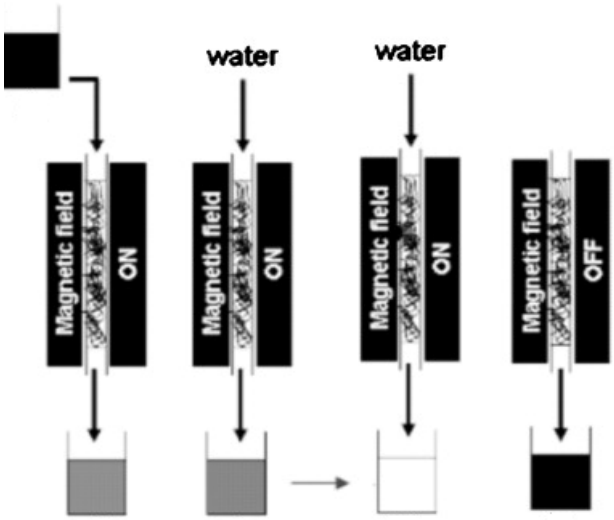

Figure 3.3 Schematic describing the HGMS. The magnetic fluid after sonication (a) is passed through the column while the electromagnet is on, (b) immediate collection of non-magnetic particles, then water passed through the column with turn on electromagnet, which washed-out non-magnetic particles, (c) the non-magnetic particles are collected, and washing continues until the effluent is clear like in (d), and (e) the electromagnet is turned off and by introducing water the captured magnetic nanoparticles are collected (Sondjaja et al., 2009).

The role of the wires is to generate a strong field gradient, which is required for capturing the magnetic nanoparticles, around the wire surface by dehomogenizing the applied magnetic field. The force applied on magnetic nanoparticles from this instrument not only depends on the gradient of the magnetic field but also depends on the size of the particles. This relationship can be seen according to the following equation (Ditsch et al., 2005):

$$F = -\mu_0 V M \nabla \boldsymbol{H}$$

Where, V is the volume of the magnetic nanoparticles, and M is the magnetization of the magnetic nanoparticles in the given magnetic field, $\boldsymbol{H}$. It has been confirmed theoretically and

experimentally that small individual magnetic nanoparticles can overcome the magnetic attraction forces to the wires, due to diffusional and drag forces (Ditsch et al., 2005; Sondjaja et al., 2009). Therefore, the capture of individual magnetic nanoparticles cannot effectively occur through high gradient magnetic separation; however, small cluster of magnetic nanoparticles, larger than 50 nm, can be efficientlycaptured by a high gradient magnetic separation process (Ditsch et al., 2005; Sondjaja et al., 2009).

Chapter 4

Drug Selective Membrane Electrode

4.1 Experimental Setup

A PrHy selective membrane electrode was used as a drug selective electrode to measure the PrHy concentration by measuring the electromotive force relative to an *Ag/AgCl* reference electrode. The experimental setup used in this study consisted of a 4-channel ion analyzer, a reference electrode, the ion selective electrode, an electrode cap, and drug selective membrane.

As illustrated in Figure 4.1, the 4-channel ion analyzer completes the circuit, along with the reference electrode and the ion selective electrode. The ion selective electrode and a membrane cap were both handmade at the University of Waterloo machine shop, as will be discussed later in this chapter. The material used for membrane can be either polyvinyl chloride or Teflon. On the tip of the membrane cap, an ion selective membrane is attached. The solution inside of the membrane cap is 10^{-3} M procaine hydrochloride (PrHy) in a 10^{-2} M *NaCl* solution. This cap completes the electrochemical cell, which is made up of two solutions with the same active ion (in this case PrHy) and a salt bridge.

The reference electrode is also based on a silver chloride (*AgCl*) construction. It is made up of an inner wire coated with *AgC*l, as well as inner and outer filling solutions, shown in Figure 4.1. The filling solution is usually saturated potassium chloride (*KCl*) or sodium chloride (*NaCl*). Saturated solutions are used because the concentration stays constant with changing temperature,

and it minimizes the effect of evaporation, purchased from Research Solution & Resources LLC. When working with ion selective electrodes, the ion selective membrane takes the place of the salt bridge, and is selective only to the target drug. As a result, it forms the basis for the entire experiment, since a potential difference builds up across the membrane.

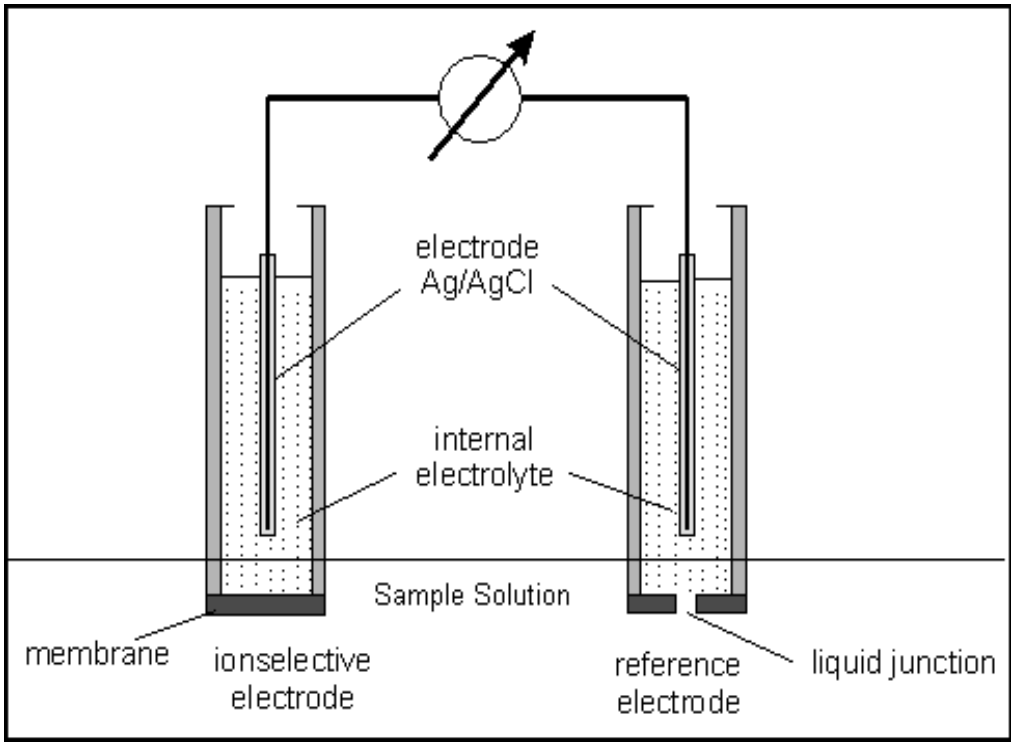

Figure 4.1 Schematic diagram of ion-selective electrode setup.

(http://www.chemistry.nmsu.edu/Instrumentation/IS_Electrod.html)

4.2 Background Reviews

Drug-selective electrodes are the subdivision of ion-selective electrodes, which are electrochemical sensors that are capable of potentiometric determination of the activity of specific ions in the presence of other ions. They become one of the most important and simple techniques for fast, precise, and low cost analysis. The main progress in the history of ion-selective electrode has occurred over the last one hundred years (Rong, 2001). Gibbs in 1875,

Arrhenius in 1887, Nernst in 1888-1889, Oswald and Planck in 1890 proposed many concepts such as diffusion potential, potential difference, and ion mobility through their relevant studies on the properties of semi-permeable membrane, thermodynamic relationships for membrane equilibrium, and the theory of electrolyte solutions. The achievement of all these early works was the birth of membrane electrochemistry (Rong, 2001).

Ion-selective electrodes can be categorized based on the nature of the basic membrane material. The crucial criterion is that the membrane remains as immiscible as possible with respect to the bathing solution and solid contacts. Therefore, ion-selective electrodes can be classified into four major groups (Vytras, 1989):

- Solid-state membrane electrode
- Liquid (plastic) ion-selective electrodes
- Glass membrane electrodes
- Electrodes with proper additional membrane

The most common type of ion-selective electrodes is the pH electrode. It utilizes a hydrogen ion H^+ selective glass electrode, which only allows H^+ ions to pass through, to record the H^+ according to the electromotive force (EMF). When the pH electrode is immersed in H^+ ions containing the solution, the external ions will diffuse through the membrane until equilibrium is reached between the external and internal concentration. The number of hydrogen ions in the bulk solution is proportional to a buildup of charge inside the membrane.

Ion-selective electrode responds selectively to the activity of ions in solution rather than their concentration. The electrode can be directly used for concentration determination, if the

relationship between the activity and concentration can be fixed through adding a constant concentration of an inert electrolyte to the samples in order to swamp out minor variations in the sample concentration. The ion-selective electrode should perfectly respond according to the Nernst equation (Rong, 2001):

$$E_{Cell} = \Delta E^{o} \pm \frac{RT}{zF} \ln a_i$$

ΔE^{o} : The standard potential of the cell containing an *i*-selective electrode and an ion *i*

a_i : The activity of ion *i*

z : The charge number of *i*,

R : Tthe universal gas constant (8.314) in J$mol^{-1}K^{-1}$

T : The temperature in K

F : The Faraday constant (96485) in Cmol^{-1}

The sign ($\pm$): When *i* is a cation, the sign is taken as positive and when it is anion the sign is taken as negative.

The drug selective electrode consists of four major parts:

1) Electrode body,

2) Inner reference electrode *Ag/AgBr*

3) Tip or end cap

4) Polymeric membrane

The silver bromide is used to coat the inner reference electrode, *Ag/AgBr* by electrolysis. In this process the silver rod was immersed in a 100 ml of 1 M *NaBr* solution for 20 minutes, in which the silver rod acts as anode and *Pt* electrode acts as the cathode. Although most of the pharmacopoeias illustrate precise techniques for analytical control, many of them are lengthy and difficult (Stefan et al., 1996). The development of membrane electrode over the past decade offers interesting advantages such as simple operation, fast response, reasonable selectivity, low cost, low detection limit, wide linear concentration range, excellent accuracy, applicability to color, turbid solution, and possible interfacing with automated and computerized system (Al Attas, 2009b; Alizadeh and Mehdipour, 2002; Frag et al., 2010; Morf et al., 2007; Shahrokhian et al., 2002; Stefan et al., 1996; Zayed et al., 2006). In addition, these electrodes can be easily fabricated in a variety of shapes and sizes, and they are less affected by the response of biological substrates, such as proteins, enzymes, and antibodies (Alizadeh and Mehdipour, 2002).

There are some disadvantages associated with electrode membrane including extensive pre-conditioning treatment, care in storage, ionic strength of the solution sensitivity to some hydrophobic counter-ions, and relatively short life-time (Alizadeh and Mehdipour, 2002; Frag et al., 2010). The formation ability of drug ions with the ion exchanger determines the potentiometric performance of the electrode. Primary amines, among other form of amines, usually present the slightest affinity to form such ion-associates causing poor response (Katsu et al., 1999).

The drug selective membrane were mostly fabricated from a liquid plasticized poly (vinyl-chloride) (PVC), which are based on a water insoluble ion-pair complex acting as an ion

exchanger (Alizadeh and Mehdipour, 2002; Frag et al., 2010). In other words, these electrodes can be made by conjugating any of the ion-exchangers or neutral-sequestering agents within a liquid plasticized PVC matrix, and they can be employed as a very practical tool for clinical, chemical, environmental analyses (Al Attas, 2009b). Applying modified PVC consisting of ionic end groups as ion exchange sites along with a plasticizer, gradually resolved many of the disadvantages and problems associated with the electrode membrane. The modified PVC prevents the dissolution of the ion-exchanger and the plasticizer yields membrane with a longer life-time (Alizadeh and Mehdipour, 2002).

In the current study, drug selective electrode consisting of procaine hydrochloride (PrHy) membrane was used to selectively determine the drug release from different nanogels. Drug release is commonly studied by many different analytical techniques including high performance liquid chromatography (HPLC), capillary zone electrophoresis, and UV-spectrometry.

In addition, most of these techniques require sophisticated instruments, and they involve time-consuming procedures, and also they cannot be automated (Al Attas, 2009b; Alizadeh and Mehdipour, 2002; Frag et al., 2010). Moreover, in all of these techniques, a dialysis membrane or centrifugal machine is needed to isolate the nanogels or nanoparticles from free drugs before the measurements are conducted. Both dialysis and centrifugation methods will affect the determination of free drug concentration, in the former released drugs may be absorbed onto the dialysis membrane surface, as the dialysis membrane acts as a diffusion barrier that restricts the accurate measurement of drugs release into the solution. Thus, the drug release profile measured the diffusion of drugs from the dialysis membrane rather than the diffusion of drugs from the drug carrier. In the latter, the high centrifugal forces can force additional drugs to be released

from the carrier (Tan et al., 2007). In UV spectrophotometry, the results could not be obtained in real time and also a limited number of data points can be acquired. With the ion-selective electrode method, electromotive force readings can be recorded during the course of actual drug release study (as frequently as every 2 seconds). In addition, the concentration of the released drug can be directly measured, without requiring any intermediate steps such as the use of dialysis membrane or centrifugation.

Selectivity and qualified response for the primary and specific ion over other interfering ions in the solution is the major characteristic of a drug selective membrane electrode. The effects of inorganic cations like Na^{+}, K^{+}, Ca^{2+}, and Mg^{2+}, on the drug selective electrode was examined by several research groups. Alizadeh and Mehdipour (Alizadeh and Mehdipour, 2002) used the Mixed Solution Method (MSM), while Frag et al. and Katsu et al. employed Separate Solution Method (SSM) (Al Attas, 2009a; Frag et al., 2010; Katsu et al., 1999) to determine the selectivity coefficients (K_{ij}) according to the Nikolsky equation (Alizadeh and Mehdipour, 2002; Frag et al., 2010; Katsu et al., 1999):

$$K_{ij}C_j^{Z_i/Z_j} = \left[\exp\left\{\frac{E_j - E_i}{RT/Z_iF}\right\}\right] - C_i$$

E_i : the potential measurements of the drug ion *i*

E_j : the potential measurements of interfering ion *j*

Z_i : the charge of drug ion *i*

Z_j : the charge of interfering ion *j*

C_i : the concentration of the drug ion *i*

C_j : the concentration of interfering ion j

In order to obtain the selectivity coefficient, the EMF values of desired solution, PrHy, in varying concentration of interfering ions were measured; afterwards, the slope of a grah $\left[\exp\left\{\frac{E_j - E_i}{RT/Z_iF}\right\}\right] - C_i$ versus $C_j^{Z_i/Z_j}$ was used to determine the selectivity coefficient (K_{ij}) (Alizadeh and Mehdipour, 2002; Frag et al., 2010; Katsu et al., 1999).

Alizade et al., Frag et al. and Katsu et al. (Alizadeh and Mehdipour, 2002; Frag et al., 2010; Katsu et al., 1999) they all reported the similar trends, that is the selectivity coefficient for monovalent cations and divalent cations were in the range of 10^{-3} and 10^{-4}, respectively. Because of the differences in ionic size of these common cations and consequently their motilities and permeability, the presence of these cations in solution will not influence the effectiveness of the drug selective electrode (Alizadeh and Mehdipour, 2002; Frag et al., 2010). Therefore, the sensitivity of the membrane can be enhanced by the incorporation of ion-exchanger. The optimum amount of ion-exchanger will convey added stability and also provide more electroactive site carriers for the efficient transfer of ions (Alizadeh and Mehdipour, 2002; Katsu et al., 1999).

The effect of pH on the drug selective electrode was also investigated by several research groups. As shown in Figure 4.2, Alizade et al. (Alizadeh and Mehdipour, 2002) reported that the EMF values of ketamine hydrochloride electrode stayed constant over the pH range of 4 to 8.5. The same trend was also observed by Tan et al. (Tan et al., 2007; Tan et al., 2008b) and Frag et al. (Frag et al., 2010) regarding procaine hydrochloride electrode and naphazoline hydrochloride electrode, respectively. The former was reported to have a stable EMF over the pH range of 3 to

8.5, while the latter one was constant over pH value of 3 to 8. The significant reduction in EMF at high pH values is due to high concentration of deprotonated ketamine. On the other hand, at low pH values, the EMF increased because of large amounts of H^+ ions which cause high ionic interference (Alizadeh and Mehdipour, 2002).

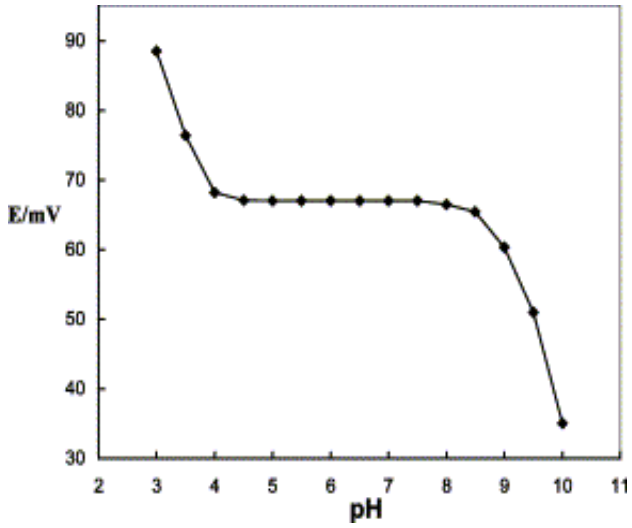

Figure 4.2 The effect of pH on the potential of the ketamine electrode, which is stable over pH range of 4 to 8.5 (Alizadeh and Mehdipour, 2002).

For potentiometric studies with ion-selective electrode, it is necessary to determine the EMF of a cell. The cell has two solutions separated by the membrane and the reference electrode in the following order (Tan et al., 2008b):

Inner *Ag/AgBr* reference electrode (2)	Internal solution (II)	Drug selective electrode	Test solution (I)	*Ag/AgCl* reference electrode (1)

The drug-selective electrodes in this study were connected to the Ion Analyzer instrument that permits the collection of data, which will be plotted as the cell electromotive force (EMF) vs. time. According to the Nernst equation, the potential of the cell in terms of concentration when the drug-selective electrode is immersed in a test solution is expressed as follow:

$$E_{Cell} = {E^o}_{Cell} \pm \frac{RT}{zF} \ln C_{Drug} = {E^o}_{Cell} \pm \frac{2.303\,RT}{zF} \log C_{Drug}$$

Therefore, by plotting E_{Cell} versus log C_{Drug} the drug concentration can be obtained according to the following equation:

$$E_{Cell} = intercept \pm (slope) \times (logC_{Drug})$$

4.3 Preparation of Drug Selective Membrane

Since the membrane is a very crucial part of the Ion Selective Electrode, the preparation methods of the membrane become critical. Drug selective membranes are commonly prepared by incorporating a suitable ion-exchanger and solvent mediator into a poly (vinyl chloride) (PVC) membrane matrix.

Carboxylated polyvinyl chloride and procaine hydrochloride were both purchased from Sigma-Aldrich Chemical Co. Tetrahydrofuran was obtained from Merck. Poly (ethylene-co-vinyl acetate-co-carbon monoxide) as a polymeric plasticizer and solvent mediator was purchased from Acros Organic. NaTPB as an ion-exhcanger was purchased from Sigma-Aldrich. The following technique with some modifications was obtained from Tan et al. (Tan et al., 2007; Tan et al., 2008b).

The first step in the membrane preparation process was to form the carboxylated polyvinyl chloride (PVC) and procaine hydrochloride (PrHy) complex. The driving force for the formation

of this complex is the electrostatic attractions between drug and carboxylated PVC. The formation of drug complex was performed by separately dissolving 0.5 g carboxylated PVC in 30 ml tetrahydrofuran (THF) and 0.955 g of PrHy in 90 ml THF and 10 ml of distilled de-ionized water. Once these solutions were dissolved separately, they were combined and allowed to stir for 48 hours. This drug complex was then precipitated in 1 L of distilled de-ionized water by steadily adding it to the water using a column. The precipitate was then filtered using a 20–25 μm filter paper and washed repeatedly with distilled de-ionized water and dried at room temperature (Tan et al., 2007; Tan et al., 2008b).

The next step involved formation of drug selective membrane by dissolving an optimum relative amount of the drug complex precipitate, polymeric plasticizer and NaTPB in 30 ml of THF. One particular recipe was used throughout the entire project, where 0.18 g of polymeric plasticizer, poly (ethylene-co-vinyl acetate-co-carbon monoxide) (PE-co-PVA-co-CO), 0.114 g of carboxylated PVC-PrHy drug complex precipitate and 0.006 g of sodium tetraphenylborate (NaTPB) were dissolved in THF. Once all the components dissolved in THF over a month, it was filtered through a glass wool using a glass funnel, a vacuum pump and a Buchner flask. The dissolved plasticizer filtered through the glass wool while the un-dissolved particles did not. Afterwards, the obtained liquid membrane was poured into a petri dish and the THF evaporated after 2-3 days, controlled evaporation at 25 °C was conducted, which formed the uniform membrane. Finally, circular disks were cut out of the membrane and adhered to the PVC or Teflon ion selective electrode caps using THF (Tan et al., 2007; Tan et al., 2008b). The membrane was then calibrated and a stability test of the membrane was done.

4.4 Manufacturing Drug Selective Electrode

As described in Figure 4.3, the drug ion selective electrode possesses four main components: electrode body, inner *Ag/AgB*r reference electrode, end cap, and drug membrane. By means of electrolysis for 20 minutes in a 100 ml of 1 M *NaBr* the silver rod was coated with silver bromide to form the inner *Ag/AgBr* reference electrode. Through electrolysis the silver rod act as anode, while the platinum electrode act as cathode (Tan and Tam, 2007; Tan et al., 2007; Tan et al., 2008b).

The previously prepared drug membrane was cut and adhered onto the contact end area of the Teflon end cap tip by THF. After the THF was evaporated, the end cap was being filled with de-ionized water in order to check leakages of the tip with drug membrane. Then, the dried end cap with drug membrane was placed in closed container and stored in a refrigerator and kept away from the light. Prior to use, the PrHy membrane was placed in a 0.01 M PrHy solution for 15 minutes (Frag et al., 2010).

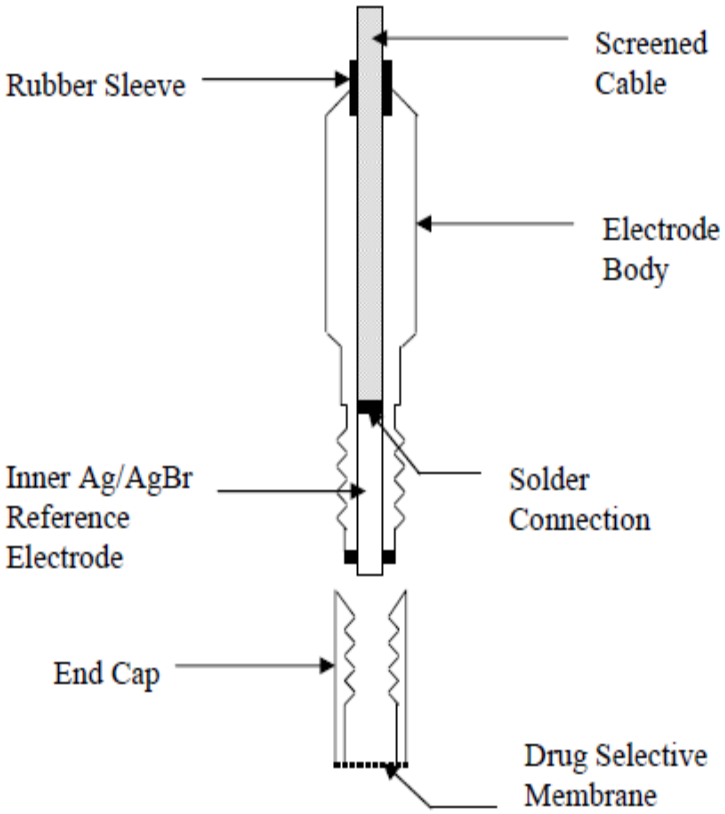

Figure 4.3 Schematic diagram of all the components of a drug selective electrode (Tan, 2007).

Chapter 5

Material and Experimental Techniques

5.1 Introduction

In this chapter the experimental technique used to synthesize various series of polyampholyte nanogels, which are the cross-linked polymeric particles that possessed both positive and negative charges on their backbone. These polyampholyte nanogels were synthesized by both emulsion polymerization and inverse emulsion polymerization. The techniques were correspondingly adopted from Tan et al. (Tan et al., 2006; Tan et al., 2007), and Ho et al. (Ho et al., 2008) with some modifications.

5.2 Cross-linked MAA-DEAEMA Nanogels

5.2.1 Materials

2 (di-ethylamino) ethyl methacrylate (DEAEMA, 99%), and methacrylic acid (MAA, 99%) were both used as monomers. Ethylene glycol dimethacrylate (EGDMA, 98%) was used as the cross-linking agent, and poly (ethylene glycol) methyl ether methacrylate (PEGMEMA, M_n 300 Da) was used as macromonomer, i.e., steric stabilizer. All of the above materials were purchased from Sigma-Aldrich, and were passed through a basic alumina column for purification and inhibitors removal. Anionic surfactant dioctyl sulfosuccinate sodium salt (Aerosol OT, 96%) was purchase from Sigma-Aldrich. Sodium persulfate as an initiator was purchased from Acros Organics, and sodium bicarbonate was obtained from Fisher Scientific to act as a buffer. They

both were used as received. 2-sulfoethyl methacrylate, which acts as a stabilizing agent was purchase from Scientific Polymer Products. De-ionized water was obtained throughout experiments from Millipore Milli-Q purification system equipped with a 0.22 μm filter, and has a resistivity of 18.2 μ.Ω.cm.

5.2.2 Synthesis Approach

Polyampholyte nanogels of methacrylic acid (MAA) and 2 (di-ethylamino) ethyl methacrylate (DEAEMA) cross-linked with ethylene glycol dimethacrylate (EGDMA) were synthesized through a conventional semi-continuous emulsion polymerization, and this technique was discussed in detail in section 2.3.1, and the synthetic procedure is represented in Figure 5.1. This technique was adopted from Tan et al. with some modifications (Tan et al., 2006). First of all, the 75% surfactant solution comprising of 15 g of Aerosol OT in mixture of 19 ml de-ionized water and 1 ml acetone was prepared. In order to obtain nanogels comprising of 60 mol% MAA, 40 mol%, and 4 wt% EGDMA, the monomer mixture consisting of 13 g MAA, 19 g DEAEMA, 1.13 g EGDMA, and 60 ml de-ionized water was added into the 250 ml beaker equipped with overhead stirrer at 250 rpm. Then, 41.5 g of a 75% solution of Aerosol OT was prepared and homogenized. An initiator solution was prepared by dissolving 0.5 g of sodium persulfate and 0.15 g of sodium bicarbonate in 5 ml previously N_2-purged de-ionized water. In another 4 ml N_2-purged de-ionized water 1 g of sodium persulfate was dissolved to form the initial catalyst solution.

Afterward, 280 ml of de-ionized water, 0.3 g of 2-sulfoethyl methacrylate, and 41.5 g of 75% solution of Aerosol OT surfactant (excess amount of surfactant above the CMC) were charged into the 500 ml three neck flask. Subsequently, the flask was placed on the hotplate and equipped

with condenser, magnetic stirrer operating at 400 rpm (the stirrer speed was adjusted to a level when a slight vortex on the surface of the liquid was evident), and under continuous N_2 purge. After 30 minutes of heating the reactor at 80 ^{o}C, and the observation of clear solution which indicate micelle formation, 10 wt% of the monomer mixture, about 12.5 g, together with the catalyst solution was added to the reactor to initiate the reaction. Once the initial monomers had reacted for 1 hour to form in situ seed products, the remaining monomer and initiator mixtures were injected into the reaction flask by means of syringe pump over two hours under continuous N_2 purge and stirring, the solution turned milky-white within 20 min of monomer mixture injection. 15 minutes before the addition of monomer and initiator mixture was completed, 10 g of PEGMEMA (20 wt% of total feed monomer) was poured into the flask to provide steric stabilization through free radical grafting reaction. Finally, the reaction was allowed to proceed for another two hours in order to consume the residual monomers. A stirred cell was used to filter the obtained nanogels through a 0.1 μm filter. Subsequently, the nanogels were dialyzed in de-ionized water using regenerated cellulose tubular membrane (M_w cut-off of 12,000-14,000 Da) over two weeks and the water was replaced every 2-3 days after checking the conductivity (Tan et al., 2006). The dialysis process was conducted to remove the excess surfactant, initiator, unreacted monomers, and any homopolymer of PEGMA, which may have formed during grafting reactions. The final nanogels were about 10% (9.96%) by weight. We observed that the nanogels remained stable over a year.

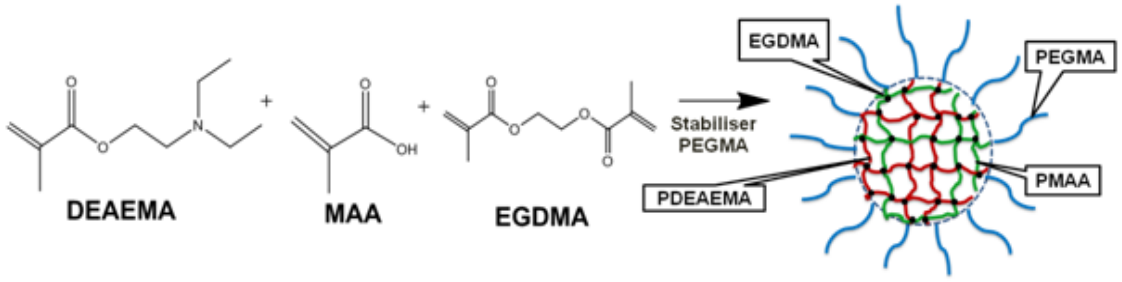

Figure 5.1 Sterically stabilized cross-linked MAA-DEAEMA nanogels.

5.3 Cross-linked MAA-DMAEMA Nanogels

5.3.1 Materials

2 (di-methylamino) ethyl methacrylate (DMAEMA, 98%), and methacrylic acid (MAA, 99%) were both used as monomer. Ethylene glycol dimethacrylate (EGDMA, 98%) was used as cross-linking agent, and poly (ethylene glycol) methyl ether methacrylate (PEGMEMA, M_n~300 Da) was used as macromonomer i.e., steric stabilizer. All of the mentioned above materials were purchased from Sigma-Aldrich, and were passed through a basic alumina column for purification and inhibitors removal. Non-ionic surfactants polyoxyethylene (2) oleyl ether (Brij 92V, HLB~4.9) and polyoxyethylene (10) oleyl ether (Brij 96V, HLB~12.4) were provided from Sigma-Aldrich and Fluka, respectively. Sodium persulfate as an initiator was purchased from Acros Organics. *n*-hexane was purchased from university chem-store. De-ionized water was obtained throughout experiments from Millipore Milli-Q purification system equipped with a 0.22 μm filter, and has a resistivity of 18.2 μ.Ω.cm.

5.3.2 Synthesis Approach

Polyampholyte nanogels of methacrylic acid (MAA) and 2 (di-methylamino) ethyl methacrylate (DMAEMA) cross-linked with ethylene glycol dimethacrylate (EGDMA) were synthesized

through an inverse emulsion polymerization. This technique was discussed in detail in section 2.3.2, and the synthetic procedure is represented in Figure 5.2. Firstly, a non-ionic surfactant mixture was prepared by mixing 14.7 g of Brij 92 and 4.4 g of Brij 96. The combined HLB is this system is ~ 7 corresponding to a phase inversion temperature of around 65 ^{o}C. This surfactant mixture was added to a 150 ml of *n*-hexane in a 500 ml three neck flask and homogenized for 30 min (Ho et al., 2008). Meanwhile, 1.72 g of MAA, 12.56 g of DMAEMA, and 0.45 g EGDMA was mixed in 150 ml of de-ionized water in a glass beaker to form a monomer mixture, in order to obtain nanogels consisting of 20 mol% PMAA, 80 mol% PDMAEMA, and 2 wt% EGDMA.

In a typical procedure for synthesis of nanogels, the monomer mixture was added to the previously homogenized surfactant mixture. The final mixture was placed on the hotplate and equipped with a condenser, a magnetic stirrer performing at 400 rpm (adjust the stirrer speed to a level when you see a slight vortex on the surface of the liquid), continuous N_2 purge, and the temperature was raised to 65 ^{o}C. Afterwards, 0.45 g of sodium persulfate was dissolved in 8 ml of de-ionized water to form initiator solution. After one hour of reaction, the initiator mixture was added to the reaction vessel to start the polymerization. The second initiator mixture comprising of 0.15 g sodium persulfate in 3 ml de-ionized water together with 5.3 g of PEGMA was added to the reaction vessel after the reaction was proceed for two hours to perform the free radical grafting reaction. Finally, the reaction was allowed to proceed for another three hours. In order to remove the hexane, the hot reaction mixture was poured into a rotary evaporator and hexane was removed under vacuum. The resulting thick nanogels sample were diluted in de-ionized water and redispersed under vigorous shaking. The obtained nanogels were dialyzed in de-ionized water using regenerated cellulose tubular membrane (M_w cut-off of 12,000-14,000

Da) over two weeks and the water was replaced every 2-3 days after checking the conductivity (Ho et al., 2008). The dialysis process was conducted to remove the excess surfactant, initiator, unreacted monomers, and any homopolymer of PEGMA that may have formed during grafting reaction. The final nanogels were about 6% (6.34%) by weight. We observed that the nanogels remained stable over a year.

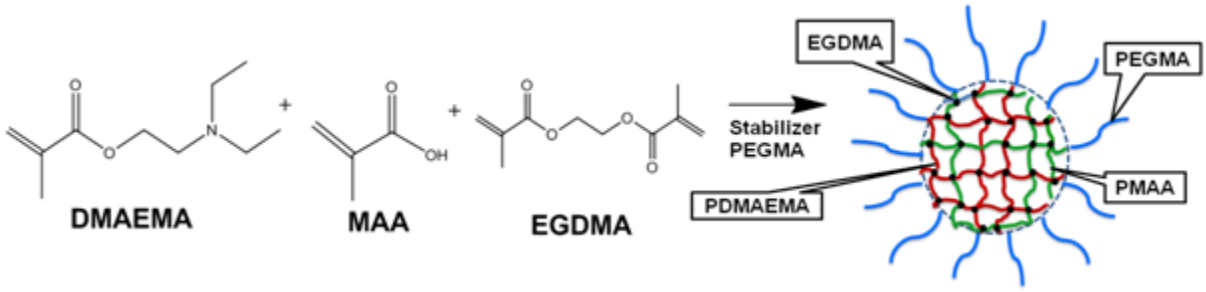

Figure 5.2 Sterically stabilized cross-linked MAA-DMAEMA nanogels.

Moreover, to compare the result of sterically stabilized nanogels and also to observe the effect of PEGMA on nanogels stabilization, unstable nanogels were also synthesized through the same technique without the addition of PEGMA at the end of the reaction.

5.4 Cross-linked EA-MAA Nanogel Coated with DMAEMA and MAA

5.4.1 Materials

Ethyl acrylate (EA, 99.50%) was purchased from Acros Organic. 2 (di-ethylamino) ethyl methacrylate (DEAEMA, 99%), and methacrylic acid (MAA, 99%) were both used as monomer, di-allyl phthalate (DAP, 99%) was used as cross-linking agent, poly (ethylene glycol) methyl ether methacrylate (PEGMEMA, M_n 300 Da) was used as macromonomer, i.e., steric stabilizer. All of the above materials were purchased from Sigma-Aldrich, and were passed through a basic alumina column for purification and inhibitors removal. Anionic surfactant dioctyl

sulfosuccinate sodium salt (Aerosol OT, 96%) was purchased from Sigma-Aldrich. Sodium persulfate as an initiator was purchased from Acros Organics, and sodium bicarbonate was provided from Fisher Scientific to act as a buffer. They both were used as received. 2-sulfoethyl methacrylate as a stabilizing agent was purchased from Scientific Polymer Products. De-ionized water was obtained throughout experiments from Millipore Milli-Q purification system equipped with a 0.22 μm filter, and has a resistivity of 18.2 μ.Ω.cm.

5.4.2 Synthesis Approach

As illustrated in Figure 5.3, EA-MAA nanogels coated with DEAEMA and MAA were prepared through sequential addition of DEAEMA and MAA onto the EA-MAA nanogels. EA-MAA mixture consisting of 1 g Aerosol OT, 0.33 g MAA, 0.4 g EA, 0.04 g DAP and 4 ml de-ionized water used as seed formation solution was prepared. In another container DEAEMA solution comprising of 5 g of 75% solution of Aerosol OT, 6.5 g of DEAEMA, 0.2 g of DAP was introduced into 6 ml of de-ionized water. In a third container MAA solution including 5 g of 75% solution of Aerosol OT, 4 g of MAA, 0.2 g of DAP in 6 ml of de-ionized water was prepared. Two initiator mixtures both comprising of 0.4 g of sodium persulfate, 0.015 g of sodium bicarbonate, and 5 ml of nitrogen-purged de-ionized water were prepared. A catalyst solution including 0.4 g of sodium persulfate dissolved in 5 ml of nitrogen-purged de-ionized water.

In the first step, 0.4 g of 75% solution of Aerosol OT along with 40 ml de-ionized water and 0.05 g 2-sulfoethyl methacrylate were charged into a 100 ml 3-neck flask equipped with a condenser and magnetic stirrer. Under a nitrogen purge, the reactor was heated to 70 ^{o}C and after 30 minutes the EA-MAA solution was added. Subsequently the catalyst solution was introduced

to the reactor to initiate the in-situ seed formation. After 30 minutes, the DEAEMA solution along with one of the initiator solutions was conveyed into the reactor by syringe pump over one hour, while the reaction mixture was under continuous nitrogen purge. During this stage a white-milky solution was formed corresponding to nanogels formation. After one hour interval, *NaOH* was added to maintain the pH level in the basic range (pH of 8-9) before adding the MAA solution. Next, the MAA mixture together with initiator solution was conveyed into the reactor through syringe pump over 1 hour. 1.2 ml PEGMA was introduced to the reactor over 15 minutes before the MAA solution was completely reacted, in order to ensure the grafting of the stabilizer onto the surface of nanogels to provide steric stabilization to the system. Lastly, the reaction was left to proceed for another hour to react residual monomers.

The obtained nanogels were dialyzed in de-ionized water using regenerated cellulose tubular membrane (M_w cut-off of 12,000-14,000 Da) over two weeks and the water was replaced every 2-3 days after checking the conductivity. The dialysis process was conducted to remove the excess surfactant, initiator, unreacted monomers, and any homopolymer of PEGMA that may have formed during grafting reaction. The final nanogels were about 12% (12.83%) by weight. We observed that the nanogels remained stable over a year.

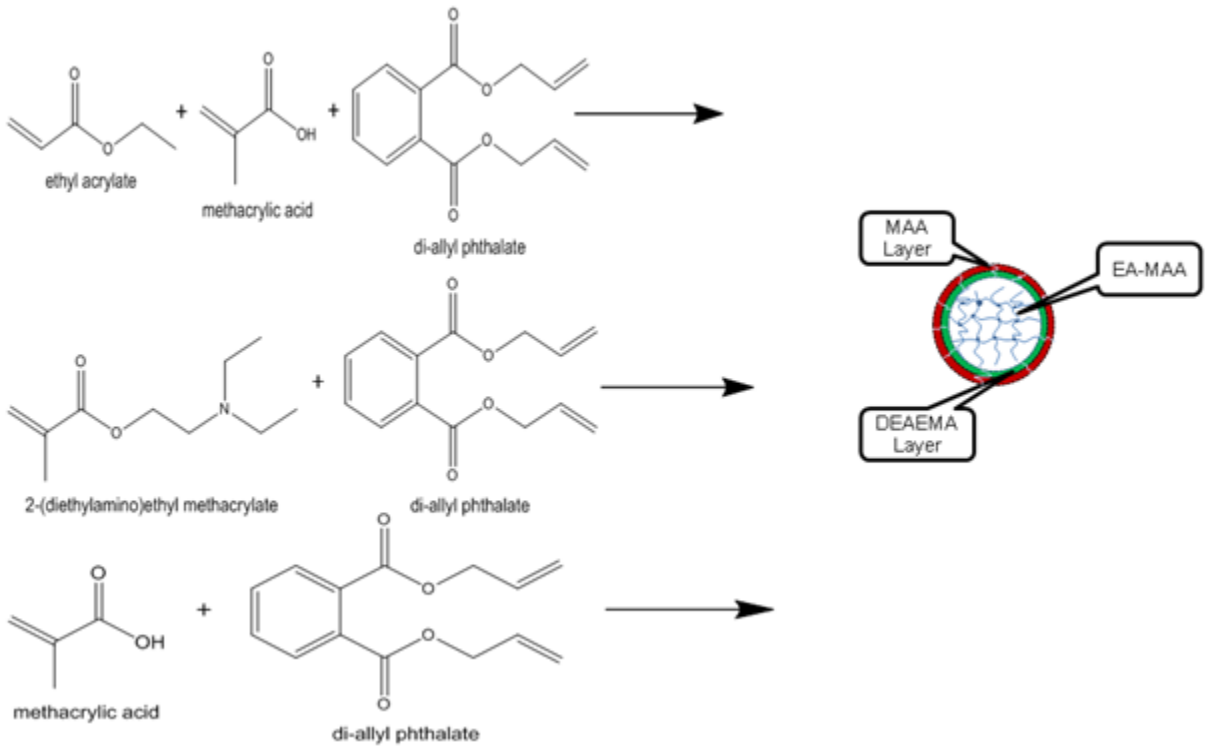

Figure 5.3 Cross-linked EA-MAA nanogels coated with DEAEMA and MAA.

5.5 Cross-linked EA-MAA Nanogels Coated with MAA and DEAEMA

5.5.1 Materials

Ethyl acrylate (EA, 99.50%) was purchased from Acros Organic. 2 (di-ethylamino) ethyl methacrylate (DEAEMA, 99%), and methacrylic acid (MAA, 99%) were both used as monomer, di-allyl phthalate (DAP, 99%) was used as cross-linking agent, poly (ethylene glycol) methyl ether methacrylate (PEGMEMA, M_n 300 Da) was used as macromonomer, i.e., steric stabilizer. All of the mentioned above materials were purchased from Sigma-Aldrich, and were passed through a basic alumina column for purification and inhibitors removal. Anionic surfactant dioctyl sulfosuccinate sodium salt (Aerosol OT, 96%) was purchased from Sigma-Aldrich. Sodium persulfate as an initiator was purchased from Acros Organics, and sodium bicarbonate

was provided from Fisher Scientific to act as a buffer. They both were used as received. 2-sulfoethyl methacrylate as a stabilizing agent was purchased from Scientific Polymer Products. De-ionized water was obtained throughout experiments from Millipore Milli-Q purification system equipped with a 0.22 μm filter, and has a resistivity of 18.2 μ.Ω.cm.

5.5.2 Synthesis Approach

As illustrated in Figure 5.5, EA-MAA nanogels coated with MAA and DEAEMA were prepared through sequential addition of DEAEMA and MAA onto the EA-MAA nanogels. EA-MAA mixture consisting of 1 g Aerosol OT, 0.33 g MAA, 0.4 g EA, 0.04 g DAPand 4 ml de-ionized water used as seed formation solution was prepared. In another container DEAEMA solution comprising of 5 g of 75% solution of Aerosol OT, 6.5 g of DEAEMA, 0.2 g of DAP was introduced into 6 ml of de-ionized water. In a third container MAA solution including 5 g of 75% solution of Aerosol OT, 4 g of MAA, 0.2 g of DAP in 6 ml of de-ionized water were prepared. Two initiator mixtures comprising of 0.4 g of sodium persulfate, 0.015 g of sodium bicarbonate, and 5 ml of nitrogen-purged de-ionized water were prepared. A catalyst solution including 0.4 g of sodium persulfate dissolved in 5 ml of nitrogen-purged de-ionized water.

In the first step, 0.4 g of 75% solution of Aerosol OT along with 40 ml de-ionized water and 0.05 g 2-sulfoethyl methacrylate were charged into a 100 ml 3-neck flask equipped with a condenser and magnetic stirrer. Under a nitrogen purge, the reactor was heated to 70 ^{o}C after 30 minutes the EA-MAA solution was added. Subsequently, the catalyst solution was introduced to the reactor to initiate the in-situ seed formation. After 30 minutes the MAA mixture along with one of the initiator solutions was conveyed into the reactor by means of syringe pump over one hour, while the reaction mixture was under continuous nitrogen purge. After one hour interval,

NaOH was added to keep the pH level high before MAA solution was introduced. Next, the MAA mixture together with initiator solution was conveyed into the reactor through syringe pump over 1 hour. The 1.2 ml PEGMA was introduced into the reactor over 15 minutes before the DEAEMA solution was completely reacted, in order to ensure the grafting of the stabilizer onto the surface of nanogels to provide steric stabilization to the system. Lastly, the reaction was left to proceed for another hour to react residual monomers.

The obtained nanogels were dialyzed in de-ionized water using regenerated cellulose tubular membrane (M_w cut-off of 12,000-14,000 Da) over two weeks and the water was replaced every 2-3 days after checking the conductivity. The dialysis process was conducted to remove the excess surfactant, initiator, unreacted monomers, and any homopolymers of PEGMA, which may have formed during grafting reactions. The final nanogels were about 12% (12.20%) by weight. We observed that the nanogels remained stable over a year.

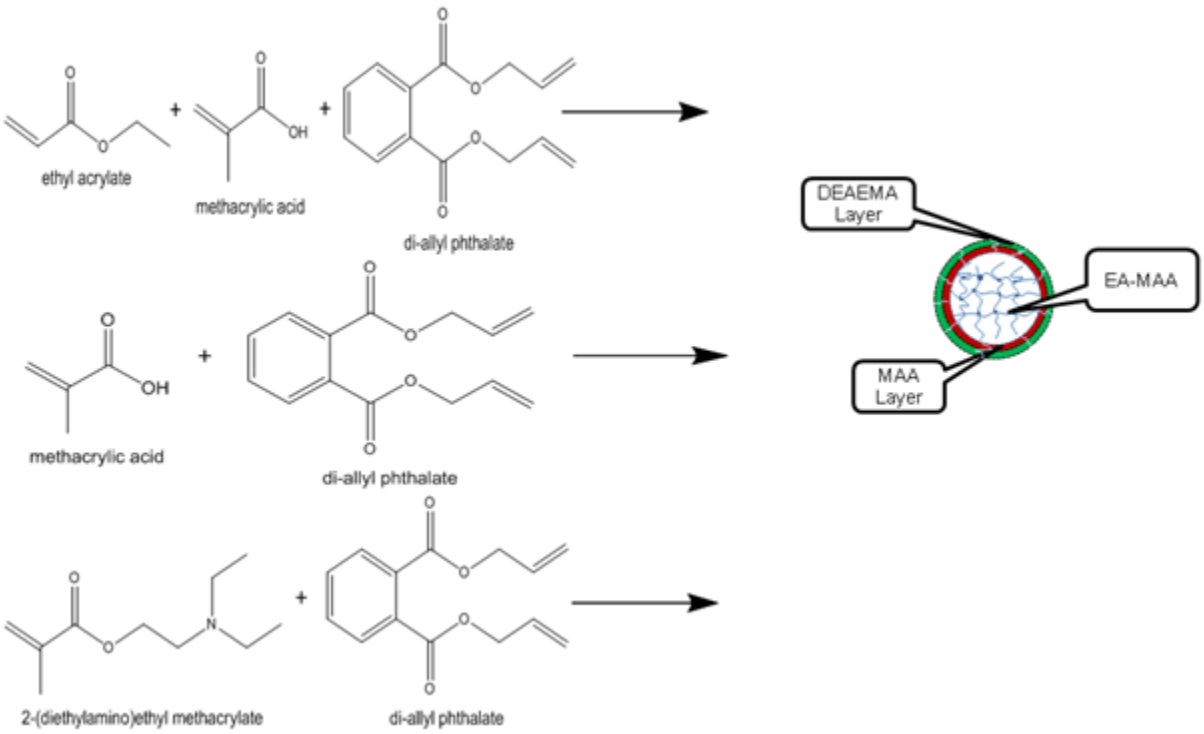

Figure 5.4 Cross-linked EA-MAA nanogels coated with DEAEMA and MAA.

Chapter 6

Characterization of MAAA-DEAEMA Nanogels

6.1 Introduction

As described earlier in section 2.4, various kinds of colloidal carriers have been reported for their applications in the field of drug delivery. Among all of the candidates, polyampholyte nanogels were chosen for the present study. Polyampholyte nanogels are known as cross-linked polymer particles whose constituent polymers possess both positive and negative charges on their backbone, which makes them capable of swelling at both high and low pH in a good solvent. The pH responsive behavior is the primary reason for synthesizing polyampholyte nanogels. As mentioned before in section 5.2.2, the amphoteric nanogels were synthesized via a semi-continuous emulsion polymerization. Then, their swelling behavior and zeta-potential were examined as a function of pH. From the potentiometric titration experiment, the exact molar ratios of MAA and DEAEMA segments were determined, which were very close to the feed molar ratio. Moreover, isothermal titration calorimetry was employed to study nanogels and procaine hydrochloride (PrHy) interaction. Besides, the temperature sensitivity of the nanogels was also studied using the differential scanning calorimetry.

6.2 Characterization of MAA-DEAEMA Nanogels

The pH and conductivity curves were obtained simultaneously by means of the Metrohm 809 Titrando autotitrator. This instrument is programmable through the Tiamo software to titrate

microliter amounts of the titrants. All experiments were performed in a closed jacketed vessel with temperature maintained at 25 ^{o}C by a water bath, and the solution was stirred with a magnetic stirrer throughout the experiment. Initially, 0.1 M *NaOH* was added to increase the pH of the 0.1 wt% nanogels to 11. Subsequently, the sample was titrated with 0.1 M *HCl* and both the pH and conductivity were measured until the pH reached a value of 2. The actual molar ratio of MAA and DEAEMA in the nanogels was confirmed by plotting the pH and conductivity curves versus concentration of *HCl*.

As illustrated in Figure 6.1, three transition points on the pH and conductivity curves were observed signifying the presence of amino and carboxylic acid groups on the nanogels. On the conductivity curve, the transition points were measured by the change in slope (inflexion points); while, on the pH curve the transition points were determined at intersection of vertical lines with the pH curve. These transition points on the pH curve were observed at pH values of 9.6, 7.9, and 3.7. The transition points on the conductivity curve exhibited four different regions. Beginning from far left of this graph, the first region before point 1 represents the neutralization of the excess amounts of *NaOH* in the nanogel solution. The first transition point at pH=9.6 corresponds to the start of the protonation of $(N\,(CH_3CH_2)_2)$ groups to $(N\,(CH_3CH_2)_2\,H^+)$ on the DEAEMA segments.

The second region indicates the protonation of $(N\,(CH_3CH_2)_2\,H^+)$ groups to $(N\,(CH_3CH_2)_2\,H^+)$ on the DEAEMA segments. The third transition point associates with completion of the protonation of COO^- groups on the MAA segments. The third region corresponds to the completion of protonation COO^-groups to *COOH* on the MAA segments. Lastly, the fourth region demonstrates the excess amount of *HCl* present in the nanogels system. In addition, there was a

change in the clarity of nanogel solution during the titration process from clear at high pH values to cloudy and milky at moderate pH and slightly cloudy and milky at low pH values. The actual molar ratio of MAA to DEAEMA was determined by applying the Homola and James method (Homola and James, 1977). According to this technique, the feed monomer mole percent of 60% MAA and 40% DEAEMA was close to the amount of actual composition of M_{MAA}: M_{DEAEMA} = 56:44. In the other words, the monomers in the system effectively participated in the polymerization.

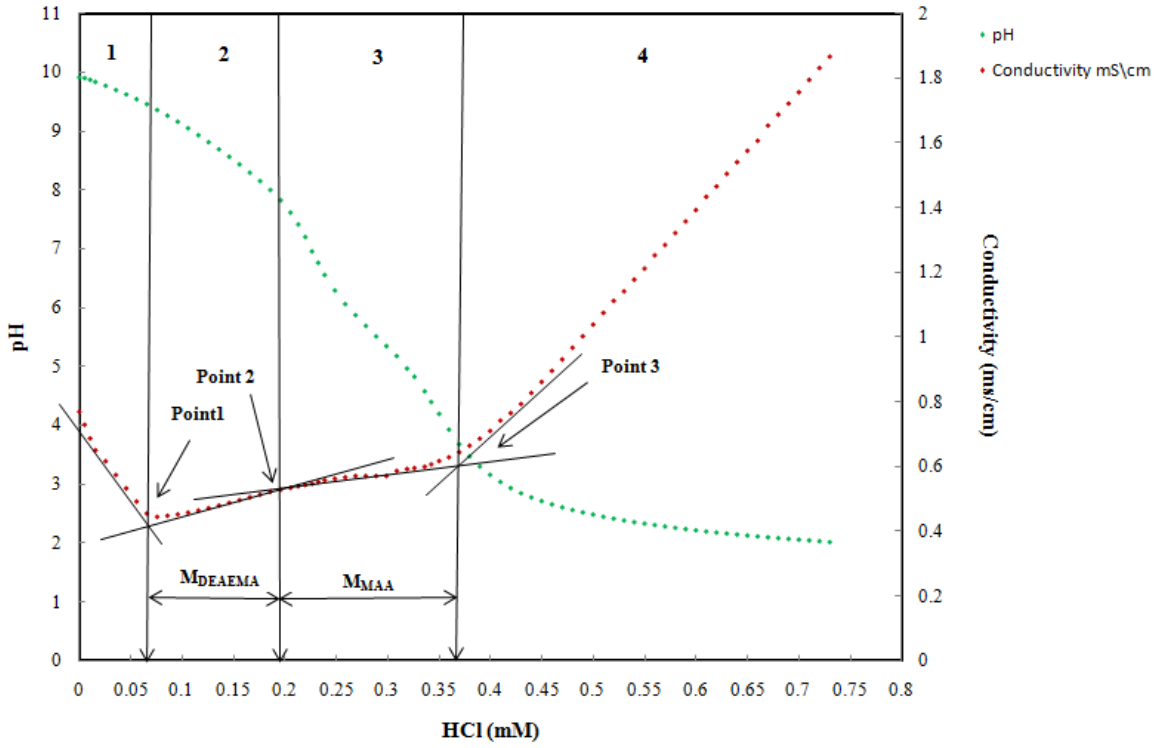

Figure 6.1 pH and conductivity titration curves for 0.1 wt% MAA-DEAEMA nanogels.

The dynamic light scattering and zeta potential measurements were conducted to determine the hydrodynamic radius (R_h), and electrophoretic mobility as a function of pH for 0.1 wt% polyampholyte nanogel sample at 25 ^{o}C, respectively. During the course of these two

experiments, the samples were allowed to equilibrate for 20 minutes to set the temperature before any measurements were performed. The refractive index, the dielectric constant and the dynamic viscosity of the dispersion medium were assumed to be similar to pure water for the calculation of the mobility, due to the dilute solution, soft, porous, and solvent-permeable structure of the nanogels.

Figure 6.2 shows the hydrodynamic radius (R_h), and electrophoretic mobility of nanogels without the addition of the PEGMA as a stabilizer; while, Figure 6.3 shows the hydrodynamic radius (R_h), and electrophoretic mobility of sterically stabilized nanogels by PEGMA. For dynamic light scattering measurement, nanogel samples with concentration of 0.1 wt% at different pH values were prepared, and the measurements were conducted at 25^{o}C and the laser wavelength was 636 nm.

A similar trend of swelling was observed for both nanogels system at high and low pH; however, at neutral pH or at isoelectric point (IEP) two distinct behaviors were observed: particle size of sterically stabilized nanogels was reduced at this pH, while particle size of unstabilized nanogels was increased dramatically. This phenomenon is associated with the fact that at the IEP, almost equal number of positive and negative charges is present in the nanogel; therefore, due to overall charge neutralization nanogels that induce the aggregation of the nanogels to form larger aggregates with as evident from Figure 6.2. Conversely, in Figure 6.3 aggregation at IEP was prevented due to the steric hindrance provided by grafted steric stabilizer on the MAA-DEAEMA nanogels. Due to the smaller repulsive force, more compact and smaller nanogels were observed.

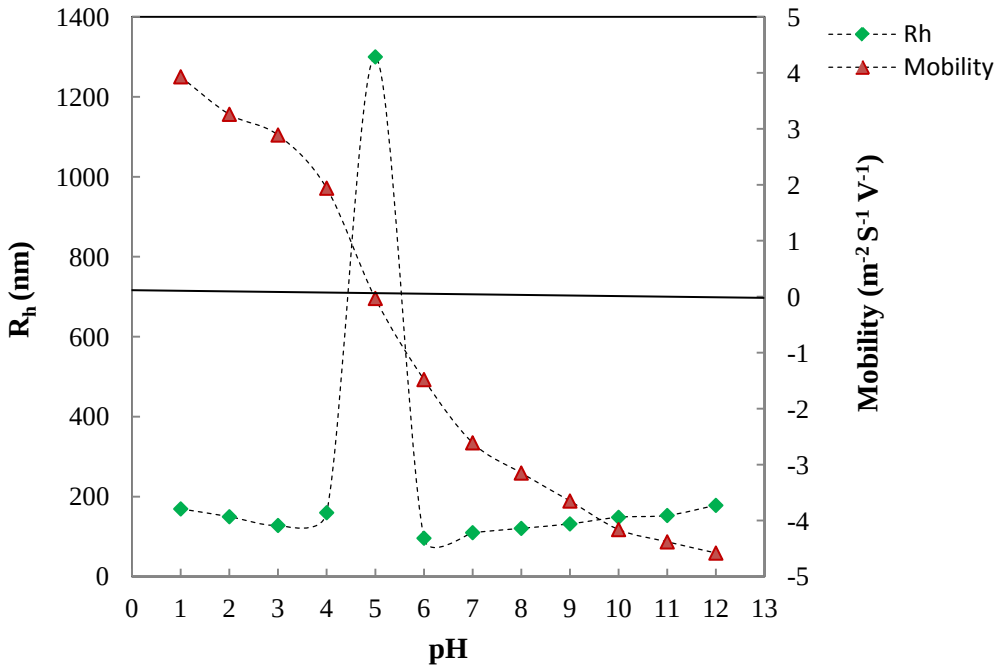

Figure 6.2 Profiles of the hydrodynamic radius (R_h), and the electrophoretic mobility of 0.1 wt% MAA-DEAEMA nanogels without steric stabilizer (PEGMA) as a function of pH at 25 ^{o}C.

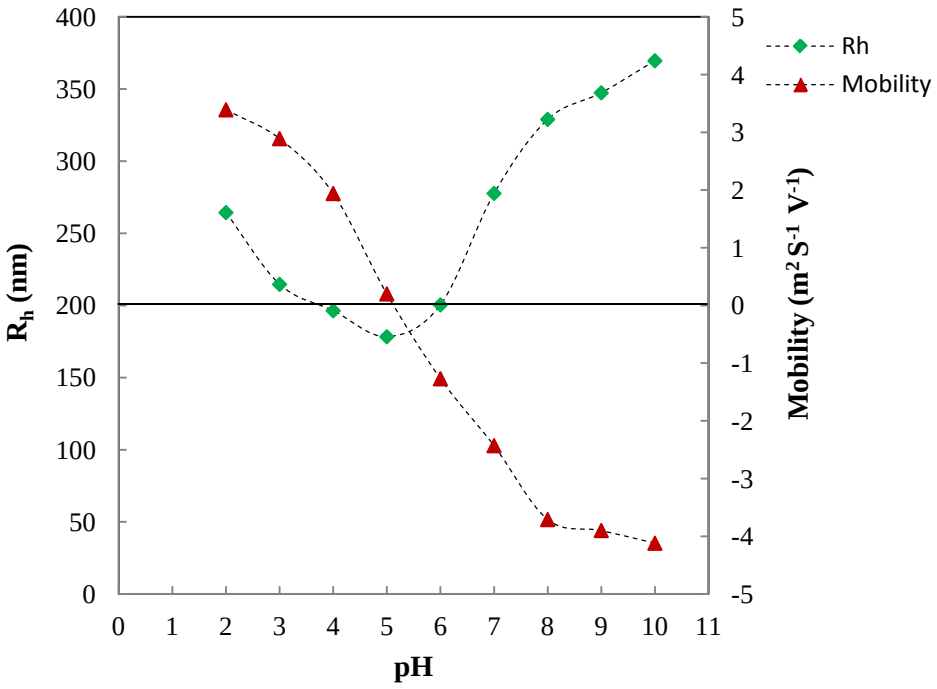

Figure 6.3 Profiles of the hydrodynamic radius (R_h), and the electrophoretic mobility of 0.1 wt% MAA-DEAEMA nanogels with steric stabilizer (PEGMA) as a function of pH at 25 ^oC.

As illustrated on the left hand side of Figure 6.4, at low pH, the *N* $(CH_3CH_2)_2$ groups on the DEAEMA segments in the nanogels were positively charged and fully protonated. This enhanced the intra-molecule Coulombic repulsive force between positively charge $(N\ (CH_3CH_2)_2\ H^+)$ groups on the DEAEMA segments, and also increased the osmotic pressure due to the counter-ion present in the nanogels matrix, which consequently induced the swelling of nanogels, and increased the size of nanogels as shown in Figure 6.4. As the pH was increased, the amount of positively charged $(N\ (CH_3CH_2)_2\ H^+)$ groups on the DEAEMA segments start to decrease; reducing osmotic pressure associated with deprotonation of DEAEMA segments, and nanogels size start to decrease. This reduction in size continued until the IEP, where the amount of positive $(N\ (CH_3CH_2)_2\ H^+)$ groups and negative COO^- were identical. As the pH was

increased over IEP, the gradual swelling in nanogels was observed, which was due to the increased osmotic pressure as a result of trapped counter-ions within the nanogels. In addition, at high pH *COOH* groups on MAA segments became negatively charged because of the deprotonation of carboxylic groups. Consequently, the intra-molecule Coulombic repulsive force between COO^- groups induced the swelling of nanogels.

The electrophoretic mobility values as illustrated in Figure 6.3, corresponded to the zeta-potential of the nanogels, which further confirmed the above results. This data demonstrated the highest electrophoretic mobility values at both low and high pH since the nanogels possessed $(N(CH_3CH_2)_2H^+)$ groups and COO^- groups, respectively. In other words, by increasing the pH from 2, the electrophoretic mobility gradually decreased due to the deprotonation of DEAEMA segments; whereas, the curve reaches zero at IEP (pH=6-6.5), since all the positive and negative charges neutralized each other. By further increasing the pH from IEP; not only the electrophoretic mobility increased gradually, but also its value shifted to a negative value. The latter corresponded to the deprotonaiton of *COOH* groups on the MAA segments.

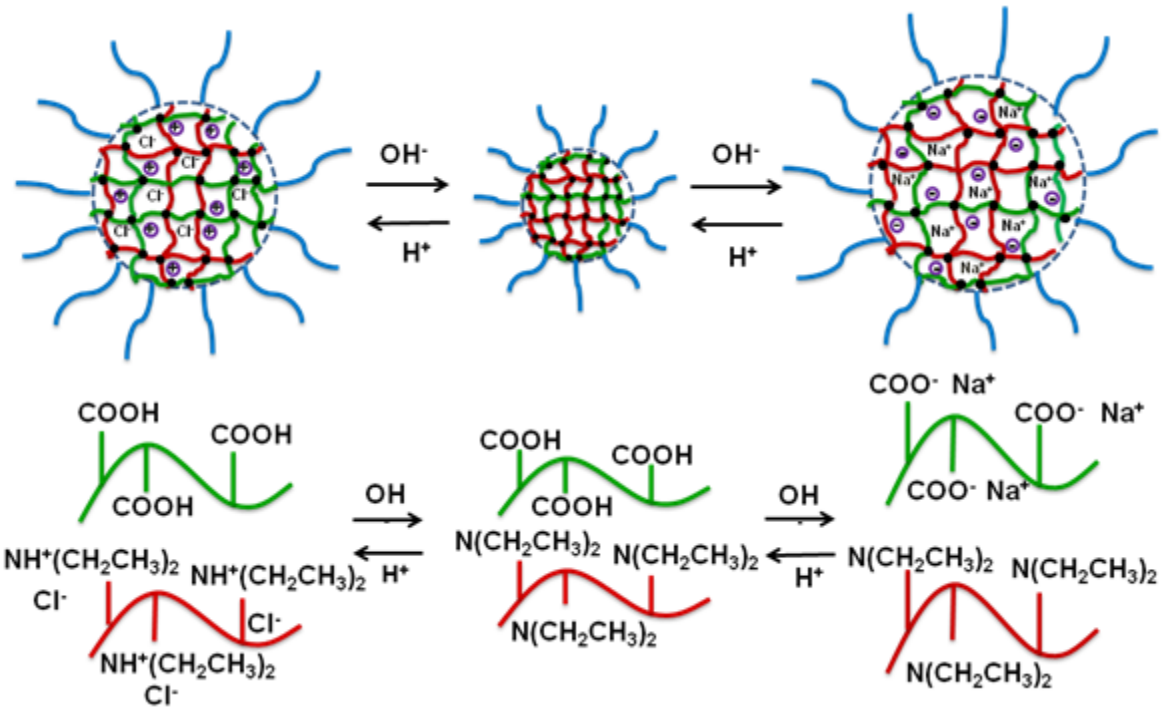

Figure 6.4 Schematic of pH-responsive behavior of MAA-DEAEMA nanogels.

From Figure 6.3 a higher value for both hydrodynamic radius and zeta potential can be observed for high pH value comparison to the lower one. This can be attributed to the higher amount of *COOH* groups in the nanogels feed monomer compared to the amount of -*N* $(CH_3CH_2)_2$ groups, 60% and 40% respectively. Besides, zeta potential analyzer is only capable of measuring the charges on the surface of the particle, hence the lower positive zeta-potential values can also be associated to the fact that some of the surface -*N* $(CH_3CH_2)_2$ groups took part in the PEGMA grafting reaction. In addition, different IEP shown in Figure 6.2 and Figure 6.3 can be a result of different synthetic conditions, errors during light scattering, and zeta potential measurements.

Figure 6.5 depicts several photographs of 0.1 wt% MAA-DEAEMA nanogels, further confirming the effect of PEGMA on the stability of nanogels, by presenting the difference in solution transmittance at IEP under conditions of nanogels without PEGMA and nanogels with

PEGMA. It can be seen that in both conditions, the nanogels demonstrated enhanced hydrophilic behavior in aqueous media at both high and low pH. In the former condition, when PEGMA was not grafted onto the nanogels, they aggregated and became very cloudy and as indicated by the milky solution at IEP. On the other hand, in latter condition, where PEGMA was grafted onto the nanogels, they became more stable and hydrophilic in aqueous media due to the steric hindrance provided by PEGMA, and the solution became clearer.

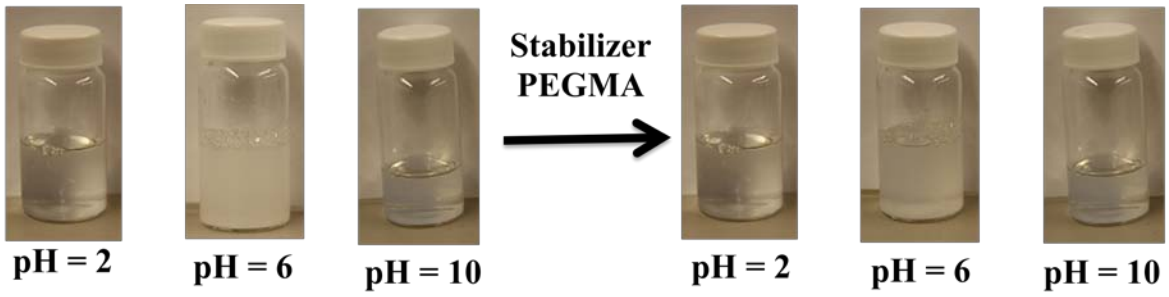

Figure 6.5 Photographs of 0.1 wt% MAA-DEAEMA nanogels with and without PEGMA stabilizer.

6.3 Drug Interaction with MAA-DEAEMA Nanogels

The cationic drug utilized during the course of this research is procaine hydrochloride (PrHy). It was purchased from Sigma-Aldrich and was used without further purification. This drug is the first chemically synthesized, nonaddictive and injectable local anesthetic used in dental surgery; nevertheless, it is no longer used for this purpose because of the short anesthetic duration and also its high allergenic properties. The chemical structure of PrHy is shown in Figure 6.6.

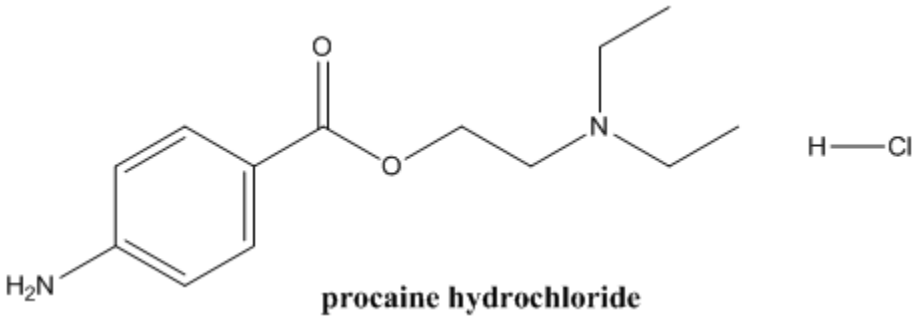

Figure 6.6 Chemical structure of procaine hydrochloride (PrHy).

The isothermal titration calorimetry was usedd to study the interactions between drug and nanogels at 25 ^{o}C. The titrant comprising of 282 μL of 600 mM procaine hydrochloride (PrHy) was titrated into 1.4551 ml of 0.1 wt% MAA-DEAEMA nanogels at different pH values. The differential enthalpies (*ΔH)* versus the concentration of titrant (PrHy) in the cell were plotted in Figure 6.7. Based on the results, the enthalpy profile for titrating PrHy into MAA-DEAEMA nanogels at different pHs exhibited similar profiles as the dilution curve (titration of PrHy into 10 mM NaCl solution). Besides, the enthalpies of dilution resembled that of all the other curves. Consequently, it can be concluded that PrHy did not bind to the MAA-DEAEMA nanogels through electrostatic attractions; this is, the titration results exhibited no evidence of electrostatic binding, between the negatively charged COO^- groups of MAA segments and positively charged N^+ of PrHy. However, diffusion and hydrophobic interactions were the driving force for binding the drug molecules into the nanogels. This phenomenon can be due to the presence of two ethyl groups surrounded the N^+, providing steric hindrance that shielded the positive charge; thus, preventing the binding of positively charged N^+ to negatively charged COO^- groups at low pHs.

Furthermore, by decreasing the pH to 4 and 2, higher values for differential enthalpy was observed. This is due to the fact that at this pH more positive charges were present on the nanogels inducing a higher hydrophobic interaction between MAA segments and benzene ring of PrHy molecules.

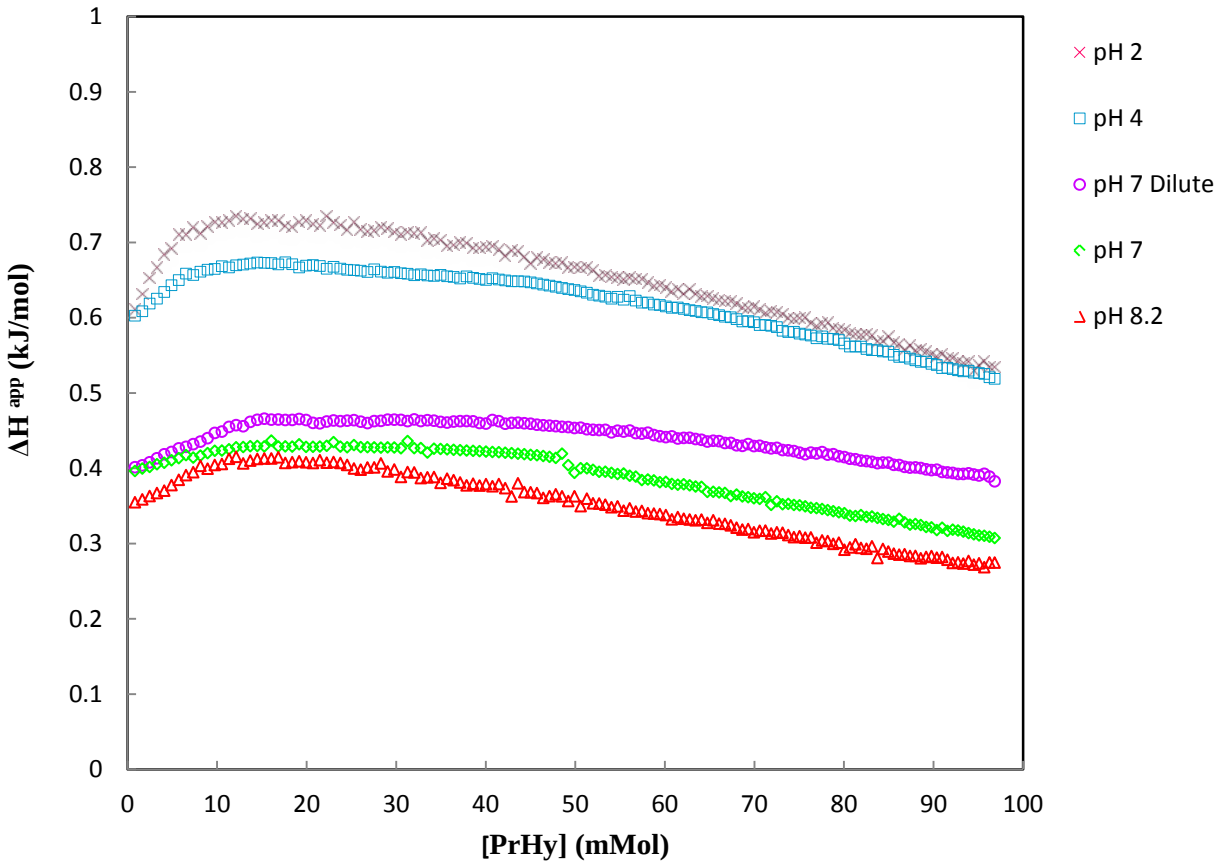

Figure 6.7 Differential enthalpy profiles for titrating 0.6 M PrHy into 0.1 wt% MAA-DEAEMA nanogels in 10 mM *NaCl* solution at different pH values.

Figure 6.8 shows the differential enthalpy curves for titrating 0.6 M PrHy into 0.1 wt% MAA-DEAEMA nanogels in 500, 300, 200, and 10 mM *NaCl* solutions. By increasing the concentration of salt in the medium, the salt molecules $Na^{+}Cl^{-}$ shielded the negatively charged COO^{-} groups on MAA segments reducing their accessibility to positively charged PrHy

molecules; hence more energy is required to induce hydrophobic interaction. These results further confirmed that the PrHy interacted with nanogels through hydrophobic bonding and diffusion rather than electrostatic attraction, because in the latter case the ΔH would be larger.

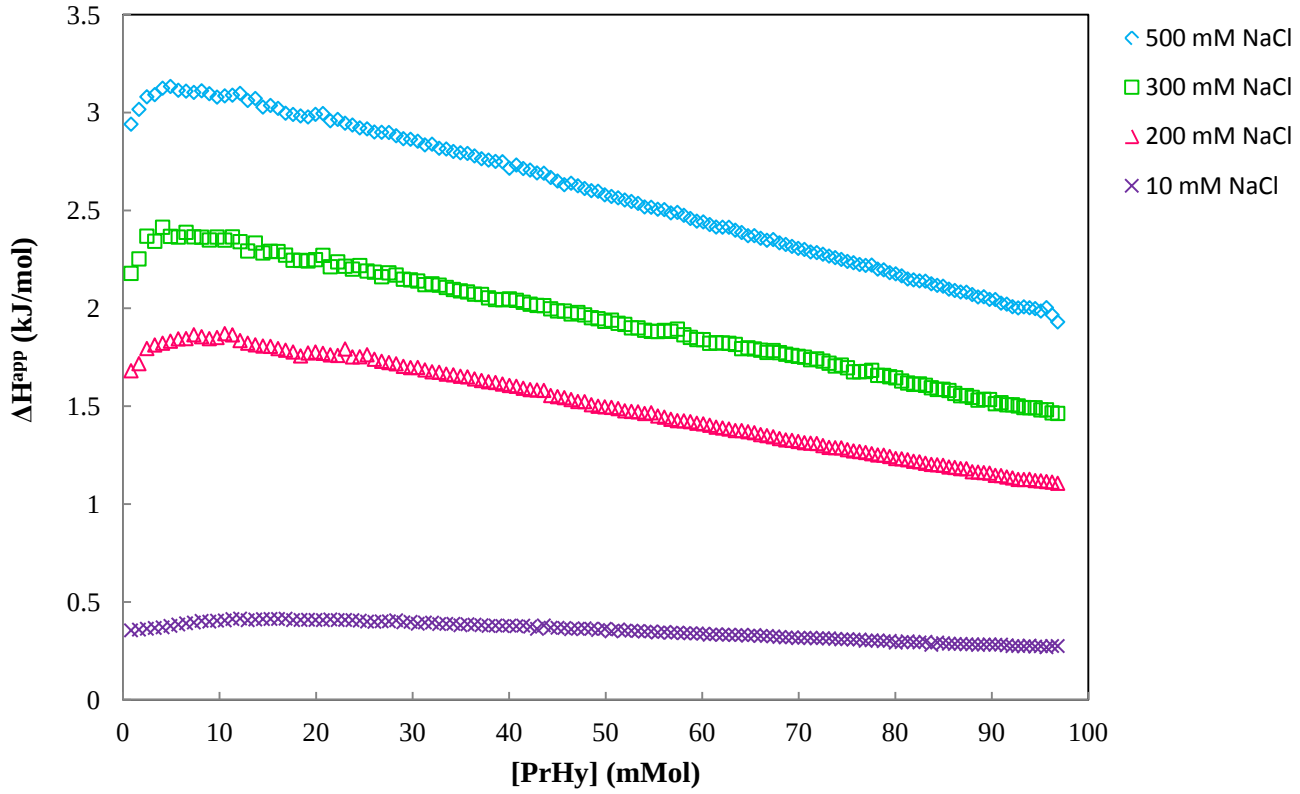

Figure 6.8 Differential enthalpy profile for titrating 0.6 M PrHy into 0.1 wt% MAA-DEAEMA nanogels at different NaCl concentration.

Figure 6.9 illustrates the differential enthalpy curves for titrating 0.6 M PrHy into 0.1 wt% MAA-DEAEMA nanogels in 10 mM NaCl solution at different temperatures. The differential enthalpy (ΔH) profiles demonstrated higher value as a result of increasing the temperature from 25 to 50 ^{o}C. This can be attributed to an increase in hydrophobic environment that induced stronger hydrophobic interaction between PrHy and MAA-DEAEMA nanogels. Thus, this result

further confirmed that binding between the loaded PrHy and the nanogels occurred through diffusion and hydrophobic interactions rather than electrostatic interactions. In other words, the concentration gradient difference between the interior and exterior of the nanogels was a driving force for the diffusion of drug molecules into the nanogels. A similar trend was reported by Tan et al. (Tan et al., 2007; Tan et al., 2008b) on the interaction between methacrylic acid-ethyl acrylate nanogels (HASE) and PrHy.

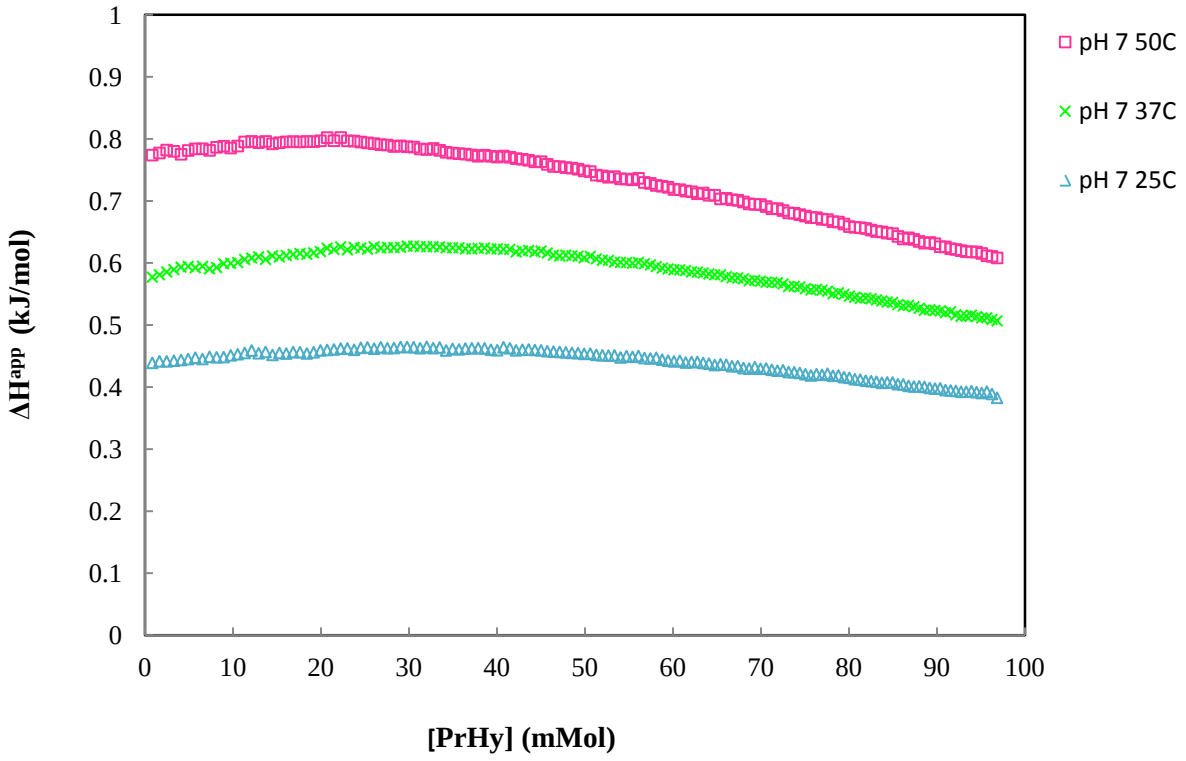

Figure 6.9 Differential enthalpy curves for titrating 0.6 M PrHy into 0.1 wt% MAA-DEAEMA nanogels in 10 mM *NaCl* solution at different temperatures.

6.3.1 Effect of Drug on Particle Size of the MAA-DEAEMA Nanogels

The relaxation rate (Γ) as a function of q^2 is shown in Figure 6.10 for 0.1 wt% MAA-DEAEMA nanogels loaded with 0.6 M PrHy in 10 mM NaCl solution. It was demonstrated that by

increasing the scattering angles, the decay function decreased. The fact that relaxation rate possessed q^2 dependence confirmed that the scattering was associated to translational diffusion. The slope of these figures corresponds to the translational diffusion coefficients, and the hydrodynamic radius (R_h) for these nanogels was calculated using the Stokes-Einstein equation. The hydrodynamic radius (R_h) of the MAA-DEAEMA nanogels loaded with 0.6 M PrHy in 10 mM NaCl solution at pH 2, 4, 7, and 8 were found to be 224.4, 177.1, 275.4, and 320.1 nm, respectively. According to the following equation the swelling degree of the nanogels can be calculated:

$$Swelling\ degree = \frac{R_{h\,(C)}}{R_{h\,(C=0)}}$$

C corresponds to the concentration of the drug. Based on the above equation the swelling degree of the drug loaded nanogels at pH 2, 4, 7, and 8 was 0.84, 0.90, 0.96, and 0.97, respectively. Therefore, the particle size decreased as a result of PrHy loading into the nanogels. These outcomes are in agreement with results reported by Xiong et al. {(Tan et al., 2008b; Xiong et al., 2005), and Lopez et al. (Lopez et al., 2005). A significant reduction in the size of the nanogels at pH 2 can be attributed to more dominant hydrophobic effect since there was larger proportion of hydrophobic MAA segments at low pH compared to DEAEMA segments in the nanogels. The more dominant hydrophobic effects led to a more compact structure.

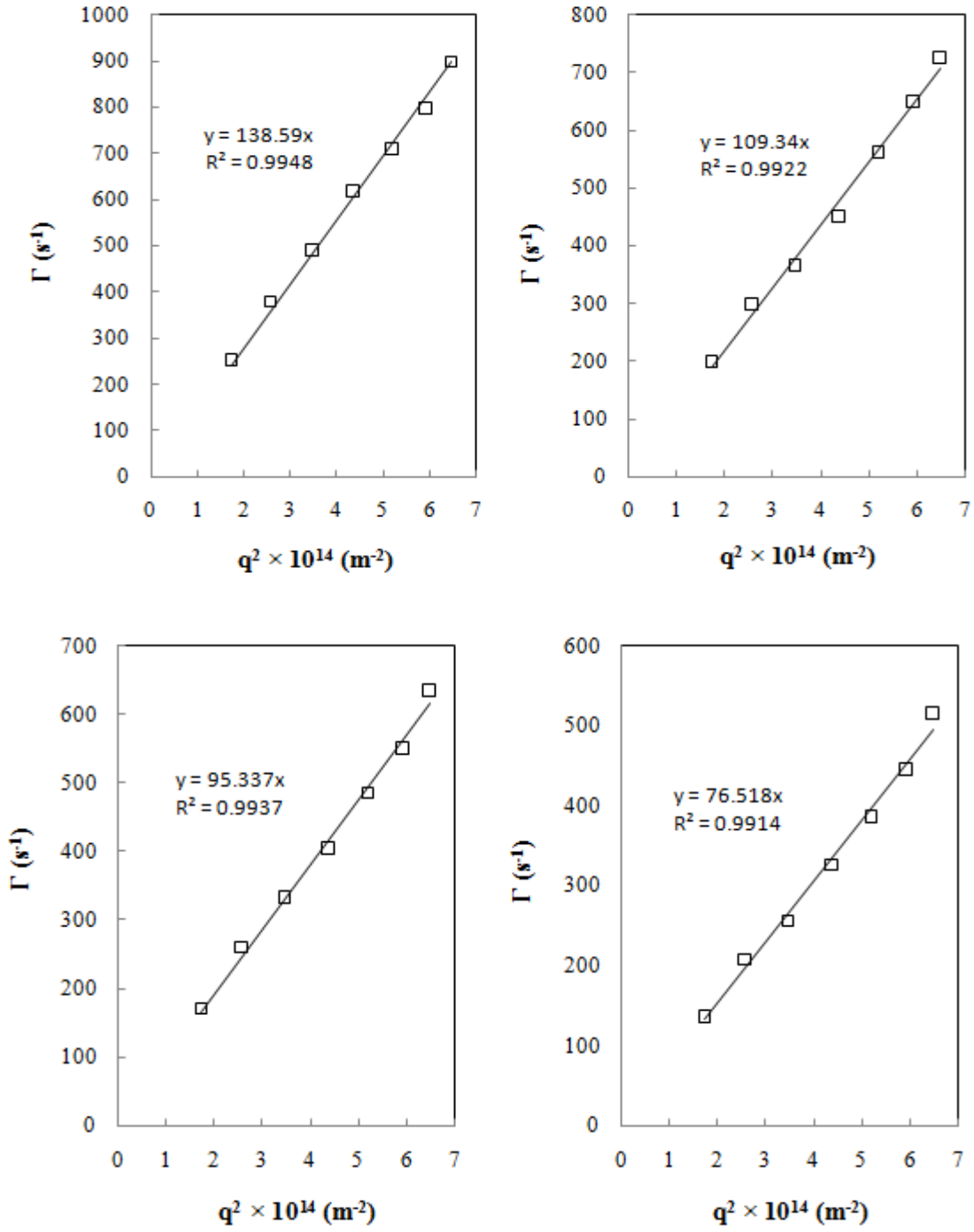

Figure 6.10 Relationship between Γ and q^2 for 0.1 wt% MAA-DEAEMA nanogels loade with 0.6 M PrHy in 10 mM NaCl solution at (a) pH 2, (b) pH 4, (c) pH 7, and (d) pH 8.

In addition, the polymer-solvent interaction was reduced forming a less polar medium within the nanogels due to the hydrophobic behavior of PrHy and nanogels at pH=2, which led to reduction in nanogel size. Similarly, at pH=7 and pH=8 shielding effect on the COO^- groups in the nanogels decreased the internal repulsion between negatively charged MAA segments, which decreased the nanogels size. Besides, reduction in polymer-solvent interaction as a result of drug incorporation formed a less polar medim within the nanogels and caused reduction in nanogel size. Furthermore, the smaller reduction in size at high pH compared to low pH can be contributed to aggregation of PrHy loaded nanogels because of a bridge effect formation; that is, PrHy incorporated on or near the surface of the nanogels could hydrophobically interact with another nanogels and consequently reduced the effect of charge shielding. However, at low pH, positively charged DEAEMA segments on the nanogels stabilized the nanogels and eliminated the bridge effect.

As shown in Figure 6.11, the zeta-potential measurements were conducted which further confirmed the results. The reduction in nanogel size improved the zeta-potential of the nanogels and correspondingly their mobility. At low pH incorporation of the positively charged PrHy to the positively charged nanogels increased the mobility in comparison to nanogels without loaded drug. On the other hand, at high pH incorporation of the positively charged PrHy, neutralized the negatively charged nanogels and reduced the mobility in comparison to nanogels without drug. Although high mobility values revealed that nanogels maintained their stability at both high and low pH, there is a slight reduction in mobility value at high pH in comparison to results obtained without PrHy incorporation. This slight instability at high pH could have contributed to aggregation between nanogels due to the presence of PrHy on the surface of the nanogels.

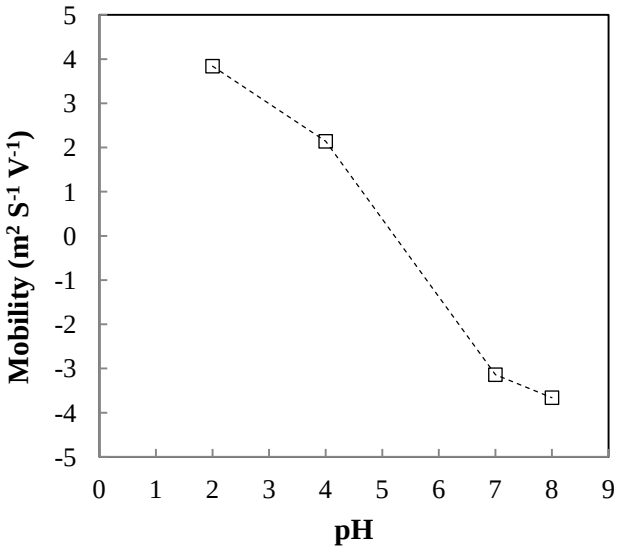

Figure 6.11 Mobility of PrHy loaded-nanogels as a function of pH.

Chapter 7

Drug Release from the MAA-DEAEMA Nanogels

7.1 Introduction

Procaine hydrochloride (PrHy) was used as a model drug for the purpose of this research. In the previous chapter we demonstrated that PrHy was loaded into the MAA-DEAEMA nanogels through hydrophobic interaction at high pH and by hydrophobic and hydrogen bonding at low pH values. These results contributed to the steric hindrance provided by the two ethyl group surrounded the N^+, which reduced the electrostatic interaction between positively charged N^+ on PrHy and negatively charged COO^- groups on MAA segments. At low pH, there is hydrophobic interaction between PrHy and MAA segments and also hydrogen bonding between *COOH* groups on MAA segments and amines on PrHy. Here, we demonstrated how the loaded drug will be released from the interior of nanogels under different conditions, such as pH and salt. In contrast with conventional methods of measuring drug released concentration, such as dialysis tubing or centrifugation, in this research the concentration of the drug released was obtained using the drug selective electrode method.

7.2 Drug Selective Electrode

The studies conducted on drug release behaviors were mostly reported as the ratio ($^{M_t}/_{M_\infty}$) of the drug released as a function of time t. M_t indicates the amount of drugs released at time t; whereas, M_∞ represents the total amount of drugs incorporated in the carrier or the amount of

drugs released at infinite time. The following assumptions were made in order to study the drug release profile. First of all, the initial swelling occurred at the surface of the nanogels; secondly, the drug was distributed uniformly in the nanogels. According to these assumptions, the primarily release of the drug was attributed to drug molecules bound to the surface of the nanogels, that led to a higher release rate; whereas, the delayed release of the drug was due to the diffusion of drug from the interior of the nanogels. Drug release experiments were conducted using a 4-channel ion instrument and drug selective electrode technique at varying conditions such as pH, concentration gradient, drug loading ratio. The temperature was maintained at 37 ^{o}C corresponding to the normal body temperature using a water bath throughout the course of experiment.

Drug membrane electrode was calibrated before and after each experiment to confirm the accuracy and stability of the electrode response time and also to ensure the reproducibility of the measurements. For calibration purpose of the PrHy membrane electrode, 10 ml of different concentrations of PrHy such as 10^{-5}, 10^{-4}, 10^{-3}, 10^{-2}, and 10^{-1} M in 10 mM *NaCl* solution was prepared, and then the membrane electrode was immersed into the solution under continuous stirring at 37 ^{o}C over 15 minutes.

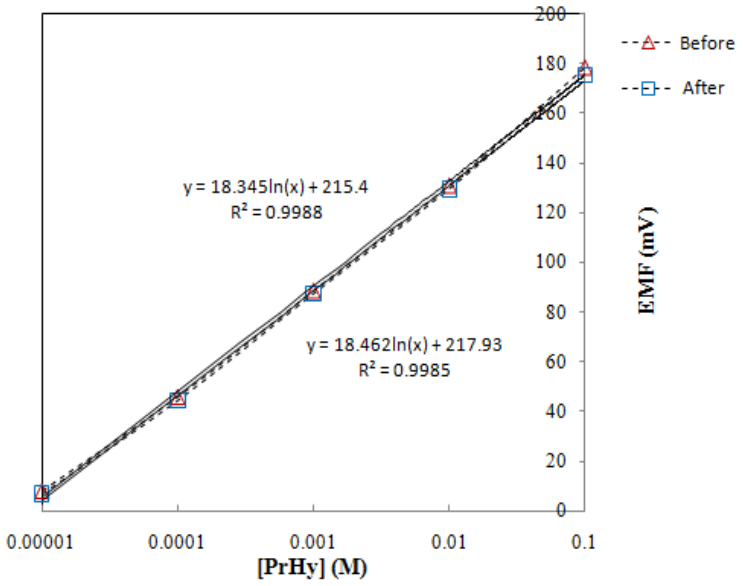

Figure 7.1 Calibration curves of PrHy membrane electrode obtained, before and after the drug release experiment 1, in different PrHy concentration in 10 mM *NaCl* solution at 37 ^{o}C.

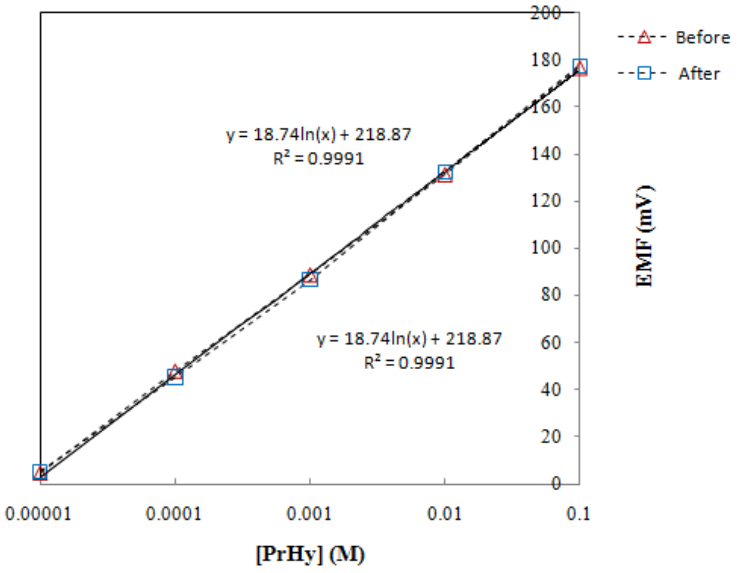

Figure 7.2 Calibration curves of PrHy membrane electrode obtained, before and after the drug release experiment 2, in different PrHy concentration in 10 mM *NaCl* solution at 37 ^{o}C.

As shown in Figures 7.1 and 7.2, calibration curves were obtained by plotting the measured electromotive force (EMF) versus different concentrations of PrHy in 10 mM NaCl solution. These figures demonstrated that the calibration curves obtained before and after the use of the membrane electrode in drug release experiment 1 and 2 respectively were reproducible. In each of the above figures, calibration curves obtained before and after experiment 1 and 2 were very identical, as they both possessed similar slopes and intercept, which proved that the results obtained during the course of experiment with unknown concentration of drug molecules were repeatable.

Moreover, each drug release experiment was performed twice under identical condition to ensure the reproducibility and stability of the results. Figure 7.3 shows the reproducibility of two drug release profiles obtained from two identical experiments conducted under the same conditions on two different days. In order to further determine the stability of the PrHy electrode response, the following experiments were performed, and stable EMF measurements were obtained by immersing PrHy electrode into the solution of 10^{-3} M PrHy and 10 mM NaCl at a temperature of 37 ^{o}C, as shown in Figure 7.4. There was only a very small drift, which was less than 0.1 *mV/hr*. This experiment was conducted to ensure the stability and reproducibility of the electrode responses.

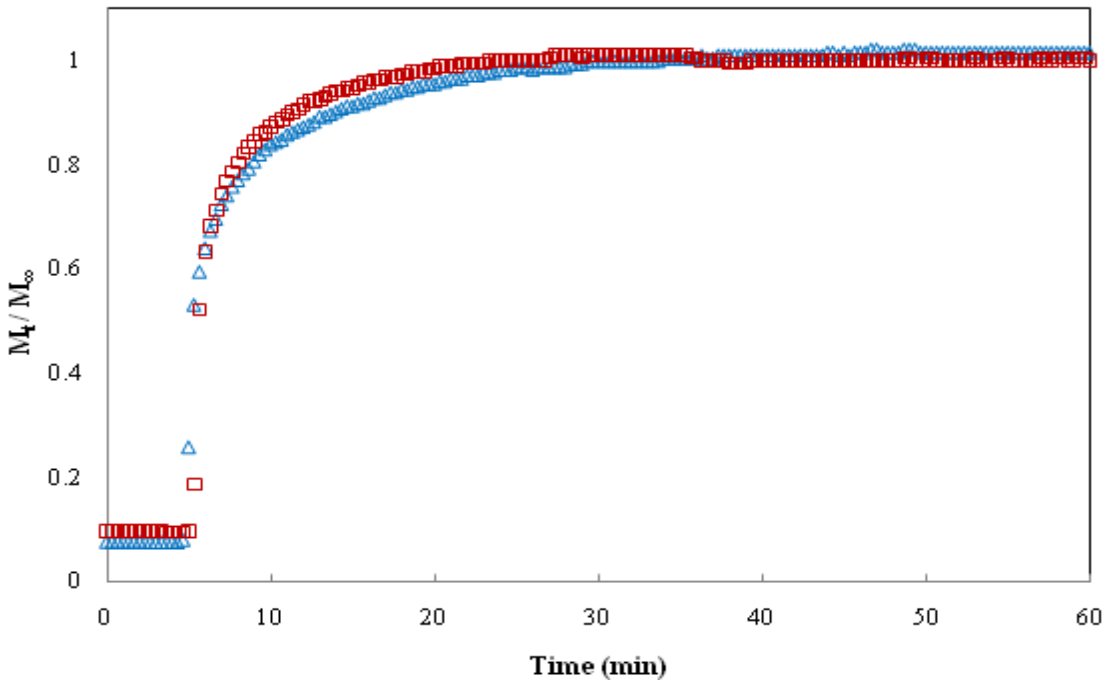

Figure 7.3 Two drug release profiles of two identical experiments conducted under similar condition on two different days.

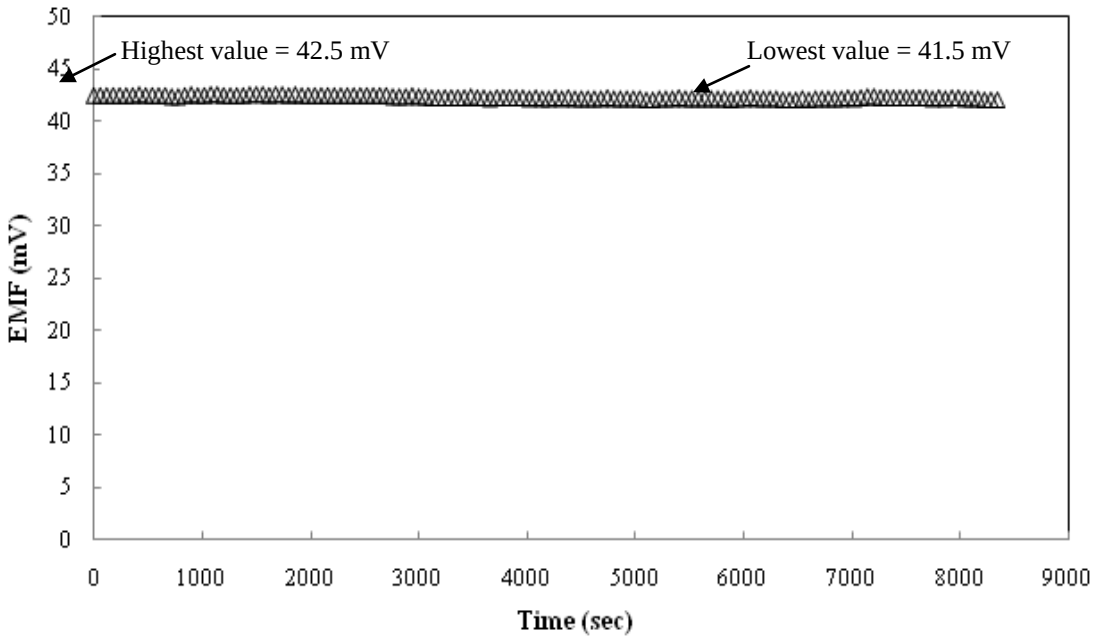

Figure 7.4 Stability profile of PrHy membrane electrode obtained in the solution of 10^{-3} M PrHy and 10 mM *NaCl* at 37 ^{o}C.

7.3 Drug loading into the MAA-DEAEMA Nanogels

In order to load the MAA-DEAEMA nanogels with hydrophilic drug PrHy, the following experiment was performed. 0.1 wt% of MAA-DEAMAE nanogels at pH=7 was prepared and based on the results and technique proposed by Tan et al. (Tan et al., 2007; Tan et al., 2008b) 2.44 g drug/ g polymer was added into the nanogels solution under continuous stirring, and the nanogel-drug solution was left to equilibrate over 24 hours at constant temperature of 25^{o}C, which was controlled by water bath. Afterwards, the loaded nanogels were passed through an ultrafiltration cell, which contain filter with a cut-off pore size of 0.02 µm. to ensure that free PrHy can pass through the filter, a pure solution of PrHy was passed through the membrane and the concentration of solution before and after filtration was measured, and it was found to be identical, confirming that free and unbound PrHy molecules can pass through the membrane.

7.3.1 Effect of pH on PrHy Release Profile

In order to investigate the effect of varying pH on the release of PrHy, the following experiment was conducted. 5 ml of 0.1 wt% nanogels loaded with 2.44 g drug/ g polymer was added into 50 ml 10 mM *NaCl* solution at different pH and constant temperature of 37^{o}C. Figure 7.5 illustrates the release profile under different pH conditions. All the profiles indicated a burst release of drugs in the first 10 minutes and afterwards the released slowed down and slightly drift after about 1.5 hour. As mentioned earlier, the drug release from the nanogels comprised of two parts. The first part associated with the drug incorporated on the surface of nanogels that led to the burst released of drug in the first 10 minutes. The second part corresponded to drugs incorporated within the nanogel network that caused the delayed exponential release due to the slow diffusion of drug from the nanogels network to the bulk solution.

The nanogels were swollen and possessed a high porosity at both high and low pH values. This increased the osmotic pressure and allowed the chains to accommodate more solvent molecules promoting the release of the drug from the nanogels by reducing the diffusion resistance. In addition, at both high and low pH, hydrophobic interactions were the predominant driving force for loading the drug molecules into the nanogels. However, the synthesized nanogels contain 60 mol% MAA compare to 40 mol% DEAEMA. Therefore, higher osmotic pressure was produced due to the presence of negatively charged COO^- and enhanced the swelling degree at high pH. Consequently, slightly higher fraction of drug will be released at high pH over longer period of time in comparison to low pH. Furthermore, at low pH as mentioned before, there was hydrogen bonding between *COOH* groups on MAA segments and amine groups on PrHy, which resulted in a lower release of PrHy from the nanogels. All these demonstrated that the surrounding pH values can effectively control the release rate from the nanogels.

Figure 7.6 indicates the release of the drug from the nanogels as a fuction of pH and R_h. These graph further comfirmed and clarified the relationship between pH values and drug release profile as discussed above. In the other words, at pH=2 the nanogels swelled due to the electrostatic repuslsion between positively charges on the DEAEMA segments; therefore, at this pH nanogels promoted the higher release of the drug from their interior, which is M_t / M_∞= 0.968. By increasing the pH to 3, less positive charges present on the nanogels, which resulted in dewelling of the nanogels and less amount of drug released from the nanogels. By further increasing the pH to 6 the abrupt reduction in drug released was observed, this phenomenon can be contributed to the isoelectric point in which nanogels possessed the lowest R_h. Thus, minimum amount of drug, M_t / M_∞= 0.213, was capable to release from the nanogels in comparison the both the lower and higher pH values. When the pH increased to 7.4 and 8 due to

the increment in osmotic pressure nanogels and electrostatic repulsion between negative charges on the MAA segments, nanogels swelled and subsequently released more amount of drug to the surrounding medium, M_t / M_∞= 0.618 and 0.74, respectively. As can be seen in both Figure 7.5 and 7.6, higher drug released was obtained at lower pH values such as pH= 2 and 3 in contrast to pH=7.4 and 8. This effect can be elucidated due to the incorporation of positively charged PrHy within the positively charged nanogels, caused less hydrophobic interaction the PrHy molecules and nanogels.

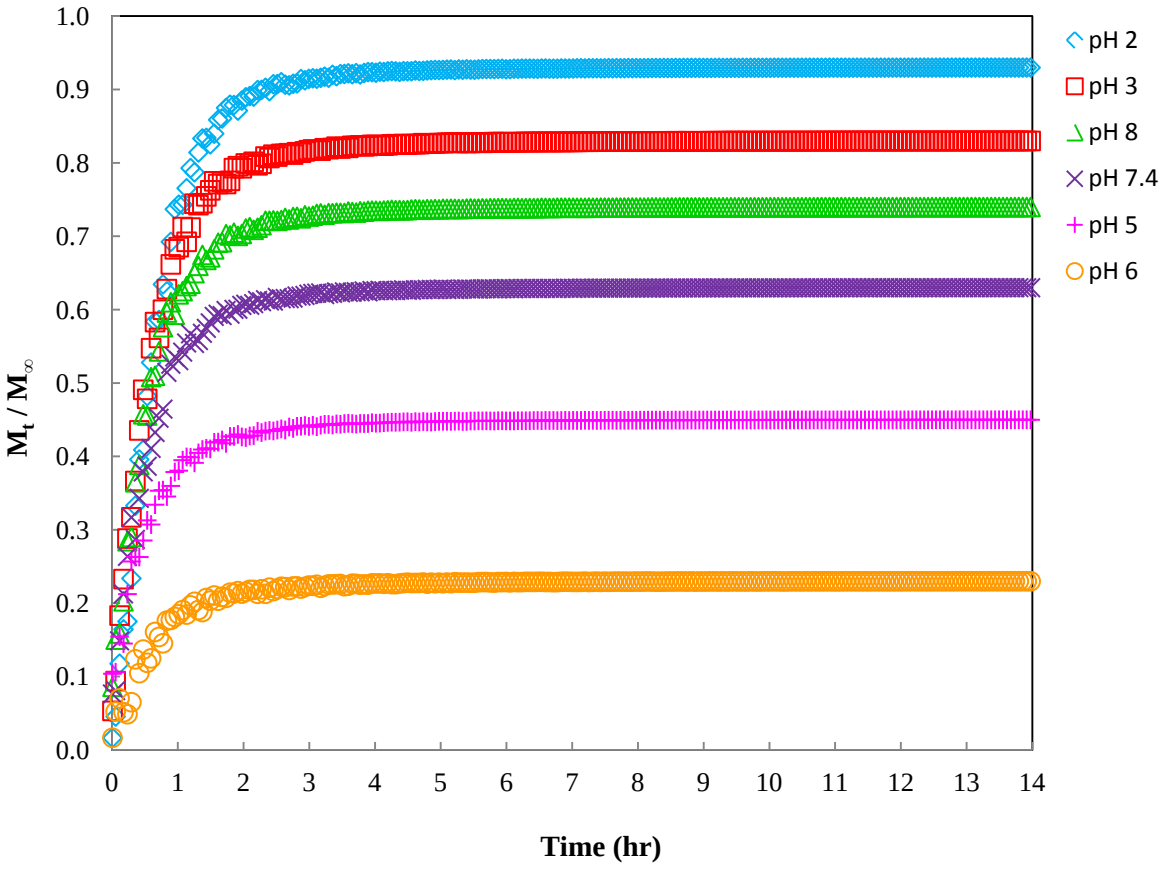

Figure 7.5 PrHy release profile from 0.1 wt% MAA-DEAEMA nanogels in 10 mM *NaCl* at 37 ^{o}C at different pH conditions.

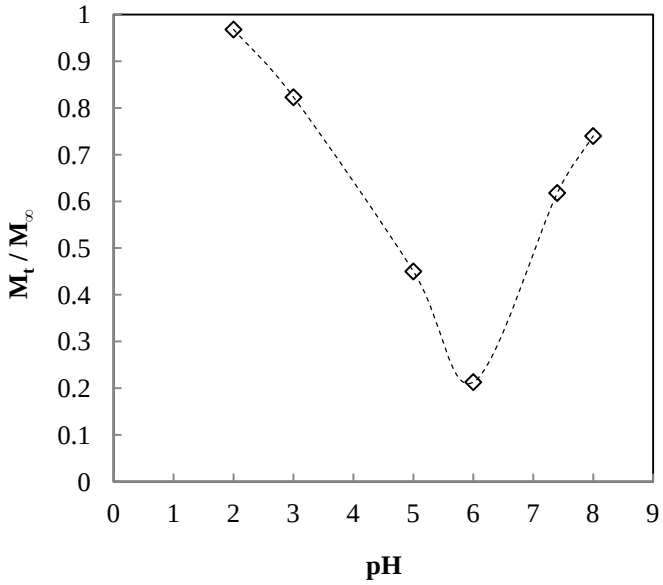

Figure 7.6 Plot of PrHy release from 0.1 wt% MAA-DEAEMA nanogels in 10 mM *NaCl* at 37 ^{o}C as a function of pH.

Figure 7.7 depicts the effect of varying pH on the release of PrHy from PrHy-loaded MAA-DEAEMA nanogels. The amount of PrHy released at pH 4 was about 62% because at this pH the nanogels were positively charged, repulsion force between *N* $(CH_3CH_2)_2H^+$ groups on the DEAEMA segments, led to swelling of the nanogels. Moreover, the concentration gradient of PrHy between the nanogels network and the medium was very high. Thus, both of these factors promoted the higher release of the PrHy molecules from the nanogels. However, by increasing the pH to 5 and 6, the release of the PrHy reduced which can contributed to the more compact structure and overall charge neutralization of the nanogels at this pH. In addition, pH=5 demonstrated more PrHy release in comparison to pH=6, which can be explained according to the zeta potential result obtained at this pH. The mobility at this pH was still positive indicating that nanogels contained slightly positive charges; besides the squeezing effect of the drug de to the reduction in nanogel size from the swollen state expelled more PrHy molecules from the

nanogels network. By increasing the pH to 7 and 8, the nanogels were still in their swollen state, the reduction in PrHy concentration gradient between the interior of the nanogels and the medium decreased the driving force for the release of the PrHy from the nanogels network. Figure 7.7, demonstrates that the drug release can be manipulated according to the different pH environments of body compartment. Therefore, the therapeutic window of the active drug can be increased and successful delivery of the drug to the targeted area is enhanced. Measurment of the concentration of the drug released in the medium with continuous change in the pH was achievable by applying the drug selective electrode rather than using conventional techniques of dialysis membrane or centrifugation (Tan et al., 2007).

A schematic diagram in Figure 7.8 illustrates that at both high and low pH, the nanogels possess swollen structure and larger porosity, as result of electrostatic repulsion between like charges and also high osmotic pressure. This led to a higher release of PrHy from the interior of the nanogels as a consequence of reduction in diffusion resistance.

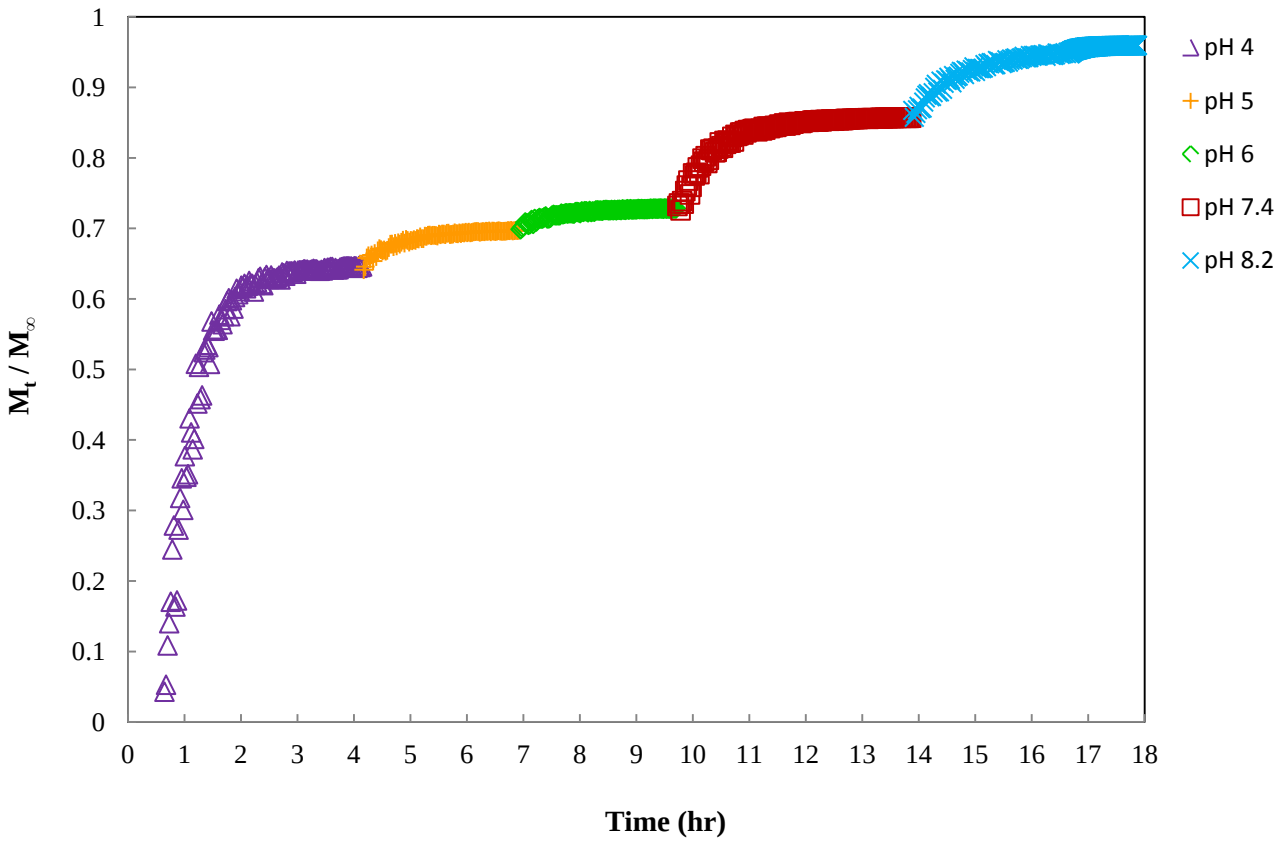

Figure 7.7 PrHy release profile from 0.1 wt% MAA-DEAEMA nanogels in 10 mM NaCl solution at 37 oC as a result of changing environmental pH.

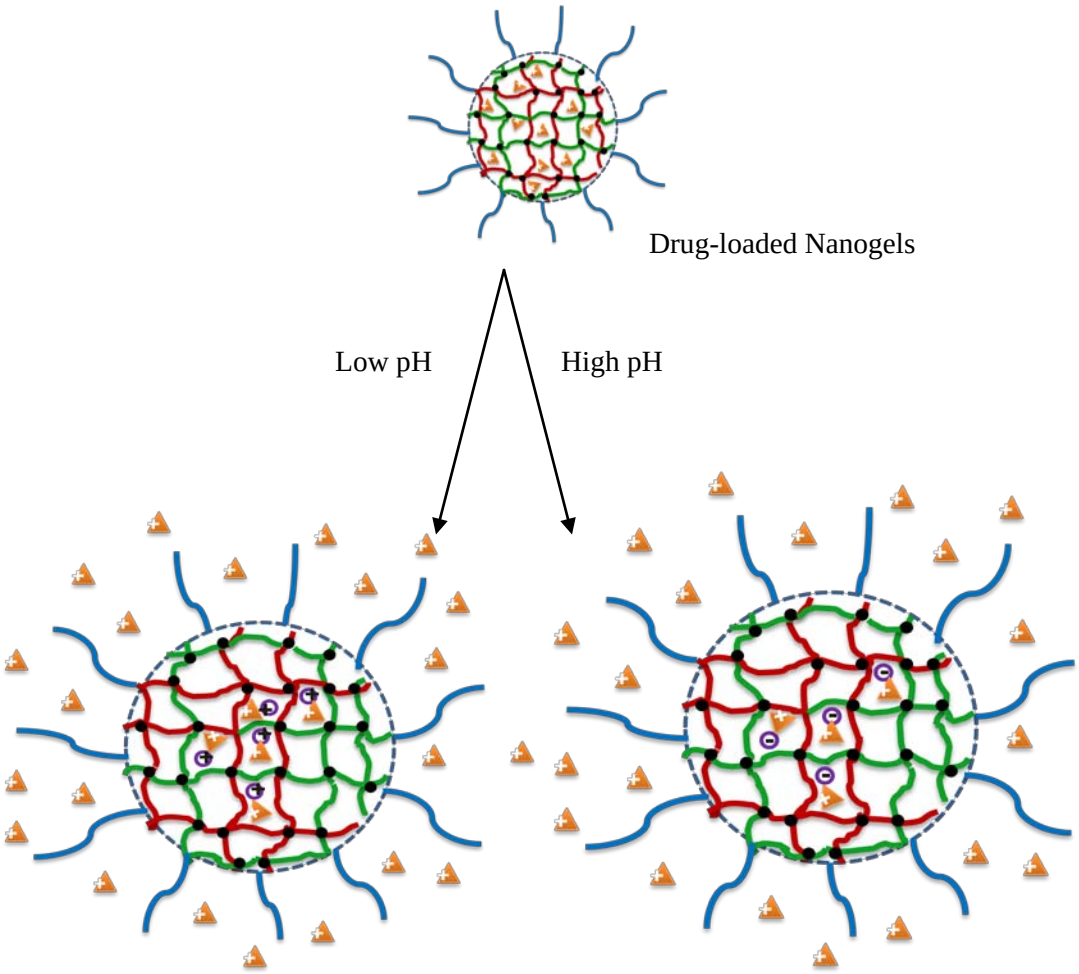

Figure 7.8 Schematic diagram of the drug release from nanogels matrix, at both high and low pH value high PrHy fractional released was observed due to the high swelling ratio and low resistance to diffusion**.**

Represents drug molecule

Represents positive or negative segment

Represents cross-linked junction

Represents DEAEMA-MAA segment

Represents PEGMA segment

7.3.2 Effect of Salt Concentration Gradient on PrHy Release

In order to investigate the effect of varying salt concentration on the release of PrHy, the following experiments were conducted. Different volume of 0.1 wt% nanogels loaded with 2.44 g drug/ g polymer was added to 50 ml 10 mM *NaCl* solution at pH 7.4 at 37 ^{o}C. The concentration gradient of 5, 7, 10, and 20 times was used. For example, to achieve the concentration gradient of 10 times, 5 ml of 0.1wt% nanogels loaded with drug was added to the 50 ml of 10 mM *NaCl* solution. That is, the volume of salt used was 10 times the volume of nanogels solution.

Figure 7.9 illustrates the effect of varying concentration gradient on the release profile of PrHy. It can be seen that the larger the concentration gradient difference, the higher the release rates. This result can be attributed to the fact that salt dissociated in the solution and formed very small size Na^+ and Cl^- ions. The very small Na^+ ions can easily diffused into the nanogel's network and replaced the positively charged PrHy molecules. Thus, the higher the concentration between the interior and exterior of the nanogels, the more Na^+ ions were able to diffuse into the nanogels. In other words, the Na^+ ions diffusion rate, which was the result of the concentration gradient between the interior and exterior of the nanogels, determined the rate at which PrHy was released from the nanogels. Since the driving force for loading PrHy into nanogels was controlled by diffusion and hydrophobic interaction, the presence of higher concentration gradient improved these driving forces and led to a faster release of PrHy from the nanogels. The larger concentration gradient created by a higher salt concentration led to a higher release rate of PrHy. On the other hand, the release rate was reduced as a result of smaller concentration gradient associated with a lower salt concentration. Moreover, by increasing the concentration

gradient between the interior and exterior of the nanogels, the time required to achieve fully drug release was increased. In other words, the higher the concentration gradient between inside and outside of the nanogels, it required longer time to reach equilibrium. Once PrHy loaded nanogels were added to the solution at pH=7.4, nanogels swelled and due to the presence of concentration gradient between the exterior and interior of nanogels, it promoted the release of the drugs.

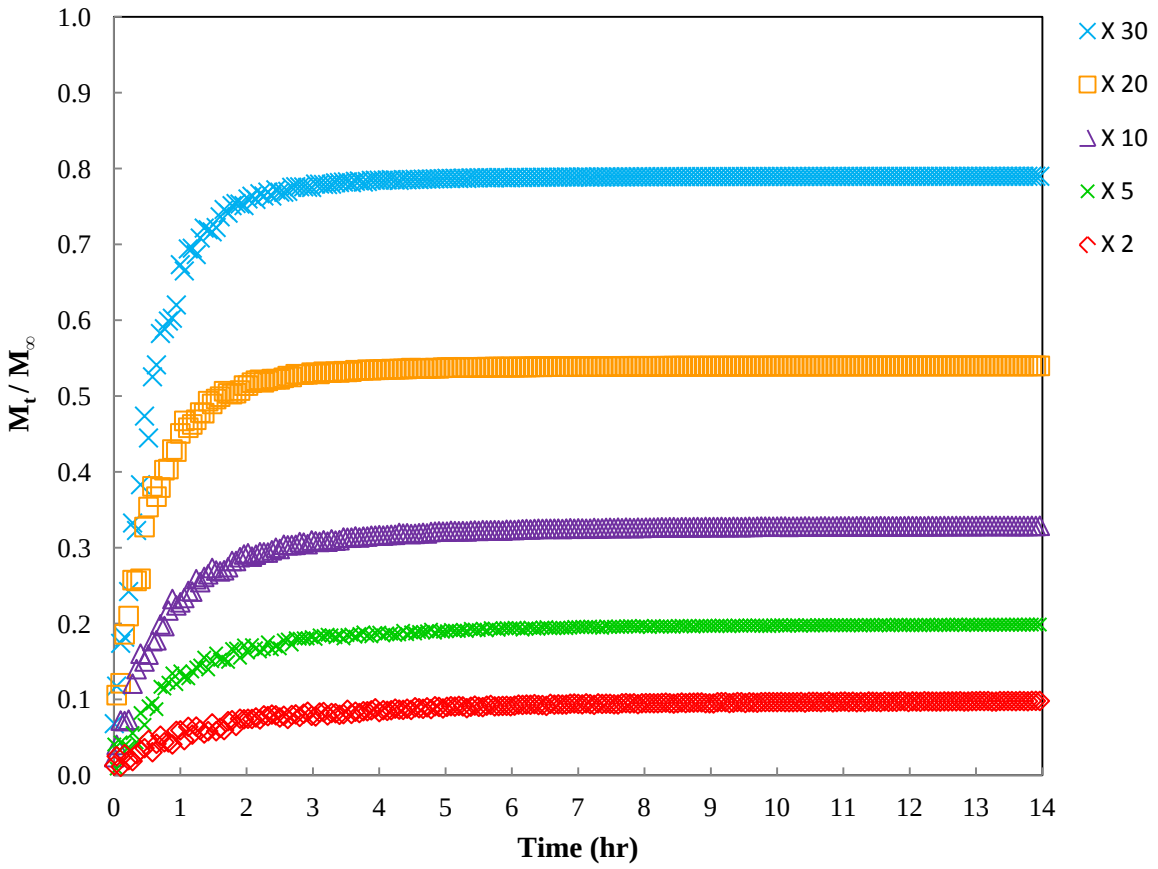

Figure 7.9 PrHy release profile from 0.1 wt% MAA-DEAEMA nanogels in 10 mM NaCl solution at pH 7.4 and temperature 37oC with varying concentration gradient difference.

Chapter 8

Layer by Layer Coating on the PrHy-Loaded Magnetic Iron-Oxide Nanogels

8.1 Introduction

As previously mentioned in section 2.4, different kinds of colloidal carriers have been investigated due to their potential in drug delivery applications. Among all of the potential candidates, polyampholyte nanogels are capable of swelling at both high and low pH in a good solvent, such as water. Aqueous magnetic fluids, possessing super-paramagnetic properties, are known as colloidal dispersions of magnetic nanoparticles in water. In this work, co-precipitated magnetic nanoparticles within nanogels were developed to investigate a more efficient approach to conduct layer-by-layer coating in order to control the burst release of drug molecules. Moreover, the nanogels developed in this research were capable of delivering drug under both spatial and temporal control. The spatially controlled delivery was achieved due to the presence of magnetic nanoparticles, which are able to respond to an externally applied magnetic field, placed on a defined location of the body. Temporally controlled delivery was obtained due to the pH responsive character of nanogels, in which varying pH value led to a different response from nanogels, like various pH values in the body compartment. Therefore, by combining both characteristics, more efficient delivery of drugs from nanogels can be accomplished (Deka et al., 2010).

8.2 Synthesis of Magnetic Iron-Oxide Nanogels

The co-precipitation of magnetic nanoparticles within nanogels was adopted and modified from the proposed method by Lee et al. (Lee et al., 2009; Lee et al., 2010). $FeSO_4.7H_2O$ was purchased from Fisher Scientific. $NaNO_2$ was obtained from Fisher Scientific.

The MAA-DEAEMA nanogels as previously described were synthesized via semi-continuous emulsion polymerization. In a typical process, 120 ml of 0.5 wt% MAA-DEAEMA nanogels was added to a three-neck round bottom equipped with overhead stirrer, to prevent accumulation of magnetic nanoparticles around magnetic stirrer bar. Then, the pH of the solution was increased to 7.5 using 1 M *NaOH*, in order to form negatively charged carboxyl groups on MAA segments, which enhanced the incorporation of positively charged ferric ions into the nanogels. In another container 2.5 g of $FeSO_4.7H_2O$ was dissolved in 30 ml of de-ionized water and deoxygenated for 30 minutes, in order to form pale green Fe^{2+} solution. The nanogels solution was heated to 75 ^{o}C, and $FeSO_4.7H_2O$ solution was added dropwise to the nanogel solution by means of a double needle under continuous nitrogen purging and vigorous stirring and Fe^{2+} were bound to the carboxyl groups of MAA resulting in the formation of a dark green suspension. After 2 hours, subsequent addition of 0.25 g of $NaNO_2$, as an oxidizing agent, and 15 ml of 28% NH_4OH was conducted, to increase the pH of the solution to pH=10.5. The reaction was left to react for another hour, changing from the dark green suspension into a black precipitate of Fe_3O_4 (Lee et al., 2009; Lee et al., 2010). In order to separate non-magnetic nanogels, the suspension was purified by passing it through the high-gradient magnetic separator. The solid content of the magnetic nanogel was about 10 wt% and possessed a hydrodynamic radius (R_h) of 292.7 nm;

there was an increment in size of the magnetic nanogels from bare nanogels, which was 277.7 nm.

8.3 Layer-by-Layer Coating of the Magnetic Iron-Oxide Nanogels

A layer-by-layer coating of polyelectrolyte on drug-loaded magnetic MAA-DEAEMA nanogels grafted with PEGMA was performed in a 0.1 M *NaCl* solution at pH=7.5. There was no sign of aggregation of the coated nanogels; however, the swelling degree of nanogels decreased as the number of polyelectrolyte layers increased. Poly (sodium 4-styrenesulfonate) (PSS) (Tan et al., 2008a; Wong et al., 2009), and low molecular weight chitosan (CS) (Diez-Pascual and Wong, 2010), both purchased from Sigma-Aldrich, acted as polyanion and polycation electrolytes to prepare coated magnetic nanogels, respectively. The drug release from the coated magnetic nanogels showed a reduction in the burst release phenomenon. The structure of CS and PSS is shown in Figure 8.1.

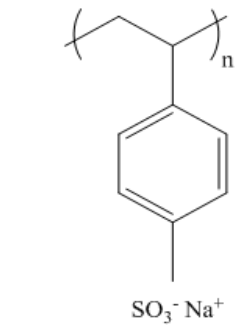

Poly (sodium 4-styrenesulfonate)

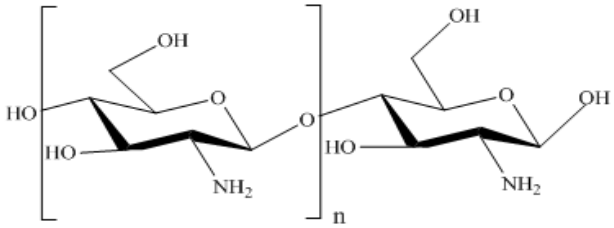

Chitosan

Figure 8.1 Schematic of PSS and CS chemical structure.

Chitosan (CS) is a linear copolymer comprising of 1, 4-linked 2-amino-2-deoxy- D glucopyranose and 2-acetamido-2-deoxy-D glucopyranose units. It is a weak cationic polysaccharide produced by the deacetylation of the natural polymer chitin. It has a variety of applications in food industry, pharmaceutical, biomaterials, medicine and cosmetic due to its attractive biological properties such as biocompatibility, biodegradability, and bioactivity. CS demonstrates great potential for its use as polycation in layer-by-layer coating. It has been revealed that low molecular weight CS possesses different biological properties such as antifungal, antibacterial, and antitumor in comparison to the high molecular weight chitosan (Diez-Pascual and Wong, 2010; Lu et al., 2011; Shu et al., 2011).

The prepared magnetic nanogels were loaded with 2.44 g drug/ g of polymer, and added to the 0.5 wt% magnetic nanogel solution and left to equilibrate over 24 hours at 25 ^{o}C. Afterwards, alternating layers of CS and PSS were deposited on the negatively charged nanogels through electrostatic attractive force. Bulk solution of 1 wt% CS was prepared by slow dissolution of CS in 3% w/v acetic acid. At the same time, 1 wt% PSS (M_w=70000) in 100 mM *NaCl* at pH=6 was prepared, and both solutions were highly charged according to their pK_a in the experiment condition. 0.5 ml CS solution was added to 10 ml of drug-loaded magnetic nanogels under continuous stirring for 30 minutes in order for CS adsorption onto the negatively charged nanogels. Istead of using the repeated filtration technique, which was commonly employed by many research group (Blasi et al., 2010; Lopez et al., 2005; Nolan et al., 2005b; Tan et al., 2007; Tan et al., 2008b; Xiong et al., 2005), high-gradient magnetic field was utilized to remove excess CS. 1.5 ml of PSS was added to 10 mL CS coated nanogels, which are positively charged under continuous stirring for 30 minutes, in order for PSS to adsorb onto the positively charged CS coated nanogels. Subsequently, by passing the coated nanogel through the high-gradient magnetic field, the excess amount of PSS was removed. Until the desire number of CS and PSS was deposited onto the nanogels, this process was repeated.

To achieve the optimum amount of CS and PSS layer to be deposited onto the PEGMA grafted nanogels the following experiment was performed. Different ratio of the volume of CS/PSS to volume of grafted nanogels was prepared and then the zeta potential and hydrodynamic radius were measured at 25 ^{o}C. For instance, a 0.5 ml of CS solution and 10 ml of nanogels solution had a ratio of 0.05.

The ratio that corresponded to the maximum zeta-potential and minimum hydrodynamic radius (R_h) yielded the most stable system. In this research, a total of 5 polyelectrolyte layers were deposited onto the nanogels, where the first, third, and fifth layer comprised of CS (positively charged) layer; whereas, the second and fourth layer consisted of PSS (negatively charged) layer.

Figures 8.3 to 8.7 demonstrate how the hydrodynamic radius and zeta potential changed with the ratio for different layers. The bare magnetic iron-oxide nanogels possessed a hydrodynamic radius (R_h) of 292.7 nm and zeta-potential of -35.63 mV. From Figure 8.3 it can be seen that by depositing a ratio of 0.05 in the first layer on the nanogels, the R_h increased significantly. This increment in R_h can be due to fact that the surface of the negatively charged magnetic nanogels was not completely covered by the small amount of CS deposited onto the surface of the nanogels; thus, nanogels aggregated and formed larger aggregates. The low value of zeta-potential further confirmed the instability of the magnetic nanogels. In other words, small amounts of chitosan were not able to fully cover the surface of the nanogels and some areas of the nanogels surface remained bare, which were prone to associate with other exposed and uncovered nanogels and to form larger aggregates. By increasing the ratio to higher than 0.05, more stable nanogels were obtained.

For the PSS (negatively charged) layers, similar trend were observed. At low PSS ratio, nanogels aggregate and the low value zeta potentials demonstrated the sign of instability. As a result, the optimum ratio used throughout the course of experiment for CS layers (first, third, and fifth layers) was 0.35, whereas the optimum ratio of 0.55 was taken into account for PSS layers (second and fourth layers). Figure 8.2 shows the schematic of the alternate adsoption of

polyelectrolytes CS and PSS onto the PrHy-loaded magnetic iron-oxide MAA-DEAEMA nanogels.

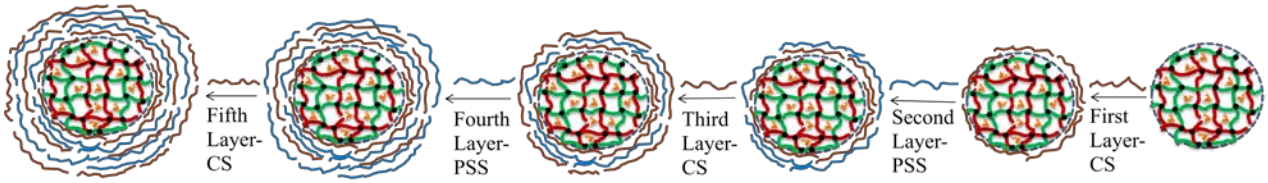

Figure 8.2 Schematic of layer-by-layer coating of CS and PSS onto PrHy-loaded magnetic MAA-DEAEAM nanogels.

Figures 8.3 to 8.7 show the relationship between R_h and zeta-potential with the number of layers of CS and PSS deposited alternately onto the negatively charged MAA-DEAEMA nanogels. The bare magnetic iron-oxide nanogels had the R_h of 292.7 nm, which increased slightly to 293.1 nm by the addition of the first positively charged polyelectrolyte layer (CS) and subsequently increased to 304.3 nm with the addition of the second negatively charged polyelectrolyte layer (PSS). The slight increase in size can be attributed to electrostatic interaction between positively charged NH_3^+ groups on the CS and negatively charged COO^- groups on MAA segments and negatively charged iron oxide. Another explanation could be attributed to the high charge density of CS, which was caused from strong acid solution of low ionic strength, and enhanced hydrophilicity of the positively charged CS. Hydrophilic behavior of charged CS, along with the porous structure of the nanogels allowed positively charged CS to easily diffuse into the nanogels and masked or neutralized the negative charges of nanogels; therefore, decreased the repulsion force between negatively charged COO^- groups of nanogels, induced reduction in R_h of the nanogels.

Besides, hydroxyl groups on the CS layer were able to form strong hydrogen bonds with solvent molecules, resulting in a reduction of nanogels R_h. The same trend was observed by Diez-Pascual and Wong (Diez-Pascual and Wong, 2010) as a result of layer by layer coating of chitosan as polycation and dextran as a polyanion onto Poly (NIPAm-MAA) microgels. The reason the size of the nanogels slightly increased rather that dramatic reduction can be contributed to the precipitation of iron oxide within the nanogels, occupying available space and preventing sufficient diffusion of positively charged CS layers. All these facts elucidate the difference in results obtained as a result of layer by layer coatings on nanogels versus those results achieved on layer by layer coating on film substrate.

On the other hand, by depositing negatively charged PSS layer, containing SO^-_3 groups, onto the chitosan-coated iron-oxide magnetic nanogels R_h increased dramatically. This can be contributed to the fact that by adding the negatively charged layer to the positive surface of CS-coated nanogels, the constant numbers of positive charges not only had to be shared between the negatively charged nanogels and the CS layer, but also had to be shared between the chitosan layer and the negatively charged PSS layer. The electrostatic interactions between the latter dominate the electrostatic interactions between the former, weaken the electrostatic interaction between positively charged CS layer and negatively charged nanogels, which consequently increased the R_h. In addition, the excess of negative charges on PSS layer due to lack of charge compensation, inducing enlargement of nanogels by repelling each other.

Furthermore, PSS layer was highly hydrophilic capable of absorbing large amounts of water, which in turn reduced the entanglement of polyelectrolyte chains and subsequently expanded coated nanogels. Porous structure of the nanogels allowed diffusion of the negatively charged

PSS into the nanogels, induced repulsion force between negative moieties of nanogels including COO^- and iron oxide. However, because of the weak interactions between polyelectrolytes and lack of hydrogen bonds, osmotic pressure induced by negative ions distributions within the nanogels dominated the interactions between the polyelectrolytes and promoted nanogels swelling. This is in agreement with the results reported by Wong et al. (Wong et al., 2009) and Tan et al. (Tan et al., 2008a), in which Poly (NIPAM-MAA) microgels were alternately coated with different layers of poly(diallyldimethylammonium chloride) (PDADMAC) and PSS, and ethyl acryl acrylate-MAA (HASE) microgels were coated through alternate addition of PAH and PSS layers.

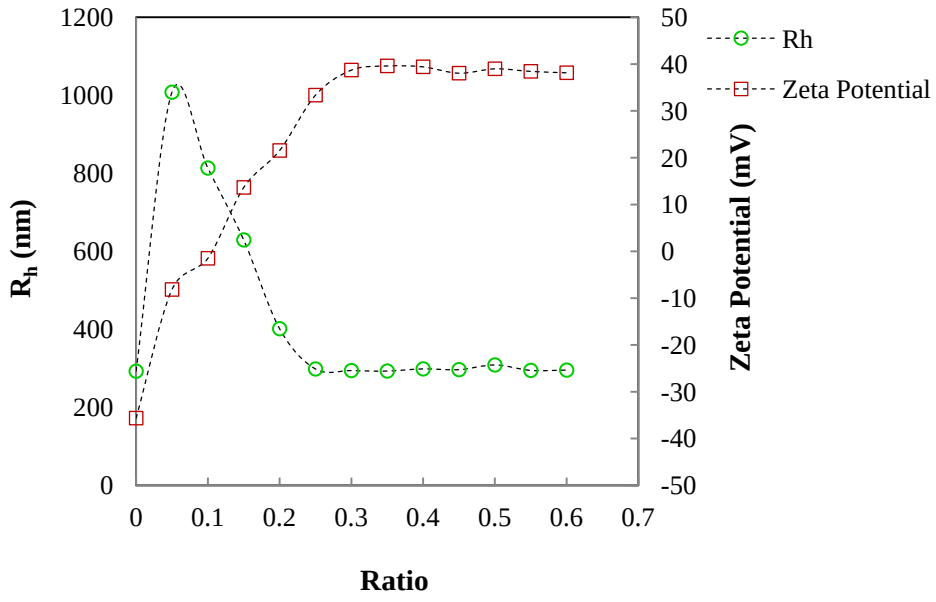

Figure 8.3 Zeta-potential and R_h as a function of ratio of volume of CS versus volume of iron-oxide magnetic MAA-DEAEMA nanogels for the first layer (CS) in 0.1 M *NaCl* at pH=7.

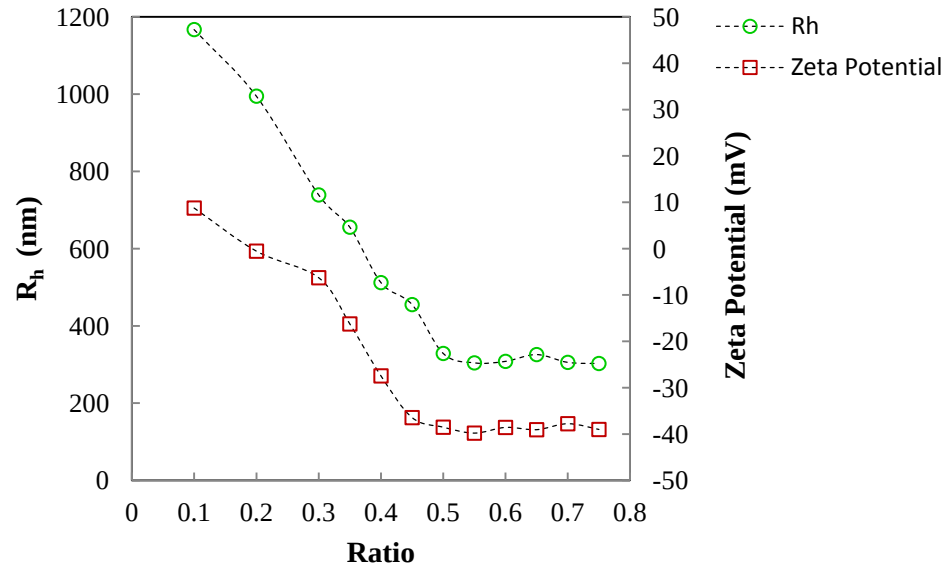

Figure 8.4 Zeta-potential and R_h as a function of ratio of the volume of PSS versus the volume of magnetic iron-oxide MAA-DEAEMA nanogels for the second layer (PSS) in 0.1 M *NaCl* at pH=7.

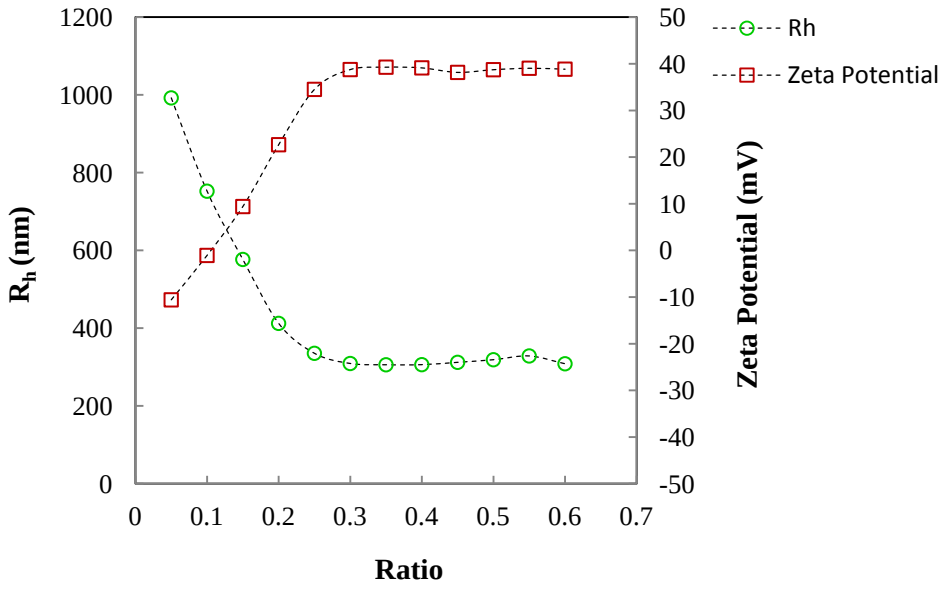

Figure 8.5 Zeta-potential and R_h as a function of ratio of the volume of CS versus the volume of magnetic iron-oxide MAA-DEAEMA nanogels for the third layer (CS) in 0.1 M *NaCl* at pH=7.

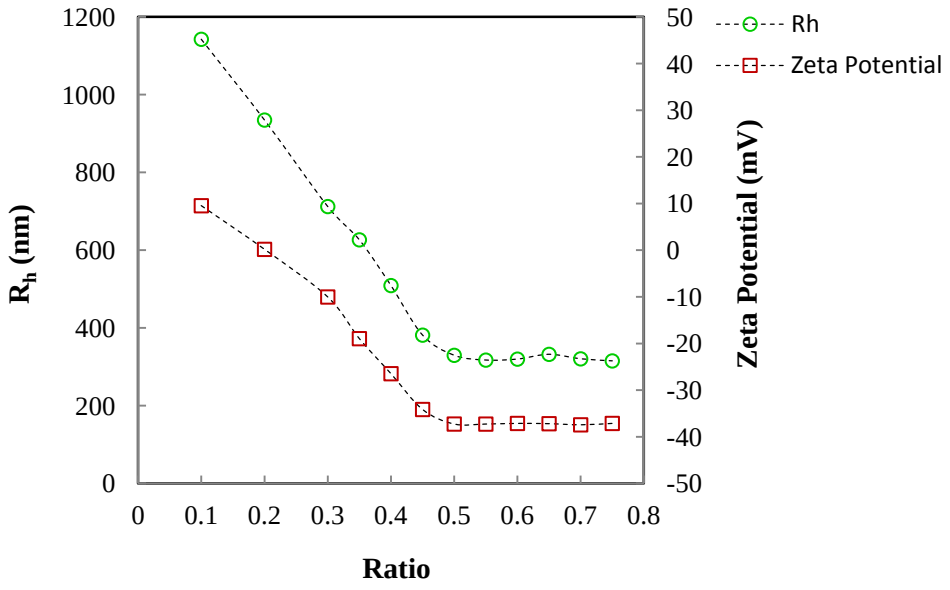

Figure 8.6 Zeta-potential and R_h as a function of ratio of the volume of CS versus the volume of magnetic iron-oxide MAA-DEAEMA nanogels for the fourth layer (CS) in 0.1 M *NaCl* at pH=7.

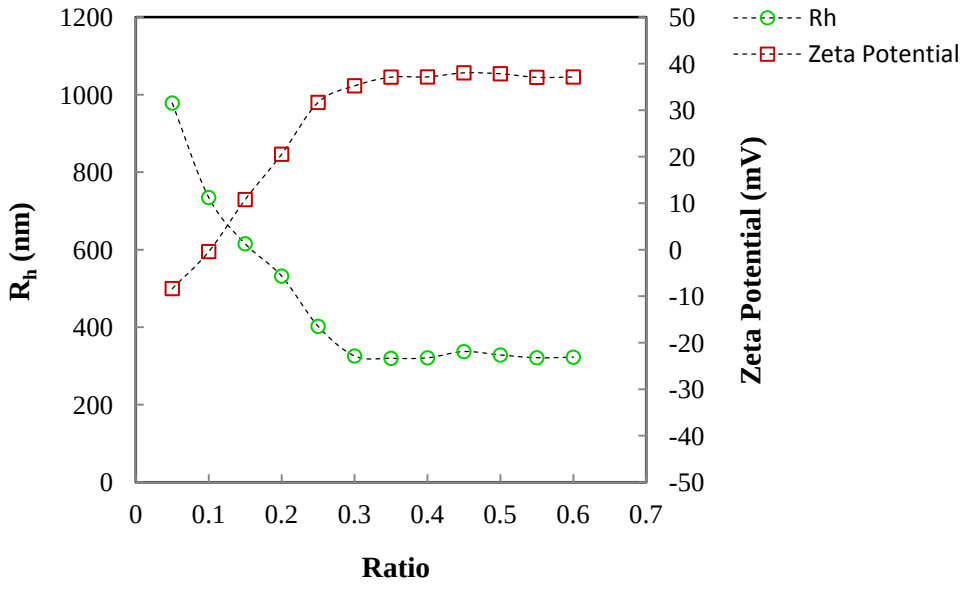

Figure 8.7 Zeta-potential and R_h as a function of ratio of the volume of CS versus the volume of magnetic iron-oxide MAA-DEAEMA nanogels for the fifthe layer (CS) in 0.1 M *NaCl* at pH=7.

Figure 8.8 also illustrates the zeta potential of the coated magnetic nanogels as a function of the number of layers at 25 ^{o}C. The successful deposition of polyelectrolyte layers onto the magnetic nanogels was further confirmed through the zeta potential data. The bare nanogels were negatively charged and upon the deposition of a first layer, the zeta potential values shifted to a positive value corresponding to the net positive surface charge of the CS layer due to the protonation of amine groups; whereas, by adding the second layer, the zeta potential value shifted to a negative value due to the negative net surface charge of the PSS layer due to presence of SO_3^-.

It can be observed that by depositing the first polyelectrolyte (chitosan), the zeta-potential increased to a higher value. This can be c nanogels due to the high charge density of CS in strong acid solution (3% w/v acetic acidexplained by the presence of higher excess of positive charges on the surface of coated-magneti) of low ionic strength. Similarly, upon the absorption of negatively charged PSS layer, the zeta-potential increased to negative value corresponding to a high surface charge density. A similar trend was reported by different research groups (Diez-Pascual and Wong, 2010; Tan et al., 2008a; Wong et al., 2009).

Furthermore, zeta-potential values decreased upon the addition of the fourth and fifth layers on the nanogels in contrast to the result achieved when solid substrate was used. This can be explained considering the fact that soft and porous structures of the nanogels provided easy diffusion and interpenetration of the polyelectrolytes, allowing the neutralization and shielding of charges trapped within the nanogels. Thus, by increasing the number of layers, the net surface charge density of the magnetic nanogels reduced as a result of interpenetration and

disappearance of the excess charges from the surface of the nanogels (Diez-Pascual and Wong, 2010; Wong et al., 2009).

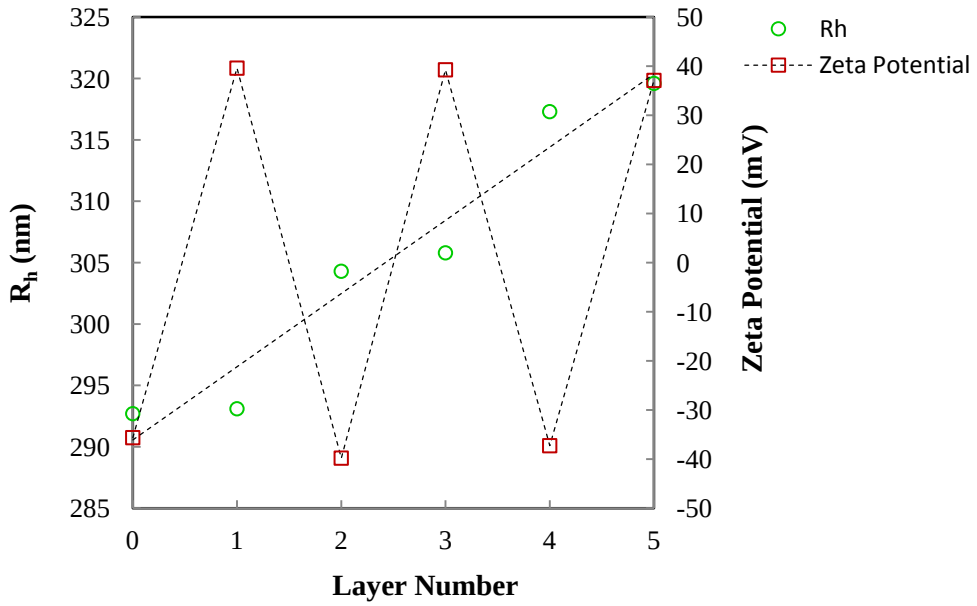

Figure 8.8 Hydrodynamic radius (R_h) and zeta-potential as a function of polyelectrolyte layer number.

8.4 PrHy Release from Layer-by-Layer Coated Magnetic Iron-Oxide DEAEMA-MAA Nanogels

In order to control the initial burst release of the PrHy from DEAEMA-MAA nanogels, the layer-by-layer method was adopted in this study. First of all, previously prepared magnetic nanogels were loaded with 2.44 g drug/ g of polymer; afterwards, as mentioned earlier the required number of layers was deposited on the PrHy-loaded magnetic nanogels, and subsequently passed through high-gradient magnetic field to remove excess amount of drug and polyelectrolytes. Finally, the concentration of released PrHy was obtained by means of the PrHy selective electrode, once the coated PrHy-loaded magnetic nanogels were introduced to 50 ml of 10 mM *NaCl* solution at physiological pH of 7.4 and body temperature of 37 ^{o}C.

The release profiles of PrHy from bare nanogels and layer coated nanogels are depicted in Figure 8.9. As shown in Figure 8.9, the initial burst release was still present for nanogels coated with the first and second layer; whereas, by increasing the number of polyelectrolyte the initial burst released was significantly reduced, which was confirmed by the smoother slope of the profile instead of a steep slope. The initial burst release observed in the bare nanogels was due to the release of the PrHy molecules present on the surface of the nanogels. In order for the surface adhered PrHy molecules to be released from the coated nanogels, they had to diffuse through the different layers of polyelectrolyte until they reached the external medium. In other words, the higher the number of polyelectrolyte layers, the more time was required by PrHy molecule to diffuse to the medium; thus, the burst release was minimized. This phenomenon can be attributed to fact that polyelectrolyte layers not only acted as diffusion barrier, but also reducing the porosity of the nanogels. As mentioned earlier, positive first, third, and fifth layer possess very small thickness in comparison to the negative second and fourth layer; however, the release profile demonstrated that the release process was mainly controlled by the total increment in layer thickness rather than being influenced by the type of the polyelectrolyte within the layers.

Figure 8.9 illustrates the schematic of drug release profile from bare and coated nanogels. Moreover, it was revealed that by increasing the nymber of coating layers, the time required for the drug molecules to reach the external medium significantly increased to 9 hours. Whereas, the bare nanogels with no coating, complete release occurred over 2 hours. In brief, it can be concluded that by manipulating the number of layers the drug release can be further controlled and also the release time can be prolonged.

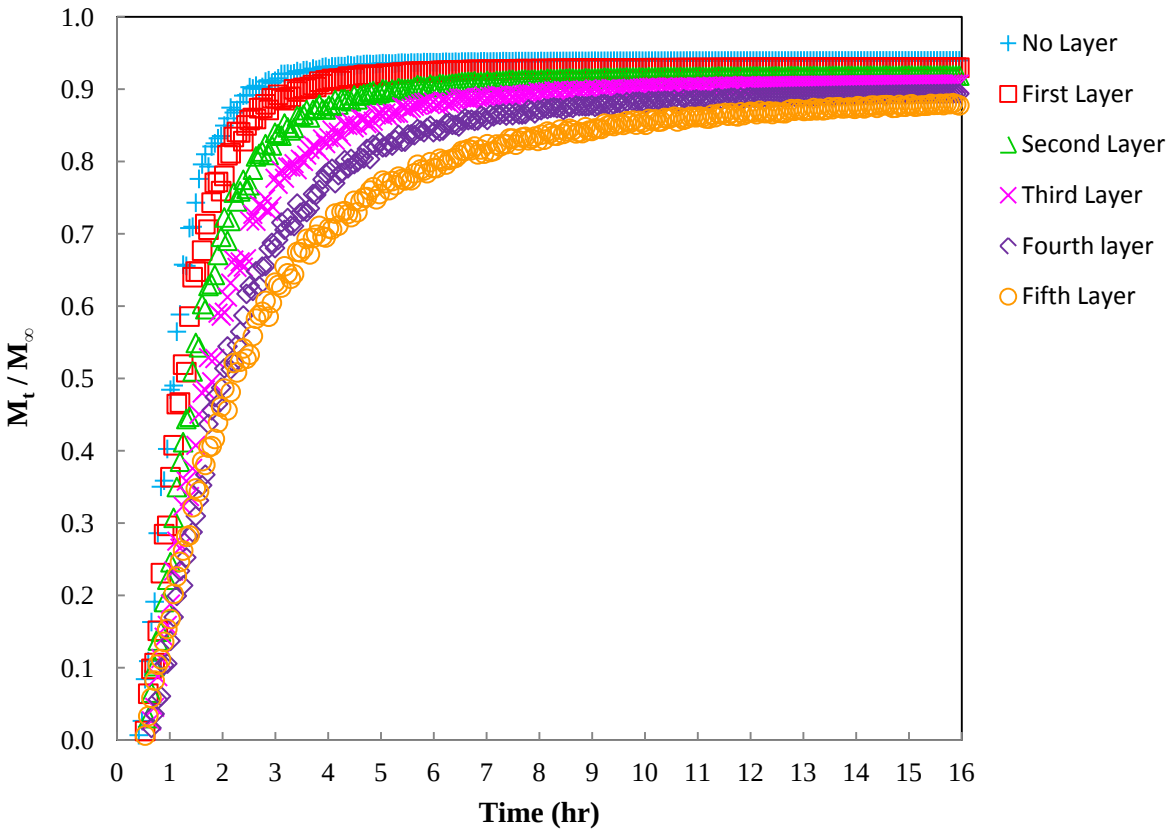

Figure 8.9 PrHy release profile from different layers of coated magnetic iron-oxide nanogels in 10 mM *NaCl* at pH=7.4 and 37^{o} C.

Chapter 9

Conclusion and Recommendation for Future Studies

In this study, polyampholyte cross-linked MAA-DEAEMA nanogels were synthesized through a semi-continuous emulsion polymerization. Polyampholytic and pH-responsive behaviour was observed in these nanogels. Dynamic light scattering and zeta-potential analyzer were used to investigate the hydrodynamic radius and surface charge density of the nanogels, correspondingly. The synthesized nanogels demonstrated great swelling ability at both high and low pH conditions, contributing to the protonation of $N\ (CH_3CH_2)_2$ groups on DEAEMA segments and ionization of *COOH* groups on MAA segments, respectively. However, at iso-electric point (IEP), confirmed by zero mobility value, the nanogels attained the most stable compact structure due to presence of steric stabilizer, PEGMA, grafting onto the surface of the nanogels. Once the pH changed from low to high, the mobility shifted from positive to negative, attributed to the positively charged ($N\ (CH_3CH_2)_2\ H^+$) groups on DEAEMA segments and negatively charged COO^- groups on MAA segments.

Isothermal titration calorimeter was used to investigate the interaction between hydrophilic drug, procaine hydrochloride (PrHy), and pH-responsive nanogels. It was revealed that the PrHy loaded into the polyampholyte nanogels network through hydrophobic interaction and hydrogen bonding at both high and low. By loading the nanogels with PrHy the hydrodynamic radius of

nanogels decreased and approached a more compact structure at high and low pH conditions comparedthe bare nanogels, as a result of hydrophobic interaction and hydrogen bonding.

The release of PrHy from MAA-DEAEMA nanogels was investigated under various conditions such as pH, salt concentration in the medium and different concentrations of loaded PrHy. The release of the PrHy was increased at low pH value and high salt concentration, which is attributed to the elevated hydrophobic interaction and larger gradient of salt concentration, respectively.

In order to induce magnetic properties to the nanogels, and also facilitate the purification step of the layer-by-layer coating of the nanogels, magnetic nanogels were synthesized through co-precipitation technique. In this method iron oxide (Fe_3O_4) was precipitated within nanogels, providing nanogels with magnetic properties. The hydrodynamic radii of the magnetic nanogels were reduced to 245.7 due to the inter-particle electrostatic interaction between iron oxide and negatively charged COO^- on MAA segments.

To reduce the initial burst release of the PrHy from magnetic nanogels, the layer by layer technique was introduced to provide diffusion barrier and increased the time required for the drug molecules to diffuse out to nanogels. Chitosan (CS) was used as polycation and Poly (sodium 4-styrenesulfonate) (PSS) was used as polyanion in the formation of coated magnetic nanogels. It was revealed that the initial burst release of the PrHy was significantly reduced and can be controlled by manipulating and increasing the number of polyelectrolyte layers.

Consequently, these coated pH-responsive magnetic iron oxide nanogels demonstrate very attractive features that make them a potential candidate for drug delivery systems. Combination of pH-responsive nanogels with magnetic nanoparticles leads to the development of functional

materials that are capable of coupling the stimulus-response of these nanogels with the magnetic properties of the nanoparticles. There are many areas for further development of coated magnetic nanogels as multifunctional drug delivery systems. Improved magnetic properties of magnetic nanogels for MR contrast agents are one area that would greatly improve the sensitivity of magnetic nanogels' detection *in vivo*. In order to increase the selectivity and safety of therapeutic nanogels, the development of a biosensor-controlled approach would be of great help. The incorporation of a biosensor-controlled therapeutic delivery would allow incorporation of more aggressive therapeutic agents without compromising safety of healthy cells and tissues.

Moreover, by incorporating biomolecules-responsive moieties, such as phenyl borate derivatives as a glucose-sensing moiety a self-regulated insulin delivery system would be constructed to treat diabetes mellitus. In addition, results from these research studies indicated that by increasing the number of coated layers, the release of drugs could be prolonged. Therefore, by incorporating a mixture of drugs at different layers different released rates can be achieved with a single dosage of drug carrier, in order to meet therapeutic requirement. For instance, a drug incorporated nearer to the matrix of nanogels would be release later and less often in comparison to drugs incorporated nearer the surface of the coated nanogels. Moreover, by modifying the ion exchangers or plasticizers a more sensitive and accurate drug-selective membrane would be obtained.

Bibliography

http://www.chemistry.nmsu.edu/Instrumentation/IS_Electrod.html

http://www.malvern.com/LabEng/technology/zeta_potential/zeta_potential_LDE.htm

http://www.med.yale.edu/wmkeck/biophysics/VP_ITC_MANUAL_11_20_02a.pdf

http://www.muschiolik.de/membrane_emulsification_process-desription.htm

Al Attas, A. S., 2009a. Construction and Analytical Application of Ion Selective Bromazepam Sensor, International Journal of Electrochemical Science 4(1), 20-29.

Al Attas, A. S., 2009b. Novel PVC Membrane Selective Electrode for the Determination of Clozapine in Pharmaceutical Preparations, International Journal of Electrochemical Science 4(1), 9-19.

Alizadeh, N., Mehdipour, R., 2002. Drug-selective electrode for ketamine determination in pharmaceutical preparations and electrochemical study of drug with BSA, Journal of pharmaceutical and biomedical analysis 30(3), 725-731.

Antipov, A. A., Sukhorukov, G. B., 2004. Polyelectrolyte multilayer capsules as vehicles with tunable permeability, Advances in Colloid and Interface Science 111(1-2), 49-61.

Arifin, D. Y., Lee, L. Y., Wang, C., 2006. Mathematical modeling and simulation of drug release from microspheres: Implications to drug delivery systems, Advanced Drug Delivery Reviews 58(12-13), 1274-1325.

Balogh, L., Nigavekar, S. S., Nair, B. M., Lesniak, W., Zhang, C., Sung, L. Y., Kariapper, M. S. T., El-Jawahri, A., Llanes, M., Bolton, B., Mamou, F., Tan, W., Hutson, A., Minc, L., Khan, M. K., 2007. Significant effect of size on the in vivo biodistribution of gold composite nanodevices in mouse tumor models, Nanomedicine: Nanotechnology, Biology and Medicine 3(4), 281-296.

Barrera, C., Herrera, A. P., Rinaldi, C., 2009. Colloidal dispersions of monodisperse magnetite nanoparticles modified with poly(ethylene glycol), Journal of colloid and interface science 329(1), 107-113.

Bergmann, N. M., Peppas, N. A., 2008. Molecularly imprinted polymers with specific recognition for macromolecules and proteins, Progress in Polymer Science 33(3), 271-288.

Berry, C. C., 2008. Intracellular delivery of nanopartides via the HIV-1 tat pepticle, Nanomedicine 3(3), 357-365.

Berry, C. C., 2009. Progress in functionalization of magnetic nanoparticles for applications in biomedicine, Journal of Physics D-Applied Physics 42(22), 224003.

Bhattacharya, S., Eckert, F., Boyko, V., Pich, A., 2007. Temperature-, pH-, and magnetic-field-sensitive hybrid microgels, Small 3(4), 650-657.

Blasi, L., Argentiere, S., Morello, G., Palama, I., Barbarella, G., Cingolani, R., Gigli, G., 2010. Uptake and distribution of labeled antibodies into pH-sensitive microgels, Acta biomaterialia 6(6), 2148-2156.

Bradley, A. J., Devine, D. V., Ansell, S. M., Janzen, J., Brooks, D. E., 1998. Inhibition of Liposome-Induced Complement Activation by Incorporated Poly(Ethylene Glycol)-Lipids, Archives of Biochemistry and Biophysics 357(2), 185-194.

Brugger, B., Vermant, J., Richtering, W., 2010. Interfacial layers of stimuli-responsive poly-(N-isopropylacrylamide-co-methacrylicacid) (PNIPAM-co-MAA) microgels characterized by interfacial rheology and compression isotherms. Phys Chem Chem Phys 12(43), 14573-8.

Burke, S. E., Barrett, C. J., 2004. pH-Dependent Loading and Release Behavior of Small Hydrophilic Molecules in Weak Polyelectrolyte Multilayer Films, Macromolecules 37(14), 5375-5384.

Calero-DdelC, V. L., Rinaldi, C., 2007. Synthesis and magnetic characterization of cobalt-substituted ferrite (CoxFe3-xO4) nanoparticles, Journal of Magnetism and Magnetic Materials 314(1), 60-67.

Capek, I., 2010. On inverse miniemulsion polymerization of conventional water-soluble monomers, Advances in Colloid and Interface Science 156(1-2), 35-61.

Chen, B., Wu, W., Wang, X., 2011. Magnetic iron oxide nanoparticles for tumor-targeted therapy, Current cancer drug targets 11(2), 184-189.

Chern, C., 2008. Principles and Applications of Emulsion Polymerization. Hoboken, N.J.: Wiley.

Chiappini, A., Guddala, S., Armellini, C., Berneschi, S., Cacciari, I., Duverger-Arfuso, C., Ferrari, M., Righini, G. C., 2010. Fabrication and Characterization of colloidal crystals infiltrated with metallic nanoparticles, Optical Components and Materials Vii 7598, 75980P.

Chonn, A., Cullis, P. R., Devine, D. V., 1991. The role of surface charge in the activation of the classical and alternative pathways of complement by liposomes, Journal of immunology (Baltimore, Md.: 1950) 146(12), 4234-4241.

Chou, L. Y. T., Ming, K., Chan, W. C. W., 2011. Strategies for the intracellular delivery of nanoparticles, Chemical Society Reviews 40(1), 233-245.

Christodoulakis, K. E., Vamvakaki, M., 2010. Amphoteric Core-Shell Microgels: Contraphilic Two-Compartment Colloidal Particles, Langmuir 26(2), 639-647.

Chu, B., 1970. Laser Light Scattering, Annual Review of Physical Chemistry 21(1), 145-174.

Dai, S., Ravi, P., Tam, K. C., Mao, B. W., Gang, L. H., 2003. Novel pH-responsive amphiphilic diblock copolymers with reversible micellization properties, Langmuir 19(12), 5175-5177.

Das, M., Kumacheva, E., 2006. From polyelectrolyte to polyampholyte microgels: comparison of swelling properties, Colloid and Polymer Science 284(10), 1073-1084.

Das, M., Mardyani, S., Chan, W. . ., Kumacheva, E., 2006. Biofunctionalized pH -Responsive Microgels for Cancer Cell Targeting: Rational Design, Advanced Materials 18(1), 80-83.

De Geest, B. G., Dejugnat, C., Verhoeven, E., Sukhorukov, G. B., Jonas, A. M., Plain, J., Demeester, J., De Smedt, S. C., 2006. Layer-by-layer coating of degradable microgels for pulsed drug delivery, Journal of Controlled Release 116(2), 159-169.

De Geest, B. G., Sukhorukov, G. B., Möhwald, H., 2009. The pros and cons of polyelectrolyte capsules in drug delivery, Expert Opin.Drug Deliv. 6(6), 613-624.

Deka, S. R., Quarta, A., Di Corato, R., Falqui, A., Manna, L., Cingolani, R., Pellegrino, T., 2010. Acidic pH-Responsive Nanogels as Smart Cargo Systems for the Simultaneous Loading and Release of Short Oligonucleotides and Magnetic Nanoparticles, Langmuir 26(12), 10315-10324.

Deng, L., Zhai, Y., Guo, S., Jin, F., Xie, Z., He, X., Dong, A., 2009. Investigation on properties of P((MAA-co-DMAEMA)-g-EG) polyampholyte nanogels, Journal of Nanoparticle Research 11(2), 365-374.

Dias, A. M. G. C., Hussain, A., Marcos, A. S., Roque, A. C. A., 2011. A biotechnological perspective on the application of iron oxide magnetic colloids modified with polysaccharides, Biotechnology Advances 29(1), 142-155.

Diez-Pascual, A. M., Wong, J. E., 2010. Effect of layer-by-layer confinement of polypeptides and polysaccharides onto thermoresponsive microgels: a comparative study. J Colloid Interface Sci 347(1), 79-89.

Discher, B. M., Bermudez, H., Hammer, D. A., Discher, D. E., Won, Y. Y., Bates, F. S., 2002. Cross-linked Polymersome Membranes: Vesicles with Broadly Adjustable Properties,106, 2848-2854.

Discher, D. E., Ortiz, V., Srinivas, G., Klein, M. L., Kim, Y., Christian, D., Cai, S., Photos, P., Ahmed, F., 2007. Emerging applications of polymersomes in delivery: From molecular dynamics to shrinkage of tumors, Progress in Polymer Science 32(8-9), 838-857.

Ditsch, A., Laibinis, P. E., Wang, D. I. C., Hatton, T. A., 2005. Controlled clustering and enhanced stability of polymer-coated magnetic nanoparticles, Langmuir 21(13), 6006-6018.

Duncan, R., Izzo, L., 2005. Dendrimer biocompatibility and toxicity, Advanced Drug Delivery Reviews 57(15), 2215-2237.

Euliss, L. E., DuPont, J. A., Gratton, S., DeSimone, J., 2006. Imparting size, shape, and composition control of materials for nanomedicine, Chemical Society Reviews 35(11), 1095-1104.

Faraji, M., Yamini, Y., Rezaee, M., 2010. Magnetic Nanoparticles: Synthesis, Stabilization, Functionalization, Characterization, and Applications, Journal of the Iranian Chemical Society 7(1), 1-37.

Farokhzad, O. C., Langer, R., 2006. Nanomedicine: Developing smarter therapeutic and diagnostic modalities, Advanced Drug Delivery Reviews 58(14), 1456-1459.

Frag, E. Y., Mohamed, G. G., El-Dien, F. A., Mohamed, M. E., 2010. Construction and performance characterization of screen printed and carbon paste ion selective electrodes for potentiometric determination of naphazoline hydrochloride in pharmaceutical preparations, The Analyst .

Gabizon, A. A., 2001. Pegylated Liposomal Doxorubicin: Metamorphosis of an Old Drug into a New Form of Chemotherapy, Cancer investigation 19(4), 424-436.

Gamarra, L. F., Amaro, E., Jr., Alves, S., Soga, D., Pontuschka, W. M., Mamani, J. B., Carneiro, S. M., Brito, G. E. S., Figueiredo Neto, A. M., 2010. Characterization of the Biocompatible Magnetic Colloid on the Basis of Fe3O4 Nanoparticles Coated with Dextran, Used as Contrast Agent in Magnetic Resonance Imaging, Journal of Nanoscience and Nanotechnology 10(7), 4145-4153.

Gao, L., Zhuang, J., Nie, L., Zhang, J., Zhang, Y., Gu, N., Wang, T., Feng, J., Yang, D., Perrett, S., Yan, X., 2007. Intrinsic peroxidase-like activity of ferromagnetic nanoparticles, Nature Nanotechnology 2(9), 577-583.

Glangchai, L. C., Caldorera-Moore, M., Shi, L., Roy, K., 2008. Nanoimprint lithography based fabrication of shape-specific, enzymatically-triggered smart nanoparticles, Journal of Controlled Release 125(3), 263-272.

Gupta, A. K., Gupta, M., 2005. Synthesis and surface engineering of iron oxide nanoparticles for biomedical applications, Biomaterials 26(18), 3995-4021.

Gupta, P., Vermani, K., Garg, S., 2002. Hydrogels: from controlled release to pH-responsive drug delivery, Drug discovery today 7(10), 569-579.

Hamidi, M., Azadi, A., Rafiei, P., 2008. Hydrogel nanoparticles in drug delivery, Advanced Drug Delivery Reviews 60(15), 1638-1649.

Hendrickson, G. R., Smith, M. H., South, A. B., Lyon, L. A., 2010a. Design of Multiresponsive Hydrogel Particles and Assemblies, Advanced Functional Materials 20(11), 1697-1712.

Hendrickson, G. R., Smith, M. H., South, A. B., Lyon, L. A., 2010b. Design of Multiresponsive Hydrogel Particles and Assemblies, Advanced Functional Materials 20(11), 1697-1712.

Heskins, M., Guillet, J. E., 1968. Solution properties of poly (N-isopropylacrylamide),2(8), 1441-1455.

Ho, B. S., Tan, B. H., Tan, J. P. K., Tam, K. C., 2008. Inverse microemulsion polymerization of sterically stabilized polyampholyte microgels, Langmuir 24(15), 7698-7703.

Hoare, T., Pelton, R., 2008. Charge-switching, amphoteric glucose-responsive microgels with physiological swelling activity, Biomacromolecules 9(2), 733-740.

Hoare, T., Pelton, R., 2004. Highly pH and temperature responsive microgels functionalized with vinylacetic acid, Macromolecules 37(7), 2544-2550.

Hoare, T. R., Kohane, D. S., 2008. Hydrogels in drug delivery: Progress and challenges, Polymer 49(8), 1993-2007.

Homola, A., James, R. O., 1977. Preparation and characterization of amphoteric polystyrene latices, Journal of colloid and interface science 59(1), 123-134.

Hong, R. Y., Feng, B., Chen, L. L., Liu, G. H., Li, H. Z., Zheng, Y., Wei, D. G., 2008. Synthesis, characterization and MRI application of dextran-coated Fe3O4 magnetic nanoparticles, Biochemical engineering journal 42(3), 290-300.

Hu, L., Chu, L., Yang, M., Wang, H., Niu, C. H., 2007. Preparation and characterization of novel cationic pH-responsive poly(N, N '-dimethylamino ethyl methacrylate# microgels, Journal of colloid and interface science 311(1), 110-117.

HUGLIN, M., 1977. Recent Trends in Classical Light-Scattering from Polymer-Solutions, Pure and Applied Chemistry 49(7), 929-940.

Hyeon, T., 2003. Chemical synthesis of magnetic nanoparticles, Chemical Communications (8), 927-934.

Ito, A., Shinkai, M., Honda, H., Kobayashi, T., 2005. Medical application of functionalized magnetic nanoparticles, Journal of Bioscience and Bioengineering 100(1), 1-11.

Ito, A., Kuga, Y., Honda, H., Kikkawa, H., Horiuchi, A., Watanabe, Y., Kobayashi, T., 2004. Magnetite nanoparticle-loaded anti-HER2 immunoliposomes for combination of antibody therapy with hyperthermia, Cancer letters 212(2), 167-175.

Jaiswal, M. K., Banerjee, R., Pradhan, P., Bahadur, D., 2010. Thermal behavior of magnetically modalized poly(N-isopropylacrylamide)-chitosan based nanohydrogel, Colloids and Surfaces B-Biointerfaces 81(1), 185-194.

Kabanov, A. V., Batrakova, E. V., Alakhov, V. Y., 2002. Pluronic® block copolymers as novel polymer therapeutics for drug and gene delivery, Journal of Controlled Release 82(2-3), 189-212.

Kabanov, A., Vinogradov, S., 2009. Nanogels as Pharmaceutical Carriers: Finite Networks of Infinite Capabilities, Angewandte Chemie International Edition 48(30), 5418-5429.

Katsu, T., Mori, Y., Furuno, K., Gomita, Y., 1999. Mexiletine-sensitive membrane electrode for medical application, Journal of pharmaceutical and biomedical analysis 19(3-4), 585-593.

Kopeček, J., 2007. Hydrogel biomaterials: A smart future? Biomaterials 28(34), 5185-5192.

Landfester, K., 2001. Polyreactions in miniemulsions, Macromolecular Rapid Communications 22(12), 896-936.

Lapeyre, V., Ancla, C., Catargi, B., Ravaine, V., 2008. Glucose-responsive microgels with a core-shell structure, Journal of colloid and interface science 327(2), 316-323.

Lapointe, J., Martel, S., 2009a. Thermoresponsive Hydrogel with Embedded Magnetic Nanoparticles for the implementation of Shrinkable Medical Microrobots and for Targeting and Drug Delivery Applications, Embc: 2009 Annual International Conference of the Ieee Engineering in Medicine and Biology Society, Vols 1-20 , 4246-4249.

Lapointe, J., Martel, S., 2009b. Thermoresponsive hydrogel with embedded magnetic nanoparticles for the implementation of shrinkable medical microrobots and for targeting and drug delivery applications. Conf Proc IEEE Eng Med Biol Soc 2009, 4246-9.

Laurent, S., Forge, D., Port, M., Roch, A., Robic, C., Elst, L. V., Muller, R. N., 2008. Magnetic Iron Oxide Nanoparticles: Synthesis, Stabilization, Vectorization, Physicochemical Characterizations, and Biological Applications, Chemical reviews 108(6), 2064-2110.

Lee, E. S. M., Chan, J., Shuter, B., Tan, L. G., Chong, M. S. K., Ramachandra, D. L., Dawe, G. S., Ding, J., Teoh, S. H., Beuf, O., Briguet, A., Tam, K. C., Choolani, M., Wang, S. C., 2009. Microgel Iron Oxide Nanoparticles for Tracking Human Fetal Mesenchymal Stem Cells Through Magnetic Resonance Imaging, Stem cells 27(8), 1921-1931.

Lee, E. S. M., Shuter, B., Chan, J., Chong, M. S. K., Ding, J., Teoh, S. H., Beuf, O., Briguet, A., Tam, K. C., Choolani, M., Wang, S. C., 2010. The use of microgel iron oxide nanoparticles in studies of magnetic resonance relaxation and endothelial progenitor cell labelling, Biomaterials 31(12), 3296-3306.

Lee, J. W., Kim, B., Kim, H. J., Han, S. C., Shin, W. S., Jin, S., 2006. Convergent Synthesis of Symmetrical and Unsymmetrical PAMAM Dendrimers, Macromolecules 39(6), 2418-2422.

Li, J., Dai, D., Zhao, B., Lin, Y., Liu, C., 2002. Properties of ferrofluid nanoparticles prepared by coprecipitation and acid treatment, Journal of Nanoparticle Research 4(3), 261-264.

Liu, H. L., Hua, M. Y., Yang, H. W., Huang, C. Y., Chu, P. C., Wu, J. S., Tseng, I. C., Wang, J. J., Yen, T. C., Chen, P. Y., Wei, K. C., 2010. Magnetic resonance monitoring of focused ultrasound/magnetic nanoparticle targeting delivery of therapeutic agents to the brain, Proceedings of the National Academy of Sciences of the United States of America 107(34), 15205-15210.

Liu, Q., Zhao, P., Chen, Y., 2007a. Divergent synthesis of dendrimer-like macromolecules through a combination of atom transfer radical polymerization and click reaction, Journal of Polymer Science Part A: Polymer Chemistry 45(15), 3330-3341.

Liu, Y., Miyoshi, H., Nakamura, M., 2007b. Nanomedicine for drug delivery and imaging: A promising avenue for cancer therapy and diagnosis using targeted functional nanoparticles, International Journal of Cancer 120(12), 2527-2537.

Lopez, V. C., Hadgraft, J., Snowden, M. J., 2005. The use of colloidal microgels as a (trans)dermal drug delivery system, International journal of pharmaceutics 292(1-2), 137-147.

Lopez-Cruz, A., Barrera, C., Calero-DdelC, V. L., Rinaldi, C., 2009. Water dispersible iron oxide nanoparticles coated with covalently linked chitosan, Journal of Materials Chemistry 19(37), 6870-6876.

Lovell, P. A., El-Aasser, M. S., 1997. Emulsion Polymerization and Emulsion Polymers. New York: J. Wiley.

Lu, C., Mu, B., Liu, P., 2011. Stimuli-responsive multilayer chitosan hollow microspheres via layer-by-layer assembly, Colloids and Surfaces B-Biointerfaces 83(2), 254-259.

Marek, S. R., Conn, C. A., Peppas, N. A., 2010. Cationic nanogels based on diethylaminoethyl methacrylate, Polymer 51(6), 1237-1243.

Matyjaszewski, K. (., Gnanou, Y., Leibler, L. (Eds), , 2007. Macromolecular Engineering : Precise Synthesis, Materials Properties, Applications . Federal Republic of Germany: WILEY-VCH Verlag GmbH & Co. KGaA.

Medina, C., Santos-Martinez, M. J., Radomski, A., Corrigan, O. I., Radomski, M. W., 2007. Nanoparticles: pharmacological and toxicological significance, British journal of pharmacology 150(5), 552-558.

Menager, C., Sandre, O., Mangili, J., Cabuil, V., 2004. Preparation and swelling of hydrophilic magnetic microgels, Polymer 45(8), 2475-2481.

Missirlis, D., Tirelli, N., Hubbell, J. A., 2005. Amphiphilic Hydrogel Nanoparticles. Preparation, Characterization, and Preliminary Assessment as New Colloidal Drug Carriers, Langmuir 21(6), 2605-2613.

Miyata, K., Kakizawa, Y., Nishiyama, N., Yamasaki, Y., Watanabe, T., Kohara, M., Kataoka, K., 2005. Freeze-dried formulations for in vivo gene delivery of PEGylated polyplex micelles with disulfide crosslinked cores to the liver, Journal of Controlled Release 109(1-3), 15-23.

Morf, W. E., Pretsch, E., De Rooij, N. F., 2007. Computer simulation of ion-selective membrane electrodes and related systems by finite-difference procedures, Journal of Electroanalytical Chemistry 602(1), 43-54.

Morimoto, N., Endo, T., Ohtomi, M., Iwasaki, Y., Akiyoshi, K., 2005. Hybrid nanogels with physical and chemical cross-linking structures as nanocarriers, Macromolecular bioscience 5(8), 710-716.

Nahar, M., Dutta, T., Murugesan, S., Asthana, A., Mishra, D., Rajkumar, V., Tare, M., Saraf, S., Jain, N. K., 2006. Functional polymeric nanoparticles: an efficient and promising tool for active delivery of bioactives, Critical reviews in therapeutic drug carrier systems 23(4), 259-318.

Nakashima, T., Shimizu, M., Kukizaki, M., 2000. Particle control of emulsion by membrane emulsification and its applications, Advanced Drug Delivery Reviews 45(1), 47-56.

Nolan, C. M., Serpe, M. J., Lyon, L. A., 2005a. Pulsatile release of insulin from Layer-by-Layer assembled microgel thin films, Macromolecular Symposia 227, 285-294.

Nolan, C. M., Serpe, M. J., Lyon, L. A., 2005b. Pulsatile release of insulin from Layer-by-Layer assembled microgel thin films, Macromolecular Symposia 227, 285-294.

Odian, G. G., 2004. Principles of polymerization, 812.

Oh, J. K., Drumright, R., Siegwart, D. J., Matyjaszewski, K., 2008a. The development of microgels/nanogels for drug delivery applications, Progress in Polymer Science 33(4), 448-477.

Oh, J. K., Drumright, R., Siegwart, D. J., Matyjaszewski, K., 2008b. The development of microgels/nanogels for drug delivery applications, Progress in Polymer Science 33(4), 448-477.

Oh, J. K., Lee, D. I., Park, J. M., 2009. Biopolymer-based microgels/nanogels for drug delivery applications, Progress in Polymer Science 34(12), 1261-1282.

Oishi, M., Nagasaki, Y., 2010. Stimuli-responsive smart nanogels for cancer diagnostics and therapy, Nanomedicine 5(3), 451-468.

Ottewill, R. H., 1982. Emulsion Polymerization Piirma, I., 1-47.

Pang, Z., Lu, W., Gao, H., Hu, K., Chen, J., Zhang, C., Gao, X., Jiang, X., Zhu, C., 2008. Preparation and brain delivery property of biodegradable polymersomes conjugated with OX26, Journal of Controlled Release 128(2), 120-127.

Park, J., An, K. J., Hwang, Y. S., Park, J. G., Noh, H. J., Kim, J. Y., Park, J. H., Hwang, N. M., Hyeon, T., 2004. Ultra-large-scale syntheses of monodisperse nanocrystals, Nature Materials 3(12), 891-895.

Park, S. I., Lim, J. H., Hwang, Y. H., Kim, K. H., Kim, S. M., Kim, J. H., Kim, C. G., Kim, C. O., 2007. In vivo and in vitro antitumor activity of doxorubicin-loaded magnetic fluids, Physica Status Solidi C - Current Topics in Solid State Physics, Vol 4, no 12 4(12), 4345-4351.

Peppas, N. A., Bures, P., Leobandung, W., Ichikawa, H., 2000. Hydrogels in pharmaceutical formulations, European Journal of Pharmaceutics and Biopharmaceutics 50(1), 27-46.

Petros, R. A., DeSimone, J. M., 2010. Strategies in the design of nanoparticles for therapeutic applications, Nature reviews.Drug discovery 9(8), 615-627.

Piao, Y., Kim, J., Bin Na, H., Kim, D., Baek, J. S., Ko, M. K., Lee, J. H., Shokouhimehr, M., Hyeon, T., 2008. Wrap-bake-peel process for nanostructural transformation from beta-FeOOH nanorods to biocompatible iron oxide nanocapsules, Nature Materials 7(3), 242-247.

Regmi, R., Bhattarai, S. R., Sudakar, C., Wani, A. S., Cunningham, R., Vaishnava, P. P., Naik, R., Oupicky, D., Lawes, G., 2010. Hyperthermia controlled rapid drug release from thermosensitive magnetic microgels, Journal of Materials Chemistry 20(29), 6158-6163.

Rhee, Y., Mansour, H. M., 2011. Nanopharmaceuticals I: nanocarrier systems in drug delivery, International Journal of Nanotechnology 8(1-2), 84-114.

Robinson, D. N., Peppas, N. A., 2002. Preparation and characterization of pH-responsive poly(methacrylic acid-g-ethylene glycol) nanospheres, Macromolecules 35(9), 3668-3674.

Rolland, J. P., Maynor, B. W., Euliss, L. E., Exner, A. E., Denison, G. M., DeSimone, J. M., 2005. Direct fabrication and harvesting of monodisperse, shape-specific nanobiomaterials, Journal of the American Chemical Society 127(28), 10096-10100.

Rong, X., 2001. Equilibrium studies of aqueous surfactant systems containing additives,.

Sahoo, S. K., De, T. K., Ghosh, P. K., Maitra, A., 1998. pH- and Thermo-sensitive Hydrogel Nanoparticles, Journal of colloid and interface science 206(2), 361-368.

Samad, A., Alam, M. I., Saxena, K., 2009. Dendrimers: a class of polymers in the nanotechnology for the delivery of active pharmaceuticals, Current pharmaceutical design 15(25), 2958-2969.

Sasaki, Y., Akiyoshi, K., 2010. Nanogel engineering for new nanobiomaterials: from chaperoning engineering to biomedical applications, Chemical record (New York, N.Y.) .

Shahrokhian, S., Hamzehloei, A., Bagherzadeh, M., 2002. Chromium(III) porphyrin as a selective ionophore in a salicylate-selective membrane electrode, Analytical Chemistry 74(14), 3312-3320.

Shu, Y., Ou, G. M., Wang, L., Zou, J. C., Li, Q. L., 2011. Surface Modification of Titanium with Heparin-Chitosan Multilayers via Layer-by-Layer Self-Assembly Technique, Journal of Nanomaterials .

Silverthorn, D. U., 2010. Human Physiology: An Integrated Approach. San Francisco: Pearson Education, Inc.

Singh, R., Lillard, J. W.,Jr, 2009. Nanoparticle-based targeted drug delivery, Experimental and molecular pathology 86(3), 215-223.

Sondjaja, R., Hatton, T. A., Tam, M. K. C., 2009. Clustering of magnetic nanoparticles using a double hydrophilic block copolymer, poly(ethylene oxide)-b-poly(acrylic acid), Journal of Magnetism and Magnetic Materials 321(16), 2393-2397.

Stefan, R. I., AboulEnein, H. Y., Baiulescu, G. E., 1996. Amiodarone-selective membrane electrode, Sensors and Actuators B-Chemical 37(3), 141-144.

Sudol, E. O., Daniel, E. S., El-Aasser, m. S., 1992. Latex: Preparation, Characterization, and Applications, 1-11.

Sukhorukov, G. B., Donath, E., Lichtenfeld, H., Knippel, E., Knippel, M., Budde, A., Mohwald, H., 1998. Layer-by-layer self assembly of polyelectrolytes on colloidal particles, Colloids and Surfaces A-Physicochemical and Engineering Aspects 137(1-3), 253-266.

Sułkowski, W. W., Pentak, D., Nowak, K., Sułkowska, A., 2006. The influence of temperature and pH on the structure of liposomes formed from DMPC, Journal of Molecular Structure 792-793, 257-264.

Sun HanWen, Zhang LianYing, Zhu XinJun, Kong ChunYan, Zhang CunLan, Yao Side, 2009. Poly(PEGMA) magnetic nanogels: preparation via photochemical method, characterization and application as drug carrier, Science in China Series B-Chemistry 52(1), 69-75.

Sun, C., Lee, J. S. H., Zhang, M. Q., 2008. Magnetic nanoparticles in MR imaging and drug delivery, Advanced Drug Delivery Reviews 60(11), 1252-1265.

Svenson, S., Tomalia, D. A., 2005. Dendrimers in biomedical applications-reflections on the field, Advanced Drug Delivery Reviews 57(15), 2106-2129.

Tan, B. H., Ravi, P., Tam, K. C., 2006. Synthesis and characterization of novel pH-responsive polyampholyte microgels, Macromolecular Rapid Communications 27(7), 522-528.

Tan, B. H., Tam, K. C., Lam, Y. C., Tan, C. B., 2005a. Microstructure and rheological properties of pH-responsive core–shell particles, Polymer 46(23), 10066-10076.

Tan, B. H., Tam, K. C., Lam, Y. C., Tan, C. B., 2005b. Microstructure and rheology of stimuli-responsive microgel systems--effect of cross-linked density, Advances in Colloid and Interface Science 113(2-3), 111-120.

Tan, B. H., Ravi, P., Tan, L. N., Tam, K. C., 2007. Synthesis and aqueous solution properties of sterically stabilized pH-responsive polyampholyte microgels, Journal of colloid and interface science 309(2), 453-463.

Tan, J. P., Tam, K. C., 2007. Application of drug selective electrode in the drug release study of pH-responsive microgels, Journal of controlled release : official journal of the Controlled Release Society 118(1), 87-94.

Tan, J. P. K., Goh, C. H., Tam, K. C., 2007. Comparative drug release studies of two cationic drugs from pH-responsive nanogels, European Journal of Pharmaceutical Sciences 32(4-5), 340-348.

Tan, J. P. K., Wang, Q., Tam, K. C., 2008a. Control of burst release from nanogels via layer by layer assembly, Journal of Controlled Release 128(3), 248-254.

Tan, J. P. K., Zeng, A. Q. F., Chang, C. C., Tam, K. C., 2008b. Release kinetics of procaine hydrochloride (PrHy) from pH-responsive nanogels: Theory and experiments, International journal of pharmaceutics 357(1-2), 305-313.

Tang, Z., Wang, Y., Podsiadlo, P., Kotov, N.., 2006. Biomedical Applications of Layer -by-Layer Assembly: From Biomimetics to Tissue Engineering, Advanced Materials 18(24), 3203-3224.

Thomas, J. B., Creecy, C. M., McGinity, J. W., Peppas, N. A., 2006. Synthesis and properties of lightly crosslinked poly((meth)acrylic acid) microparticles prepared by free radical precipitation polymerization, Polymer Bulletin 57(1), 11-20.

Thorek, D. L. J., Chen, A., Czupryna, J., Tsourkas, A., 2006. Superparamagnetic iron oxide nanoparticle probes for molecular imaging, Annals of Biomedical Engineering 34(1), 23-38.

Tirelli, N., 2006. (Bio)Responsive nanoparticles, Current Opinion in Colloid & Interface Science 11(4), 210-216.

Torchilin, V. P., 2007. Micellar nanocarriers: pharmaceutical perspectives, Pharmaceutical research 24(1), 1-16.

Veiseh, O., Gunn, J. W., Zhang, M., 2010. Design and fabrication of magnetic nanoparticles for targeted drug delivery and imaging, Advanced Drug Delivery Reviews 62(3).

Veiseh, O., Sun, C., Gunn, J., Kohler, N., Gabikian, P., Lee, D., Bhattarai, N., Ellenbogen, R., Sze, R., Hallahan, A., Olson, J., Zhang, M., 2005. Optical and MRI Multifunctional Nanoprobe for Targeting Gliomas, Nano Letters 5(6), 1003-1008.

Vytras, K., 1989. The use of ion-selective electrodes in the determination of drug substances, Journal of pharmaceutical and biomedical analysis 7(7), 789-812.

Whitesides, G., 2005. Nanoscience, Nanotechnology, and Chemistry, Small 1(2), 172-179.

Wong, J. E., Diez-Pascual, A. M., Richtering, W., 2009. Layer-by-Layer Assembly of Polyelectrolyte Multilayers on Thermoresponsive P(NiPAM-co-MAA) Microgel: Effect of Ionic Strength and Molecular Weight, Macromolecules 42(4), 1229-1238.

Wong, J. E., Richtering, W., 2008. Layer-by-layer assembly on stimuli-responsive microgels, Current Opinion in Colloid & Interface Science 13(6), 403-412.

Wu, X., Mansour, H. M., 2011. Nanopharmaceuticals II: application of nanoparticles and nanocarrier systems in pharmaceutics and nanomedicine, International Journal of Nanotechnology 8(1-2), 115-145.

Xie, J., Xu, C., Kohler, N., Hou, Y., Sun, S., 2007. Controlled PEGylation of Monodisperse Fe3O4 Nanoparticles for Reduced Non-Specific Uptake by Macrophage Cells, Advanced Materials 19(20), 3163-3166.

Xiong, X. Y., Tam, K. C., Gan, L. H., 2005. Release kinetics of hydrophobic and hydrophilic model drugs from pluronic F127/poly(lactic acid) nanoparticles, Journal of Controlled Release 103(1), 73-82.

Xu, C., Sun, S., 2007. Monodisperse magnetic nanoparticles for biomedical applications, Polymer International 56(7), 821-826.

Xu, R., Sun, G. Y., Li, Q. Y., Wang, E. B., Gu, J. M., 2010. A dual-responsive superparamagnetic Fe3O4/Silica/PAH/PSS material used for controlled release of chemotherapeutic agent, keggin polyoxotungstate, PM-19, Solid State Sciences 12(10), 1720-1725.

Ye, L., CormackPresent address: Department of Pure and Applied Chemistry, University of Strathclyde, Thomas Graham Building, 295 Cathedral Street, Glasgow, G1 1XL, UK.,Peter A.G., Mosbach, K., 2001. Molecular imprinting on microgel spheres, Analytica Chimica Acta 435(1), 187-196.

Yi, D. K., Lee, S. S., Papaefthymiou, G. C., Ying, J. Y., 2006. Nanoparticle Architectures Templated by SiO2/Fe2O3 Nanocomposites, Chemistry of Materials 18(3), 614-619.

Yoon, T., Yu, K., Kim, E., Kim, J., Kim, B., Yun, S., Sohn, B., Cho, M., Lee, J., Park, S., 2006. Specific Targeting, Cell Sorting, and Bioimaging with Smart Magnetic Silica Core–Shell Nanomaterials, Small 2(2), 209-215.

Zayed, S. I., Issa, Y. M., Hussein, A., 2006. Construction and performance characterization of ion-selective electrodes for potentiometric determination of pseudoephedrine hydrochloride applying batch and flow injection analysis techniques, Annali di Chimica 96(7-8), 421-433.

Zhou, L. L., Yuan, W. Z., Yuan, J. Y., Hong, X. Y., 2008. Preparation of double-responsive SiO2-g-PDMAEMA nanoparticles via ATRP, Materials Letters 62(8-9), 1372-1375.

Zhou, L., Yuan, J., Yuan, W., Sui, X., Wu, S., Li, Z., Shen, D., 2009a. Synthesis, characterization, and controllable drug release of pH-sensitive hybrid magnetic nanoparticles, Journal of Magnetism and Magnetic Materials 321(18), 2799-2804.

Zhou, L., Yuan, J., Yuan, W., Zhou, M., Wu, S., Li, Z., Xing, X., Shen, D., 2009b. Synthesis and characterization of multi-functional hybrid magnetite nanoparticles with biodegradability, superparamagnetism, and fluorescence, Materials Letters 63(18-19), 1567-1570.

Zou, P., Yu, Y., Wang, Y. A., Zhong, Y., Welton, A., Galban, C., Wang, S., Sun, D., 2010. Superparamagnetic Iron Oxide Nanotheranostics for Targeted Cancer Cell Imaging and pH-Dependent Intracellular Drug Release, Molecular Pharmaceutics 7(6), 1974-1984.